



EDU-QOP1(/M) Quantum Optics Kit

User Guide

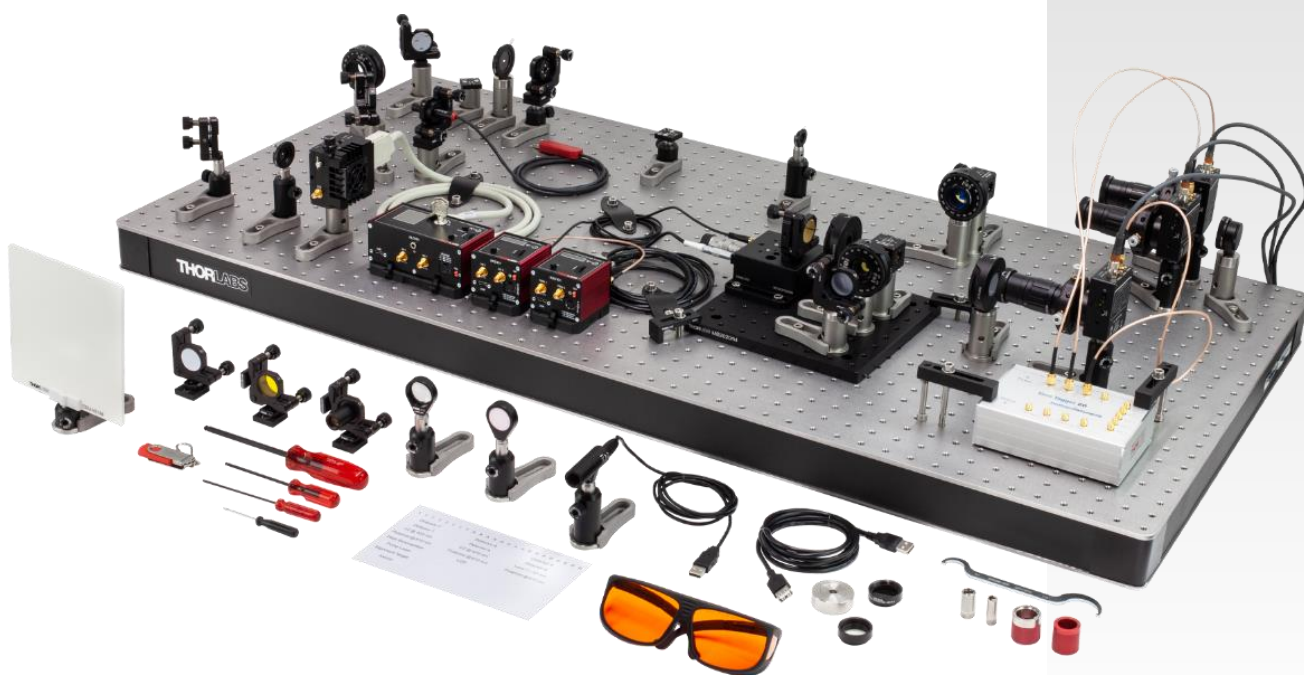


Table of Contents

Chapter 1	Safety	1
1.1	Warning Symbol Definitions	1
1.2	Laser Radiation Warning.....	1
1.3	Piezo Controller Warnings	1
Chapter 2	Product Description.....	2
Chapter 3	Principles of Quantum Optics	4
3.1	Classical Description of Light.....	4
3.1.1	Behavior at a Beamsplitter	4
3.1.2	Interference	5
3.1.3	Polarization	6
3.2	Mathematical Formalism of Quantum Mechanics.....	8
3.2.1	Dirac Notation	8
3.2.2	General Case	8
3.2.3	Application in Quantum Mechanics and Quantum Optics	8
3.2.4	Linear Operators	8
3.2.5	Eigenstates and Eigenvalues	9
3.2.6	Commutator Relations	9
3.2.7	Bases of the Hilbert Space.....	10
3.2.8	Observables.....	10
3.2.9	Measurements and Superposition of Quantum States	11
3.2.10	Expectation Values	11
3.2.11	Mixed States.....	11
3.2.12	Combination of Quantum Systems	12
3.3	Quantum Description of Light.....	12
3.3.1	Fock States	12
3.3.2	Coherent States.....	13
3.3.3	Thermal States	14
3.4	Proof of Quantized Light - Theory	14
3.4.1	Second-Order Correlation Function	15
3.4.2	Quantum Mechanical Treatment of a Beamsplitter.....	16
3.4.3	Quantum Fields	17
3.5	Proof of Quantized Light - Experiment	18
3.5.1	Hanbury-Brown-Twiss Experiment.....	18
3.5.2	Correlation Function for Single Photon Detectors	19
3.5.3	Grangier-Roger-Aspect Experiment	20
3.5.4	Triple Coincidence Detection Scheme.....	21
3.5.5	Triple Coincidence Detection Scheme: Explanation 1	22
3.5.6	Triple Coincidence Detection Scheme: Explanation 2	22
3.5.7	Accidental Coincidences.....	23
3.6	Single Photon Interference	24
3.6.1	Theoretical Description	24
3.6.2	Experimental Realization.....	25
3.7	Quantum Treatment of Polarization	26
3.7.1	Theoretical Description	26
3.7.2	Experimental Realization.....	27
3.8	The Quantum Eraser	28
3.8.1	Theoretical Description	28
3.8.2	Experimental Realization.....	29
3.9	Spontaneous Parametric Down-Conversion	29

Chapter 4	Experimental Concepts	33
4.1	Single Photon Detectors	33
4.2	Time Tagging	34
4.2.1	Time Tagging versus Coincidence Electronics	34
4.2.2	Jitter and Coincidence Window	34
4.2.3	Delay Compensation	35
Chapter 5	Kit Components	37
5.1	Pump and Alignment Laser	37
5.2	Crystal and Adjustment Aids.....	38
5.3	Optics.....	38
5.4	Detectors	40
5.5	Michelson Interferometer	41
5.6	Time Tagger and Software	42
5.7	Quantum Eraser	43
5.8	Mounting and Tools	43
5.9	Included Hardware	44
5.9.1	Imperial Kit.....	44
5.9.2	Metric Kit	44
Chapter 6	Quick Setup	45
Chapter 7	Setup and Adjustment	48
7.1	Assembly of Components	48
7.1.1	Pump Laser	48
7.1.2	Alignment Laser	50
7.1.3	Mirrors	51
7.1.4	Iris Apertures	52
7.1.5	Half-Wave Plates.....	53
7.1.6	Crystal, Axicon, and Filter	54
7.1.7	Beamsplitter	56
7.1.8	Detectors	56
7.1.9	Detector Optics	57
7.1.10	Beam Trap.....	58
7.1.11	Alignment Target	58
7.1.12	Economy Beamsplitter.....	59
7.1.13	Screen	59
7.1.14	Mirrors for Michelson Interferometer	60
7.1.15	Lens.....	61
7.1.16	Mounting the LED	62
7.1.17	Polarizers for Quantum Eraser.....	63
7.1.18	Labelling the Time Tagger	64
7.2	Preliminary Alignment.....	65
7.2.1	Software Installation.....	65
7.2.2	Collimating the Pump Laser	65
7.2.3	Calibrating the Polarizer	68
7.3	Setting Up the HBT Experiment with the Alignment Laser	70
7.4	Setting Up the Photon Pair Source.....	73
7.4.1	Setting up the Pump Laser Beam Path.....	73
7.4.2	Aligning Both Pump and Alignment Laser on the Same Path	75
7.4.3	Detector Positioning	78
7.4.4	Detector Fine Adjustment.....	81
7.4.5	Crystal Angle Adjustment	83

7.5	Setting Up the Grangier-Roger-Aspect Experiment	84
7.5.1	Beamsplitter Positioning	85
7.5.2	Third Detector Positioning	86
7.5.3	Third Detector Fine Adjustment	86
7.5.4	Test Measurement	87
7.6	Setting Up the Michelson Interferometer	88
7.6.1	Additional Alignment Path	89
7.6.2	Interferometer Adjustment	90
7.6.3	Detector Positioning	97
7.6.4	Detector Fine Adjustment	97
7.6.5	Single Photon Interference Adjustment	98
7.6.6	Michelson Interferometer Test Measurement	99
7.7	Setting Up the Quantum Eraser	100
Chapter 8	Learning Goals and Misconceptions.....	104
Chapter 9	Experiments	106
9.1	HBT-Experiment with Attenuated Laser	106
9.2	Photon Pair Source	107
9.3	HBT Experiment with one Arm of the Pair Source	108
9.4	Grangier-Roger-Aspect Experiment.....	108
9.5	GRA Experiment with Classical Light	109
9.6	Malus' Law for Single Photons	110
9.7	Single Photon Michelson Interferometer	111
9.8	Quantum Eraser	114
Chapter 10	Additional Experiments	116
10.1	Coherence Length.....	116
10.2	The Three-Polarizer-Paradox	118
10.3	Quantum Computing	118
10.3.1	Qubits and Gates	119
10.3.2	Deutsch-Jozsa Algorithm	120
10.3.3	Optical Implementation	121
10.3.4	Experimental Realization.....	123
10.3.5	Sample Measurements.....	126
10.3.6	Discussion of Error Sources	127
10.3.7	Further Algorithm Ideas	128
10.4	Direct Event Pulse Observation.....	128
Chapter 11	Software.....	131
11.1	Software Installation	131
11.2	General Remarks	131
11.3	Saving Results.....	131
11.4	Alignment Tab	132
11.5	Delay Adjust Tab	132
11.6	HBT and GRA Tabs	134
11.7	Malus' Law Tab.....	135
11.8	Michelson Interferometer Tab.....	136

11.9	Configuration Tab.....	137
11.10	Hidden Settings	138
Chapter 12	Technical Notes.....	139
12.1	Different Detection Schemes	139
12.1.1	Standard Triple Coincidences.....	139
12.1.2	Gated Detection Scheme	140
12.1.3	Changing the Detection Scheme in the Software	141
12.2	Environmental Conditions	142
12.3	Avoiding Fluctuations in the Michelson Interferometer	142
12.4	Accidental Coincidences	144
12.5	Maximizing the Count Rate	146
12.6	Choice of Polarizers	147
12.7	Polarizers vs. Quarter-Wave Plates.....	147
12.8	Axicon Design.....	148
12.9	Temperature Dependence of Pump Laser Wavelength	148
12.10	Adjustable Count Rate Ratio.....	148
12.11	Movable Michelson Interferometer.....	149
12.12	Polarization In the SPDC Process.....	150
Chapter 13	Troubleshooting.....	151
13.1	Pump Laser not Working	151
13.2	Low Count Rates with Filter	151
13.3	Low Count Rates with BBO crystal	151
13.4	Low Coincidence Count Rates	152
13.5	Malus' Law Measurement is Asymmetric	152
13.6	Michelson Interferometer Problems.....	153
13.7	Quantum Eraser Problems.....	153
Chapter 14	Laser Safety Calculation	154
14.1	Laser System	154
14.2	Laser Class Calculation.....	154
14.3	Laser Safety Glasses Calculation	154
Chapter 15	Acknowledgements	156
Chapter 16	Warranty and RMA Information	157
16.1	Return of Devices	157
Chapter 17	Thorlabs Worldwide Contacts	158

Chapter 1 Safety

1.1 Warning Symbol Definitions

Below is a list of warning symbols you may encounter in this manual or on your device



Warning: Laser Radiation



General Warning

1.2 Laser Radiation Warning

Warning



The class 3B laser diode used in this kit can emit more than 50 mW of optical power, which can cause damage to the eyes if viewed directly. The laser driver is equipped with a key switch and safety interlock, which should be used appropriately to avoid injury. Additionally, we recommend wearing appropriate laser safety glasses when using this kit.



1.3 Piezo Controller Warnings

General Warnings



If this equipment is used in a manner not specified by the manufacturer, the protection provided by the equipment may be impaired. In particular, excessive moisture may impair operation.

This product generates, uses, and outputs high voltages from the SMC connector (HV Output) that are hazardous and can cause serious injury. In any installation that uses the KPZ101 piezo controller, it is the user's responsibility to ensure adequate insulation and precautions are taken to avoid shock risk. Cables for HV Out must be rated for 250 V RMS.

Spillage of fluid, such as sample solutions, should be avoided. If spillage does occur, clean up immediately using absorbant tissue. Do not allow spilled fluid to enter the internal mechanism.

Chapter 2 Product Description

The field of quantum physics evolves quickly: quantum computers, quantum cryptography networks, and quantum-based sensing are all nearing introduction into real world applications. Highlighting this, the 2022 Nobel Prize in Physics was awarded to Alain Aspect, John F. Clauser, and Anton Zeilinger for their groundbreaking work in quantum optics. In turn, teaching quantum concepts is becoming ever more important. Our Quantum Optics Educational Kit allows students to investigate the quantum properties of light first-hand in an open and accessible environment.

One particularly important aspect of the kit is to educate people about what constitutes a non-classical light source. E.g., students can measure that an attenuated laser does not constitute a single photon source. The source that is set up and analyzed in this kit is a so-called photon pair source; pairs of 810 nm photons are generated inside a nonlinear, type-I BBO crystal from the output of a 405 nm pump laser. The photons in the pair are time-energy entangled (though not polarization-entangled). The use of nonlinear crystals is widespread in the quantum optics community because of their ease of alignment and their high count rates. Since all measurements are performed with these pairs, this type of non-classical light source is also called a heralded single photon source (i.e., one photon signaling the arrival of the other).

A look at this educational system, as displayed in Figure 1, reveals the open design that allows students to investigate each component's properties and function. Moreover, we do not utilize optical fibers which are often used to guide light from the table to detectors housed somewhere else. Instead, we use free space optics and very small single photon detectors which allow us to place the detectors in the system and perform the measurement in that spot. This is even more important since the discussion of when and where a measurement occurs is fundamental in quantum mechanics. The open setup requires a darkened room; see Section 12.2 for more details.

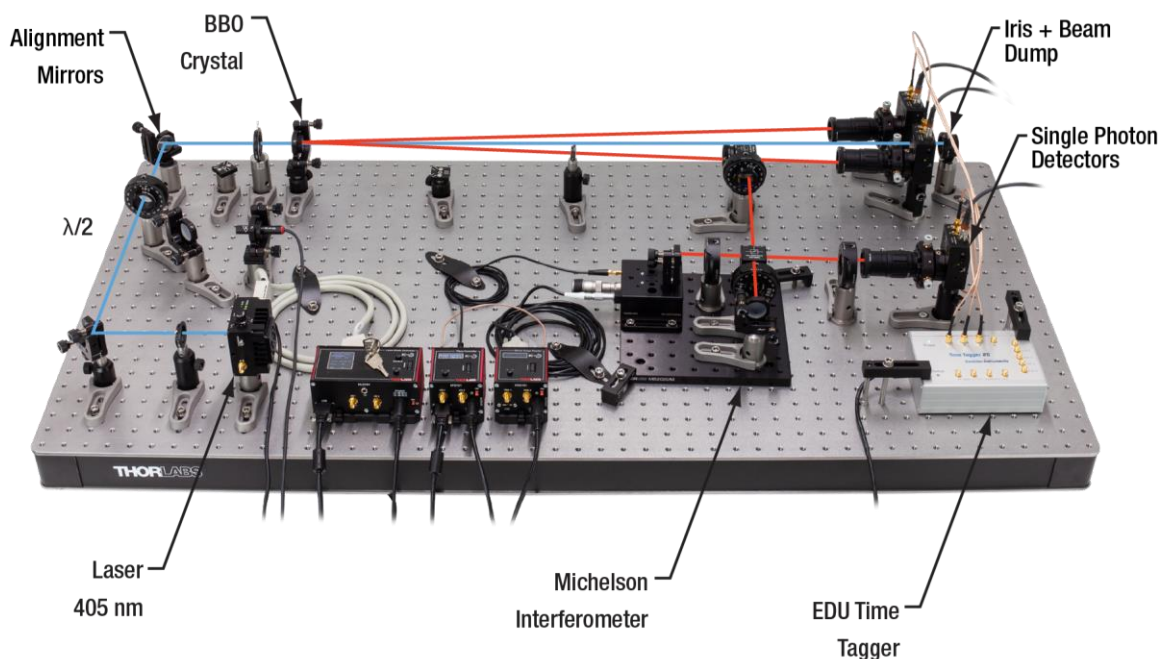


Figure 1 *Overview of the Quantum Optics Setup (Breadboard not included: We recommend the B2448FX (B60120AX) optical breadboard with the AV5(/M) damping feet.)*

To analyze and correlate the signals coming from the three single photon detectors, modern time-tagging electronics is employed. There are several experiments that students can set up and measure themselves:

- The pair source itself
- The experimental proof of a non-classical light source (Grangier-Roger-Aspect experiment)
- Experimental falsification of the misconception that attenuated lasers are single photon sources
- Behavior of single photons at a linear polarizer

- Single photon interference in a Michelson interferometer
- Quantum eraser experiment

All these experiments are described in detail in this manual and are made experimentally accessible by clear alignment procedures and experimental alignment tools that greatly help in reliably finding the signals of interest.

Chapter 3 Principles of Quantum Optics

3.1 Classical Description of Light

In this section, a summary of the classical description of light is given, focused on the properties that play a role in the experiments in this kit. It is often useful to compare the quantum mechanical results derived in later sections to the classical results of this section.

Classically, light is described as an electromagnetic field governed by the Maxwell equations.

$$\nabla \cdot \vec{E} = \frac{\rho}{\epsilon_0} \quad (1)$$

$$\nabla \cdot \vec{B} = 0 \quad (2)$$

$$\nabla \times \vec{E} = -\frac{\partial \vec{B}}{\partial t} \quad (3)$$

$$\nabla \times \vec{B} = \mu_0 \left(\vec{J} + \epsilon_0 \frac{\partial \vec{E}}{\partial t} \right) \quad (4)$$

Here, \vec{E} and \vec{B} are the electric and magnetic fields, ρ is the charge density, \vec{J} is the electric current density, ϵ_0 is the vacuum permittivity constant, and μ_0 is the vacuum permeability constant.

By combining the Maxwell equations, the electromagnetic wave in vacuum can be described by a single equation:

$$\left(\nabla^2 - \frac{1}{c^2} \frac{\partial^2}{\partial t^2} \right) \vec{E}(\vec{r}, t) \quad (5)$$

One solution of this equation is a plane wave with:

$$\vec{E}(\vec{r}, t) = \vec{E}_0 \cdot e^{i(\vec{k}\vec{x} - \omega t)} \quad (6)$$

Here, \vec{k} is the wave vector and ω is the angular frequency.

A Cartesian coordinate system can be chosen in such a way that the propagation of the wave is along the z-direction, i.e., the wave vector is $\vec{k} = k \cdot \vec{u}_z$, with \vec{u}_z being the unit vector in the z-direction. The following equation therefore applies:

$$k = \frac{2\pi}{\lambda} = \frac{2\pi f}{c} = \frac{\omega}{c} \quad (7)$$

Here, λ is the wavelength, f is the frequency, and c is the speed of light.

The electric field emitted by a laser can be approximated as a plane wave and the intensity is the square of the electric field $I = |\vec{E}_0|^2$.

3.1.1 Behavior at a Beamsplitter

If a plane wave with an amplitude \vec{E}_i is incident on the input port of a beamsplitter with a transmission coefficient t and a reflection coefficient r , the output fields are still plane waves with amplitudes of $\vec{E}_t = t \cdot \vec{E}_i$ and $\vec{E}_r = r \cdot \vec{E}_i$, respectively. The output intensities are then:

$$I_t = t^2 \cdot |\vec{E}_i|^2 = t^2 \cdot I_i \quad (8)$$

$$I_r = r^2 \cdot |\vec{E}_i|^2 = r^2 \cdot I_i \quad (9)$$

Under the assumption of an ideal lossless beamsplitter, the squares of the coefficients add up to 1:

$$t^2 + r^2 = 1 \quad (10)$$

3.1.2 Interference

Assume the experimental setup¹ shown in Figure 2: An incoming light wave, \vec{E}_i (green arrow), is split at a beamsplitter. The light from each output port, \vec{E}_α and \vec{E}_β (blue dashed arrows), then hits a mirror at normal incidence and is reflected backwards into the beamsplitter. The waves from the two arms recombine at the beamsplitter and leave in the direction of the detector, \vec{E}_d (such as a screen, camera, or eye) as well as back towards the light source, \vec{E}_s (red dashed arrows).

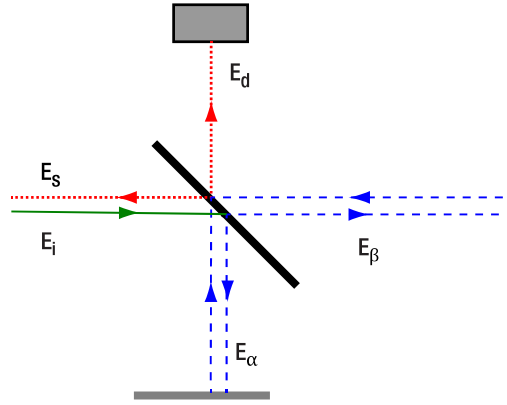


Figure 2 Schematic of a Michelson Interferometer

If the input field has an amplitude E_i and the beamsplitter ratio is 50:50, then the amplitudes E_α and E_β in the arms are:

$$E_\alpha = E_\beta = \frac{1}{\sqrt{2}} \cdot E_i \quad (11)$$

Due to the path length difference Δl of arms α and β , the fields in the arms become out of phase with a phase difference ϕ :

$$\phi = \frac{2\pi\Delta l}{\lambda} \quad (12)$$

The amplitude of the field E_d at the output port is then:

$$E_d = \frac{1}{\sqrt{2}} (E_\alpha + E_\beta \cdot e^{i\phi}) = \frac{1}{\sqrt{2}} \cdot \left(\frac{1}{\sqrt{2}} \cdot E_i + \frac{1}{\sqrt{2}} \cdot E_i \cdot e^{i\phi} \right) = \frac{1}{2} \cdot E_i \cdot (1 + e^{i\phi}) \quad (13)$$

The intensity I_d measured at the detector on the output path is then:

$$I_d = |E_d|^2 = \frac{|E_i|^2}{4} \cdot (1 + e^{i\phi}) \cdot (1 + e^{-i\phi}) = \frac{I_i}{4} (2 + 2 \cos \phi) = \frac{I_i}{2} (1 + \cos \phi) \quad (14)$$

Where I_i is the intensity of the initial input. Hence, depending on the path length difference, the output intensity can reach from 0 (destructive interference) to I_i (constructive interference).

When combining two beams at a beamsplitter, energy conservation dictates that in one of the outgoing beams, the incoming beams are phase-shifted by an additional π to each other². In which outgoing beam this occurs depends on the actual design of the beamsplitter. Here, we assign the additional phase-shift to the output beam going back towards the laser, \vec{E}_s . The field E_s and intensity I_s in this path are then:

$$E_s = \frac{1}{\sqrt{2}} (E_\alpha + E_\beta \cdot e^{i(\phi+\pi)}) = \frac{1}{2} \cdot E_i \cdot (1 + e^{i(\phi+\pi)}) \quad (15)$$

$$I_s = |E_s|^2 = \frac{|E_i|^2}{4} \cdot (1 + e^{i(\phi+\pi)}) \cdot (1 + e^{-i(\phi+\pi)}) = \frac{I_i}{4} (2 + 2 \cos(\phi + \pi)) = \frac{I_i}{2} (1 - \cos \phi) \quad (16)$$

¹ Thorlabs offers the EDU-MINT2(/M) Educational Kit for Classical Interferometry. The manual is freely available on the product webpage and introduces the Michelson interferometer in more detail.

² M. Fox, Quantum Optics: An Introduction. (Oxford University Press, Oxford, 2006).

It is apparent that the sum of the intensities in the two output arms is always equal to the input intensity I_i , meaning that the energy is conserved.

3.1.3 Polarization

The Maxwell equations show that the electromagnetic field is a traverse field, i.e., the field vectors are perpendicular to the propagation direction². Figure 3 shows an example of such a wave.

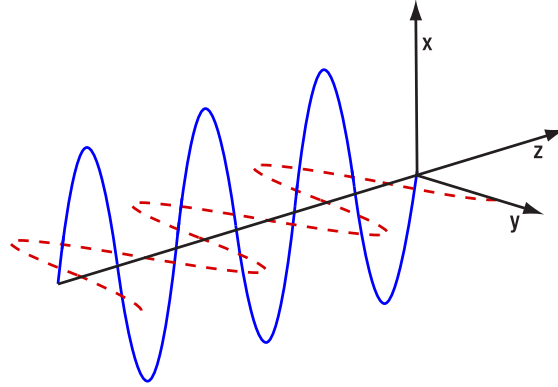


Figure 3 An electromagnetic wave propagating along the z-direction. The electric field is marked as a solid blue line, and the magnetic field is marked as a red dashed line.

The polarization is defined by the direction of the electric field; hence the magnetic field is omitted in the following equations. For a plane wave propagating in z-direction, the electric field vector is in the xy-plane and can be described as:

$$\vec{E} = E_x \cdot \vec{u}_x + E_y \cdot \vec{u}_y \quad (17)$$

For this plane wave, the following equations apply:

$$E_x = E_{0x} \cdot \cos(kz - \omega t) \quad (18)$$

$$E_y = E_{0y} \cdot \cos(kz - \omega t + \phi) \quad (19)$$

Here, E_{0x} and E_{0y} are the amplitudes of the fields in x- and y-direction, respectively, and ϕ is the phase factor, describing the fact that the field can oscillate in separate phases in the x- and y-direction. The overall amplitude of the electric field E_0 is then:

$$E_0 = \sqrt{E_{0x}^2 + E_{0y}^2} \quad (20)$$

The polarization vector $\vec{\epsilon}$ describes the direction of the electric field oscillation and is defined as:

$$\vec{\epsilon} = \frac{E_{0x}}{E_0} \cdot \vec{u}_x + \frac{E_{0y}}{E_0} \cdot e^{i\phi} \cdot \vec{u}_y \quad (21)$$

and the electric field \vec{E} can be described in terms of the polarization vector (see the literature³ for a more detailed derivation) as:

$$\vec{E} = E_0 \cdot e^{i(kz - \omega t)} \cdot \vec{\epsilon} \quad (22)$$

To understand the meaning of the polarization vector, it is helpful to investigate several special cases.

Linear Polarization

If $\phi = 0$, i.e., the x- and y-components of the electric field are oscillating in phase, then $\vec{\epsilon}$ is a real vector, describing a line which is offset by an angle θ from the x-axis:

$$\theta = \tan^{-1} \left(\frac{E_{0y}}{E_{0x}} \right) \quad (23)$$

³ M. Beck, *Quantum Mechanics, Theory and Experiment*. (Oxford University Press, Oxford, 2012).

The electric field oscillates along this line, and the light is called linearly polarized. Figure 4 displays an example of a linearly polarized electric field.

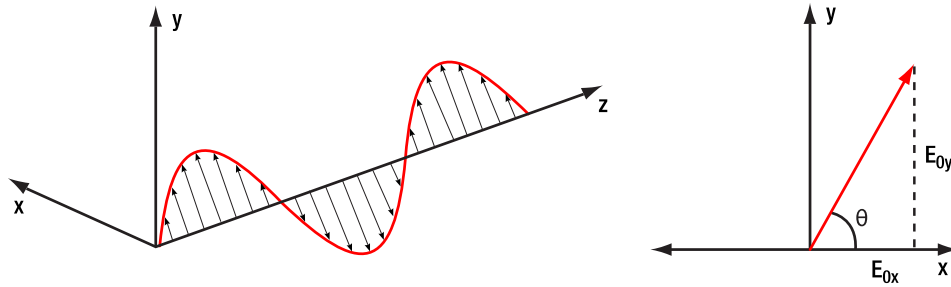


Figure 4 Electric Field of a Linearly Polarized Wave. The perspective in the right graph is along the negative z-direction (towards the source).

Circular Polarization

If $\phi = \frac{\pi}{2}$ and $E_{0x} = E_{0y}$, the polarization vector becomes $\vec{\epsilon}_L = \frac{1}{\sqrt{2}} \cdot (\vec{u}_x + i\vec{u}_y)$. The subscript L denotes left-circular polarization. Calculating the electric fields in this case and setting $z = 0$ to only view the oscillation in time at a fixed point, one obtains:

$$E_x = \frac{E_0}{\sqrt{2}} \cdot \cos(\omega t) \tag{24}$$

$$E_y = \frac{E_0}{\sqrt{2}} \cdot \sin(\omega t) \tag{25}$$

This means that the direction of the electric field is constantly changing and tracing a circle in the x-y-plane, hence the name circular polarization. The rotation is counter-clockwise (when looking towards the source) and called left-circularly polarized.

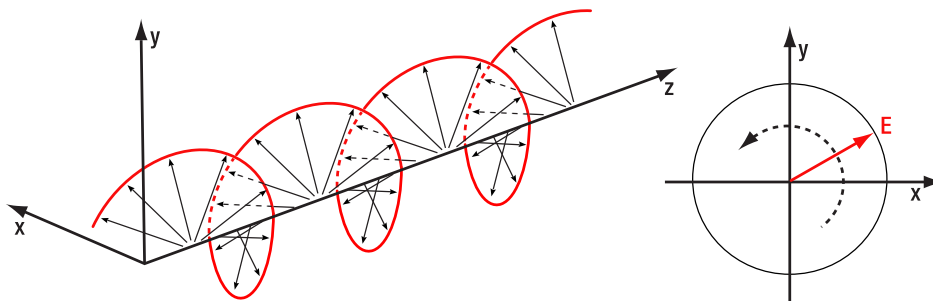


Figure 5 Electric Field of a Left-Circularly Polarized Wave. The perspective in the right graph is along the negative z-direction (towards the source).

A phase difference of $\phi = -\frac{\pi}{2}$ results in clockwise rotation (again, when looking towards the source) and the light is then called right-circularly polarized. In this case, the polarization vector becomes:

$$\vec{\epsilon}_R = \frac{1}{\sqrt{2}} \cdot (\vec{u}_x - i\vec{u}_y) \tag{26}$$

Elliptical Polarization

Elliptical polarization is the general case when none of the special cases above apply. The phase shift and the ratio of the amplitudes in the x- and y-directions determine the orientation and eccentricity of the ellipse.

Linear Polarizers

Linear polarizers are optical elements that only transmit the component of incoming light that is linearly polarized along the polarizer axis. The light after the polarizer is then linearly polarized along this axis.

The polarization of linearly polarized light passing a linear polarizer will be projected onto the polarizer axis, and the intensity will be attenuated according to Malus' Law:

$$I_{out} = I_{in} \cdot \cos^2(\theta_{in} - \theta_{pol}) \quad (27)$$

Here, I_{in} and I_{out} are the intensities before and after the polarizer, respectively. θ_{in} is the angle between the polarization of the incoming light and the x-axis, while θ_{pol} is the angle between the polarizer axis and the x-axis.

The intensity of circularly-polarized light will always be attenuated by a factor of $\frac{1}{2}$ when passing through a linear polarizer, irrespective of the polarizer axis.

3.2 Mathematical Formalism of Quantum Mechanics

Before the quantum mechanical treatment of the electromagnetic field is introduced in the next section, a very brief introduction to quantum mechanics is given in this section, only as far as will be required for the calculations in the remainder of the chapter. A more comprehensive introduction can be found in the literature^{4,5}.

3.2.1 Dirac Notation

In this chapter, the Bra-Ket notation introduced by Dirac will be used. In the following subsection, a brief overview of the components and their mathematical and physical meanings are given.

3.2.2 General Case

A ket is written in the form $|w\rangle$. Mathematically it is a vector in a vector space V .

A bra is written in the form $\langle f|$. Mathematically it is a linear form $f: V \rightarrow \mathbb{C}$, mapping a vector into the plane of complex numbers.

Letting the linear form $\langle f|$ act on a ket $|w\rangle$ is denoted as $\langle f|w\rangle$. The result of this operation is a complex number.

3.2.3 Application in Quantum Mechanics and Quantum Optics

In quantum physics, quantum states can be represented by vectors in a complex Hilbert space (the exact nature of that space depends on the problem at hand), which facilitates calculation in most cases. These vectors are denoted by kets. The symbol(s) inside the ket are a label denoting the state, they are not a mathematical entity on which operations can be performed. For example, in general $|1\rangle + |2\rangle \neq |3\rangle$ and $\frac{1}{2}|2\rangle \neq |1\rangle$.

As an inner product (\cdot, \cdot) is defined in every Hilbert space (the " \cdot " being a placeholder for any possible element of the Hilbert space), the bra $\langle v|$ can be understood as positioning the vector $v \equiv |v\rangle$ in the first position of this inner product $(v, \cdot) \equiv \langle v|$. A bra $\langle v|$ acting on a ket $|w\rangle$ is then understood as the inner product $(v, w) \equiv \langle v|w\rangle$. This is typically interpreted as a projection of state $|w\rangle$ onto the state $|v\rangle$, i.e., the probability amplitude for the state $|w\rangle$ to collapse into the state $|v\rangle$. The inner product is antilinear, i.e., exchanging the components gives the complex conjugate:

$$\langle v|w\rangle = \langle w|v\rangle^* \quad (28)$$

3.2.4 Linear Operators

Linear operators are denoted \hat{A} and when acting on a ket, output a ket, e.g., $\hat{A}|w\rangle = |x\rangle$. A typical way to construct linear operators is the outer product. If $|w\rangle$ is a ket and $\langle v|$ is a bra, then the outer product is defined as $|w\rangle\langle v|$ and acts on a ket $|x\rangle$ in the following way:

$$|w\rangle\langle v|(|x\rangle) \equiv |w\rangle\langle v|x\rangle = \langle v|x\rangle \cdot |w\rangle \quad (29)$$

Linear operators are distributive, i.e.:

⁴ M. Beck, *Quantum Mechanics, Theory and Experiment*. (Oxford University Press, Oxford, 2012).

⁵ R. Loudon, *The Quantum Theory of Light*. (Oxford University Press, Oxford, 1965).

$$(\hat{A} + \hat{B}) |w\rangle = \hat{A}|w\rangle + \hat{B}|w\rangle \quad (30)$$

$$\hat{A}(|w_1\rangle + |w_2\rangle) = \hat{A}|w_1\rangle + \hat{A}|w_2\rangle \quad (31)$$

In the following, we will list some special types of operators which are of importance later.

Adjoint Operator

For every linear operator \hat{A} there exists an operator \hat{A}^\dagger , for which the following holds true:

$$\text{If } \hat{A}|w\rangle = |x\rangle, \text{ then } \langle w|\hat{A}^\dagger = \langle x| \text{ for all } |w\rangle \text{ and } |x\rangle \quad (32)$$

The operator \hat{A}^\dagger (pronounced “A-dagger”) is called the adjoint operator to \hat{A} .

Identity Operator

The identity operator $\hat{1}$ has no effect on any state, i.e.:

$$\hat{1}|w\rangle = |w\rangle \text{ for all } |w\rangle \quad (33)$$

Inverse Operator

The inverse operator to \hat{A} is denoted as \hat{A}^{-1} and defined as:

$$\hat{A}\hat{A}^{-1} = \hat{A}^{-1}\hat{A} = \hat{1} \quad (34)$$

Unitary Operators

A unitary operator is an operator for which the following equation holds true:

$$\hat{U}\hat{U}^\dagger = \hat{U}^\dagger\hat{U} = \hat{1} \quad (35)$$

Projection Operators

An operator of the form $\hat{P}_w = |w\rangle\langle w|$ is called a projection operator because it projects any state in the Hilbert space onto the state $|w\rangle$. Projection operators are idempotent, i.e.:

$$\hat{P}_w^2 = \hat{P}_w \quad (36)$$

This means that after projecting once onto the state $|w\rangle$ any subsequent projection onto the same state does not change anything.

Hermitian Operators

An operator is called Hermitian or self-adjoint, if it is identical to its own adjoint operator, i.e.:

$$\hat{O} = \hat{O}^\dagger \quad (37)$$

Hermitian operators play a key role in quantum mechanics as they represent measurable physical quantities, such as energy or momentum.

3.2.5 Eigenstates and Eigenvalues

For a linear operator \hat{A} , if there exist one or more state vectors $|A_i\rangle$ for which:

$$\hat{A}|A_i\rangle = A_i|A_i\rangle \quad (38)$$

these vectors are called eigenstates of \hat{A} and the A_i (in general complex numbers) are called eigenvalues.

If $|A_i\rangle$ is an eigenstate of \hat{A} , then the following relation applies to the corresponding bra vector $\langle A_i|$ and the adjoint operator \hat{A}^\dagger :

$$\langle A_i|\hat{A}^\dagger = A_i^* \cdot \langle A_i| \quad (39)$$

Here, A_i^* is the complex conjugate value of A_i .

3.2.6 Commutator Relations

In general, operators are not commutative, i.e.: $\hat{A}\hat{B} \neq \hat{B}\hat{A}$. The commutator of two operators is defined as:

$$[\hat{A}, \hat{B}] \equiv \hat{A}\hat{B} - \hat{B}\hat{A} \quad (40)$$

If $[\hat{A}, \hat{B}] = 0$, the operators are said to be commuting.

3.2.7 Bases of the Hilbert Space

In any Hilbert space, there exists at least one orthonormal basis, i.e., a set of vectors $|b_i\rangle$ for which the following relation holds:

$$\langle b_i | b_j \rangle = \delta_{ij} \quad (41)$$

With δ_{ij} being the Kronecker delta function defined as:

$$\delta_{ij} = \begin{cases} 1 & \text{for } i = j \\ 0 & \text{for } i \neq j \end{cases} \quad (42)$$

An orthonormal basis contains exactly as many elements as the dimension of the Hilbert space and a linear combination of these bases vectors can be used to describe any vector in the Hilbert space. Let $|b_i\rangle$ be the basis vectors in an N-dimensional Hilbert space, then any vector-normalized vector $|w\rangle$ (meaning $\langle w | w \rangle = 1$) can be expressed as:

$$|w\rangle = \sum_i c_i \cdot |b_i\rangle \quad i = 1, 2, \dots, N \quad (43)$$

Here, the c_i are complex coefficients for which the following holds:

$$\sum_i |c_i|^2 = 1 \quad i = 1, 2, \dots, N \quad (44)$$

If a ket $|w\rangle$ is expressed via a basis of the Hilbert space, the corresponding bra is:

$$\langle w | = \sum_i c_i^* \cdot \langle b_i | \quad (45)$$

Here, the basis vectors are replaced by their corresponding bra and the coefficients are the complex conjugates of the ones used to express the ket.

Additionally, for an orthonormal basis, the following relation applies:

$$\hat{1} = \sum_i \hat{P}_{b_i} = \sum_i |b_i\rangle \langle b_i| \quad i = 1, 2, \dots, N \quad (46)$$

Here, $\hat{P}_{b_i} = |b_i\rangle \langle b_i|$ is called a projection operator as explained in Section 3.2.4. The eigenstates of a Hermitian operator in a finite dimensional Hilbert space always form an orthonormal basis, and the eigenvalues are real numbers.

3.2.8 Observables

An observable is any physically measurable quantity, such as momentum, energy, polarization, and many more. Every observable corresponds to a Hermitian operator, and the possible results of a measurement of the observable are the eigenvalues of the corresponding operator.

For a system in any normalized state $|\psi\rangle$, the probability of measuring the value λ is:

$$P(\lambda | \psi) = |\langle \lambda | \psi \rangle|^2 \quad (47)$$

Here, λ is the eigenvalue corresponding to the eigenstate $|\lambda\rangle$.

Using Equation (46) and the fact that the eigenvectors of a Hermitian operator form a basis of the Hilbert space, we can rewrite any Hermitian operator \hat{O} with the eigenvectors $|\lambda_i\rangle$ as

$$\hat{O} = \hat{O}\hat{1} = \sum_i \hat{O}|\lambda_i\rangle \langle \lambda_i| = \sum_i \lambda_i \cdot |\lambda_i\rangle \langle \lambda_i| \quad (48)$$

3.2.9 Measurements and Superposition of Quantum States

Hidden in the prior subsection is an integral property of quantum physics, the superposition of states. As stated previously, measuring an observable O of a particle in the state $|\psi\rangle$ can in general result in any eigenvalue λ_i of the operator \hat{O} . This is because, prior to the measurement, the particle is in a superposition of all states $|\lambda_i\rangle$.

$$|\psi\rangle = \sum_i c_i \cdot |\lambda_i\rangle$$

The result of the measurement is not defined beforehand! The superposition coefficients c_i give the probabilities of different measurement results (and define the state $|\psi\rangle$).

When considering multiple measurements, there are two cases to distinguish:

Multiple measurements on the same particle:

After a measurement that yielded λ_i as a result, the state is changed to $|\lambda_i\rangle$. This means that every consecutive measurement of the same observable will yield λ_i with 100% probability (unless the state was changed in the meantime, e.g., by measuring a different observable). This process of changing the state due to a measurement is often called a collapse of the state (superposition of states), as in: “The measurement resulted in λ_i so the state collapsed to $|\lambda_i\rangle$.”

Multiple measurements on identical particles:

Here, a critical difference between classical and quantum physics becomes visible: in classical physics, a quantity like momentum is always well defined (even if unknown). When performing measurements of this quantity on an ensemble of identical particles in the same state, one will always get the same result. This is not the case in quantum physics: measurements on an ensemble of particles in the identical state can have different results. The result before the measurement is not only unknown, but unknowable!

3.2.10 Expectation Values

If many measurements of an observable O are performed on a state $|\psi\rangle$ (not on the same system, but on an ensemble of systems in the identical state), then the expected average of the measurement results is called the expectation value $\langle O \rangle$ of the measurement. It is calculated as follows:

$$\langle O \rangle = \langle \psi | \hat{O} | \psi \rangle \quad (49)$$

The probability of measuring a specific eigenvalue λ of \hat{O} is:

$$P(\lambda | \psi) = |\langle \lambda | \psi \rangle|^2 = \langle \lambda | \psi \rangle^* \cdot \langle \lambda | \psi \rangle = \langle \psi | \lambda \rangle \cdot \langle \lambda | \psi \rangle = \langle \psi | \hat{P}_\lambda | \psi \rangle = \langle P_\lambda \rangle \quad (50)$$

For the third equality we used the antilinear property of the inner product; see Equation (28). We can see that the probability of measuring an eigenvalue is the expectation value of the projection operator \hat{P}_λ onto the corresponding eigenstate $|\lambda\rangle$.

The variance of the measurement is:

$$\Delta O^2 = \langle \hat{O}^2 \rangle - \langle \hat{O} \rangle^2 \quad (51)$$

3.2.11 Mixed States

States that can be expressed by a single ket vector are called pure states. However, there are states of the electromagnetic field that cannot be represented by a pure state. Instead, they are statistical mixtures of pure states, i.e., one can only give the probabilities for the system to behave as being in one of two or more pure states. These states are called mixed states⁶ and are expressed by the so-called density operator:

$$\hat{\rho} = \sum_{n=1}^N P_n |n\rangle \langle n| \quad \text{with} \quad 0 < P_n \leq 1 \quad \text{and} \quad \sum_{n=1}^N P_n = 1 \quad (52)$$

⁶ R. Loudon, *The Quantum Theory of Light*. (Oxford University Press, Oxford, 1965).

The P_n are the weights for the pure state and can be interpreted as the probabilities of the mixed state to behave as if being in the corresponding pure state when an observable is being measured. Note that they are not the probability of the mixed state being the pure state. The number N here can be any number.

3.2.12 Combination of Quantum Systems

Assume you have two quantum systems (such as particles), called A and B . Each system has a corresponding Hilbert space, H_A and H_B , and a set of orthonormal basis vectors $|A_i\rangle$ and $|B_j\rangle$. If the two quantum systems interact, then the state of the combined system is an element of the enlarged Hilbert space $H_{AB} = H_A \otimes H_B$. The symbol \otimes denotes the tensor product. The dimension of H_{AB} is the product of the dimensions of H_A and H_B and $|A_i\rangle \otimes |B_j\rangle$ is an orthonormal basis of H_{AB} .

Let $|\psi_A\rangle_A$ be a normalized vector in H_A and $|\psi_B\rangle_B$ be a normalized vector in H_B . Then $|\psi_A\rangle_A \otimes |\psi_B\rangle_B$ is also normalized and an element of H_{AB} . To simplify the notation, we define:

$$|\psi_A\rangle_A \otimes |\psi_B\rangle_B \equiv |\psi_A, \psi_B\rangle \equiv |\psi_A\rangle|\psi_B\rangle \quad (53)$$

Expressed in the orthonormal basis $|A_i\rangle \otimes |B_j\rangle$, the state is:

$$|\psi_A, \psi_B\rangle = \sum_{i,j} c_{ij} |A_i\rangle|B_j\rangle \quad \text{with} \quad \sum_{i,j} |c_{ij}|^2 = 1 \quad (54)$$

The inner product between two vectors $|\psi_A, \psi_B\rangle$ and $|\phi_A, \phi_B\rangle$ in H_{AB} is defined as:

$$\langle \psi_A, \psi_B | \phi_A, \phi_B \rangle \equiv \langle \psi_A | \phi_A \rangle \cdot \langle \psi_B | \phi_B \rangle \quad (55)$$

An observable of a subsystem is still represented by an operator. Let O_A be an observable in subsystem A . Then the operator is $\hat{O}_A \hat{1}_B$, acting only on the part of the combined state that describes subsystem A and leaving subsystem B unchanged. Often, this is only written as \hat{O}_A .

The expectation value of O_A for a combined state $|\psi_A, \psi_B\rangle$ is:

$$\langle \hat{O}_A \rangle = \langle \psi_A, \psi_B | \hat{O}_A | \psi_A, \psi_B \rangle \quad (56)$$

3.3 Quantum Description of Light

In this section, we will give a brief overview of the quantum description of light, focusing on the light states that are most important for the experiments in this kit. A more comprehensive introduction can be found in the literature⁷.

To treat the electromagnetic field quantum mechanically, it is assumed that every mode of the field corresponds to a harmonic oscillator⁸. The Hamiltonian of a mode of the electromagnetic field can then be written as:

$$\hat{H} = \hbar\omega \left(\hat{n} + \frac{1}{2} \right) \quad (57)$$

Here, $\hbar = \frac{h}{2\pi}$ with h being the Planck constant, ω is the resonance angular frequency, and \hat{n} is the number operator. The number operator can be expressed in terms of the annihilation operator \hat{a} and the creation operator \hat{a}^\dagger :

$$\hat{n} = \hat{a}^\dagger \hat{a} \quad (58)$$

Quantum mechanics thus treats the electromagnetic field as quantized excitation in (energy) packages of $\hbar\omega$. These packages are called photons.

3.3.1 Fock States

A single photon is the fundamental excitation quantum of the electromagnetic field, i.e., the smallest possible excitation of the field. It is described by the so-called Fock state $|1\rangle$. Fock states in general describe the

⁷ R. Loudon, *The Quantum Theory of Light*. (Oxford University Press, Oxford, 1965).

⁸ M. Beck, *Quantum Mechanics, Theory and Experiment*. (Oxford University Press, Oxford, 2012).

fundamental excitations of the electromagnetic field. They are the eigenstates $|n\rangle$ of the Hamiltonian and of the number operator:

$$\hat{n}|n\rangle = n|n\rangle \quad n = 0, 1, 2, \dots \quad (59)$$

The following equations hold for Fock states:

$$\hat{a}|n\rangle = \sqrt{n} \cdot |n-1\rangle \quad (60)$$

$$\hat{a}^\dagger|n\rangle = \sqrt{n+1} \cdot |n+1\rangle \quad (61)$$

Here, the names of the operators \hat{a} and \hat{a}^\dagger becomes clear. The annihilation operator acting on a Fock state results in a Fock state with one less photon, while the creation operator acting on a Fock state results in Fock state with one additional photon. The ground state of the electromagnetic field is $|0\rangle$ and is called the vacuum state. It describes the complete absence of photons.

The operators \hat{a} and \hat{a}^\dagger do not commute. We can calculate the commutator by letting it act on a state $|n\rangle$ and apply the definitions above:

$$\begin{aligned} [\hat{a}, \hat{a}^\dagger]|n\rangle &= \hat{a}\hat{a}^\dagger|n\rangle - \hat{a}^\dagger\hat{a}|n\rangle = \sqrt{n+1} \cdot \hat{a}|n+1\rangle - \sqrt{n} \cdot \hat{a}^\dagger|n-1\rangle \\ &= \sqrt{n+1}\sqrt{n+1} \cdot |n\rangle - \sqrt{n}\sqrt{n} \cdot |n\rangle = (n+1-n)|n\rangle = 1 \cdot |n\rangle \end{aligned} \quad (62)$$

As this holds for any state $|n\rangle$, we obtained:

$$[\hat{a}, \hat{a}^\dagger] = 1 \quad (63)$$

The expectation value and the variance of the photon number in a Fock state are:

$$\langle n|\hat{n}|n\rangle = n \cdot \langle n|n\rangle = n \quad (64)$$

$$\Delta n^2 = \langle n|\hat{n}^2|n\rangle - \langle n|\hat{n}|n\rangle^2 = n^2 - n^2 = 0 \quad (65)$$

This means that a field mode in a Fock state contains exactly n photons; see the left graph in Figure 6. Generating Fock states experimentally has long been a challenge. Nowadays, reliable methods exist to prepare light in the state $n = 1$, but Fock states with higher numbers require increasingly complex techniques.

3.3.2 Coherent States

A plane electromagnetic wave with constant amplitude, such as one emitted by a (strongly attenuated) laser, is **different** from a Fock state, with a number of photons that matches the energy contained in the wave. Instead, such a plane wave is described by a coherent state.

Such a coherent state can be expressed as a linear combination of Fock states because Fock states form an orthonormal basis of the Fock space. The coherent state $|\alpha\rangle$ is:

$$|\alpha\rangle = e^{-\frac{|\alpha|^2}{2}} \cdot \sum_{n=0}^{\infty} \left(\frac{\alpha^n}{\sqrt{n!}} \cdot |n\rangle \right) \quad (66)$$

Coherent states are the eigenstates of the annihilation operator \hat{a} , i.e., $\hat{a}|\alpha\rangle = \alpha \cdot |\alpha\rangle$. The annihilation operator is not Hermitian, so in general, the eigenvalues α are complex numbers. Coherent states are the closest quantum mechanical analog to classical oscillators.

The mean photon number (expectation value of the number operator) of a coherent state is:

$$\langle n \rangle = \langle \alpha|\hat{n}|\alpha \rangle = \langle \alpha|\hat{a}^\dagger\hat{a}|\alpha \rangle = \alpha^* \cdot \alpha \cdot \langle \alpha|\alpha \rangle = |\alpha|^2 \quad (67)$$

The variance of such a state is:

$$\begin{aligned} \Delta n^2 &= \langle \alpha|\hat{n}^2|\alpha \rangle - \langle \alpha|\hat{n}|\alpha \rangle^2 = \langle \alpha|\hat{a}^\dagger\hat{a}\hat{a}^\dagger\hat{a}|\alpha \rangle - |\alpha|^4 = \alpha^* \cdot \alpha \cdot \langle \alpha|\hat{a}\hat{a}^\dagger|\alpha \rangle - |\alpha|^4 \\ &= |\alpha|^2 \cdot \langle \alpha|1 + \hat{a}^\dagger\hat{a}|\alpha \rangle - |\alpha|^4 = |\alpha|^2 \cdot (1 + |\alpha|^2) - |\alpha|^4 = |\alpha|^2 \end{aligned} \quad (68)$$

Here, we used the commutator relation of the annihilation and creation operators: $\hat{a}\hat{a}^\dagger = 1 + \hat{a}^\dagger\hat{a}$ (see Section 3.3.1). The variance is equal to the expectation value, which hints at a Poisson

distribution of the photon numbers. Indeed, it can be proven that the probabilities of a coherent state measured in different Fock states is Poissonian⁹, as depicted in the center graph of Figure 6.

3.3.3 Thermal States

Besides Fock states and coherent states, there are other, more chaotic states of light. This includes thermal radiation emitted by a black body, fluorescent light sources, and LEDs. Chaotic light cannot be described by a pure quantum state. Instead, it is a statistical mixture of pure states; for more information, see Section 3.2.11.

All the chaotic light sources above share the same photon number distribution for a fixed mean photon number $\langle \hat{n} \rangle$:

$$P(n) = \frac{\langle n \rangle^n}{(1 + \langle n \rangle)^{1+n}} \quad (69)$$

It can be shown that the variance for the probability distribution in Equation (69) is always:

$$\Delta n^2 = \langle n^2 \rangle - \langle n \rangle^2 = \langle n \rangle^2 + \langle n \rangle \quad (70)$$

As a black body is the most prominent example of this kind of light source, all states with this probability distribution are called thermal states in the following even if the explicit density matrix depends on the exact type of the source. For example, the state of a black body with a temperature T can be expressed by the following density matrix¹⁰:

$$\hat{\rho} = \left(1 - e^{\left(\frac{-\hbar\omega}{k_b T} \right)} \right) \cdot e^{\left(\frac{-\hbar\omega \hat{n}}{k_b T} \right)} \quad (71)$$

Here, ω is the angular frequency, k_b is the Boltzmann constant, and the exponential of the number operator is defined by a power series expansion. One can see from Equation (70) that the photon number variance of thermal states is always larger than for a Poissonian statistic such as displayed by coherent states. Figure 6 shows a graph of the photon number probabilities for a Fock state, a coherent state, and a thermal state with the same mean photon number 5.

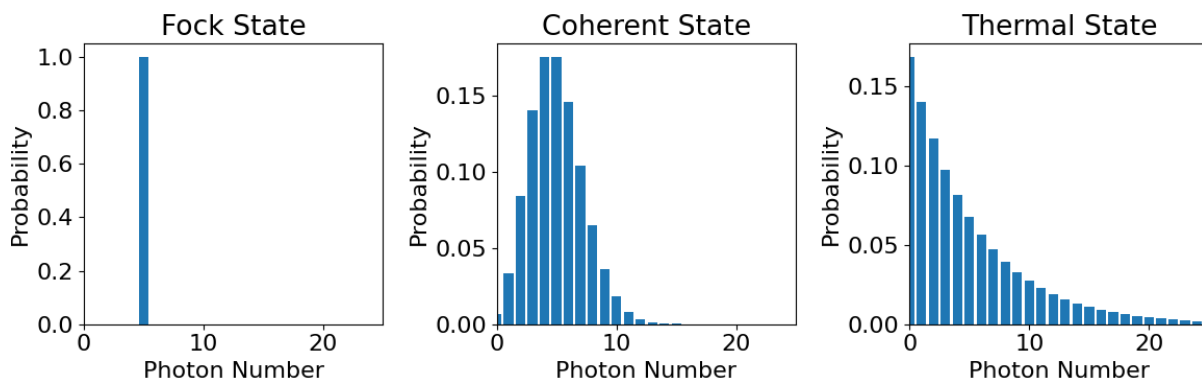


Figure 6 Photon number probabilities for a Fock state (left), a coherent state (center), and a thermal state (right), all with the same mean photon number $\langle n \rangle = 5$. Be aware that the scaling for the first plot is different than for the second and third to provide better visibility.¹¹

3.4 Proof of Quantized Light - Theory

In educational literature, the quantization of light is often motivated by the photoelectric effect¹². However, this phenomenon can be completely described by semiclassical theories that do not require a quantization of the electromagnetic field. Only the energy levels of the atoms in the matter are quantized in these theories¹³, while

⁹ M. Fox, *Quantum Optics: An Introduction*. (Oxford University Press, Oxford, 2006).

¹⁰ R. Loudon, *The Quantum Theory of Light*. (Oxford University Press, Oxford, 1965).

¹¹ The figure was composed with the Qutip Quantum Toolbox for Python.

¹² B. J. Pearson and D. P. Jackson, *American Journal of Physics*, **78**(5), 471 (2010).

¹³ R. Loudon, *The Quantum Theory of Light*. (Oxford University Press, Oxford, 1965).

the light field is still defined by the classical Maxwell equations. Therefore, different experiments are required to test the quantum nature of light.

3.4.1 Second-Order Correlation Function

A conceptually simple test is to send a light beam with extremely low intensity through a beamsplitter with two detectors at the two possible outputs of the splitter. If light is indeed quantized, then it should be impossible for the two detectors to detect light at the exact same time (in coincidence), because a single quantum of light can only be detected in one of the detectors. A sketch of such a setup, often called an intensity interferometer as introduced by Hanbury Brown and Twiss (HBT)¹⁴, is shown in Figure 7.

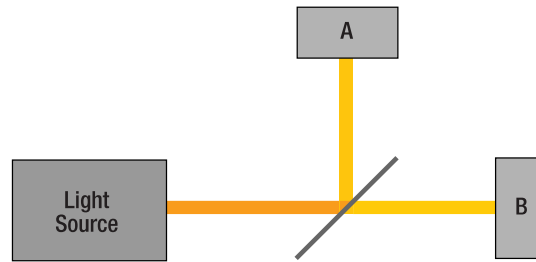


Figure 7 Schematic of an Intensity Interferometer

Here, we will focus on the definition of important quantities, while the experiment is described in Section 3.5.1. The measured quantity in this setup is the second-order correlation function. For the classical electromagnetic field and two detectors A and B, this function is defined as follows:

$$g^{(2)}(\tau) = \frac{\langle I_A(t + \tau) \cdot I_B(t) \rangle}{\langle I_A(t + \tau) \rangle \cdot \langle I_B(t) \rangle} \quad (72)$$

Here, $I_A(t)$ and $I_B(t + \tau)$ are the intensities at detector A at the time t and at detector B at the time $t + \tau$, respectively. The angle brackets denote a time average. This function is called “second order” because it describes the correlation of intensities. A first-order correlation function indicates correlations between amplitudes.

Second-order correlations give insight into the nature of the light entering the setup. The most important aspect is the correlation of the detector signals at the same time, i.e., at $\tau = 0$.

$$g^{(2)}(0) = \frac{\langle I_A \cdot I_B \rangle}{\langle I_A \rangle \cdot \langle I_B \rangle} \quad (73)$$

If $g_{AB}^{(2)}(0)$ takes a value of 1, this means that the detector signals are completely uncorrelated. A value larger than 1 means correlation of the detector signals, i.e., if one detector measures a large (small) signal, the other detector is more likely to also measure a large (small) signal than expected for complete randomness. $g^{(2)}(0) < 1$, on the other hand, indicates anti-correlation of the signals, i.e., a high (low) signal on one detector is more likely to coincide with a small (large) signal on the other one.

Using Equations (8) and (9) in Section 3.1.1, we can rewrite Equation (73) in terms of the input intensity I_i for the setup displayed in Figure 7 (irrespective of the transmission and reflection coefficients of the beamsplitter):

$$g_{HBT}^{(2)}(0) = \frac{\langle I_i^2 \rangle}{\langle I_i \rangle^2} \quad (74)$$

The subscript HBT indicates that the equation is valid for an intensity interferometer as introduced by HBT and shown in Figure 7. Using the Cauchy-Schwarz inequality, it can be proven that:

$$g_{HBT}^{(2)}(0) = \frac{\langle I_i^2 \rangle}{\langle I_i \rangle^2} \geq 1 \quad (\text{classical fields}) \quad (75)$$

This means that for classical fields, the second-order correlation function is always larger than or equal to 1 and there can be no anti-correlation of the detector signals. This is intuitive, as the beamsplitter always splits the wave

¹⁴ R. H. Brown and R. Q. Twiss, *Nature*, **177**, 27 (1956).

into two parts with a constant ratio. The signals at the detectors can then either be uncorrelated (amplitude constant in time) or correlated (amplitude varies in time, both detectors “see” the same increase and decrease of the signal) and there is no way that the signal on one detector increases while the signal on the other decreases. In the case of a constant amplitude and hence uncorrelated detector signals, we expect $g_{HBT}^{(2)}(0) = 1$.

This means that any experiment showing anti-correlation in an HBT setup violates the classical description of light.

3.4.2 Quantum Mechanical Treatment of a Beamsplitter

To calculate the quantum mechanical expectation for the HBT experiment, it is important to understand how a beamsplitter is treated in quantum mechanics. Assume a lossless beamsplitter with the geometry shown in Figure 8, with \hat{a}_1 and \hat{a}_2 being the annihilation operators of the input ports and \hat{a}_3 and \hat{a}_4 being the annihilation operators of the output ports.

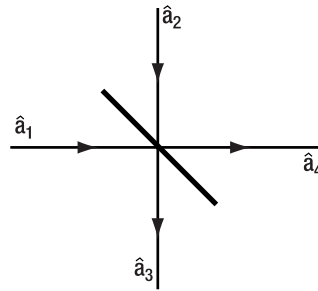


Figure 8 Geometry of Beamsplitter

With the transmission and reflection coefficients of the beamsplitter being t and r , it can be shown¹⁵ that the following relations hold for the annihilation and creation operators of the ports:

$$\hat{a}_1 = r \cdot \hat{a}_3 + t \cdot \hat{a}_4 \quad (76)$$

$$\hat{a}_2 = t \cdot \hat{a}_3 - r \cdot \hat{a}_4 \quad (77)$$

$$\hat{a}_1^\dagger = r \cdot \hat{a}_3^\dagger + t \cdot \hat{a}_4^\dagger \quad (78)$$

$$\hat{a}_2^\dagger = t \cdot \hat{a}_3^\dagger - r \cdot \hat{a}_4^\dagger \quad (79)$$

These operator relations can then be used to transform the input states of the beamsplitter to the output states. As an important example, take the input mode $|1\rangle_1|0\rangle_2$, i.e., a Fock state with a photon number of 1 at input port 1 and the vacuum state at input port 2 (a single photon incident on the beamsplitter at port 1). This transforms to:

$$|1\rangle_1|0\rangle_2 = \hat{a}_1^\dagger|0\rangle = (r \cdot \hat{a}_3^\dagger + t \cdot \hat{a}_4^\dagger)|0\rangle = r \cdot |1\rangle_3|0\rangle_4 + t \cdot |0\rangle_3|1\rangle_4 \quad (80)$$

The single photon at input port 1 transforms to a superposition state of the photon being in the output ports 3 or 4. Calculating the expectation value of the photon number at output port 3 yields:

$$\begin{aligned} & (r \cdot \langle 1|_3 \langle 0|_4 + t \cdot \langle 0|_3 \langle 1|_4) \hat{n}_3 (r \cdot |1\rangle_3|0\rangle_4 + t \cdot |0\rangle_3|1\rangle_4) \\ &= (r \cdot \langle 1|_3 \langle 0|_4 + t \cdot \langle 0|_3 \langle 1|_4) (1 \cdot r \cdot |1\rangle_3|0\rangle_4 + 0 \cdot t \cdot |0\rangle_3|1\rangle_4) \\ &= (r \cdot \langle 1|_3 \langle 0|_4 + t \cdot \langle 0|_3 \langle 1|_4) (r \cdot |1\rangle_3|0\rangle_4) \\ &= r^2 \cdot 1 + r \cdot t \cdot 0 = r^2 \end{aligned} \quad (81)$$

As long as there is no measurement, the photon is in a superposition state of both outputs; see Section 3.2.9. The probability of the photon being measured at one of the outputs is distributed the same as the intensity in the classical description. Measuring a single photon is a statistical process: only the probabilities are known, and the result cannot be predicted with certainty. However, the distribution of the photons will approach the classical result for large numbers of photons.

¹⁵ M. Beck, *Quantum Mechanics, Theory and Experiment*. (Oxford University Press, Oxford, 2012).

3.4.3 Quantum Fields

Classically, $g^{(2)}(0)$ in an intensity interferometer cannot be smaller than 1, as shown in Section 3.4.1. In this section, the limits and expected values of $g^{(2)}(0)$ are derived depending on the characteristics of the incoming light.

The quantum mechanical second-order correlation function is defined as¹⁶:

$$g^{(2)}(0) = \frac{\langle : \hat{I}_A \hat{I}_B : \rangle}{\langle \hat{I}_A \rangle \cdot \langle \hat{I}_B \rangle} \quad (82)$$

Here, \hat{I}_A and \hat{I}_B are the intensity operators at detector A and B and the colons denote so-called normal ordering, meaning all creation operators appear to the left of all annihilation operators. This function has the same properties as its classical counterpart¹⁷.

The intensity operator is proportional to the photon number operator¹⁸, so that we can write:

$$g^{(2)}(0) = \frac{\langle : \hat{n}_A \hat{n}_B : \rangle}{\langle \hat{n}_A \rangle \cdot \langle \hat{n}_B \rangle} \quad (83)$$

Expressing the number operators via creation and annihilation operators and taking care of the normal ordering, this can be written as:

$$g^{(2)}(0) = \frac{\langle : \hat{a}_A^\dagger \hat{a}_A \hat{a}_B^\dagger \hat{a}_B : \rangle}{\langle \hat{a}_A^\dagger \hat{a}_A \rangle \cdot \langle \hat{a}_B^\dagger \hat{a}_B \rangle} = \frac{\langle \hat{a}_B^\dagger \hat{a}_A^\dagger \hat{a}_A \hat{a}_B \rangle}{\langle \hat{a}_A^\dagger \hat{a}_A \rangle \cdot \langle \hat{a}_B^\dagger \hat{a}_B \rangle} \quad (84)$$

Now assume an intensity interferometer as described in Section 3.4.1. The field at port 1 is an arbitrary state $|\psi\rangle$ and the field at port 2 is in the vacuum state $|0\rangle$. The annihilation and creation operators after the beamsplitter can then be expressed via the corresponding operators of the incoming field via Equations (76) - (79) (with $\hat{a}_A = \hat{a}_3$ and $\hat{a}_B = \hat{a}_4$) so that the numerator becomes:

$$\begin{aligned} \langle \hat{a}_B^\dagger \hat{a}_A^\dagger \hat{a}_A \hat{a}_B \rangle &= \langle (t\hat{a}_1^\dagger - r\hat{a}_2^\dagger)(r\hat{a}_1^\dagger + t\hat{a}_2^\dagger)(r\hat{a}_1 + t\hat{a}_2)(t\hat{a}_1 - r\hat{a}_2) \rangle \\ &= {}_1\langle \psi | {}_2\langle 0 | (t\hat{a}_1^\dagger - r\hat{a}_2^\dagger)(r\hat{a}_1^\dagger + t\hat{a}_2^\dagger)(r\hat{a}_1 + t\hat{a}_2)(t\hat{a}_1 - r\hat{a}_2) | \psi \rangle_1 | 0 \rangle_2 \\ &= {}_1\langle \psi | (t\hat{a}_1^\dagger)(r\hat{a}_1^\dagger)(r\hat{a}_1)(t\hat{a}_1) | \psi \rangle_1 = r^2 t^2 \cdot {}_1\langle \psi | \hat{a}_1^\dagger \hat{a}_1^\dagger \hat{a}_1 \hat{a}_1 | \psi \rangle_1 \end{aligned} \quad (85)$$

The expectation values in the denominator can be similarly written as:

$$\langle \hat{a}_A^\dagger \hat{a}_A \rangle = r^2 \cdot {}_1\langle \psi | \hat{a}_1^\dagger \hat{a}_1 | \psi \rangle_1 \quad (86)$$

$$\langle \hat{a}_B^\dagger \hat{a}_B \rangle = t^2 \cdot {}_1\langle \psi | \hat{a}_1^\dagger \hat{a}_1 | \psi \rangle_1 \quad (87)$$

Combining these results leads to the following expression of the second order correlation function of the intensity interferometer:

$$g_{HBT}^{(2)}(0) = \frac{\langle \hat{a}_B^\dagger \hat{a}_A^\dagger \hat{a}_A \hat{a}_B \rangle}{\langle \hat{a}_A^\dagger \hat{a}_A \rangle \cdot \langle \hat{a}_B^\dagger \hat{a}_B \rangle} = \frac{\langle \hat{a}_1^\dagger \hat{a}_1^\dagger \hat{a}_1 \hat{a}_1 \rangle}{\langle \hat{a}_1^\dagger \hat{a}_1 \rangle^2} \quad (88)$$

With the help of this equation, the expected values of $g_{HBT}^{(2)}(0)$ can be determined for different states of the incoming light.

Single Photons

The first example is $|1\rangle$, the Fock state with the photon number 1, called a single photon.

$$g_{HBT}^{(2)}(0) = \frac{\langle 1 | \hat{a}_1^\dagger \hat{a}_1^\dagger \hat{a}_1 \hat{a}_1 | 1 \rangle}{\langle 1 | \hat{a}_1^\dagger \hat{a}_1 | 1 \rangle^2} = \langle 1 | \hat{a}_1^\dagger \hat{a}_1^\dagger \hat{a}_1 \hat{a}_1 | 1 \rangle = \langle 1 | \hat{a}_1^\dagger \hat{a}_1^\dagger \hat{a}_1 | 0 \rangle = 0 \quad (89)$$

The expected value for the second order correlation function with a single photon incident on the beamsplitter is zero. This describes complete anti-correlation, i.e., if the photon is detected at one output of the beamsplitter it

¹⁶ J. J. Thorn et al., *American Journal of Physics*, **72**(9), 1210 (2004)

¹⁷ R. Loudon, *The Quantum Theory of Light*. (Oxford University Press, Oxford, 1965).

¹⁸ M. Beck, *Quantum Mechanics, Theory and Experiment*. (Oxford University Press, Oxford, 2012).

can never be detected at the other output. This agrees with intuition: as the photon is the smallest possible excitation of the electromagnetic field, it cannot be split further. This can be experimentally confirmed in this kit; see Section 9.4.

Laser Light

What about a strongly attenuated laser? This would be represented quantum-mechanically by a coherent state $|\alpha\rangle$, as seen in Section 3.3.2.

$$g_{HBT}^{(2)}(0) = \frac{\langle \alpha | \hat{a}_1^\dagger \hat{a}_1^\dagger \hat{a}_1 \hat{a}_1 | \alpha \rangle}{\langle \alpha | \hat{a}_1^\dagger \hat{a}_1 | \alpha \rangle^2} = \frac{|\alpha|^4}{(|\alpha|^2)^2} = 1 \quad (90)$$

The second order correlation function for coherent states is 1 irrespective of the mean photon number $\langle n \rangle = |\alpha|^2$ of the state, i.e., the detector signal in the intensity interferometer will be completely uncorrelated. This means that even a very strongly attenuated laser is not a suitable source to perform quantum optic experiments. The experimental confirmation is part of this kit, as seen in Section 9.1.

Thermal Light

To obtain the expected value for the second order correlation of thermal light, it helps to express $g_{AB}^{(2)}(0)$ in terms of the expectation value and the variance of the photon number:

$$\begin{aligned} g_{HBT}^{(2)}(0) &= \frac{\langle \hat{a}_1^\dagger \hat{a}_1^\dagger \hat{a}_1 \hat{a}_1 \rangle}{\langle \hat{a}_1^\dagger \hat{a}_1 \rangle^2} = \frac{\langle \hat{a}_1^\dagger (\hat{a}_1 \hat{a}_1^\dagger - 1) \hat{a}_1 \rangle}{\langle \hat{a}_1^\dagger \hat{a}_1 \rangle^2} = \frac{\langle \hat{a}_1^\dagger \hat{a}_1 \hat{a}_1^\dagger \hat{a}_1 - \hat{a}_1^\dagger \hat{a}_1 \rangle}{\langle \hat{a}_1^\dagger \hat{a}_1 \rangle^2} = \frac{\langle \hat{n}^2 - \hat{n} \rangle}{\langle \hat{n} \rangle^2} = \frac{\langle \hat{n}^2 \rangle - \langle \hat{n} \rangle}{\langle \hat{n} \rangle^2} \\ &= \frac{(\Delta n)^2 + \langle \hat{n} \rangle^2 - \langle \hat{n} \rangle}{\langle \hat{n} \rangle^2} = \frac{\langle \hat{n} \rangle^2 + \langle \hat{n} \rangle + \langle \hat{n} \rangle^2 - \langle \hat{n} \rangle}{\langle \hat{n} \rangle^2} = 2 \end{aligned} \quad (91)$$

For the first equality, the commutator relation between \hat{a}_1^\dagger and \hat{a}_1 is used. For the penultimate equality we used a variance $(\Delta n)^2 = \langle \hat{n}^2 \rangle + \langle \hat{n} \rangle$, as derived in Section 3.3.3.

As a result, the second order correlation for thermal light is 2, i.e., the detector signals in the intensity interferometer are correlated. Descriptively formulated, the source emits no photons most of the time, but when it does, it tends to emit multiple at the same time, which are split evenly at the beamsplitter. The correlated/dense bursts of photons increase $g_{HBT}^{(2)}(0)$ above 1.

3.5 Proof of Quantized Light - Experiment

3.5.1 Hanbury-Brown-Twiss Experiment

The concept of the intensity interferometer (see Section 3.4.1) was first introduced by Hanbury Brown and Twiss (HBT) in 1956¹⁹ when they were looking for a method to measure the angular size of stars. This was a purely classical experiment.

However, when simulating their experiment in the laboratory and using a strongly attenuated spectral line from a mercury vapor lamp as the light source, they found that the signals at the two detectors were positively correlated, i.e., $g_{HBT}^{(2)}(0) > 1$.

Following the publication of these results, there was a dispute about the interpretation, which was resolved by Hanbury Brown and Twiss showing that the result $g_{HBT}^{(2)}(0) > 1$ is consistent with semi-classical theories, as seen in Section 3.4.1. The reason that no anti-correlation is detected, even though the light consists of photons, lies in the state of the incoming light. The mercury vapor lamp is a thermal source, so the light will be in a thermal mixture of states, as defined in Section 3.3.3. The second order correlation function for this case is calculated in Equation (91):

$$g_{HBT}^{(2)}(0) = 2 \quad (\text{Thermal Light}) \quad (92)$$

¹⁹ R. H. Brown and R. Q. Twiss, *Nature*, **177**, 27 (1956).

Please note that this value can only be measured in the limit of idealized detectors with perfect time resolution. The time resolution of real detectors will reduce the measured value of $g_{HBT}^{(2)}(0)$ towards the limit of 1, as seen in Section 3.5.2.

3.5.2 Correlation Function for Single Photon Detectors

To detect the extremely low intensities that are common in quantum optics, single photon detectors are used. These detectors do not output a continuous signal, but single output pulses (called counts or clicks). It is important to be clear that the clicks of such a detector do not in themselves prove the quantization of the light field. In semi-classical theories, only the quantization of the energy levels in the detector is required to explain the detector behavior. The pulse generation is a random process, and the pulse rate is proportional to the intensity of the light hitting the detector²⁰.

$$P_i = \eta_i \cdot \langle I_i(t) \rangle \cdot Dt \quad (93)$$

Here, P_i is the probability of a detection event at detector i in the short time window Dt , η_i is the detection efficiency of detector i , and $I_i(t)$ is the intensity of the light hitting detector i .

To calculate the correlation function for single photon detectors, Equation (72) can be modified to incorporate count rates instead of intensities.

The probability of a detection event at detector i in a short time window Dt followed by a detection event at detector j (also in a short time window Dt) after a time τ is:

$$P_{ij}(\tau) = \eta_i \cdot \eta_j \cdot \langle I_i(t + \tau) \cdot I_j(t) \rangle \cdot Dt^2 \quad (94)$$

Substituting Equations (93) and (94) (for $i = A$ and $j = B$) into Equation (72) yields:

$$g^{(2)}(\tau) = \frac{P_{AB}(\tau)}{P_A \cdot P_B} \quad (95)$$

The probabilities are just the average count rates R_A and R_B of the detectors A and B, respectively, and the average count rate of coincidences R_{AB} multiplied by the time window Δt .

$$P_A = R_A \cdot \Delta t \quad P_B = R_B \cdot \Delta t \quad P_{AB}(\tau) = R_{AB}(\tau) \cdot \Delta t \quad (96)$$

Substituting this in Equation (95) yields:

$$g^{(2)}(\tau) = \frac{R_{AB}(\tau)}{R_A \cdot R_B \cdot \Delta t} \quad (97)$$

For $\tau = 0$, this is written as:

$$g^{(2)}(0) = \frac{R_{AB}(0)}{R_A \cdot R_B \cdot \Delta t} = \frac{R_{AB}}{R_A \cdot R_B \cdot \Delta t} \quad (98)$$

This two-detector correlation function is used in two distinct ways in this kit:

- 1.) As a characterization of the pair source: Here, the photon pairs generated in a BBO crystal (see Section 3.9) are directly sent to the two detectors. In this case, one measures significantly more coincidences than expected for uncorrelated light, thus $g_{PS}^{(2)}(0) \gg 1$. The subscript PS stands for "Pair Source." The quantity $g_{PS}^{(2)}(0)$ is used as an indicator for the quality of the pair source (the larger, the better) and is measured at about 100 in the setup in this kit.
- 2.) As a measurement for the correlation of light in an HBT experiment: This is the quantity $g_{HBT}^{(2)}(0)$ as described in Section 3.5.1. Here, a value lower than 1 would indicate non-classical light.

Strictly speaking, what is called $g_{HBT}^{(2)}(0)$ here is not the value at the point $t = 0$ anymore, but an integration of $g_{HBT}^{(2)}(\tau)$ over the time window Δt centered at $t = 0$ ²¹. As long as $g_{HBT}^{(2)}(\tau)$ is not rapidly changing over Δt , there

²⁰ M. Beck, *Quantum Mechanics, Theory and Experiment*. (Oxford University Press, Oxford, 2012).

²¹ R. W. Boyd, S. G. Lukishova, and V. N. Zadkov, *Quantum Photonics: Pioneering Advances and Emerging Applications*. (Springer, New York City, 2019), p. 3.

is no difference between the two. Most importantly, the inequalities that include the $g_{HBT}^{(2)}(0)$ term always remain valid.

For thermal sources (see Section 3.3.3), the time-dependent correlation function drops from 2 at $t = 0$ to 1 for $\tau \gg \tau_c$, with τ_c being the coherence time of the light²², as seen in Figure 9. The coherence time of a light source is a measure of the duration over which the phase of the light emitted by the source remains stable.

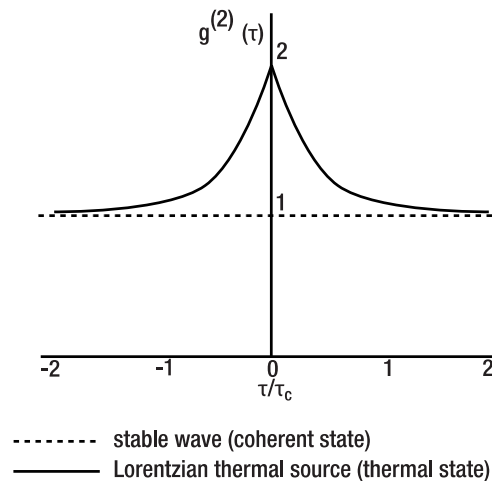


Figure 9 Time Dependent Second-Order Correlation Function

Even for spectrally filtered thermal sources, τ_c is on the order of femtoseconds²³, while typical values of Δt are in the order of 1 ns. Thus, $g_{HBT}^{(2)}(\tau)$ is 1 for the vast majority of the window, resulting in measured values of $g_{HBT}^{(2)}(0) \approx 1$ for the time-integrated correlation.

This is confirmed experimentally in this kit; see Section 9.3 for more details. Only with extremely fast detectors and electronics could one measure $g_{HBT}^{(2)}(0) = 2$ for thermal sources.

In the literature, there are several approaches to constructing a pseudo-thermal light source that shows the same statistics as thermal light but with fluctuations on a much longer time scale. Prominent examples are moving laser speckles induced by a rotating diffuser²⁴ or an LED programmed to output randomized intensity²⁵. With such sources, $g_{HBT}^{(2)}(0) \approx 2$ can be measured with the setup in this kit.

3.5.3 Grangier-Roger-Aspect Experiment

In the 1970s, several experiments^{26,27,28} were performed with various kinds of single photon sources that experimentally proved effects that could only be explained by a quantization of the light field.

An experimental concept, which forms the basis of the experiments in this kit, was introduced by Grangier, Roger, and Aspect (GRA) in 1986²⁹. They used an atomic cascade that produced pairs of photons, with the two photons leaving the source in different directions (see Figure 10). One of these photons was used as a trigger (when detected at detector T) to “announce” the presence of the other one, with which a correlation experiment analog to the Hanbury-Brown-Twiss intensity interferometer (detectors A and B) was performed.

²² R. Loudon, *The Quantum Theory of Light*. (Oxford University Press, Oxford, 1965).

²³ M. Beck, *Quantum Mechanics, Theory and Experiment*. (Oxford University Press, Oxford, 2012), p. 461.

²⁴ F. T. Arecchi, *Physical Review Letters*, **15**(24), 912 (1965).

²⁵ R. Scholz et al., *European Journal of Physics*, **37**(5), 055302 (2016).

²⁶ D. C. Burnham and D. L. Weinberg, *Physical Review Letters*, **25**(2), 84 (1970).

²⁷ J. F. Clauser, *Physical Review D*, **9**(4), 853 (1974).

²⁸ H. J. Kimble et al., *Physical Review Letters*, **39**(11), 912 (1974).

²⁹ P. Grangier et al., *Europhysics Letters*, **1**(4), 173 (1986).

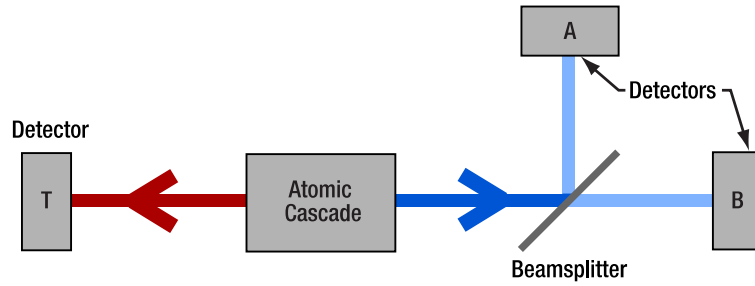


Figure 10 Schematic of the Grangier-Roger-Aspect Experiment

Using this approach, they obtained $g_{GRA}^{(2)}(0) = 0.18$, a result that can only be explained by the quantization of the electromagnetic field (the subscript GRA indicates the change in setup compared to a HBT intensity interferometer). Later, advantages in photon pair sources and detectors allowed experiments that show even more significant violations of $g_{GRA}^{(2)}(0) \geq 1$. The mathematical treatment of the GRA setup is explained in the following section.

A big advantage of the GRA setup is that if one does experiments with the photons in one arm after the beamsplitter, such as the Michelson interferometry described in Section 3.6, a test of the non-classical nature of the light can be run in parallel, validating the single photon nature of the main experiment.

3.5.4 Triple Coincidence Detection Scheme

In the GRA experiment, one photon of the pair reaches detector T directly, while the other one passes a beamsplitter with detectors A and B at the output ports. As the source produces pairs of photons, one could assume that the light in each arm consists of single photons. However, this is **not** the case. An HBT experiment while disregarding detector T would lead to the result $g_{HBT}^{(2)}(0) = 1$ (to within the error of the measurement), showing that the photon statistics in a single arm are of classical character.

To show the quantization of the light field, the information about the photon distribution at detector T must be used. The two photons of a pair are emitted at the same time. Measuring a photon at detector T yields the information that at this exact point of time, there must be another photon in the A-B arm. At this point of time, the quantum state in the A-B arm is then not thermal anymore but becomes the single photon Fock state. The thermal state is said to collapse into the Fock state. Counting only such heralded events at detectors A and B will yield the non-classical result $g_{HBT}^{(2)}(0) < 1$. This is why a photon pair source is also called a heralded single photon source. This process is called a triple coincidence detection scheme and is described in more detail in the remainder of this subsection.

Each count on A or B is only counted when in coincidence with a count on T. The coincidence window is Δt . If an event is registered at detector A in coincidence with T, this contributes to the count rate R_{TA} . The count rate R_{TB} is obtained in the same fashion. Detection events at A and B that are not in coincidence with events at T are discarded. A coincidence count between A and B is only registered when both detector A and B register an event in coincidence with the **same** event at detector T, resulting in the triple coincidence count rate R_{TAB} . The definition for the second order correlation function remains (see Section 3.5.2):

$$g_{GRA}^{(2)}(0) = \frac{P_{TAB}}{P_{TA} \cdot P_{TB}} \quad (99)$$

Here, the subscript GRA indicates that the correlation function is measured with the detection scheme of the original GRA experiment.

The probabilities in the triple coincidence case can be normalized to the count rate of the trigger detector T, as this is the maximum rate of counts at the other detectors³⁰. Thus:

³⁰ Technically, this is only true if the count rates are low enough that it is very improbable that multiple events are registered at a detector during a gate window. However, as the detectors normally exhibit dead times much larger than the window; see Section 4.1, this is automatically the case.

$$P_A = \frac{R_{TA}}{R_T}, \quad P_B = \frac{R_{TB}}{R_T}, \quad P_{AB} = \frac{R_{TAB}}{R_T} \quad (100)$$

Substituting this into Equation (99), the result is:

$$g_{GRA}^{(2)}(0) = \frac{R_{TAB} \cdot R_T}{R_{TA} \cdot R_{TB}} \quad (101)$$

3.5.5 Triple Coincidence Detection Scheme: Explanation 1

Why does this process enable measuring $g_{GRA}^{(2)}(0) < 1$ when the simpler HBT experiment with one arm of the pair source does not? There are multiple ways to answer this question. Here, we will give a quantum mechanical answer, while the next section offers a more intuitive explanation.

There are different techniques that produce photon pairs that are entangled in time. One example is the Spontaneous Parametric Down-Conversion (SPDC) process used in this kit (see Section 3.9). If one photon of the time-entangled photon pair is measured at a time t at one detector, the second photon is guaranteed to be detected at nearly exactly the same time at the second detector (if it is placed the same distance from the pair source). The uncertainty of the arrival time of the second photon is much smaller than the typical time resolution of the experiment. Therefore, one can approximate the system in the second arm to be in a Fock state $|1\rangle$ whenever a photon is measured in the first arm and $|0\rangle$ at all other times. The triple coincidence detection scheme ensures that we are only looking at the system in the state $|1\rangle$ (when the counts are in coincidence with the trigger detector T), instead of the thermal state as in the simpler two-detector HBT setup.

3.5.6 Triple Coincidence Detection Scheme: Explanation 2

A second, maybe more intuitive, explanation goes as follows:

First, assume a completely randomly distributed stream of photons with 10000 photons per second arriving at two detectors with 100% efficiency.

When performing the HBT experiment (with a 50:50 beamsplitter), the single detector count rates will be $R_A = R_B = 5000$ Hz (half of the photons going to each detector). We set the coincidence window to $\Delta t = 1 \mu\text{s}$ ³¹, i.e., a coincidence is defined as detector B registering a count within a $1 \mu\text{s}$ window around detector A.

We do the experiment and measure a coincidence count rate $R_{AB} = 25$ Hz. We then calculate $g_{HBT}^{(2)}(0)$ from Equation (98) to be:

$$g_{HBT}^{(2)}(0) = \frac{R_{AB}}{R_A \cdot R_B \cdot \Delta t} = \frac{25 \text{ Hz}}{5 \text{ kHz} \cdot 5 \text{ kHz} \cdot 1 \mu\text{s}} = 1 \quad (102)$$

So far, everything is as expected. But now we have a second photon stream that is identical to the first one (as the photons are generated in pairs). We can use that to limit the time we are watching our experiment. We place detector T at the same distance from the pair source and send the second photon stream to detector T. We only watch our experiment for a $1 \mu\text{s}$ window around counts at detector T. This means that if the experiment is running for a time T , we watch it only for a time T_c :

$$T_c = R_T \cdot \Delta t \cdot T = 10000 \text{ Hz} \cdot 1 \mu\text{s} \cdot T = 0.01 \cdot T \quad (103)$$

so only 1/100th of the time. However, we get the same number of counts, because all the events at detectors A and B happen within the $1 \mu\text{s}$ window around events at T.

If we write Equation (101) with counts instead of rates, we immediately see the influence of the shortened measurement time at constant counts:

$$g_{GRA}^{(2)}(0) = \frac{R_{TAB} \cdot R_T}{R_{TA} \cdot R_{TB}} = \frac{N_{TAB} \cdot T \cdot 0.01}{N_{TA} \cdot N_{TB} \cdot \Delta t} = 0.01 \cdot g_{HBT}^{(2)}(0) = 0.01 \quad (104)$$

³¹ The window length must be much lower than the average time between two counts, which is the case here. The exact length is chosen to facilitate the calculation, and any window length fulfilling the constraint above would work.

Here, we used the relation $R_T = \frac{0.01}{\Delta t}$ which can be derived from Equation (103) and the fact that the rates are the numbers divided by the measurement time, e.g. $R_{TA} = \frac{N_{TA}}{T}$. The gating process allowed us to measure $g_{GRA}^{(2)}(0) = 0.01$ because we were able to shorten the effective measurement time by the factor $R_T \cdot \Delta t$ without losing any counts due to the time correlation between the photons in the two arms.

3.5.7 Accidental Coincidences

As shown in Section 3.4.3, the expectation is $g_{HBT}^{(2)}(0) = 0$ for a single photon Fock state in an HBT experiment. When using the GRA setup and the triple coincidence detection scheme, one still expects $g_{GRA}^{(2)}(0) = 0$. However, in an experiment, several factors can lead to measurement results higher than that. In the case of the GRA experiment, the main factor is accidental triple coincidences.

There are two types of accidental triple coincidences:

- **Purely accidental triple coincidence:** A photon from photon pair 1 hits detector T, and during the coincidence window detectors A and B register counts due to uncorrelated events (such as other pairs generated during the gate window, background light, or detector dark counts). The rate $R_{acc}^{(3)}$ of such purely accidental triple coincidences³² is:

$$R_{acc}^{(3)} = R_T \cdot R_A \cdot R_B \cdot \Delta t^2 \quad (105)$$

Here, Δt is the width of the coincidence window.

- **Normal double coincidence with accidental third count:** In this case, two photons of a pair generate a coincidence event at either T&B or T&A and an uncorrelated event leads to a count at the third detector during the coincidence window. The rate $R_{acc}^{(2+1)}$ for this type of accidental triple coincidence is:

$$R_{acc}^{(2+1)} = (R_{TA} \cdot R_B + R_{TB} \cdot R_A) \cdot \Delta t \quad (106)$$

An example calculation with values typical for this kit with $R_T = 200$ kHz, $R_A = R_B = 100$ kHz, $R_A^{(g)} = R_B^{(g)} = 10$ kHz, and $\Delta t = 5$ ns yields:

$$R_{acc}^{(3)} = R_T \cdot R_A \cdot R_B \cdot \Delta t^2 = 2 \cdot 10^{15} \text{ Hz} \cdot 25 \cdot 10^{-18} \text{ s} = 0.05 \text{ Hz} \quad (107)$$

$$R_{acc}^{(2+1)} = (R_{TA} \cdot R_B + R_{TB} \cdot R_A) \cdot \Delta t = 2 \cdot 10^9 \text{ Hz} \cdot 5 \cdot 10^{-9} \text{ s} = 10 \text{ Hz} \quad (108)$$

It is apparent that the second type of accidental triple coincidences dominates. Inserted into Equation (101), these accidental coincidences result in an expectation for $g_{GRA}^{(2)}(0)$ with the example values above of

$$g_{GRA}^{(2)}(0) = \frac{R_{acc}^{(2+1)} \cdot R_T}{R_{TA} \cdot R_{TB}} = \frac{10 \text{ Hz} \cdot 200 \text{ kHz}}{10 \text{ kHz} \cdot 10 \text{ kHz}} = 0.02 \quad (109)$$

All single detector count rates are proportional to the pair generation rate R_{pp} (the absolute rate of generated photon pairs, whether detected or not) and independent of Δt . The twofold coincidence count rates are also proportional to R_{pp} (with a different proportionality factor) and independent of Δt . Substituting this in Equation (108) yields that $R_{acc}^{(2+1)}$ is proportional to $R_{pp} \cdot \Delta t$. Thus:

$$g_{GRA}^{(2)}(0) \propto \frac{R_{pp}^2 \cdot R_{pp} \cdot \Delta t}{R_{pp} \cdot R_{pp}} = R_{pp} \cdot \Delta t \quad (110)$$

This agrees with intuition. Both a larger rate of photons and wider coincidence windows increase the probability of two uncorrelated events being registered as if they were correlated, increasing $g_{GRA}^{(2)}(0)$. As a result, there are two ways to limit accidental triple coincidences and move $g_{GRA}^{(2)}(0)$ closer to 0:

³² B. J. Pearson and D. P. Jackson, *American Journal of Physics*, **78**(5), 471 (2010).

- Shorten the coincidence window. This is limited by the time resolution of the detectors and electronics. In the case of this kit, the jitter of the EDU Time Tagger is 720 ps (see Section 4.2.2), so coincidence windows shorter than 1 ns do not improve the result.
- Lower the rate of photon pairs. This is most easily achieved by lowering the power of the pump laser. The drawback is of course a reduction of the count rates, which means that longer measurements are required to avoid larger error bars. For details, see Section 12.4.

The standard values for the coincidence window and laser power given in this manual are optimized for satisfactory results and comfortable measurement times.

3.6 Single Photon Interference

3.6.1 Theoretical Description

Here, the experimental case explained in Section 3.1.2 and shown in Figure 2 is treated quantum mechanically. We label the ports “i” for input, “d” for detector and “α” and “β” for the two arms of the interferometer.

If the state $|1\rangle_i \otimes |0\rangle_d$ is incident on the beamsplitter, describing a single photon at the input port and vacuum at the detector port (see Section 3.2.12 for the explanation of combined states), the state after the beamsplitter is (according to Equation (80) in Section 3.4.2):

$$\frac{1}{\sqrt{2}}(|1\rangle_\alpha|0\rangle_\beta + |0\rangle_\alpha|1\rangle_\beta) \tag{111}$$

The difference in the lengths of the interferometer arms Δl induces a relative phase shift $\phi = \frac{2\pi\Delta l}{\lambda}$. This can be represented by a phase shift of the creation operator in one of the arms³³ (here β): $\hat{a}_\beta^\dagger \rightarrow e^{i\phi} \cdot \hat{a}_\beta^\dagger$, so that the state before recombination at the beamsplitter becomes:

$$\frac{1}{\sqrt{2}}(|1\rangle_\alpha|0\rangle_\beta + e^{i\phi}|0\rangle_\alpha|1\rangle_\beta) \tag{112}$$

The recombination at the beamsplitter is described by the same equations as the splitting process. However, instead of $|1\rangle$ and $|0\rangle$, the input is now the split state of Equation (112). To adjust for the fact that the input and output ports are switched when compared to the splitting process (see right side of Figure 11), ports “i” and “β” and ports “d” and “α” are switched in Equations (78) and (79). With $t = r = \frac{1}{\sqrt{2}}$ (to account for the 50:50 beamsplitter) these two equations then become:

$$\hat{a}_\beta^\dagger = \frac{1}{\sqrt{2}} \cdot (\hat{a}_i^\dagger + \hat{a}_d^\dagger) \tag{113}$$

$$\hat{a}_\alpha^\dagger = \frac{1}{\sqrt{2}} \cdot (\hat{a}_d^\dagger - \hat{a}_i^\dagger) \tag{114}$$

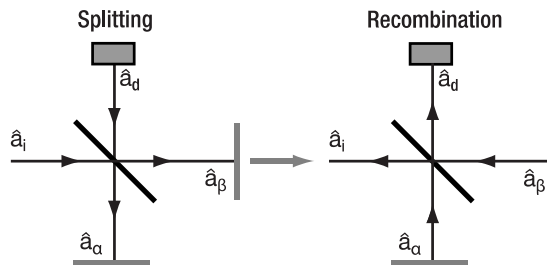


Figure 11 Geometry of Michelson Interferometer. Left: Splitting, Right: Recombination

³³ M. Beck, Quantum Mechanics, Theory and Experiment. (Oxford University Press, Oxford, 2012).

The state after recombination is then:

$$\begin{aligned}
 |\psi_{rec}\rangle &= \frac{1}{\sqrt{2}}(|1\rangle_\alpha|0\rangle_\beta + e^{i\phi}|0\rangle_\alpha|1\rangle_\beta) \\
 &= \frac{1}{\sqrt{2}}(\hat{a}_\alpha^\dagger|0\rangle + e^{i\phi}\hat{a}_\beta^\dagger|0\rangle) = \frac{1}{\sqrt{2}}\left(\frac{1}{\sqrt{2}}(\hat{a}_d^\dagger|0\rangle - \hat{a}_i^\dagger|0\rangle) + \frac{1}{\sqrt{2}}(\hat{a}_i^\dagger|0\rangle + \hat{a}_d^\dagger|0\rangle)\right) \\
 &= \frac{1}{\sqrt{2}}\left(\frac{1}{\sqrt{2}}(|0\rangle_i|1\rangle_d - |1\rangle_i|0\rangle_d) + \frac{1}{\sqrt{2}}e^{i\phi} \cdot (|1\rangle_i|0\rangle_d + |0\rangle_i|1\rangle_d)\right) \\
 &= \frac{1}{2}\left((-1 + e^{i\phi})|1\rangle_i|0\rangle_d + (1 + e^{i\phi})|0\rangle_i|1\rangle_d\right)
 \end{aligned}
 \tag{115}$$

The quantity of interest is the probability $P(1_d)$ of the photon leaving the interferometer through port 2:

$$P(1_d) = \langle \psi_{rec} | \hat{P}_{n_d=1} | \psi_{rec} \rangle = \langle \psi_{rec} | 1\rangle_d \langle 1|_d | \psi_{rec} \rangle
 \tag{116}$$

Here, $\hat{P}_{n_d=1} = |1\rangle_d \langle 1|_d$ is the projection operator on the state $|1\rangle_d = |0,1\rangle + |1,1\rangle$, i.e., the state describing a photon leaving through the detection port. Substituting this definition into Equation (116) yields:

$$P(1_d) = \frac{1}{2}(1 + e^{-i\phi})\langle 0,1|0,1\rangle \cdot \frac{1}{2}(1 + e^{i\phi})\langle 0,1|0,1\rangle = \frac{1}{4}(1 + 1 + e^{-i\phi} + e^{i\phi}) = \frac{1}{2} \cdot (1 + \cos(\phi))
 \tag{117}$$

The last transformation uses the relation $\cos(\phi) = \frac{e^{i\phi} + e^{-i\phi}}{2}$.

This result is analogous to the classic one; see Section 3.1.2. The probability of the photon leaving the interferometer through the detection port depends on the arm length difference and can reach from 0 to 1. The probability of the photon leaving through the input port can be analogously calculated as:

$$P(1_i) = \frac{1}{2} \cdot (1 - \cos \phi)
 \tag{118}$$

The sum $P(1_d) + P(1_i) = 1$ for all phase differences ϕ , hence the energy is conserved.

3.6.2 Experimental Realization

In the experiment in this kit, which follows the original setup by GRA, as well as others after³⁴, a Michelson interferometer is placed between the beamsplitter and detector B. The basic setup geometry is displayed in Figure 12.

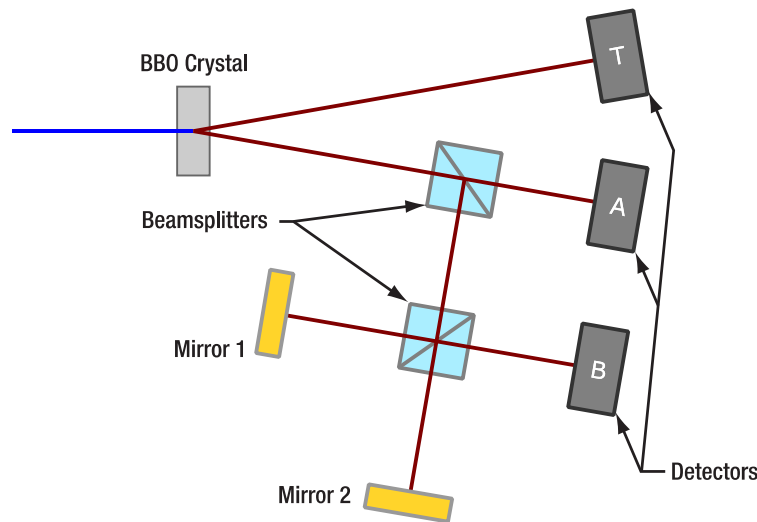


Figure 12 Setup Geometry of Michelson Interferometer Coupled with GRA Experiment

³⁴ E. J. Galvez et al., *American Journal of Physics*, **73**(2), 127 (2005).

Mirror 1 is positioned on a movable stage. In the experiment, the stage position and therefore the path length difference Δl is varied and the coincidence count rate R_{TB} is plotted. The expected count rate is then a function of the arm length difference:

$$R_{TB} = R_{TB}^{max} \cdot \frac{1}{2} \left(1 + \cos\left(\frac{2\pi\Delta l}{\lambda}\right) \right) \quad (119)$$

with $\lambda \approx 810$ nm being the wavelength of the single photons and R_{TB}^{max} an experimentally obtained maximum count rate. Parallel to this interferogram, the second-order correlation function $g_{GRA}^{(2)}(0)$ is recorded as described in Equation (101) to continuously verify the single photon character of the light in the experiment.

By moving the mirror over a length l and counting the number N of maxima during this movement, the wavelength of the photons can be determined via:

$$\lambda = 2 \cdot \frac{l}{N} \quad (120)$$

3.7 Quantum Treatment of Polarization

3.7.1 Theoretical Description

Single photons have a polarization. As polarization is associated with spin angular momentum³⁵, photons are usually described to have either left-circular or right-circular polarization (for the classical definition, see Section 3.1.3) or a superposition of the two. The state of a single photon (Fock state with $n = 1$) with left-circular polarization (spin 1) is denoted as $|L\rangle$ and with right-handed polarization (spin -1) as $|R\rangle$. The spin state 0 is not possible as photons are massless and always move at the speed of light.

Those two states are orthogonal, i.e., $\langle L|R\rangle = 0$. They also form a basis in the Hilbert space of polarization states, meaning that every polarization state can be described by a linear combination of $|L\rangle$ and $|R\rangle$. As an example, the photon state $|H\rangle$ corresponding to linear polarization along the x-axis in the coordinate system introduced in Section 3.1.3 is described as follows:

$$|H\rangle = \frac{1}{\sqrt{2}} \cdot (|L\rangle - |R\rangle) \quad (121)$$

This polarization is called horizontal. The vertical polarization state $|V\rangle$ (linear polarization along the y-axis) is:

$$|V\rangle = \frac{1}{i\sqrt{2}} \cdot (|L\rangle - |R\rangle) \quad (122)$$

$|H\rangle$ and $|V\rangle$ also form an orthonormal basis of the Hilbert space and as such can be used to describe every polarization state. For example, the circular polarization states written as linear combinations of $|H\rangle$ and $|V\rangle$ are:

$$|L\rangle = \frac{1}{\sqrt{2}} \cdot (|H\rangle + i|V\rangle) \quad (123)$$

$$|R\rangle = \frac{1}{\sqrt{2}} \cdot (|H\rangle - i|V\rangle) \quad (124)$$

A linear polarization state along a line with an angle θ to the x-axis is denoted $|\theta\rangle$ and calculated as:

$$|\theta\rangle = \cos(\theta) \cdot |H\rangle + \sin \theta \cdot |V\rangle \quad (125)$$

If a photon passes a linear polarizer with a polarizer axis that forms an angle θ with the x-axis, it is either completely transmitted or completely absorbed. If it is transmitted, it is then linearly polarized in the direction of the polarizer axis, i.e., its state is transformed to $|\theta\rangle$. This constitutes a measurement of the polarization; see Section 3.2.9. The measured observable is the polarization along the θ -axis, the corresponding Hermitian operator is called $\hat{\rho}_\theta$, and its eigenvectors are $|\theta\rangle$ and $|\theta + \frac{\pi}{2}\rangle$ with the eigenvalues 1 and -1 , respectively. A photon in an arbitrary polarization state $|\psi\rangle$ being transmitted by the polarizer is equal to measuring the photon to be in state $|\theta\rangle$. As such, the probability of transmission is given as (see Section 3.2.10):

³⁵ L. He et al., *Science Advances*, **2**(9), (2016).

$$P(\theta \parallel \psi) = |\langle \theta | \psi \rangle|^2 \quad (126)$$

It is instructive to look at the special case of in the incoming photon being linearly polarized with an angle ϕ , i.e., in the state $|\phi\rangle$. Combining Equations (125) and (126) yields:

$$\begin{aligned} P(\theta \parallel \phi) &= |\langle \theta | \phi \rangle|^2 = |(\cos(\theta) \cdot \langle H | + \sin \theta \cdot \langle V |)(\cos(\phi) \cdot |H\rangle + \sin \phi \cdot |V\rangle)|^2 \\ &= |\cos \theta \cos \phi + \sin \theta \sin \phi|^2 = |\cos(\theta - \phi)|^2 = \cos^2(\theta - \phi) \end{aligned} \quad (127)$$

For large numbers of photons, this result is the same as the classical Malus' Law (see Section 3.1.3), as the expectation value of the transmitted photon number is proportional to the classical intensity. The experimental validation of this result is part of the kit; see Section 9.6.

In the classical description, polarizers act on the intensities of the beam. The quantum mechanical formalism, however, describes the probability of each single photon to propagate through optical elements and/or be measured in a certain state (here the polarization angle). The fact that the polarizer not only determines the transmission probability of the photon but also alters its state can be shown with a three-polarizer experiment³⁶, as explained in Section 10.2.

If only very few events are measured, we cannot tell the underlying probability distribution from the measurement. For a large number of measurements of photons prepared in the same state, the probabilistic result converges towards the classical expectation.

3.7.2 Experimental Realization

In the experiment in this kit, a linear polarizer is placed in front of detector B in a GRA setup geometry as displayed in Figure 13.

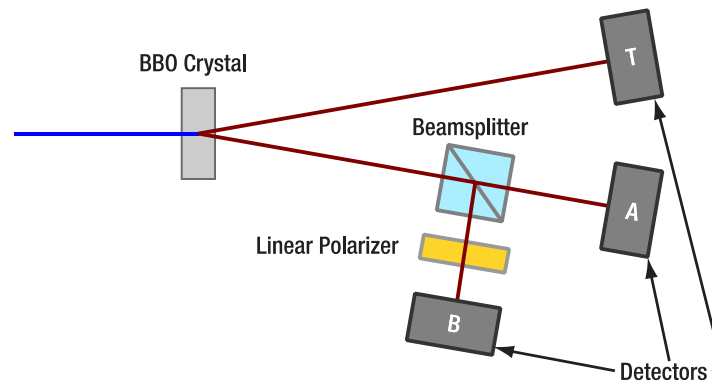


Figure 13 Schematic of a Setup for Measuring Malus' Law for Single Photons

This polarizer is then rotated and the coincidence count rate R_{TB} is recorded with respect to the polarizer angle θ . According to the theory above, the expected result is:

$$R_{TB} = R_{TB}^{max} \cdot \cos^2(\theta - \phi) \quad (128)$$

with ϕ being the polarization angle of the single photons and R_{TB}^{max} being the maximum coincidence count rate (reached when the polarization axes of the polarizer and the photons are identical). This measurement can then additionally be used to determine ϕ . At the same time, $g_{GRA}^{(2)}(0)$ is calculated according to Equation (101) to verify the single photon character of the light in the experiment for every data point.

Due to the process of generating the photon pairs (described in detail in Section 3.9), the polarization in both arms of the pair photon source is expected to be parallel. This can be verified by positioning the polarizer in front of detector T instead of B and repeating the experiment.

³⁶ J. M. Brom and F. Rioux, *The Chemical Educator*, 7, 200 (2002).

3.8 The Quantum Eraser

3.8.1 Theoretical Description

In Section 3.6, we discussed the Michelson interferometer. What happens when we insert polarizers into the interferometer? This will link polarization with the information about the interferometer arms. To demonstrate that, we will use combined states of the form $|n_\alpha, n_\beta, p\rangle$ and $|n_i, n_d, p\rangle$ with n_x being the photon number at the x -port of the beamsplitter and p being the polarization as described in Section 3.7.

We start with the state $|1_i, 0_d, 45^\circ\rangle$ at the beamsplitter. The beamsplitter itself does not affect the polarization, so we can use Equation (80) to calculate the state after the beamsplitter as:

$$\frac{1}{\sqrt{2}}(|1_\alpha, 0_\beta, 45^\circ\rangle + |0_\alpha, 1_\beta, 45^\circ\rangle) \quad (129)$$

Now we insert a linear polarizer with a polarization axis along 0° in the α -arm and a second linear polarizer with a polarization axis along 90° in the β -arm. The polarizers act only on the third part of the combined states in the same way as described in Section 3.7. Thus, the states in the arms are transformed by the polarizers in the following way:

$$|1_\alpha, 0_\beta, 45^\circ\rangle \rightarrow \frac{1}{\sqrt{2}}|1_\alpha, 0_\beta, H\rangle \quad (130)$$

$$|0_\alpha, 1_\beta, 45^\circ\rangle \rightarrow \frac{1}{\sqrt{2}}|0_\alpha, 1_\beta, V\rangle \quad (131)$$

Additionally, the path length difference induces a phase difference, just as explained in Section 3.6:

$$\frac{1}{\sqrt{2}}|0_\alpha, 1_\beta, V\rangle \rightarrow \frac{e^{i\phi}}{\sqrt{2}}|0_\alpha, 1_\beta, V\rangle \quad (132)$$

Recombination at the beamsplitter is handled analog to Section 3.6. The creation operators pick up subscripts denoting the polarization of the created photon but Equations (113) and (114) remain unchanged in their structure:

$$\begin{aligned} |\psi_{rec}\rangle &= \frac{1}{2}(|1_\alpha, 0_\beta, H\rangle + e^{i\phi}|0_\alpha, 1_\beta, V\rangle) = \frac{1}{2}(\hat{a}_{\alpha,H}^\dagger|0\rangle + e^{i\phi}\hat{a}_{\beta,V}^\dagger|0\rangle) \\ &= \frac{1}{2}\left(\frac{1}{\sqrt{2}}(|0_i, 1_d, H\rangle - |1_i, 0_d, H\rangle) + \frac{e^{i\phi}}{\sqrt{2}}(|1_i, 0_d, V\rangle + |0_i, 1_d, V\rangle)\right) \\ &= \frac{1}{2\sqrt{2}}(|0_i, 1_d, H\rangle - |1_i, 0_d, H\rangle + e^{i\phi}|1_i, 0_d, V\rangle + e^{i\phi}|0_i, 1_d, V\rangle) \end{aligned} \quad (133)$$

We want to know the probability of the photon leaving the interferometer through the detection port. Analog to Section 3.6, this is the probability $P(1_d)$ which is the expectation value of the projection operator $\hat{P}_{n_d=1} = |1\rangle_d\langle 1|$. The calculation is the same as in Section 3.6, only this time with a different $|1\rangle_d$ (accounting for the polarization base):

$$|1\rangle_d = |0,1,H\rangle + |0,1,V\rangle + |1,1,H\rangle + |1,1,V\rangle \quad (134)$$

$$P(1_d) = \langle\psi_{rec}|1\rangle_d\langle 1|\psi_{rec}\rangle = \frac{1}{(2\sqrt{2})^2}(\langle 0,1,H|0,1,H\rangle)^2 + \frac{e^{-i\phi} \cdot e^{i\phi}}{(2\sqrt{2})^2}(\langle 0,1,V|0,1,V\rangle)^2 = \frac{1}{8} + \frac{1}{8} = \frac{1}{4} \quad (135)$$

The probability is now independent of the phase difference ϕ , meaning that there is no interference pattern when changing the length difference of the interferometer arms³⁷. This can be interpreted as follows:

The polarizers in the interferometer arms provide “which-way” (WW) information. By measuring the polarization of a photon after the interferometer output, one can tell which path it took. Horizontally polarized photons went through the α -arm and vertically polarized photons went through the β -arm. Interference of a photon with itself

³⁷ Note, the probability is only $\frac{1}{4}$ instead of $\frac{1}{2}$ as one may expect. The reason is that half of the photons get absorbed by the polarizers in the interferometer arms.

is only possible if the paths are indistinguishable, so there can be no interference pattern when WW information is available. The polarization measurement does not need to be performed; its mere possibility is sufficient.

However, it is possible to remove the WW information. In our case, this can be done by placing a third linear polarizer in front of the detector in the interferometer output and setting its polarization axis to 45° . In this case we measure the probability $P(0,1,45^\circ)$ that the photon is in state $|0_i, 1_d, 45^\circ\rangle = \frac{1}{\sqrt{2}}(|0_i, 1_d, H\rangle + |0_i, 1_d, V\rangle)$:

$$\begin{aligned} P(0,1,45^\circ) &= |\langle 0_i, 1_d, 45^\circ | \psi_{rec} \rangle|^2 = \frac{1}{2} |\langle 0_i, 1_d, H | \psi_{rec} \rangle + \langle 0_i, 1_d, V | \psi_{rec} \rangle|^2 = \frac{1}{16} |1 + e^{i\phi}|^2 \\ &= \frac{1}{8} (1 + \cos \phi) \end{aligned} \quad (136)$$

This is the same result as for the interferometer without any polarizers! The probability of a detected photon is again dependent on the arm length difference of the paths, meaning that the interference pattern is recovered. The only difference is a factor of $\frac{1}{4}$, which represents that twice in the experiment, half of the photons are absorbed (first at the polarizers in the interferometer and again at the polarizer in front of the detector). This is interpreted as follows:

By inserting the third polarizer, the WW information is erased (the probability of a photon to be measured as 45° -polarized is the same for photons going through arms α and β). After the polarizer, the arms are again indistinguishable, allowing interference to occur.

Interestingly, it is also possible to change the recovered interference pattern. If the axis of the third polarizer is chosen to be -45° , then the above calculation yields:

$$P(0,1,-45^\circ) = \frac{1}{8} (1 - \cos \phi) \quad (137)$$

In this case, the minima and maxima of the interference pattern are switched compared to the 45° polarizer.

The phenomenon of the Quantum Eraser³⁸ can also be understood without the use of WW information by regarding the “erasing” process more as an “editing” process, where a different subset of photons is probed³⁹ or by explaining it in the framework of projecting the beams from the arms to a different polarization basis.

3.8.2 Experimental Realization

The setup geometry is the same as in Section 3.6.2. The coincidence count rate R_{TB} is plotted over the stage position Δl .

The experiment consists of three measurements with the following expected results:

- 1.) Both polarizers at 0° , no eraser: $R_{TB} = R_{TB}^{max} \cdot \frac{1}{4} \left(1 + \cos\left(\frac{2\pi\Delta l}{\lambda}\right)\right)$
- 2.) Polarizers at $0^\circ/90^\circ$, no eraser: $R_{TB} = R_{TB}^{max} \cdot \frac{1}{2}$
- 3.) Polarizers at $0^\circ/90^\circ$, eraser polarizer at 45° : $R_{TB} = R_{TB}^{max} \cdot \frac{1}{8} \left(1 + \cos\left(\frac{2\pi\Delta l}{\lambda}\right)\right)$

With $\lambda = 810$ nm being the wavelength of the single photons and R_{TB}^{max} the maximum count rate of experiment 1. Parallel to the interferograms, the second-order correlation function $g_{GRA}^{(2)}(0)$ is recorded as described in Equation (101) to continuously verify the single photon character of the light in the experiment.

3.9 Spontaneous Parametric Down-Conversion

The atomic cascade that Grangier, Roger, and Aspect used to obtain photon pairs is a very inefficient and complicated source. Nowadays, most experiments use a process called Spontaneous Parametric Down-Conversion (SPDC) to generate photon pairs. In SPDC, pairs of photons are generated inside a nonlinear crystal from pump

³⁸ Thorlabs offers the EDU-QE1(/M) Quantum Eraser Analogy Kit. The manual is freely available on the product webpage and introduces the quantum eraser experiment in more detail.

³⁹ P. G. Kwiat et al., *AIP Conference Proceedings*, **461**(1), 69 (1999).

light, typically the output of a pump laser. These photons are created virtually simultaneously, so that one of the photons can be used to signal the existence of the other, making it possible to perform measurements on single photons. That is why the photons of the pair are historically called the “idler” and “signal” photon. A schematic drawing of the SPDC process is shown in Figure 14.

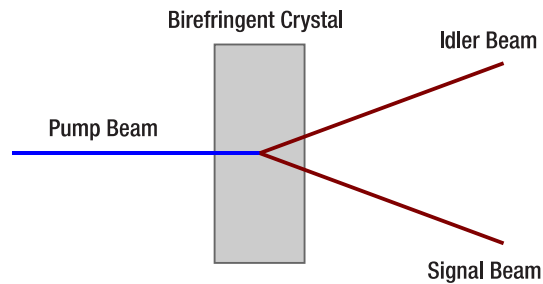


Figure 14 Schematic Drawing of the SPDC Process (Top View)

The process⁴⁰ is called spontaneous (as opposed to stimulated) because the photon pair is created without the presence of an external electromagnetic field at the target wavelength. It is called parametric because it has a relation to the parametric oscillator model. The term down-conversion is used because the photons of the pair have a lower energy than the incoming photon.

SPDC is the reverse process to Second Harmonic Generation (SHG), a process used very commonly in optics labs for multiple applications, such as creating 532 nm wavelength lasers. Unlike SHG, however, it cannot be explained by classical fields. Classical theories only allow for the generation of an idler and signal beam if a weak signal beam already exists, a process called parametric amplification. Therefore, the existence of the SPDC process can only be explained quantum-mechanically.

For the complete derivation, we refer to the literature⁴¹, but we will highlight some of the important properties of the process in the following.

Energy and momentum need to be conserved by the SPDC process. This means:

$$\omega_p = \omega_s + \omega_i \quad (138)$$

$$\vec{k}_p = \vec{k}_s + \vec{k}_i \quad (139)$$

Here, ω is the angular frequency of the photon and \vec{k} is the wave vector. The indices p, i, and s stand for pump, idler, and signal, respectively. The frequencies and wave vectors are not independent, but linked via the dispersion relation. As all three indices would have the same representative equation, the pump photon is given as an example below:

$$k_p = \frac{n_p \cdot \omega_p}{c} \quad (140)$$

Here, n_p is the index of refraction of the crystal at the pump frequency ω_p and c is the speed of light in vacuum. The index of refraction depends on the frequency of the light. For most materials it increases with increasing frequency in the optical regime, the so-called normal dispersion.

For SPDC, however, if we assume the wavelengths of the signal and idler photons to be similar, we need the same index of refraction for both pump and signal/idler photons. That is the reason birefringent crystals are used for SPDC. Those crystals have different indices of refraction for different polarizations. In Type-I crystals, such as the barium borate (BBO) crystal used in this kit, the polarization of the signal and idler photons is parallel and determined by the crystal orientation. If the pump is polarized orthogonally to the signal and idler polarization, a different dispersion relation applies. This makes it possible to find orientations of the crystal (in relation to \vec{k}_p and the pump polarization), that satisfy both equations (138) and (139).

⁴⁰ M. Beck, *Quantum Mechanics, Theory and Experiment*. (Oxford University Press, Oxford, 2012).

⁴¹ C. Couteau, *Contemporary Physics*, **59**(3), 291 (2018).

The refractive index as a function of the wavelength for BBO is shown in Figure 15. The red solid curve marks the refractive index for the ordinary beam (n_o). The black dashed curve is the refractive index for the extraordinary beam (n_e) if the input beam is orthogonal to the crystal plane. By rotating the crystal axes, the refractive index curve can be moved until $n_e(405 \text{ nm}) = n_o(810 \text{ nm})$. This is called phase matching and allows efficient SPDC from pump photons at 405 nm to signal/idler photon pairs at about 810 nm each. The BBO crystal in this kit is cut at an angle of 29.2° to ensure optimal phase matching for a pump beam under normal incidence. Section 12.12 provides more details about the crystal angle and polarization.

Another factor in the experiment is the thickness of the crystal. Thicker crystals provide a higher pair generation rate per pump power as there is more volume for the light to interact with the crystal. However, increasing thickness also blurs the wavelength-position correlation of the SPDC photons, as pairs created at different spots in the crystal have a different point of origin for the cone on which they are emitted.

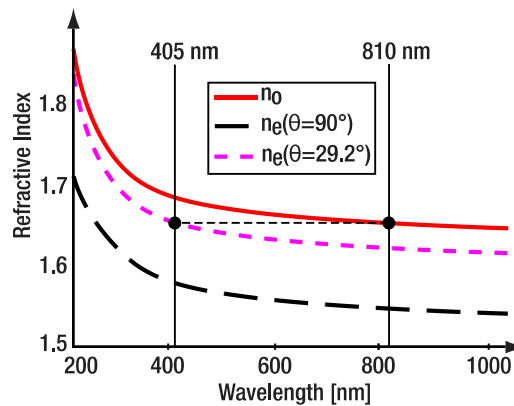


Figure 15 Refractive Indices for the Ordinary Beam (n_o , Red Curve), the Extraordinary Beam (n_e) at 0° (Black Curve), and 29.2° (Pink Curve) Crystal Orientation

Depending on the exact phase matching parameters, the signal and idler pairs either leave the crystal collinearly or on a cone with a small opening angle. The k -vectors of the photons in this case are schematically shown in Figure 16. For this kit, the half opening angle of the cone is 3° .

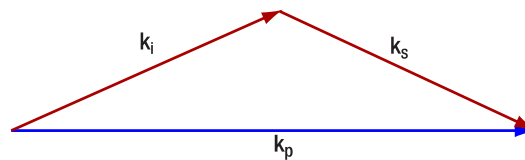


Figure 16 Schematic of the k -vectors of the Pump (p), Idler (i) and Signal (s) Photons in a SPDC process with Non-Collinear Emission

It is important to note that for a pump wavelength of 405 nm, the wavelength of the signal and idler photons will not always be 810 nm. Equation (138) also allows for pairs of different wavelengths, such as 812 nm / 808 nm⁴². In those cases, the photon with the longer wavelength makes a slightly larger angle with the pump beam and vice versa. This wavelength deviation is limited by how well the phase matching is fulfilled at the different wavelengths, as the efficiency of the SPDC process will drop sharply with non-optimal phase matching. In the configuration of this kit, the photon pairs are emitted under a range of wavelengths of up to several 10 nm and angles up to several degrees^{43,44}. Figure 17 shows a theoretically calculated plot for the normalized signal intensity depending on the signal wavelength for a pump wavelength of 405 nm and crystal parameters matching the crystal in the kit. In the experiment, this means that the photons generated by the SPDC process are distributed over a rather large angle.

⁴² Be aware that the wavelength of the pairs is calculated by $\frac{1}{\lambda_p} = \frac{1}{\lambda_s} + \frac{1}{\lambda_i}$, not by $\lambda_p = \frac{\lambda_s + \lambda_i}{4}$. The example above would therefore be 812.00 nm / 808.01 nm when given with more precision.

⁴³ M. Beck, *Quantum Mechanics, Theory and Experiment*. (Oxford University Press, Oxford, 2012).

⁴⁴ N. Beouf et al., *Optical Engineering*, 39(4), (2000).

When measuring with two detectors in coincidence, one must be careful that the detectors are positioned in such a way that they are able to detect photons from the same pair. Furthermore, when measuring wavelength-dependent quantities like the coherence length of the SPDC generated photons, one must consider that the wavelengths are spatially separated. This makes it likely that not all generated wavelengths are detected.

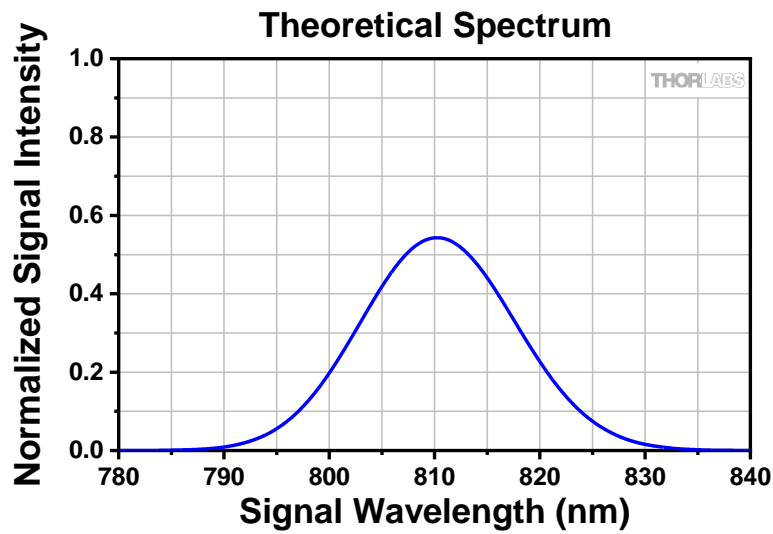


Figure 17 Theoretical Spectrum of Signal Intensity as a Function of Pump Wavelength (Calculation via spdcalc.org)

Chapter 4 Experimental Concepts

4.1 Single Photon Detectors

Single Photon Detectors are based on the Avalanche Photodiode (APD) design. An incoming photon creates an electron-hole pair in the semiconductor material of the APD (silicon for the detectors in this kit). A strong reverse voltage is applied to the semiconductor, accelerating the electron to the point that it creates additional free electrons via impact ionization, which in turn create even more electrons. This effect generates a large internal gain factor, resulting in a measurable voltage pulse even with a single photon as the original signal. In that sense the functional principle is remarkably close to a Geiger-Müller counter (the detectors are said to be operated in Geiger mode) but works at much lower photon energies. This output pulse is often shaped by internal electronics of the detector to match an international standard, such as TTL. A typical output pulse of Thorlabs' SPDMA Single Photon Detection Module, included in this kit, is displayed on the left graph of Figure 18.

After an avalanche event, the detector is unresponsive to additional photons for a small amount of time, which is called the dead time (<35 ns for the SPDMA detectors). This is the main contribution to the maximum count rate the detector can detect (20 MHz for the SPDMA detectors).

The photon detection efficiency (i.e., the percentage of incoming photons that result in a signal pulse) of such a detector depends on the detector material and the wavelength of the photons. The SPDMA detectors used in this kit provide a maximum efficiency of 65% at about 600 nm. At the design wavelength of this kit (810 nm), they still detect about 45% of all incoming photons, as seen in the right graph of Figure 18.

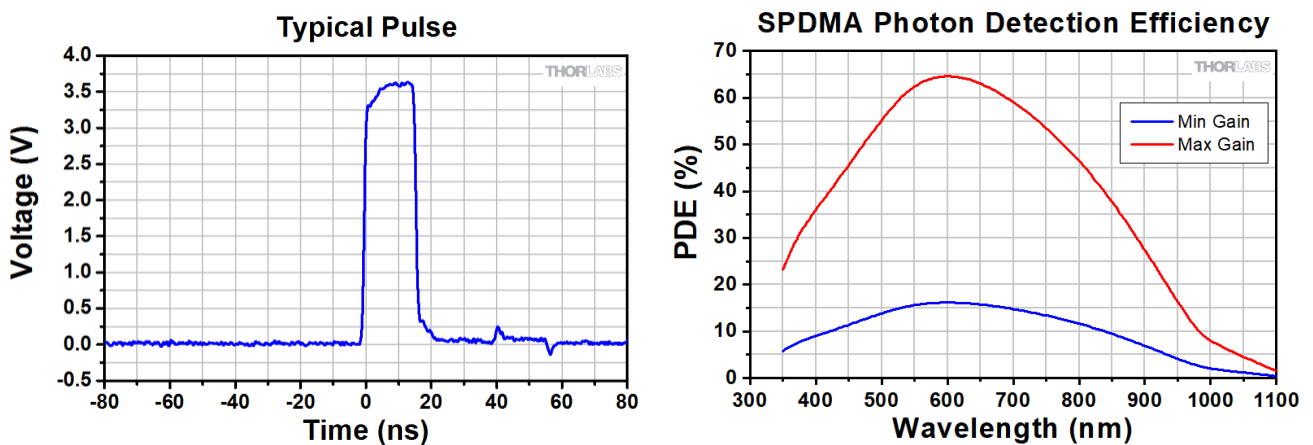


Figure 18 Typical Output Pulse (Left) and Spectral Photon Detection Efficiency (Right) for the SPDMA Detectors Used in this Kit

Sometimes, an avalanche event occurs without an external photon hitting the detector. Such an event is called a “dark count.” Dark counts are undesirable, as they cause errors in the measurement, especially at low signal count rates. The typical dark count rate of the SPDMA detectors is <300 Hz. As the signal count rates in the experiments described here are typically several 10s or even 100s of kHz, the negative impact of the dark counts on the results is negligible. Furthermore, the coincidence counting method, described in Section 4.2, further reduces the impact of dark counts.

The SPDMA detectors offer the function of reducing the reverse voltage (gain) at the diode, decreasing the dark count rate but at the same time reducing the photon detection efficiency. As described above, dark counts are not a problem in the experiments of this kit, so the detectors should be operated at maximum gain all the time (see Section 7.1.8).

Sometimes, a detection event does not generate a single output pulse from the detector but two or more. This unwanted effect is called afterpulsing. There are several mechanisms contributing to this effect. For our detectors, the probability of afterpulsing rises with increasing gain, but is low even at maximum gain. In the experiments described in this manual, afterpulsing results in a slight overestimation of all detector count rates but does not meaningfully change any of the results.

4.2 Time Tagging

4.2.1 Time Tagging versus Coincidence Electronics

A fundamental part of doing quantum optic experiments with a photon pair source is the counting of coincidence events. There are two main technical implementations to determine whether two events are temporally close enough to be counted as a coincidence:

- 1.) Coincidence Electronics: By constructing a gated circuit with serial logic elements or on a field programmable gate array (FPGA), one can count events in which the pulses of two detectors arrive in a given coincidence window in real time.
- 2.) Time Tagging: A time tagging device associates every detector event with a very precise timestamp. The number of coincidences can then be calculated from the time differences derived from the timestamps.

Coincidence electronics can be designed in the price range of a few hundred dollars, while time tagging devices with the precision required for quantum optics are more expensive. However, time tagging offers several advantages over coincidence electronics, most importantly flexibility. While coincidence electronics are often limited in their parameters (e.g., by the rate of the processor clock) and must be designed for the specific experiment, time tagging is only limited by the precision of the timestamps and different experiments can easily be accounted for by changing the calculation parameters. Additionally, time tagging electronics allows for more versatile post-processing: different input channels can be compared after the measurements were performed. In this kit, we use a time tagging device, hence the remainder of this section will focus on the specifics of time tagging. Please note that the time tagger in the kit has four active channels, which allows you to extend your range of experiments beyond the ones in the kit. If you need even more active channels, please contact Swabian Instruments.

4.2.2 Jitter and Coincidence Window

The time tagger assigns timestamps to both the rising and falling edges of the input pulses (only the rising edges are used in this kit). This association of the timestamps to events is never perfect. The deviation of the timestamp values of two channels relative to each other can be tested by applying a very stable periodic signal to both channels, measuring many events, and plotting the differences between the measured times of the two channels. Typically, the time differences will show a Gaussian distribution with a standard deviation of σ . The jitter is then defined as $\sqrt{\frac{1}{2}}\sigma$. For the educational version of the time tagger used in this kit, the jitter is specified to be <720 ps. As the typical coincidence window for the experiments is several nanoseconds long, this jitter is acceptable. Research grade time taggers approach jitter levels as low as 1 ps.

Assume there are two channels of the time tagger called A and B and a user-defined tagger window of Δt_t . Whenever an event is counted on one of the two detectors at the time t_1 , the window opens. If an event on the other detector is measured at a time t_2 and $t_2 - t_1 \leq \Delta t_t$, a coincidence event is counted. It does not matter if the event is measured first at detector A or detector B. This scheme is shown in Figure 19. Please note that the window Δt_t (which is a parameter to control the time tagger) and the coincidence window Δt used in Section 3.5 (which is the full coincidence window describing when a count on B may come to generate a coincidence with a fixed count on A) differ⁴⁵ by a factor of 2:

$$\Delta t = 2 \cdot \Delta t_t$$

⁴⁵ This difference is handled automatically by the software. The input value is Δt .

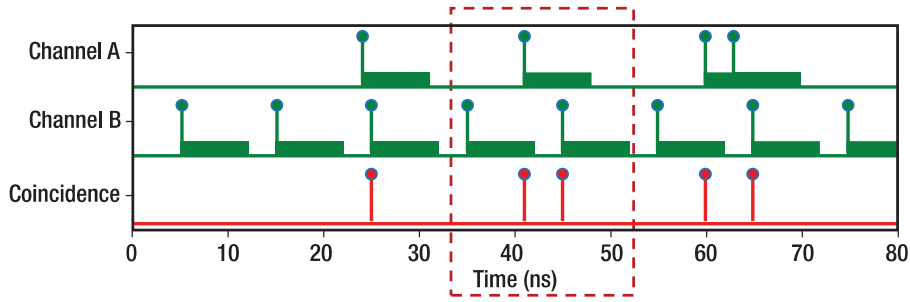


Figure 19 Definition of a Coincidence Between Two Channels of the Time Tagger (Bars Mark the Length of the Coincidence Window). The dashed rectangle marks an unwanted case of two coincidences created by only one event in Channel A.⁴⁶

At first glance, this looks to be unsuitable for quantum optic applications, because a single detection event on one detector can cause two coincidence events, as marked with a red rectangle in Figure 19, while a photon of a photon pair should of course cause a single coincidence count at maximum.

However, Figure 19 does not take the dead time of the detectors into account (see Section 4.1). This dead time is much larger than the coincidence window of a typical experiment, so the events on channel B in Figure 19 can never be close enough to cause the critical case marked with the red rectangle. Given this, the definition of coincidences as used by the time tagger is suitable for the experiments laid out in this manual.

In the quantum optics experiments in this kit, we often require triple coincidences between three channels T, A, and B, with T being the trigger detector indicating the presence of a single photon in the arm that includes detectors A and B. In this special case, triple coincidences are defined by a coincidence between the two-channel-coincidences T&A and T&B. Any two-channel coincidence event gets the time stamp of the earlier of its two counts, as seen in Figure 20.

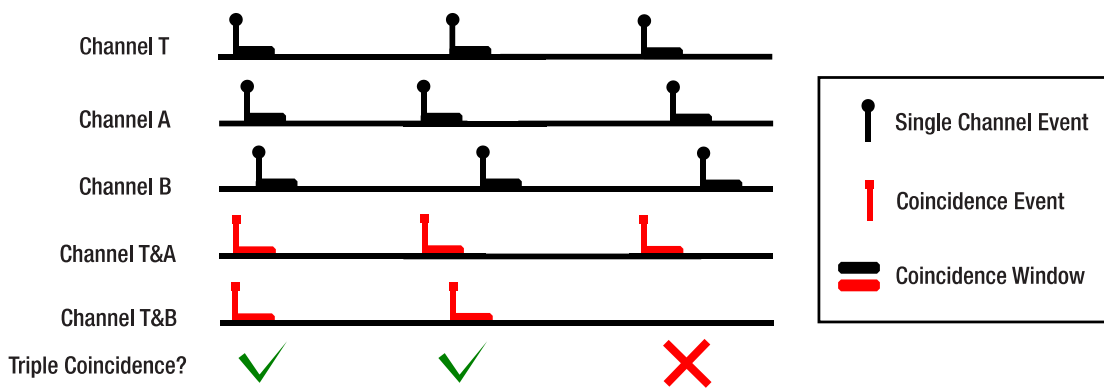


Figure 20 Triple Coincidences Detection Scheme. Between the second and third case, only the timing of the counts at T and A was exchanged, but the third case does not result in a triple coincidence as no two-channel coincidence between T&B is registered. This exemplifies the special role of the trigger detector in this scheme.

While triple coincidences can be defined in other ways and different detection schemes are possible, the method and definition here are the best fit for the experiments in this kit. More details are given in Section 12.1.

4.2.3 Delay Compensation

If two or more detectors are connected to different channels of the time tagger, their signal will arrive at different times even if the events that caused the signals happened simultaneously. There are two causes for this:

⁴⁶ Figure copied from documentation of Time Tagger 20 by Swabian Instruments

- 1.) Arbitrary delays caused by jitter in the detectors and timing electronics.
- 2.) Systematic delays caused by different cable lengths, slight differences in detector circuits, differences in the path lengths to the detectors (30 cm \approx 1 ns for light in air), etc.

The systematic delays are often much larger than the arbitrary ones (on the order of several ns) but can be compensated for by just adding or subtracting a constant time from every timestamp on a given channel before calculating coincidences.

To determine the systematic delay offsets in this kit, we use the following method:

- Use a large coincidence window (20 ns or more) to find coincidences of photon pairs even with the systematic delays.
- Go back to a small coincidence window (5 ns), vary the delay of detectors A and B (compared to detector T) stepwise (0.5 ns step width) and record the number of coincidences between detectors T&A and T&B for every step. Figure 21 shows an example for such a measurement.
- The maximum number of coincidences for T&A (T&B) occurs at the delay of channel A (B) which offers the best compensation for the systematic delay differences. These delays are then used for all further measurements.

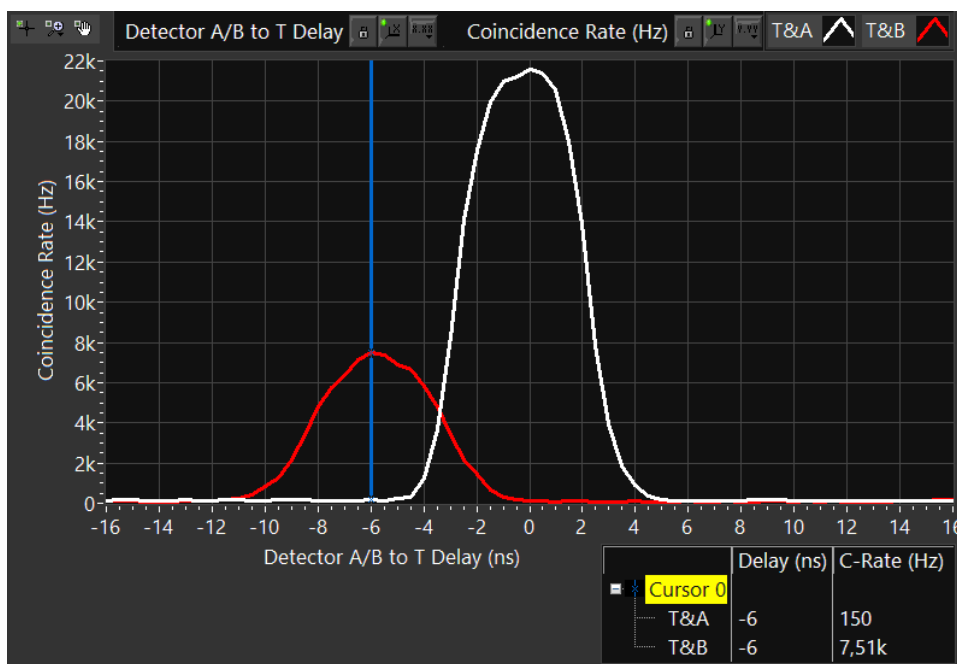


Figure 21 Example Measurement of Detector Delay. In this case, detector B has a delay of -6 ns compared to detector T.

Chapter 5 Kit Components

In cases where the metric and imperial kits contain parts with different item numbers, metric part numbers and measurements are indicated by parentheses unless otherwise noted.

5.1 Pump and Alignment Laser

 <p>1 x LDM9T(M) Laser Diode Mount with Integrated Temperature Controller</p>	 <p>1 x L405P20⁴⁷ Laser Diode 405 nm, 20 mW</p>	 <p>1 x KLD101 K-Cube Laser Diode Controller</p>	 <p>1 x C230TMD-A Aspheric Lens, Mounted f = 4.51 mm, NA = 0.55</p>
 <p>1 x S1TM09 Lens Adapter SM1 to M9 x 0.5</p>	 <p>1 x TPS002 15 V Power Supply for up to Two K-Cubes</p>	 <p>1 x CAB400 Cable, 9-Pin D-Sub 1.5 m Long</p>	 <p>1 x PL202 USB Laser Module 635 nm, 0.9 mW</p>
 <p>1 x AD11NT Adapter without Threads for Ø11 mm Components</p>	 <p>1 x KM100CP(M) Kinematic Mirror Mount with Centering Plate for Ø1" Optics</p>	 <p>1 x DS5 USB Power Supply, 5 VDC</p>	 <p>1 x RS2P8E (RS2P4M) Ø1" (Ø25.0 mm) Pedestal Post, 8-32 (M4) Tap, 2" (50 mm) Long</p>
 <p>1 x RS1.5P8E (RS1.5P4M) Ø1" (Ø25.0 mm) Pedestal Post, 8-32 (M4) Tap, 1.5" (38 mm) Long</p>	 <p>1 x KB1X1 (KB25/M) Magnetic Base, 1" x 1" (25 mm x 25 mm)</p>	 <p>1 x KBB1X1 (KBB25/M) Magnetic Bottom Plate, 1" x 1" (25 mm x 25 mm)</p>	 <p>1 x PH1E⁴⁸ Ø1/2" (Ø12.7 mm) Pedestal Post Holder, Magnetic, 1.19" (30.1 mm) Long</p>
 <p>1 x TR1 (TR30/M) Ø1/2" (Ø12.7 mm) Post, 1" (30 mm) Long</p>			

⁴⁷ Pre-selected to be within ± 1 nm. This laser diode comes with a spec sheet that includes the LIV curve.

⁴⁸ The EDU-QOP1/M kit comes with a 30.1 mm tall post holder. For a replacement, please contact Tech Support (techsupport@thorlabs.com).

5.2 Crystal and Adjustment Aids

 <p>1 x BBO-Crystal Type 1 3 mm Thick, Cutting Angle: 29.2°</p>	 <p>1 x FGL515 Ø25 mm Colored Glass Filter, 515 nm Long Pass</p>	 <p>2 x KM100CP(/M) Kinematic Mirror Mount with Centering Plate for Ø1" Optics</p>	 <p>1 x Marked Mirror Mount⁴⁹ Kinematic Mirror Mount with Centering Plate with Extra Markings</p>
 <p>1 x KB1X1 (KB25/M) Magnetic Base, 1" x 1" (25 mm x 25 mm)</p>	 <p>2 x KBT1X1 (KBT25/M) Magnetic Top Plate, 1" x 1" (25 mm x 25 mm)</p>	 <p>1 x Axicon Ø1/2", 3° Half Opening Angle of Light Cone for 635 nm</p>	 <p>1 x SM05L10 SM05 Lens Tube, 1" Thread Depth</p>
 <p>1 x SM05S5M Ø1/2" Brass Optic Spacer, 5 mm in Length</p>	 <p>1 x SM05S10M Ø1/2" Brass Optic Spacer, 10 mm in Length</p>	 <p>1 x AD1T Ø1" OD Adapter for Ø1/2" Optics, Internally SM05 Threaded</p>	 <p>1 x PH1E⁵⁰ Ø1/2" (Ø12.7 mm) Pedestal Post Holder, Magnetic, 1.19" (30.1 mm) Long</p>
 <p>1 x TR1 (TR30/M) Ø1/2" (Ø12.7 mm) Post, 1" (30 mm) Long</p>			

5.3 Optics

 <p>4 x PF10-03-F01 Ø1" UV-Enhanced Aluminum Mirror</p>	 <p>4 x KM100 Kinematic Mirror Mount for Ø1" Optics</p>	 <p>4 x KCP1(/M) Centering Plate for Ø1" Mirror Mounts</p>	 <p>5 x RS2P8E (RS2P4M) Ø1" (Ø25.0 mm) Pedestal Post, 8-32 (M4) Tap, 2" (50 mm) Long</p>
---	---	--	--

⁴⁹ This is a KM100CP(/M) mount with extra engravings. For a replacement, please contact Tech Support (techsupport@thorlabs.com).

⁵⁰ The EDU-QOP1/M kit comes with a 30.1 mm tall post holder. For a replacement, please contact Tech Support (techsupport@thorlabs.com).

 <p>1 x RS1.5P8E (RS1.5P4M) \varnothing1" (\varnothing25.0 mm) Pedestal Post, 8-32 (M4) Tap, 1.5" (38 mm) Long</p>	 <p>1 x KB1X1 (KB25/M) Magnetic Base 1" x 1" (25 mm x 25 mm)</p>	 <p>1 x CCM5-BS017(/M) Mounted Beamsplitter, Non-Polarizing, Anti-Reflection Coated: 700 nm - 1100 nm</p>	 <p>1 x RS2.5P(/M) \varnothing1" (\varnothing25.0 mm) Pedestal Post, 1/4"-20 (M6) Tap, 2.5" (65 mm) Long</p>
 <p>1 x Unmounted Iris⁵¹ \varnothing15.0 mm Max Aperture, with 8-32 (M4) Stud</p>	 <p>1 x Unmounted Iris⁵² \varnothing25.0 mm Max Aperture, with 3/4" (20 mm) Long 8-32 (M4) Setscrew</p>	 <p>1 x RSP1D(/M) Rotation Mount for \varnothing1" Optics</p>	 <p>1 x WPH10ME-405 \varnothing1" Mounted Polymer Zero-Order Half-Wave Plate, SM1-Threaded Mount, 405 nm</p>
 <p>1 x LMR1(/M) \varnothing1" Lens Holder</p>	 <p>1 x VRC4D1 \varnothing1" Visible and IR Alignment Disk</p>	 <p>1 x EDU-VS1(/M) Polysterene Viewing Screen, 5.91" x 5.91"</p>	 <p>1 x SMR1(/M) \varnothing1" Lens Mount with SM1 Internal Threads and No Retaining Lip</p>
 <p>2 x SM1D12D SM1 Iris, Ring Actuated, \varnothing12 mm Max Aperture</p>	 <p>1x SM1CP2 Externally SM1-Threaded End Cap</p>	 <p>1 x SM05CP2 Externally SM05-Threaded End Cap</p>	 <p>1 x PH2E (PH50E/M) \varnothing1/2" (\varnothing12.7 mm) Pedestal Post Holder, Magnetic, 2.19" (54.7 mm) Long</p>
 <p>1 x TR2 (TR50/M) \varnothing1/2" (\varnothing12.7 mm) Post, 2" (50 mm) Long</p>	 <p>1 x PH1.5E (PH40E/M) \varnothing1/2" (\varnothing12.7 mm) Pedestal Post Holder, Magnetic, 1.69" (44.7 mm) Long</p>	 <p>2 x TR1.5 (TR40/M) \varnothing1/2" (\varnothing12.7 mm) Post, 1.5" (40 mm) Long</p>	 <p>1 x PH1E (PH30E/M) \varnothing1/2" (\varnothing12.7 mm) Pedestal Post Holder, Magnetic, 1.19" (34.7 mm) Long</p>






⁵¹ This is a modified ID15(/M) iris where the TR3 (TR75/M) post is not included. For a replacement, please see the ID15(/M) iris on the website.

⁵² This is a modified ID25(/M) iris where the TR3 (TR75/M) post is not included and a longer 8-32 (M4) setscrew is utilized. For a replacement, please contact Tech Support (techsupport@thorlabs.com).













 <p>1 x PH082E (PH20E/M) $\varnothing 1/2"$ ($\varnothing 12.7$ mm) Pedestal Post Holder, Magnetic, 1" (25 mm) Long</p>	 <p>1 x TR075 (TR20/M) $\varnothing 1/2"$ ($\varnothing 12.7$ mm) Post, 0.75" (20 mm) Long</p>	 <p>1 x RS4M (RS5M) Spacer for $\varnothing 25$ mm Posts, 4 mm (5 mm) Thick</p>	 <p>2 x RS10M Spacer for $\varnothing 25$ mm Posts, 10 mm Thick</p>
 <p>1 x RS3M (RS1M) Spacer for $\varnothing 25$ mm Posts, 3 mm (1 mm) Thick</p>	 <p>1 x RS06M Spacer for $\varnothing 25$ mm Posts, 0.6 mm Thick</p>	 <p>1x AP8E25E (AP6M4M) Adapter with External 8-32 (M4 x 0.7) Threads and External $1/4"-20$ (M6 x 1.0) Threads</p>	 <p>1 x SM1L03 SM1 Lens Tube, 0.3" Thread Depth</p>
 <p>1 x EBP1 $\varnothing 1"$ 30:70 Beamsplitter, AOI: 45°</p>	 <p>1 x NE30A $\varnothing 25$ mm Absorptive ND Filter, SM1-Threaded Mount, Optical Density: 3.0</p>	 <p>1 x SM1A1 Adapter with External SM05 Threads and Internal SM1 Threads</p>	

















5.4 Detectors

 <p>3 x SPDMA Single Photon Detector 350 nm - 1100 nm $\varnothing 500$ μm Detector Area</p>	 <p>3 x CXY1A XY Translation Mount for $\varnothing 1"$ Optics</p>	 <p>3 x SM1NR05 SM1 Zoom Housing for $\varnothing 1/2"$ Optics</p>	 <p>3 x AC127-050-B $\varnothing 1/2"$ Achromatic Doublet, f = 50 mm, Anti-Reflection Coated, 650 nm - 1050 nm</p>
 <p>3 x $\varnothing 1"$ Bandpass Filter CWL = 810 ± 2 nm, FWHM = 10 ± 1 nm</p>	 <p>3 x SM1D12D SM1 Ring-Actuated Iris, $\varnothing 12$ mm Max Aperture</p>	 <p>3 x SM1L05 SM1 Lens Tube, 0.5" Thread Depth</p>	 <p>3 x Dovetail Adapter</p>

 <p>3 x DTSM1 External SM1 Threads to Female D4T Dovetail Adapter</p>	 <p>3 x SM1NT1 SM1 (1.035"-40) Locking Ring, 1.25" Outer Diameter, Slots for Spanner Wrench</p>	 <p>3 x PH2E (PH50E/M) Ø1/2" (Ø12.7 mm) Pedestal Post Holder, Magnetic, 2.19" (54.7 mm) Long</p>	 <p>3 x TR2 (TR50/M) Ø1/2" (Ø12.7 mm) Post, 2" (50 mm) Long</p>
 <p>3 x AP8E4M (Metric Kit Only) Adapter with External 8-32 Threads and External M4 x 0.7 Threads</p>			

5.5 Michelson Interferometer

 <p>1 x MB8 (MB2020/M) Aluminum Breadboard 8" x 8" (200 mm x 200 mm)</p>	 <p>1 x NFL5DP20S(/M) 5 mm Travel Translation Stage with Differential Drive and 20 µm Closed-Loop Piezo Driver</p>	 <p>1 x NFL5P1(/M) Adapter Plate for Translation Stage</p>	 <p>1 x KPZ101 K-Cube Piezo Controller</p>
 <p>1 x KSG101 K-Cube Strain Gauge Controller</p>	 <p>1 x TPS002 15 V Power Supply for up to Two K-Cubes</p>	 <p>2 x PF10-03-M01 Ø1" Protected Gold Mirror</p>	 <p>2 x KM100 Kinematic Mirror Mount for Ø1" Optics</p>
 <p>1 x KCP05(/M) Centering Plate</p>	 <p>1 x RS1.5P8E (RS1.5P4M) Ø1" (Ø25.0 mm) Pedestal Post, 8-32 (M4) Tap, 2" (50 mm) Long</p>	 <p>1 x RS6M Spacer for Ø25 mm Posts, 6 mm Thick</p>	 <p>1 x CCM5-BS017(/M) Mounted Beamsplitter, Non-Polarizing, Anti-Reflection Coated: 700 nm - 1100 nm</p>

 <p>1 x RS2P(/M) $\text{\O}1''$ ($\text{\O}25.0$ mm) Pedestal Post, $1/4''$-20 (M6) Tap, 2'' (50 mm) Long</p>	 <p>1 x AP8E25E (AP6M4M) Adapter with External 8-32 (M4 x 0.7) Threads and External $1/4''$-20 (M6 x 1.0) Threads</p>	 <p>1 x RS3M Spacer for $\text{\O}25$ mm Posts, 3 mm Thick</p>	 <p>1 x LEDMT1F USB Powered LED Mount, $62 \text{ }\Omega$ Resistance, USB to Micro-B USB Cable Included</p>
 <p>2 x LED660L LED, 660 nm, 13 mW, 18° Half Opening Angle FWHM: 14 nm</p>	 <p>1 x SMR05(/M) Lens Mount without Retaining Lip for $\text{\O}1/2''$ Optics</p>	 <p>1 x SM05L10 SM05 Lens Tube, 1'' Thread Depth</p>	 <p>1 x USB-C-72 72'' USB 2.0 Type-A Extension Cable</p>
 <p>1 x LMR1(/M) $\text{\O}1''$ Lens Mount</p>	 <p>1 x LB1471 $\text{\O}1''$ Lens Biconvex $f = 50$ mm, Uncoated</p>	 <p>1 x Unmounted Iris⁵³ $\text{\O}8.0$ mm Max Aperture, with 8-32 (M4) Stud</p>	 <p>2 x PH2E (PH50E/M) $\text{\O}1/2''$ ($\text{\O}12.7$ mm) Pedestal Post Holder, Magnetic, 2.19'' (54.7 mm) Long</p>
 <p>2 x TR2 (TR50/M) $\text{\O}1/2''$ ($\text{\O}12.7$ mm) Post, 2'' (50 mm) Long</p>	 <p>1 x PH1.5E (PH40E/M) $\text{\O}1/2''$ ($\text{\O}12.7$ mm) Pedestal Post Holder, Magnetic, 1.69'' (44.7 mm) Long</p>	 <p>1 x TR1.5 (TR40/M) $\text{\O}1/2''$ ($\text{\O}12.7$ mm) Post, 1.5'' (40 mm) Long</p>	 <p>1 x CA2912 SMA Coaxial Cable, SMA Male to SMA Male, 12'' (304 mm)</p>

5.6 Time Tagger and Software

 <p>1 x EDU Time Tagger</p>	 <p>3 x CA2924 SMA Coaxial Cable Male-to-Male 24'' (609 mm) Long</p>	 <p>1 x USB Stick EDU-QOP1 Software</p>
---	--	---





⁵³ This is a modified ID15(/M) iris where the TR3 (TR75/M) post is not included. For a replacement, please see the ID8(/M) iris on the website.

5.7 Quantum Eraser

 <p>2 x LPNIRB050 Ø1/2" Unmounted Linear Polarizer, 650 - 1100 nm</p>	 <p>1 x LPNIRE100-B Ø1" Unmounted Linear Polarizer, 600 nm - 1100 nm</p>	 <p>1 x WPH10ME-808 Ø1" Mounted Polymer Zero-Order Half-Wave Plate, SM1-Threaded Mount, 808 nm</p>	 <p>4 x RSP1D(/M) Rotation Mount for Ø1" Optics</p>
 <p>2 x SM1A6T Adapter with External SM1 Threads and Internal SM05 Threads</p>	 <p>2 x RS1.5P8E (RS1.5P4M) Ø1" (Ø25.0 mm) Pedestal Post, 8-32 (M4) Tap, 1.5" (38 mm) Long</p>	 <p>2 x RS2P8E (RS2P4M) Ø1" (Ø25.0 mm) Pedestal Post, 8-32 (M4) Tap, 2" (50 mm) Long</p>	 <p>2 x RS4M (RS5M) Spacer for Ø25 mm Posts, 4 mm (5 mm) Thick</p>
 <p>2 x RS4M Spacer for Ø25 mm Posts, 4 mm Thick</p>	 <p>1 x PS3 1/2" Tall Mounting Post Spacer</p>		





5.8 Mounting and Tools

 <p>5 x CF125-P5 Clamping Fork, 1.24" Counterbored Slot, Universal, 5 Pack</p>	 <p>2 x Clamping Fork 0.40" Counterbored Slot, Universal</p>	 <p>2 x CL2(/M) Heavy-Duty Variable Height Clamp, 1/4"-20 (M6) Tapped</p>	 <p>2 x CL5A Table Clamp, L-Shape, Rounded Lip</p>
 <p>1 x SPW606 Spanner Wrench for SM1-Threaded Retaining Rings, Length = 1"</p>	 <p>1 x SPW909 Spanner Wrench for SM1-Threaded Adapters, Length = 1"</p>	 <p>1 x SPW603 Spanner Wrench for SM05-Threaded Retaining Rings, Length = 1"</p>	 <p>1 x SPW301 Spanner Wrench for Aspheric Lenses</p>





 1 x SPW502 Spanner Wrench for Slotted SM05, SM1, and C-Mount Locking Rings	 1 x CS1 Screw-On Cable Straps (Qty. 15)	 1 x LG3 Laser Safety Glasses	 1 x Label Sheet
---	--	--	---

5.9 Included Hardware

5.9.1 Imperial Kit

To Combine Components		To Mount Assemblies to Breadboard	
Type	Qty.	Type	Qty.
8-32 x 1/4" Cap Screw	14	1/4"-20 x 1/4" Cap Screw	14
8-32 x 5/8" Cap Screw	1	1/4"-20 x 3/8" Cap Screw	37
8-32 x 1/2" Setscrew	2	1/4"-20 x 1" Cap Screw	2
8-32 x 5/8" Setscrew	1	1/4"-20 x 2" Cap Screw	2
8-32 x 3/4" Setscrew	6	1/4"-20 x 2.5" Cap Screw	2
Hex Keys: 0.05", 1/16"		1/4" Washer	100
Ball Drivers			Slit Screwdriver
 1 x BD-5/64 5/64" Ball Driver	 1 x BD-9/64 Ball Driver for 8-32 Cap Screws	 1 x BD-3/16 Ball Driver for 1/4"-20 Cap Screws	 1 x Screwdriver 1.8 mm x 0.5 mm

5.9.2 Metric Kit

To Combine Components		To Mount Assemblies to Breadboard	
Type	Qty.	Type	Qty.
M4 x 6 mm Cap Screw	14	M6 x 6 mm Cap Screw	14
M4 x 16 mm Cap Screw	1	M6 x 10 mm Cap Screw	37
M4 x 12 mm Setscrew	2	M6 x 25 mm Cap Screw	2
M4 x 16 mm Setscrew	1	M6 x 50 mm Cap Screw	2
M4 x 20 mm Setscrew	6	M6 x 65 mm Cap Screw	2
Hex Keys: 1.3 mm, 1.5 mm		M6 Washer	100
Ball Drivers			Slit Screwdriver
 1 x BD-2M 2 mm Ball Driver	 1 x BD-3M Ball Driver for M4 Cap Screws	 1 x BD-5M Ball Driver for M6 Cap Screws	 1 x Screwdriver 1.8 mm x 0.5 mm

Chapter 6 Quick Setup

This chapter provides a summary of the setup procedure for experienced users or as a reminder when rebuilding the setup several times. The assembly of the components is explained in Section 7.1 and a detailed guide to building the setup is provided in the remainder of Chapter 7.

Preliminary Alignments (Section 7.2)

- Make sure that the pump laser is collimated.
- Make sure that the scales of all three polarizer elements are correctly calibrated (the scale should match the actual polarizer rotation). The process is described in Section 7.2.3.

HBT Experiment with Alignment Laser (Section 7.3)

- Position the components as shown in Figure 22.

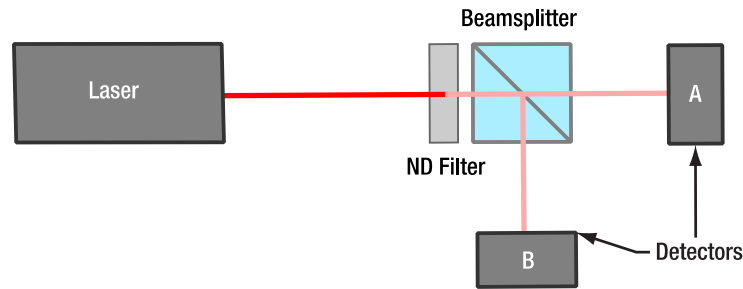


Figure 22 HBT Experiment with Alignment Laser

Pair Source (Section 7.4)

- Position the components as shown in Figure 23.
- Make sure that the pump and alignment beam paths are identical (via beam walk through the two iris apertures).
- Use the axicon with the alignment laser to position the detectors in the light cone.
- Use the fluorescent filter to adjust the detector optics for maximum count rate.
- Use the BBO crystal and adjust the tilt (lower kinematic screw) for maximum coincidence count rate. If required, use a larger coincidence window (20 ns).
- Set the detector delay in the software.

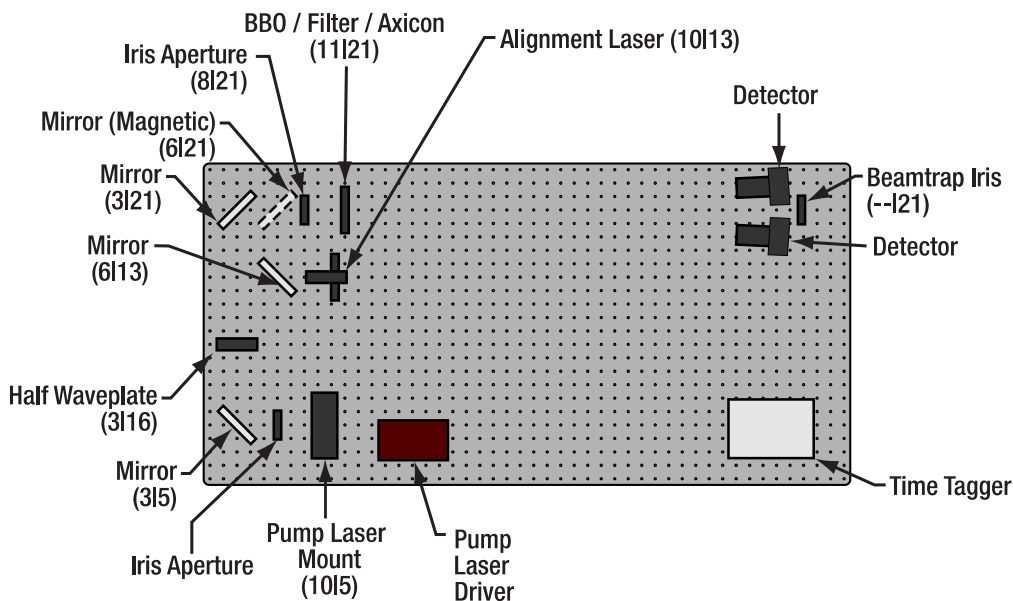


Figure 23 Pair Source Setup. The numbers in parentheses are breadboard hole numbers (from left / from bottom).

GRA Experiment (Section 7.5)

- Align a beamsplitter in the path to detector A and position detector B in the other output of the splitter.
- Position detector B analog to detectors T and A (axicon → filter → BBO).
- Set the delay of detector B in the software.

Michelson Interferometer (Section 7.6)

- Set up an additional alignment path between the BBO crystal and the beamsplitter with one additional iris aperture.
- Replace detector B with the Michelson interferometer on the small breadboard (see Figure 24)
- Adjust the interferometer with the alignment laser and red LED.
- Position detector B in the output of the interferometer. Align and set delay as before.
- Connect the stage to the KPZ101 and KSG101. And connect the KPZ101 to the KSG101.

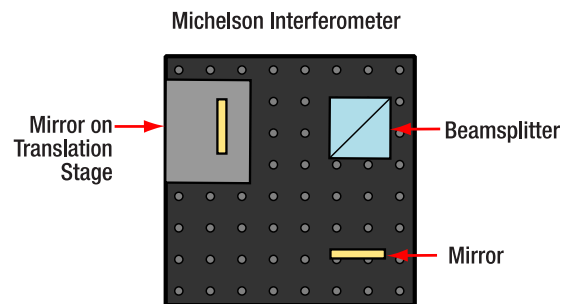


Figure 24 *Michelson Interferometer Board*

Quantum Eraser (Section 7.7)

- Insert a half-wave plate between the two beamsplitters and set it to 22.5° .
- Place the two $1/2$ " diameter polarizers in the arms of the interferometer and set them to 0° .
- Use the red LED to realign the interferometer.
- Figure 25 shows the complete setup.

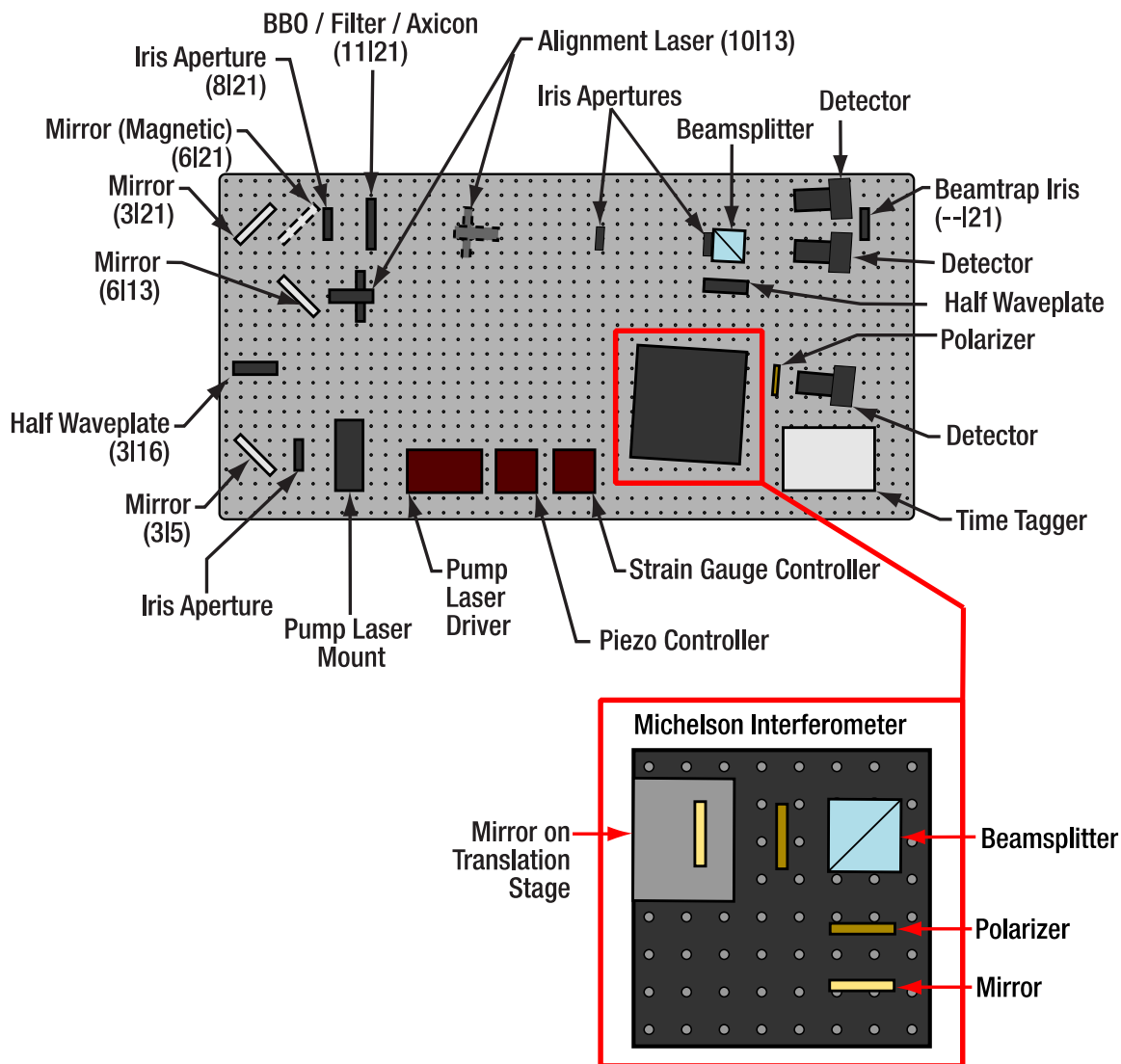


Figure 25 Complete Setup Overview. The numbers in parentheses are breadboard hole numbers (from left / from bottom).

Chapter 7 Setup and Adjustment

This chapter gives detailed and thorough instructions for setting up all the components and experiments in the kit. Chapter 6 offers a very brief summary for experienced users or repeated rebuilds.

7.1 Assembly of Components

7.1.1 Pump Laser

- It is recommended that the user wears ESD protection equipment while assembling the pump laser to avoid damage to the laser diode via electric discharge.
- Take the LDM9T(/M) Laser Diode Mount and lay it on a table with the front plate pointing upwards. Remove the four screws in the corners of the front plate and take it off. On the inside of the diode mount are two switches for LD (Laser Diode) and PD (Photodiode). Both should be set to CG (Cathode Grounded) and the J2 jumper should not be connected, as shown in Figure 26.

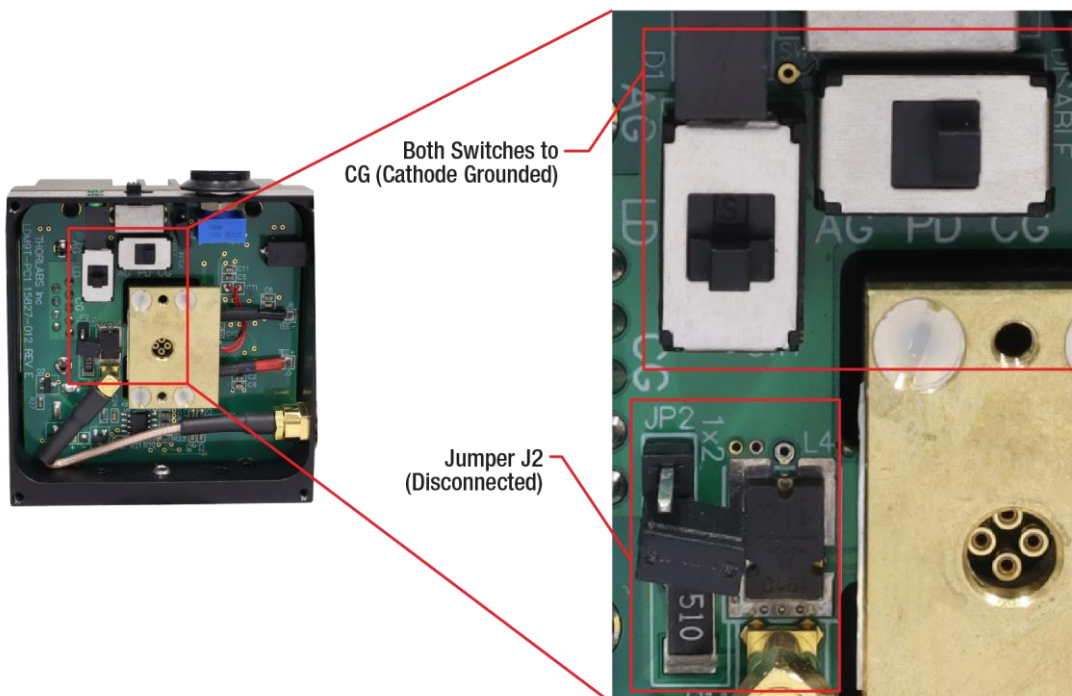


Figure 26 Correct Switch Position of LDM9T(/M) Laser Diode Mount

- Remove the mounting flange (if pre-installed) and assemble the pump laser as shown in Figure 27.
- Please note:
 - For steps 1-5, keep the LDM9T(/M) mount on a flat surface with the front face pointing upwards.
 - In step 1, fit the diode legs to the holes of the laser mount as shown in Figure 28.
 - The LDM9T(/M) mount comes with two different flanges. Use the smaller one in step 2.
 - During step 3, make sure that the front plate is centered on the mount.
 - Use the SPW301 spanner wrench for step 4 and the SPW909 spanner wrench for step 5.
 - During step 5, screw the S1TM09 adapter into the front plate until you notice an increased resistance due to the rubber lip of the S1TM09 adapter engaging the SM1 threading.

- During step 6, use a 5/64" (2 mm) hex key to screw the setscrew as far into the post as possible.
- In step 7, use the torque hole of the post to tighten the connection between LDM9T(/M) mount and the post.
- After completion, set the temperature of the controller to 25°C.

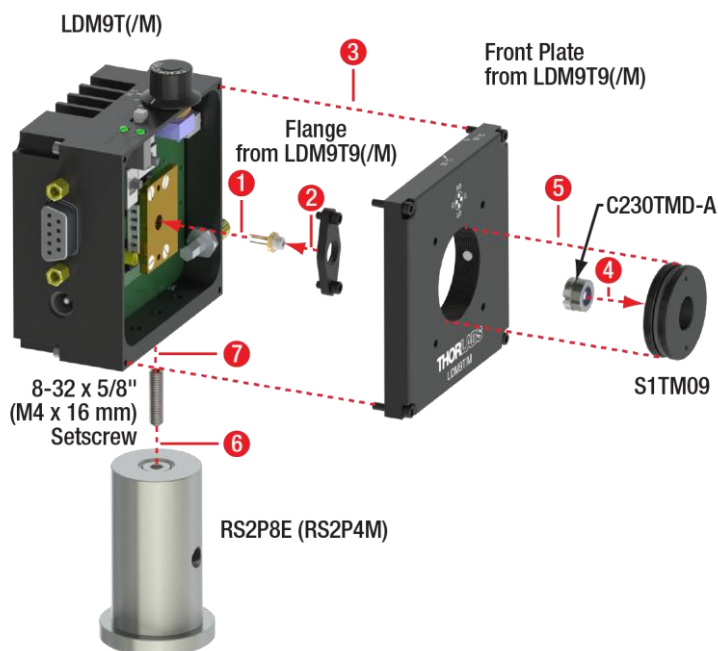


Figure 27 Assembly of Pump Laser

Laser Diode Bottom View

Laser Mount Front View

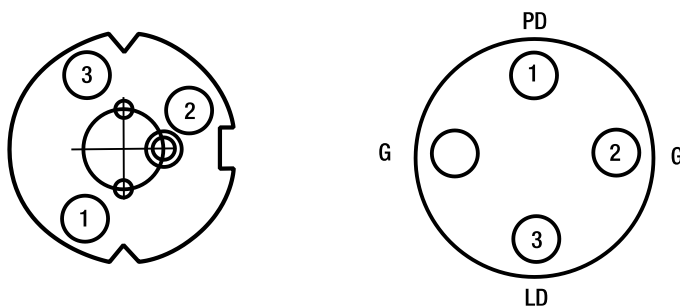


Figure 28 Correct Mounting of L405P20 Laser Diode into LDM9T(/M) Mount

7.1.2 Alignment Laser

- Assemble the alignment laser as shown in Figure 29.
- Please note:
 - The KM100CP(/M) mirror mount has two threaded bases. Attach the one labeled “Thorlabs” to the magnetic plate (as shown as step 2 in Figure 29). This allows better access to the adjusters when placed in the setup.
 - In step 3, use a 1/16" (1.5 mm) hex key to lock the PL202 laser in the AD11NT adapter.
 - The AD11NT adapter should be positioned approximately at the center of the PL202 laser.

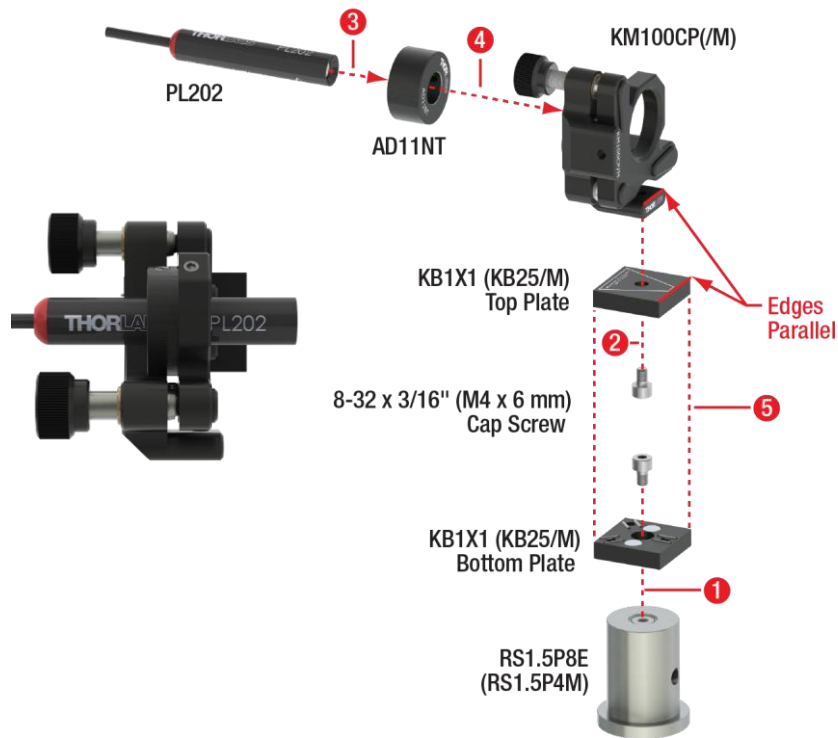


Figure 29 Assembly of Alignment Laser and Finished Component (Inset)

7.1.3 Mirrors

- Assemble two mirror setups as shown in Figure 30, one as shown in Figure 31, and one as shown in Figure 32.
- Please note:
 - The cap screws that connect the KM100 mount to the KCP1(/M) plate are included with the KM100 mount. The metric screws are colored black for easier distinction.
 - Take care to align the edges marked in the figures as parallel as possible.
 - Only touch the circumference of the mirrors, do not touch the mirror surface.
 - Use the nylon-tipped screw of the KM100 mount to hold the mirror in place.

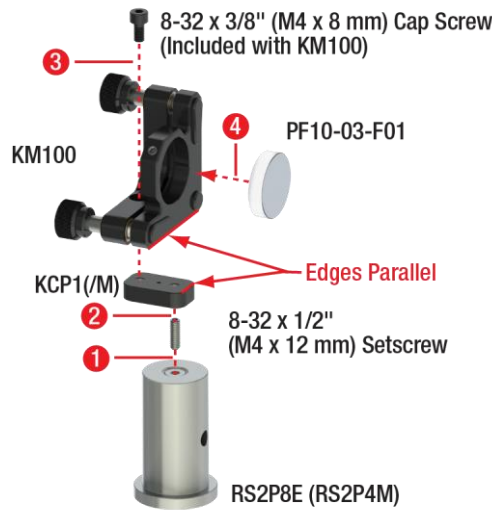


Figure 30 First Mirror Assembly (Build Two)

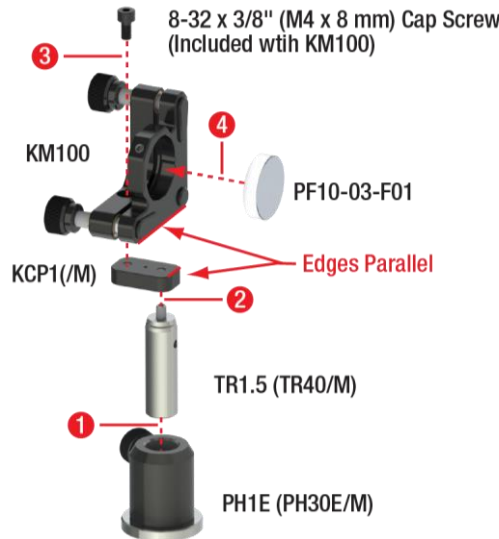


Figure 31 Second Mirror Assembly (Build One)

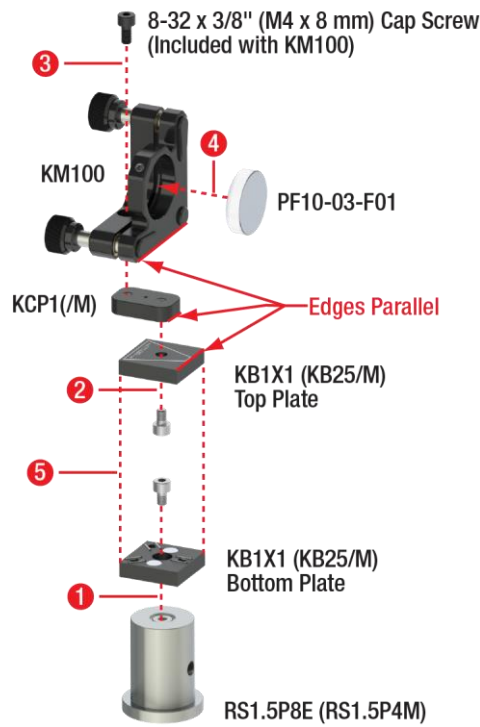


Figure 32 *Third Mirror Assembly (Build One)*

7.1.4 Iris Apertures

- Assemble three iris aperture assemblies as shown in Figure 33.



Figure 33 *Iris Aperture Components*

7.1.5 Half-Wave Plates

- Assemble the wave plates as shown in Figure 34.
- Please note:
 - During step 1, use a 5/64" (2 mm) hex key to screw the setscrew as far into the RSP1D(/M) rotation mount as possible.
 - After completion, use a 5/64" (2 mm) hex key to loosen the two locking screws on the front of the RSP1D(/M) mount, move the scale until the 0° setting is aligned with the fast axis marker on the wave plate, and re-tighten the locking screws. Do this for both wave plates.



Figure 34 Half-Wave Plate Components

7.1.6 Crystal, Axicon, and Filter

- Remove the retaining ring from an SM05L10 lens tube and assemble the axicon as shown in Figure 35.
- Please note:
 - In step 1, the conical side of the axicon should face the bronze spacers (see Figure 36). Only touch the circumference of the axicon. Do not touch the axicon surface.
 - For step 2, use an SPW603 spanner wrench.
 - During step 5, take care to align the marked edges.

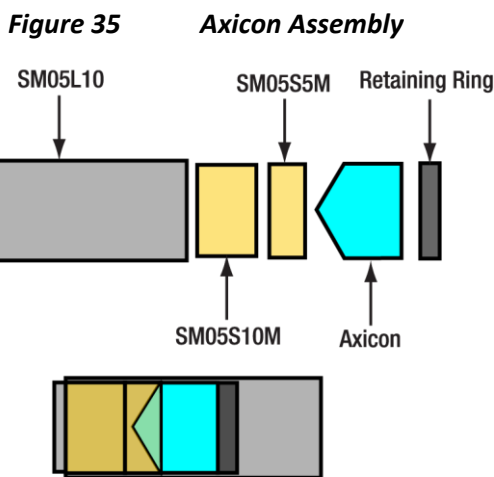
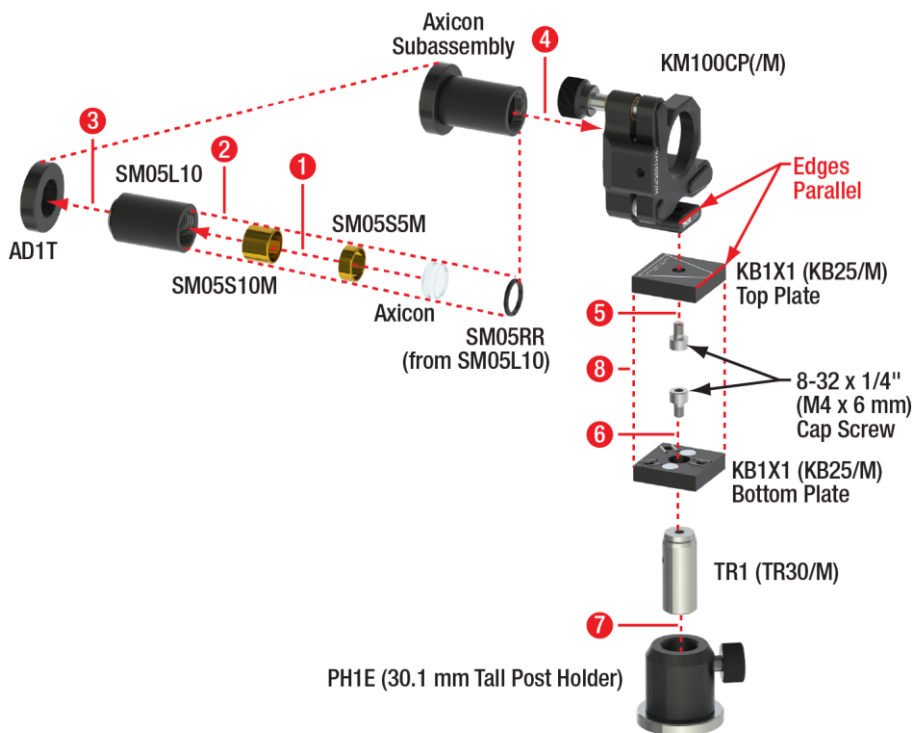


Figure 36 *Sketch of the Elements of the Axicon Component Before (Upper Image) and After (Lower Image) Assembly. The axicon angle is strongly exaggerated.*

- Assemble the BBO Crystal as shown on the left side of Figure 37.
- Please note:
 - During step 1, make sure to align the marked edges as parallel as possible.
 - Make sure to align the crystal with respect to the markings on the KM100CP(/M) mount as shown on the right side of Figure 37. Use the nylon-tipped screw of the KM100CP(/M) mount to hold the crystal in place.

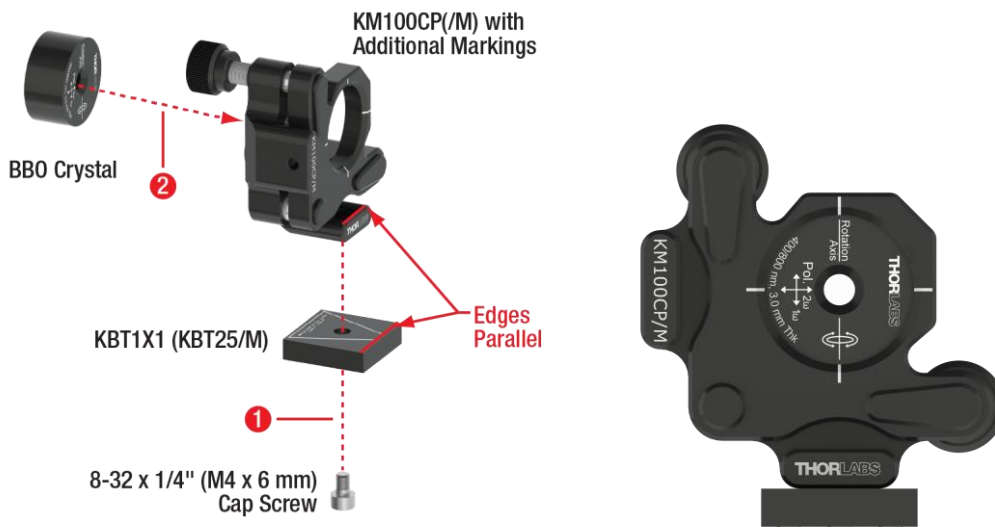


Figure 37 BBO Crystal Assembly

- Assemble the colored glass filter as shown in Figure 38.
- Please note:
 - During step 1, align the marked edges as parallel as possible.
 - During step 2, only touch the circumference of the glass filter; do not touch the filter surface. Use the nylon-tipped screw of the KM100CP(/M) mount to hold the filter in place.



Figure 38 Glass Filter Assembly

7.1.7 Beamsplitter

- Assemble the beamsplitters as shown in Figure 39.
- Please note:
 - Before step 4 on the left side of Figure 39, use a 0.05" (1.3 mm) hex key to tighten the locking screw of the SM1D12 iris. This avoids damaging the iris blades during step 4. Loosen the locking screw after completing the assembly.

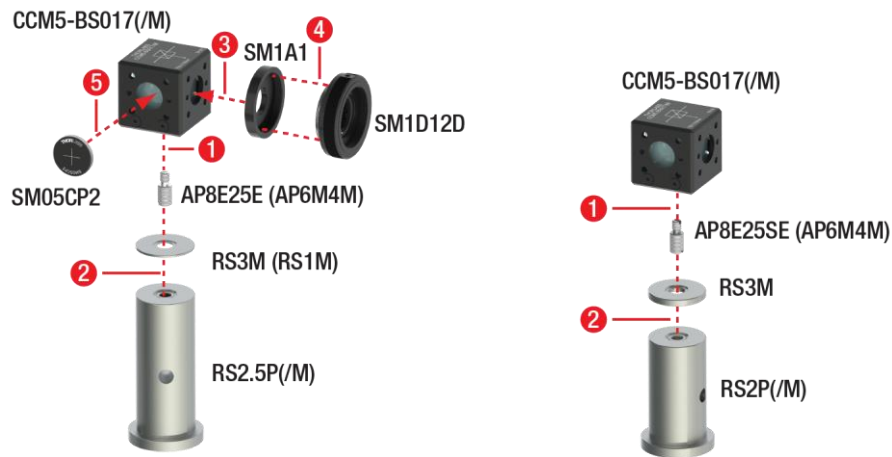


Figure 39 Beamsplitter Components

7.1.8 Detectors

- Remove the lens tubes from the three SPDMA detectors and assemble three detectors as shown on the left side of Figure 40.
- Please note:
 - After step 2, put a 5/64" (2 mm) ball driver through the hole in the TR2 (TR50/M) post and use it as a lever to strongly tighten the post against the SPDMA detector.
 - Use the flat head screwdriver to turn the gain screw of all three detector clockwise until a hard stop is reached (gain set to maximum), as seen on the right side of Figure 40.

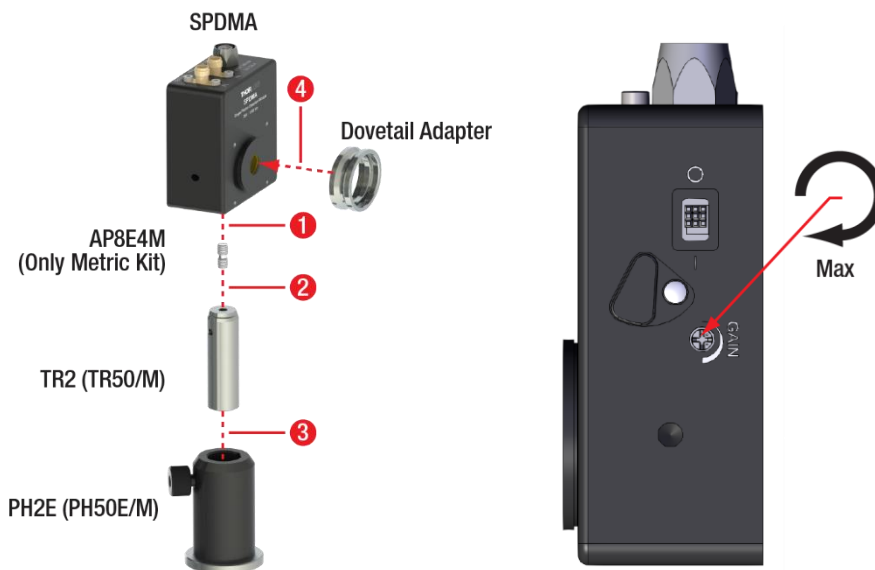


Figure 40 Detector Component (Build Three)

7.1.9 Detector Optics

- Assemble three detector optics as shown in Figure 41.
- Please note:
 - Before beginning the assembly, remove the SM05RR retaining ring from the SM1NR05 zoom housing and the SM1RR retaining ring from the SM1L05 lens tube.
 - During step 1, the convex side of the lens should face the SM1NR05 (see Figure 41). Only touch the circumference of the lens, do not touch the lens surface.
 - For step 2, use an SPW603 spanner wrench.
 - During step 4, the arrow on the filter mount should point towards the lens tube. Only touch the circumference of the filter, do not touch the filter surface.
 - For step 5, use an SPW606 spanner wrench.
 - Before step 6, tighten the locking screw of the SM1D12 iris with a 0.05" (1.3 mm) hex key. This avoids accidentally damaging the iris blades. Loosen the locking screw after step 6.
 - During steps 8 and 9, rotate the DTSM1 such that its locking screw is located between both kinematic screws of the CXY1A mount, as seen in the bottom figure of Figure 41. Use the SPW502 spanner wrench to lock the rotation by screwing the SM1NT1 towards the CXY1A mount.

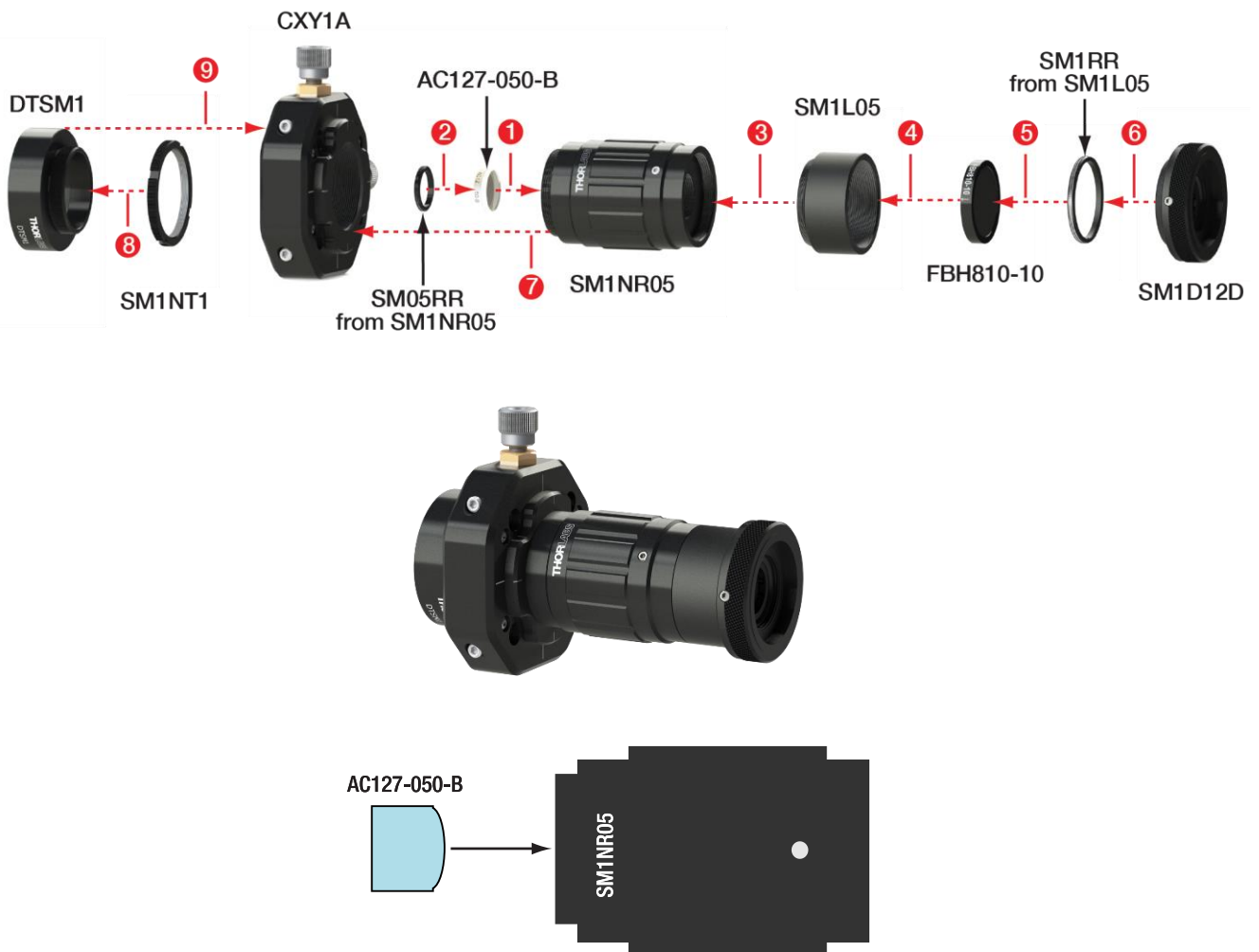


Figure 41 Exploded View (Top) and Assembled (Middle) Detector Optics Component (Build Three). The correct orientation of AC127-050-B lens in SM1NR05 zoom housing is shown on the bottom.

7.1.10 Beam Trap

- Assemble the beam trap as shown in Figure 42.
- Please note:
 - In step 1, screw the setscrew all the way into the SMR1(/M) mount. Use a 9/64" (3 mm) hex key.
 - Before step 3, use a 0.05" (1.3 mm) hex key to tighten the locking screw of the SM1D12 iris. This avoids damaging the iris blades during step 3. Loosen the locking screw after completing the assembly.



Figure 42 Beam Trap Component

7.1.11 Alignment Target

- Unscrew the retaining ring from an LMR1(/M) lens mount and assemble the alignment target as shown in Figure 43.
- For step 4, use an SPW606 spanner wrench.

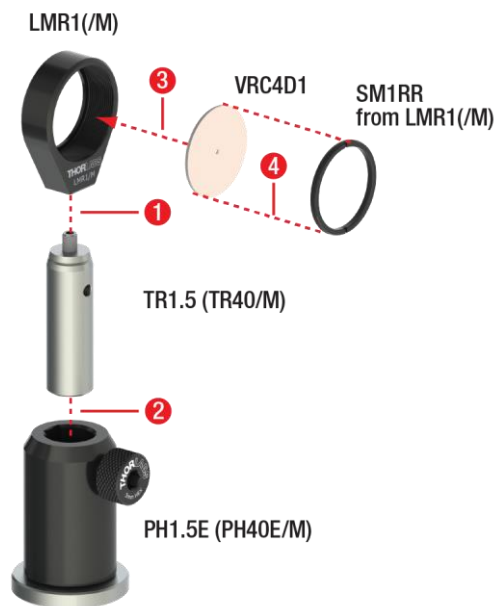


Figure 43 Alignment Target Component

7.1.12 Economy Beamsplitter

- Remove the retaining ring from an SM1L03 lens tube and assemble the economy beamsplitter as shown in Figure 44.
- Please note:
 - Only touch the circumference of the beamsplitter. Do not touch the beamsplitter surface.
 - For step 2, use an SPW606 spanner wrench.



Figure 44 Economy Beamsplitter Component

7.1.13 Screen

- Assemble the screen as shown in Figure 45.

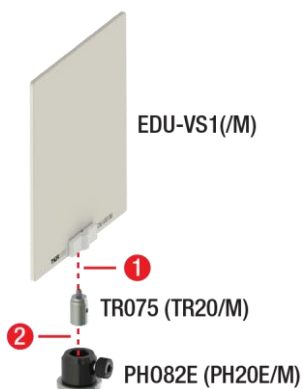


Figure 45 Screen Component

7.1.14 Mirrors for Michelson Interferometer

- Assemble the mirror on the stage as shown in Figure 46.
- Please note:
 - During step 2, make sure that you are using the correct screw length. Longer screws may damage the stage!
 - During steps 2 and 3, make sure that the edges marked in Figure 46 are aligned as parallel as possible.
 - During step 4, only touch the circumference of the mirror, do not touch the mirror surface. Use the nylon-tipped screw of the KM100 to hold the mirror in place.

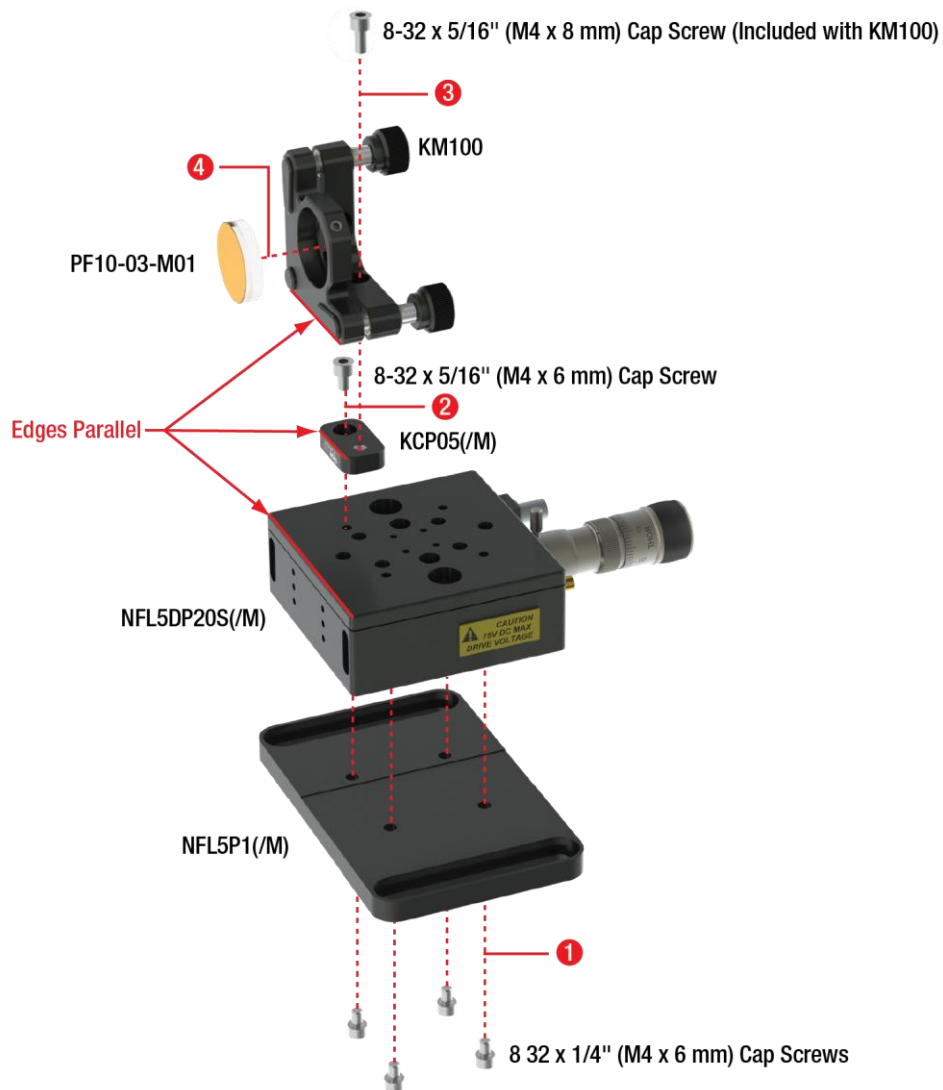


Figure 46 First Mirror for Michelson Interferometer

- Assemble the second mirror for the Michelson interferometer as shown in Figure 47.
- Please note:
 - During step 2, only touch the circumference of the mirror, do not touch the mirror surface. Use the nylon-tipped screw of the KM100 to hold the mirror in place.

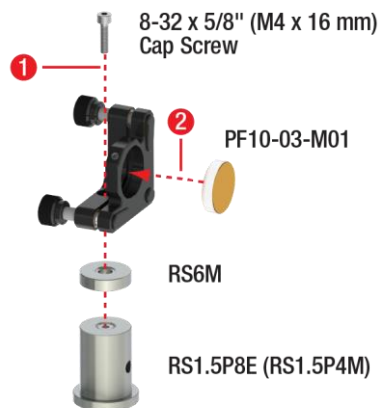


Figure 47 *Second Mirror for Michelson Interferometer*

7.1.15 Lens

- Unscrew the retaining ring from an LMR1(/M) lens mount and assemble the alignment lens as shown in Figure 48.
- Please note:
 - During step 3, make sure to touch the lens only on the outer circumference. Do not touch the lens surface.
 - For step 4, use an SPW606 spanner wrench.



Figure 48 *Lens Component*

7.1.16 Mounting the LED

- Assemble the LED as shown in Figure 49.
- Please note:
 - During step 3, take care of the polarity of LED and mount. The correct orientation is shown in Figure 50.



Figure 49 LED Assembly



Figure 50 Polarity of LED

7.1.17 Polarizers for Quantum Eraser

- Remove the retaining ring from an RSP1D(M) mount and assemble a polarizer component as shown in Figure 51.
- Please note:
 - During step 1, use a 5/64" (2 mm) hex key to screw the setscrew as far into the RSP1D(/M) mount as possible.
 - During step 3, make sure to touch the polarizer only on the outer circumference. Do not touch the polarizer surface.
 - During step 4, use an SPW606 spanner wrench.



Figure 51 Large Polarizer Assembly

- Remove the retaining rings from two RSP1D(M) mounts and assemble two polarizer components as shown in Figure 52.
- Please note:
 - During step 1, use a 5/64" (2 mm) hex key to screw the setscrew as far into the RSP1D(/M) mount as possible.
 - The SM1A6T adapter contains two retaining rings. Instead of removing them both and then do step 3, just remove only one.
 - During step 4, make sure to touch the polarizer only on the outer circumference. Do not touch the polarizer surface.
 - During step 5, use an SPW603 spanner wrench.
 - During step 6, use an SPW909 spanner wrench.

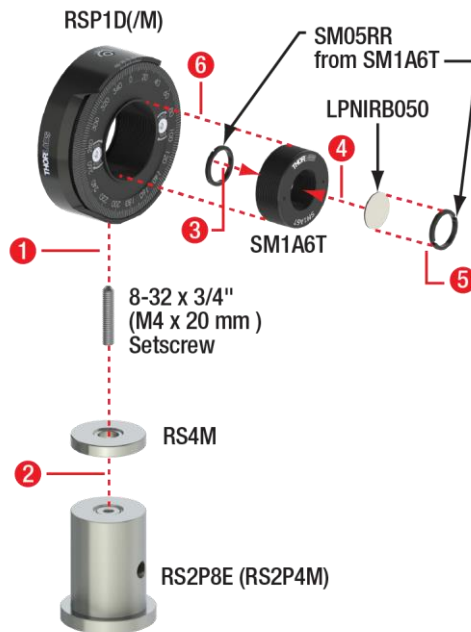


Figure 52 Small Polarizer Assembly

7.1.18 Labelling the Time Tagger

- Use the label sheet to label the first three channels of the Time Tagger as shown in Figure 53.
 - Channel 1 → T
 - Channel 2 → A
 - Channel 3 → B



Figure 53 Time Tagger Labels

- Label the three detectors with labels T, A, and B, respectively as shown for detector B in Figure 54. Labeling is optional, however in the remainder of this manual we will refer to the detectors as “detector T,” etc.



Figure 54 **Detector Labeling**

7.2 Preliminary Alignment

7.2.1 Software Installation

- Install the software of the kit as described in Section 11.1.

7.2.2 Collimating the Pump Laser

- Place the pump laser on the left side of the breadboard pointing to the right and secure its position with a CF125 clamp and a 1/4"-20 x 3/8" (M6 x 10 mm) cap screw plus washer. Connect the power supply coming with the LDM9T(/M) to the laser mount.
- Remove the KLD101 laser controller from its baseplate by opening the clamps. Mount the baseplate to the breadboard on the position marked in Figure 55 via two 1/4"-20 x 3/8" (M6 x 10 mm) cap screws plus washers. Connect the KLD101 controller to the baseplate and close the clamps.

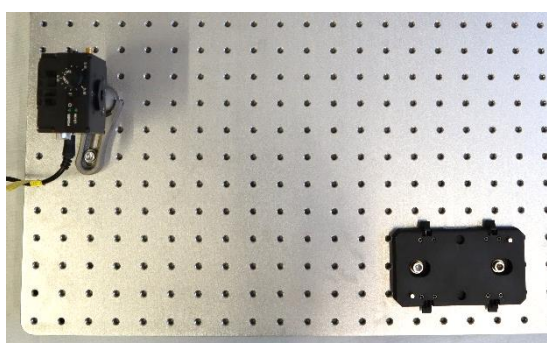


Figure 55 **Position of KLD101 Baseplate**

- Connect the KLD101 laser controller to the power grid via the TPS002 power supply and to the LDM9T(/M) mount via the CAB400 cable. Switch on both the laser mount and driver.
- Use the wheel menu of the KLD101 controller to select **2: Polarity** and make sure that the setting is **Cathode Grounded**.
- Use the wheel menu of the KLD101 controller to select **3: Max Current** and set the maximum current to 50 mA, as seen in Figure 56.



Figure 56 Maximum Current Setting for the KLD101 Controller

- Turn the key on the KLD101 controller and set the laser current to 15 mA by turning the wheel on the controller.
- In the next step, the laser will be switched on. **You should always wear laser safety glasses when the pump laser is turned on!** Hold a sheet of white paper in front of the laser and press the *Enable* button on the KLD101. If the pump laser hits white paper, the paper will show green fluorescence that can be seen through the glasses.
- You will see some super-luminescent light, but not yet lasing. Carefully increase the laser current until the intensity jumps to a higher level. You have now crossed the laser threshold. Use this setting for beam alignment. You can use the datasheet that ships with your laser diode as a reference for the threshold current.
- Fix one of the alignment cards that are included with the controllers to the front of the screen component and position it about 20 cm to the right of the laser, as seen in Figure 57. The laser should now hit the screen, as seen in Figure 58. If you do not see any light on the screen, the laser is too divergent. In this case, move the screen closer until you see the laser.

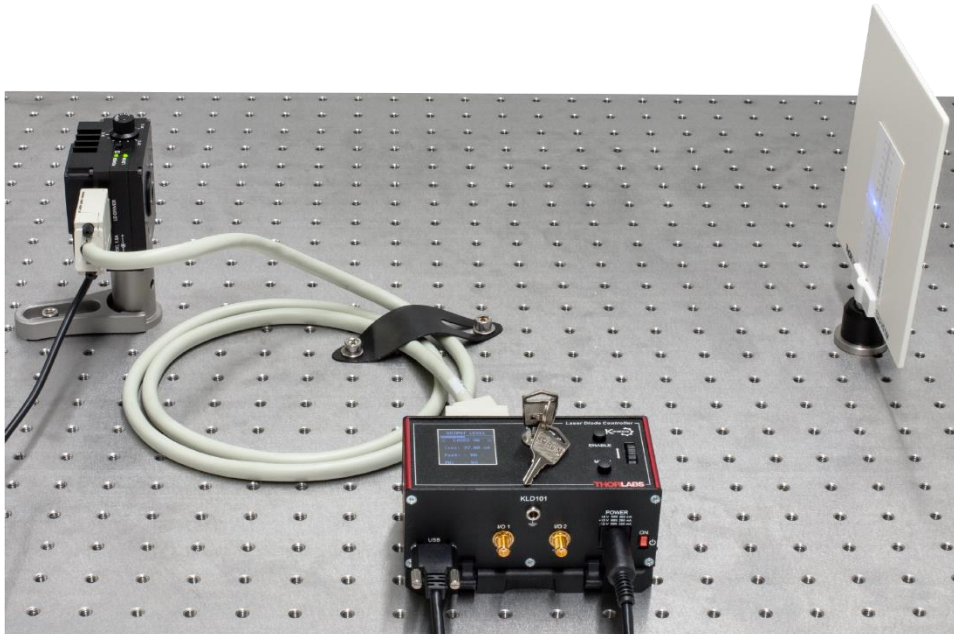


Figure 57 Basic Collimation Setup



Figure 58 Laser on Screen Before Collimation

- Use the SPW909 spanner to rotate the lens adapter in front of the pump laser clockwise to change the lens position, decreasing the laser divergence until the laser on the screen looks like the one in Figure 59.

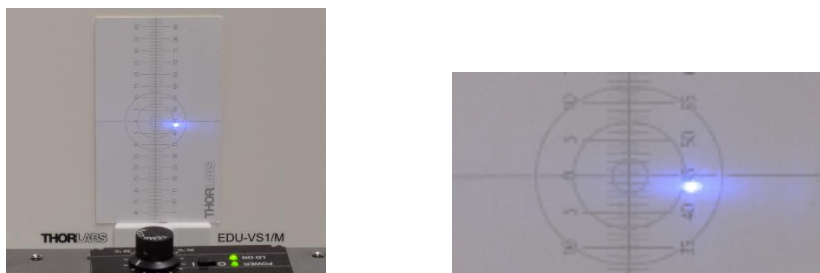


Figure 59 Laser Spot on Screen After Collimation (Left) and Zoomed View (Right)⁵⁴

- Increase the distance between screen and laser by about 30 cm and check if the spot size on the screen changes in the process. Adjust the lens position to achieve a uniform beam profile over the whole distance from laser to screen, i.e., a collimated beam. Make sure that there is no focus between the laser and the screen. If there is one, you did not move the lens close enough to the diode. In that case, turn the adapter clockwise a bit more.
- Sometimes, the laser diode emits at a small angle. In this case you might not be able to hit the screen at larger distances because the beam height becomes too high or low. If that happens, turn the laser so that it emits in direction of the far breadboard edge and use a mirror angled at 45° to reflect the laser towards the screen⁵⁵. You can now correct the beam deviation with the kinematic screws of the mirror so that the beam has a constant height after the mirror and is visible on the screen, as seen in Figure 60.



Figure 60 Collimation Setup for Compensation of Deviating Emission Angle

- Once you achieve a similar spot size on the screen directly after the laser and in 30 cm distance, move the screen all the way across the breadboard. Fine-tune the lens adapter on the laser mount until you see a laser spot like the one in Figure 59 over the whole path.

⁵⁴ This photo was taken with a camera. If you wear the laser safety goggles (as you should at this point!) the laser spot will look slightly different in color and brightness.

⁵⁵ Alternatively, you can slightly offset the front plate of the laser diode mount by loosening (not unscrewing) the 4 screws that hold it. This slightly moves the collimating lens in relation to the diode and may improve the angle deviation as well as the beam profile (more symmetric). Retighten the screws after you have found a suitable front plate position.

- Switch off the laser driver and laser mount.
- Move the pump laser (in the LDM9T(/M) laser mount) to the 10th breadboard hole from the left and the 5th breadboard hole from the front, pointing towards the left edge of the breadboard as shown in Figure 70. Secure it with a CF125 clamp and a 1/4"-20 x 3/8" (M6 x 10 mm) cap screw plus washer. Use CS1 cable straps and 1/4"-20 x 1/4" (M6 x 6 mm) cap screws plus washers to secure the power cable and the CAB400 to the breadboard as shown in Figure 70.

7.2.3 Calibrating the Polarizer

The goal of this procedure is to ensure that the scale of the Ø1" polarizer is calibrated⁵⁶.

- Position the alignment laser on the left side of the breadboard, pointing to the right. Secure its position with a CF125 clamp and a 1/4"-20 x 3/8" (M6 x 10 mm) cap screw plus washer. Connect the USB cable of the alignment laser to a PC or to the power grid via the DS5 power adapter. Switch on the alignment laser.
- Position the polarizer with the 1" diameter in the alignment laser beam path and put the screen component behind the polarizer, as seen in Figure 61.

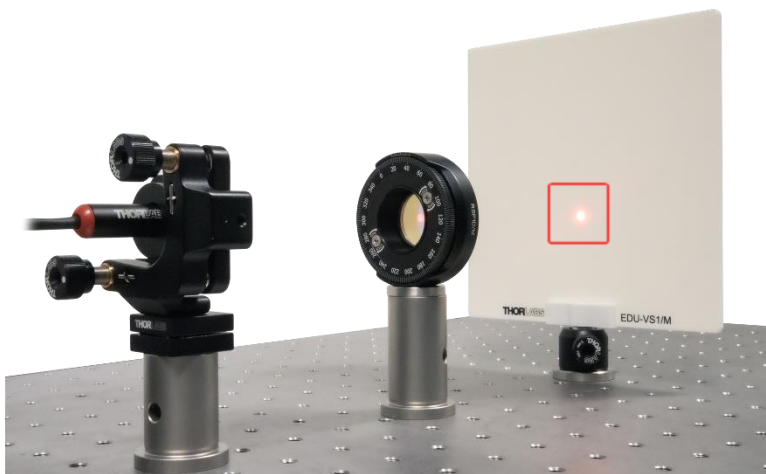


Figure 61 Initial Position for Polarizer Calibration

- Rotate the polarizer until the intensity on the screen is minimized and note the value on the polarizer scale (122° in the example in Figure 62).

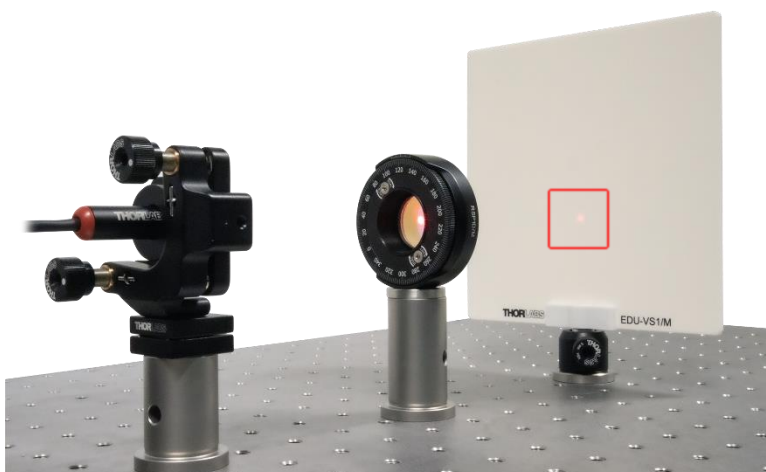


Figure 62 Polarizer after Minimizing Transmission

- Switch the front and back sides of the polarizer component, as seen in Figure 63.

⁵⁶ A video detailing the process is available at: https://www.thorlabs.com/newgrouppage9.cfm?objectgroup_id=14062#VideoPolarizerHVAAlign

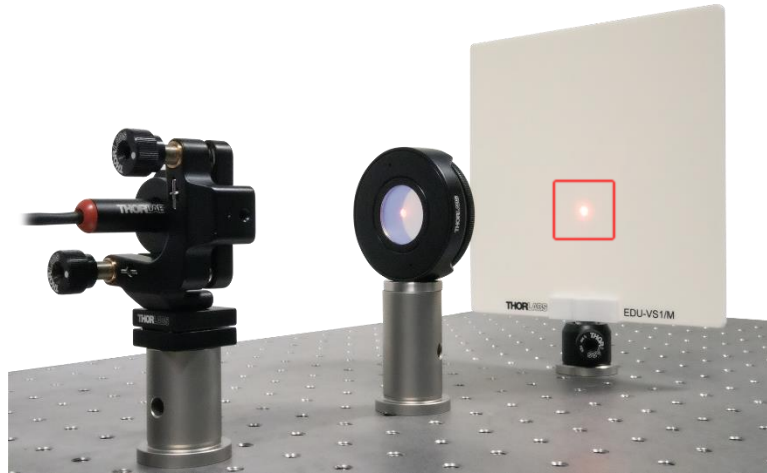


Figure 63 Polarizer after Rotation

- Rotate the polarizer until the intensity on the screen is minimized and note the value on the scale.
- Rotate the polarizer to the position exactly in the middle of the two scale values you noted, then tighten the locking screw of the rotation mount.
- Loosen the two screws on the front face of the rotation mount and rotate the scale until the current position is 0°. Retighten the two screws.
- You have now aligned this polarizer to be oriented either perpendicular or parallel to the table plane in the 0° setting. You will later determine which of the two directions it is.
- Figure 64 shows a schematic of this method and why it ensures that the polarizer is s- or p-polarized.

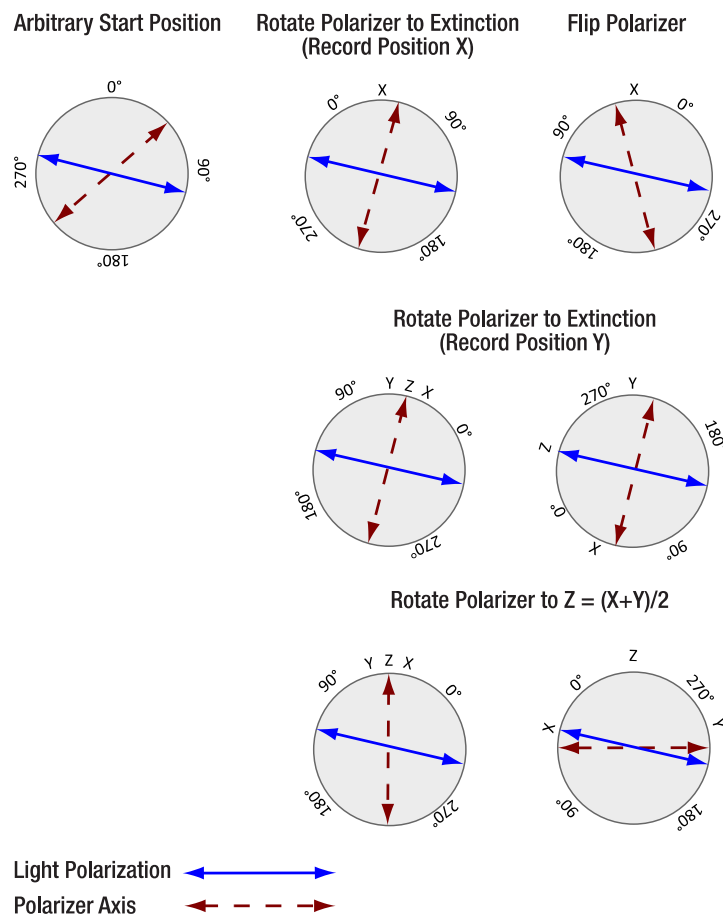


Figure 64 Schematic of the Polarizer Calibration Procedure

7.3 Setting Up the HBT Experiment with the Alignment Laser

As a first experiment, it is recommended to show that an attenuated laser is not suitable as a single photon source. The experimental setup is shown schematically in Figure 65.

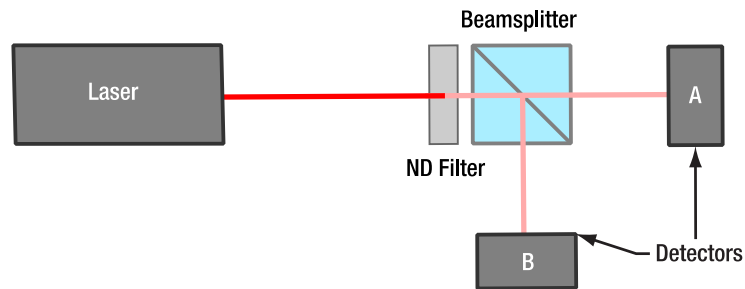


Figure 65 Schematic of the HBT Experiment with the Alignment Laser

Set this experiment up as follows:

- Place the alignment laser component on the left side of the breadboard, pointing towards the right side. Secure it with a CF125 clamp and a 1/4"-20 x 3/8" (M6 x 10 mm) cap screw plus washer.
- Place the beamsplitter component with the attached iris aperture in the beam path of the alignment laser, about 20 cm away (iris facing the laser).
- Position the alignment target halfway between the alignment laser and the beamsplitter.
- Switch on the alignment laser and move the alignment target until the hole is hit by the laser.
- Move and rotate the beamsplitter until the laser passes the center of the iris **and** the reflection from the beamsplitter passes back through the hole in the target⁵⁷. Secure the beamsplitter with a CF125 clamp and a 1/4"-20 x 3/8" (M6 x 10 mm) cap screw plus washer.
- Connect the lens tube with the economy beamsplitter to the detector labeled "A." Position the detector in the transmission path of the beamsplitter, about 20 cm away.
- Place the alignment target about 10 cm in front of the detector so that the laser passes through the hole. Now adjust the height, position, and angle of the detector in such a way, that **both**:
 - The reflection from the beamsplitter passes back through the hole of the target.
 - The light passing the hole of the target is centered on the detector chip, as seen in Figure 66.



Figure 66 Laser Spot Centered on Detector Chip (Shown without Economy Beamsplitter)

⁵⁷ In case the alignment laser does not emit a beam parallel to the table plane, the reflection of the beamsplitter may always be above or below the hole in the target. In this case, use the upper adjuster of the laser mount to roughly align the laser parallel to the table plane.

- Figure 67 shows the back side of the target before alignment. The clear red spot is the reflection from the beamsplitter. There can be a diffuse red spot which is the reflection from the detector chip and can be ignored.

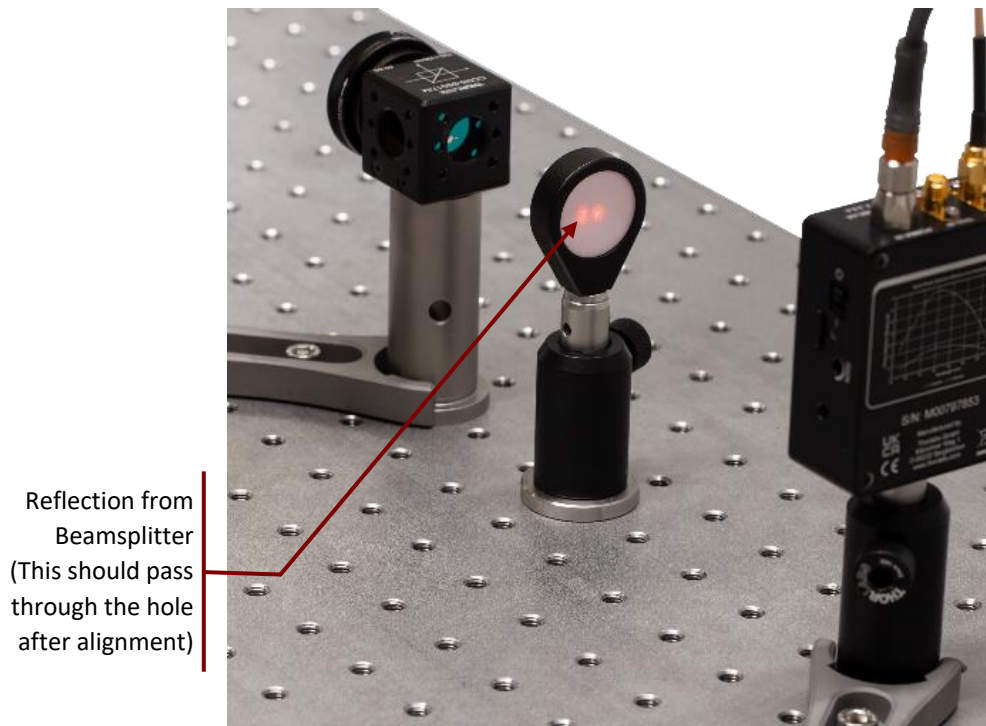


Figure 67 Back Side of the Alignment Tool Prior To Detector Alignment

- Secure the position of the detector with a CF125 clamp and a 1/4"-20 x 3/8" (M6 x 10 mm) cap screw plus washer. Then remove the lens tube with the beamsplitter from the detector.
- Repeat the same procedure with the detector labeled "B" in the reflection path of the beamsplitter.
- Screw the NE30A neutral density filter on the iris aperture.
- Take one of the prepared detector optics and loosen the locking screw of the DTSM1 dovetail adapter almost completely. Slide it over the dovetail adapter on the front of the detector labeled "A." Rotate the optics until one of the adjusters is pointing straight upwards and the other one is pointing away from you. Then tighten the locking screw of the DTSM1 coupler to securely connect the optics to the detector.
- Repeat this step for the detector labeled "B."
- Connect the detectors to the power grid via the included power supplies.
- Place the Time Tagger on the breadboard and connect **detector A to channel 2 and detector B to channel 3 of the tagger** via SMA-to-SMA cables.
- Connect the Time Tagger to your PC via the included USB cable and start the software.
- You might see very high count rates of both detectors in the software because of the ambient light. It may also be that you see no count rates at all because the Time Tagger is saturated.
- Darken the room as much as possible (switch off all lights, shutter windows if existing, and turn other light sources, such as computer screens, away from the setup). The count rates should now be significantly below 50 kHz⁵⁸. If they are higher, the room needs to be darkened further⁵⁹.

⁵⁸ The count rates of the two detectors may be different, e.g., because some stray light source, such as a computer screen, illuminates one more than the other. This is not a problem if both count rates are below the 50 kHz threshold.

⁵⁹ If further darkening is not possible, take note of the tips at the end of Section 13.2 for dealing with large background signals.

- Rotate the zoom housing of the left detector (when looking from the perspective of the filter) to about the middle of its range (test how far it can be turned in both directions and then try to turn it halfway from one endpoint). Now turn one of the differential screws of the CXY1A mount in both directions until you observe a significant increase in the count rate of detector A in the software. If you see such a signal increase, then maximize the signal. If you do not see a signal increase, return the screw to the center position (align the marks on the front side of the CXY1A mount) and try the other differential screw⁶⁰.
- Once you found the maximum in one axis, optimize further with the other differential screw.
- Once you have maximized the count rate via the differential screws, carefully turn the zoom housing again to further increase the count rate. Afterwards, you may be able to increase the count rate further via slight changes of the differential screws. Iteratively turn the zoom housing and the screws until you have reached a stable maximum count rate. This should be at least 150 kHz with alignment iris and detector apertures completely open.
- Repeat the prior two steps for the second detector, this time maximizing the count rate for detector B in the software. You should reach a similar count rate as for detector A⁶¹.
- The setup is now complete and should look like Figure 68. You can now perform the HBT experiment for the alignment laser; see Section 9.1 for more details.

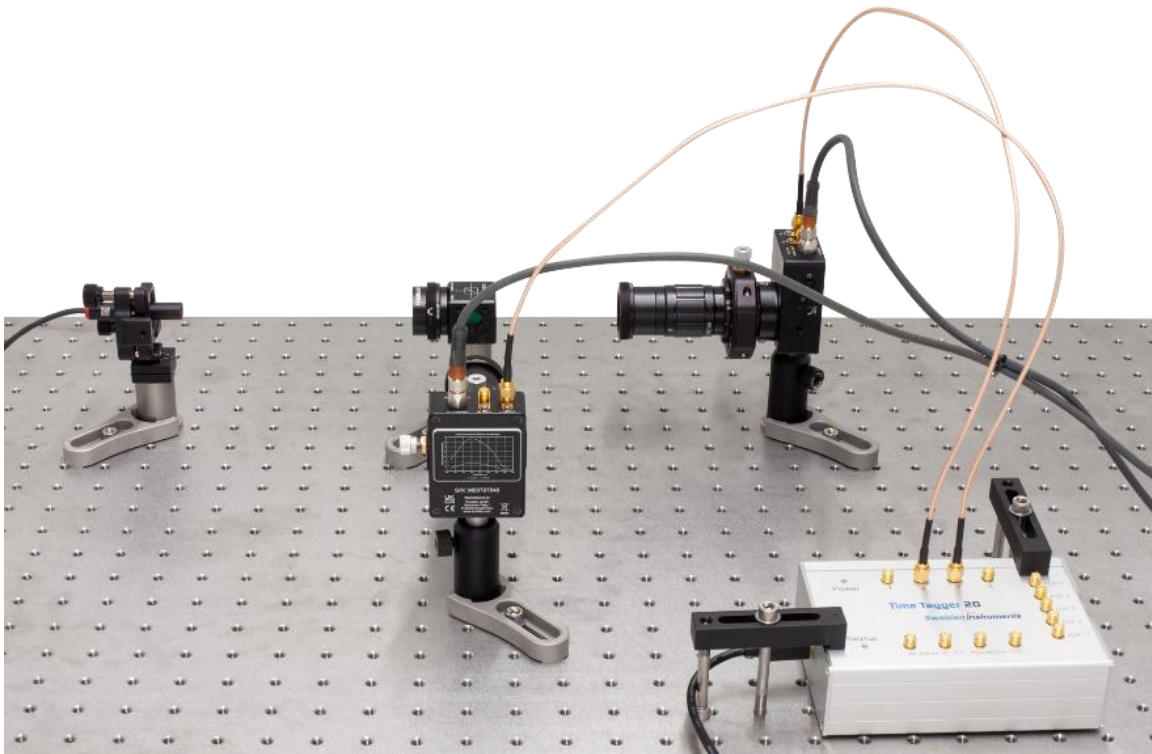


Figure 68 HBT Setup after Detector Placement

⁶⁰ Sometimes, it seems like the count rate keeps increasing in one turning direction of the screw until the end of travel is reached, because more stray light is reaching the detector from that direction. This is not the goal of the adjustment process. You can check this by turning the laser off. If the signal does not decrease significantly then you have optimized only for stray light. In this case, turn the screw back to the center position and try to find the actual signal (resulting in a much stronger and steeper count rate increase) via adjusting the other screw or the zoom housing.

⁶¹ Again, slightly different count rates are not problematic, one detector might be slightly more efficient than the other or capture more stray light, resulting in an offset. Larger differences (like a factor of 2) point to one detector alignment being not fully optimized.

7.4 Setting Up the Photon Pair Source

In this Section, the photon pair source is set up. This source forms the basis of all quantum optic experiments in this kit. In Figure 69, an overview of the photon pair setup is given. The following subsections include detailed instructions for the placement and adjustment of the components.

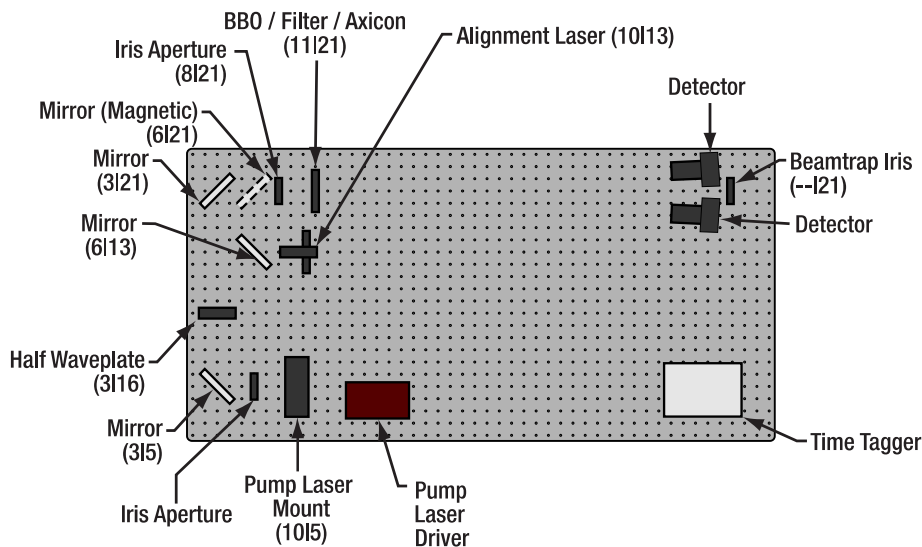


Figure 69 Overview of the Pair Source Setup. The numbers in parentheses are breadboard hole numbers (from left / from bottom). Components are not to scale and exact positions may deviate slightly from those given in text.

7.4.1 Setting up the Pump Laser Beam Path

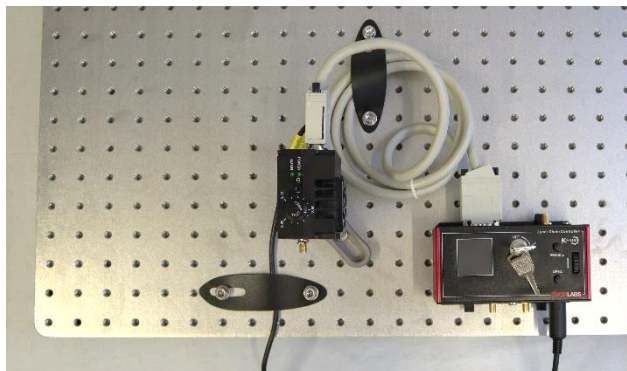


Figure 70 Positioning of Pump Laser and Driver

- If you followed the procedure in Section 7.2.2, the pump laser is already at the correct position on the breadboard. If your laser was already collimated for you and you skipped Section 7.2.2, then position it according to the last bullet point there (10th breadboard hole from the left, 5th hole from the front, laser pointing to the left).
- Position the mirror component in the PH1E (PH30E/M) post holder to the left of the pump laser (3rd breadboard hole from the left, 5th from the front). The mirror should be angled at about 45°, so that the laser will be reflected towards the far edge of the breadboard. Secure the mirror with a CF125 clamp and a 1/4"-20 x 3/8" (M6 x 10 mm) cap screw plus washer. Place the screen in the expected beam path of the laser after the mirror, as seen in Figure 71.

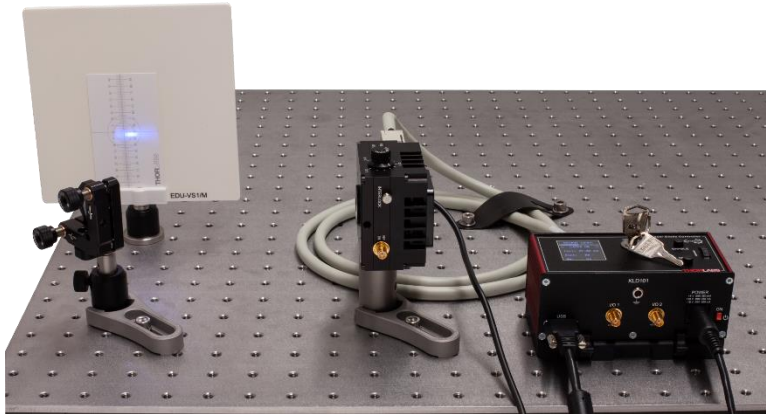


Figure 71 Setup after Placement of First Pump Laser Mirror

- Switch on the LDM9T(/M) mount. Set the temperature knob to 25°C.
- Switch on the KLD101 driver and set the laser current to 15 mA. Switch on the pump laser via the button on the KLD101 driver. **Be sure to always wear laser safety glasses when working with the pump laser!** Follow the beam path of the laser with a sheet of white paper and increase the laser current until the laser threshold is surpassed (brightness of the spot increases sharply).
- Loosen the clamp of the laser mount and rotate it carefully to horizontally center the beam on the mirror, then secure the clamp again.
- Adjust the height of the mirror to vertically center the laser on the mirror.
- Switch off the pump laser and position the $\varnothing 15.0$ mm iris between the laser and the first mirror. Switch on the laser and adjust the position and height of the iris until the laser is centered on the iris. Here, it can be helpful to close the iris and hold a sheet of paper behind it. Adjust the iris aperture so that only the center of the laser profile is passing, and divergent stray radiation is blocked, as seen in Figure 72. This aperture will be used for all following adjustment steps and experiments. It should never be changed from now on, so that stray light from the laser diode cannot inadvertently influence experiments.



Figure 72 Beam Profile of the Pump Laser in Front of (Left) and Behind (Right) the Beam Cleaning Iris

- Switch off the pump laser. Place a second mirror component (with a KCP1(/M) centering plate but without a magnetic mount) on the 21st breadboard hole from the front and the 3rd from the left. It should be angled 45° to reflect the laser towards the right edge of the breadboard. Secure the mirror with a CF125 clamp and a 1/4"-20 x 3/8" (M6 x 10 mm) cap screw plus washer. Move the screen to block the expected beam path of the laser after the second mirror, as seen in Figure 74.
- Switch on the pump laser again and follow the beam with a sheet of paper. The beam should hit the center of the second mirror. Correct deviations to the left or right by either turning the lower kinematic screw of the first mirror (small deviations) or by loosening the CF125 clamp of the first mirror and turning the whole mirror component before securing it again (larger deviations). Correct deviations in the vertical axis via the upper kinematic screw of the first mirror.

- The cards included in the K-Cube controller packages can be used to see the laser spot while centering the beam on the mirror, as shown in Figure 73.

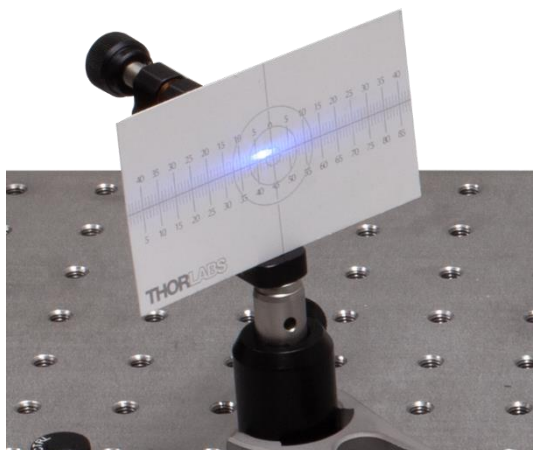


Figure 73 **Alignment on The Mirror**

- Place the WPH10ME-405 half-wave plate between the two mirrors on the 16th breadboard row from the front so that the laser hits the wave plate in the center and under normal incidence, as seen in Figure 74. Secure the wave plate position with a CF125 clamp and a 1/4"-20 x 3/8" (M6 x 10 mm) cap screw plus washer. Set the wave plate to 45°.

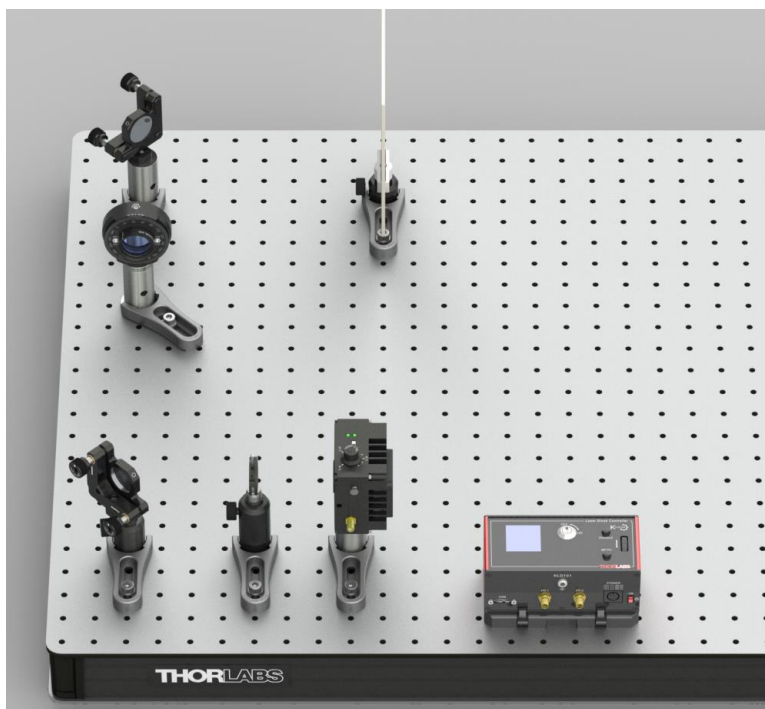


Figure 74 **Setup During Coarse Alignment of Pump Laser**

- Switch off the pump laser. It is now roughly aligned. It will be aligned more precisely in a later step.

7.4.2 Aligning Both Pump and Alignment Laser on the Same Path

- Place the Alignment Laser on the 10th breadboard hole from the left and 13th from the front, pointing towards the left edge of the breadboard as shown in Figure 75. Secure its position with a CF125 clamp and a 1/4"-20 x 3/8" (M6 x 10 mm) cap screw plus washer.
- Connect the USB plug of the alignment laser to either a PC/laptop or to the power grid via the DS5 power supply. To switch on the laser, press the small button on the red USB plug.

- Place a mirror (with a KCP1(/M) mount, without a magnetic base) on the 6th breadboard hole from the left and 13th from the front. It should be angled by 45°, so that the alignment laser is reflected towards the far edge of the breadboard. Fix its position with a CF125 clamp via a 1/4"-20 x 3/8" (M6 x 10 mm) cap screw plus washer.
- The alignment laser beam should be centered on the newly placed mirror. If that is not the case, use the lower kinematic screw of the alignment laser to adjust the beam position.
- Place the mirror with the magnetic base on the 6th breadboard hole from the left and the 21st from the front. Angle it by 45°, so that the alignment laser is reflected towards the right edge of the breadboard. Fix its position with a CF125 clamp via a 1/4"-20 x 3/8" (M6 x 10 mm) cap screw plus washer (the long end of the clamp should point towards the first alignment laser mirror). The setup should now look like Figure 75.

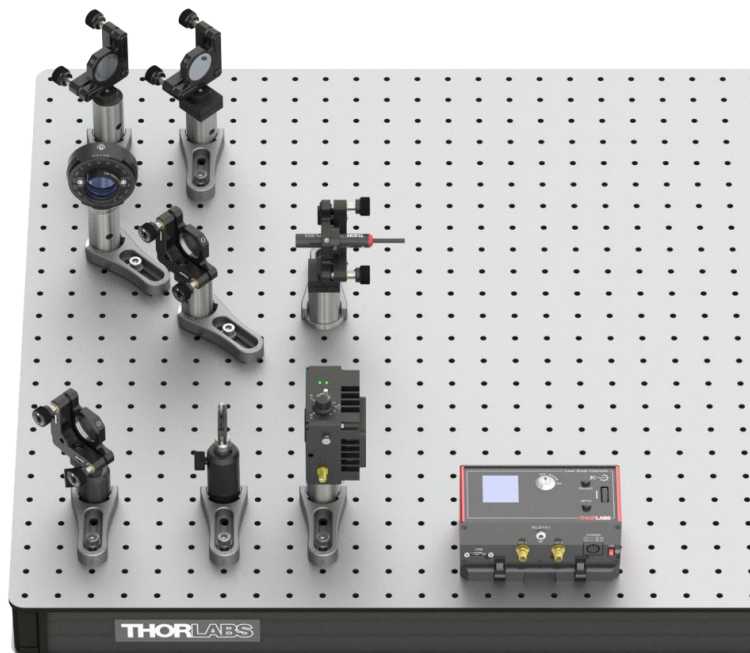


Figure 75 **Setup with Alignment Laser**

- The alignment laser beam should be centered on the newly placed mirror. If that is not the case, use the kinematic screws of the first mirror in the alignment laser beam path to adjust the beam position. In case of large deviations in the horizontal axis, you might need to loosen the CF125 clamp of the first mirror temporarily to rotate the whole mirror component (do not move it laterally).
- Place the beam trap iris on the 21st breadboard hole row from the front and on the 4th hole from the right edge of the breadboard. The iris should point towards the second mirror. The precise centering on the hole row is especially important for this element. Secure the iris position with a CF125 clamp and a 1/4"-20 x 3/8" (M6 x 10 mm) cap screw plus washer.
- The alignment laser should be centered on the beam trap iris. Use the kinematic screws of the second mirror in the alignment laser beam path to adjust. In case of large deviations in the horizontal axis, you might need to loosen the CF125 clamp of the second mirror temporarily to rotate the whole mirror component (do not move it laterally).
- Place the ID25(/M) iris on the 21st breadboard hole row from the front and the 8th hole from the left. The precise centering on the hole row is especially important for this element. Secure the iris position with a CF125 clamp and a 1/4"-20 x 3/8" (M6 x 10 mm) cap screw plus washer (long end of the clamp should point towards the front edge of the breadboard). This iris will be called "alignment iris" in the following. The setup should now look like Figure 76.

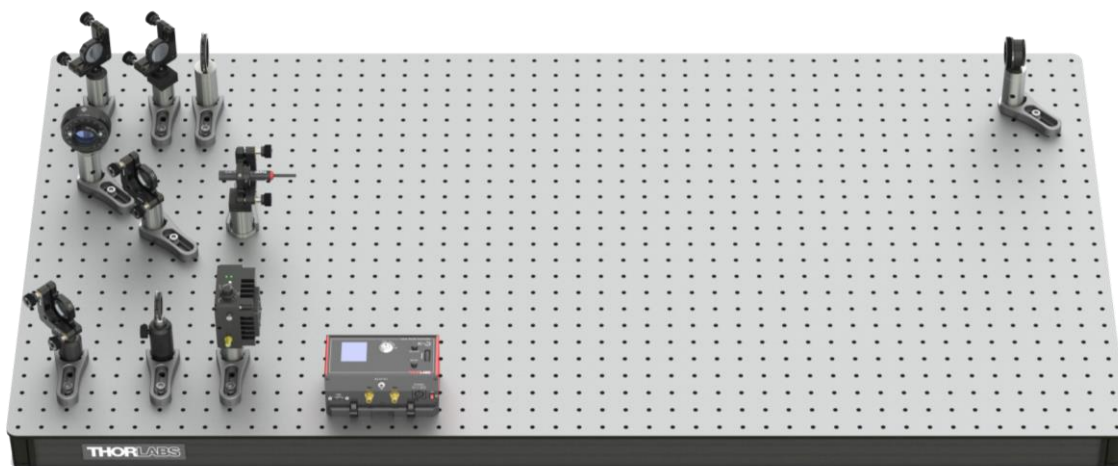


Figure 76 Setup for Beam Alignment

- The next step is to align the alignment laser through both irises on the 21st hole row. This can be achieved by a so called beamwalk⁶² which is described in the following:
 - Close the alignment iris nearly completely.
 - Use the kinematic screws of the first mirror in the alignment laser beam path to center the beam on this iris. Then open it.
 - Close the beam trap iris nearly completely.
 - Use the kinematic screws of the second mirror in the alignment laser beam path to center the beam on the beam trap iris.
 - Repeat all the above steps iteratively until the alignment laser is centered on both iris apertures as shown in Figure 77.

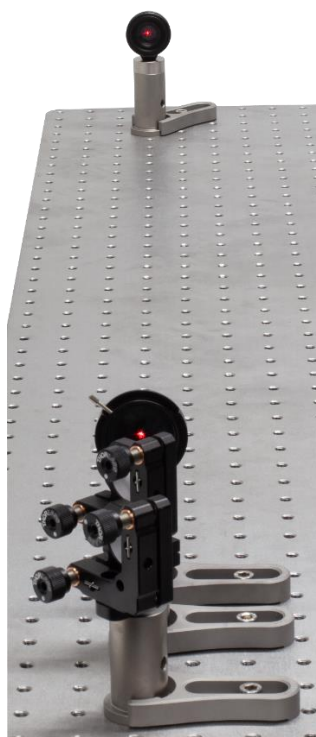


Figure 77 Beam Path after Successful Beamwalk

⁶² For more details and a video, see https://www.thorlabs.com/newgrouppage9.cfm?objectgroup_id=14221

- Switch off the alignment laser and remove the mirror from the magnetic base.
- The next step is to align the pump laser on the exact same beam path as the alignment laser, as defined by the two iris apertures. **Remember to wear laser safety glasses when working with the pump laser!**
- Switch on the pump laser and repeat the beamwalk as described above. Again, use the first mirror to center on the alignment iris and the second mirror to center on the beam trap iris. As the pump laser is not easily visible on the iris apertures, use a sheet of paper to help. It can also be helpful to watch the beam behind the iris apertures to better see if it is centered. Remove the end cap of the beam trap for this step (as seen in Figure 78) but return it afterwards.

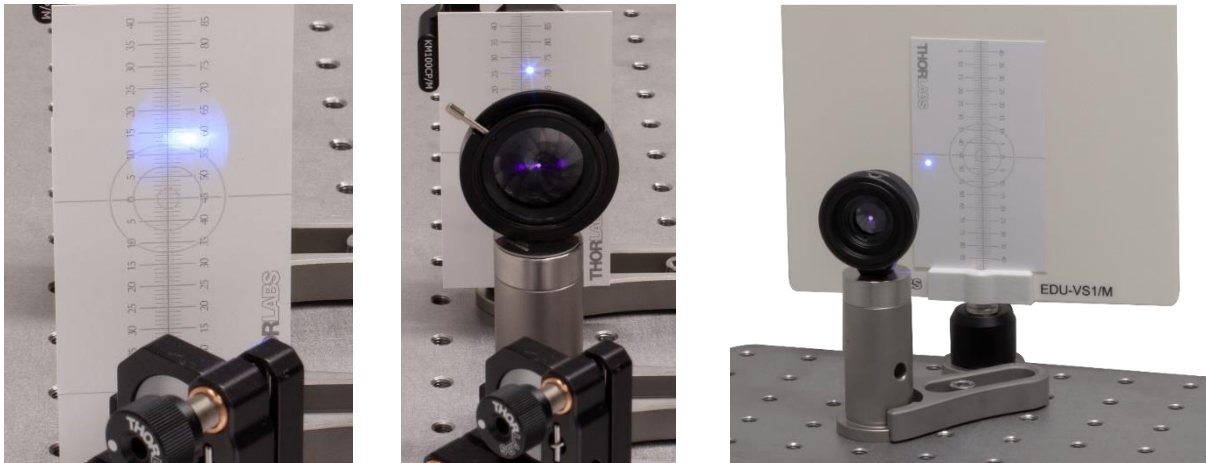


Figure 78 *Beamwalk for the pump beam path. From left to right: rough alignment with card in front of iris, test fine alignment with card behind iris, and beam trap with end cap removed and EDU-VS1(/M) viewing screen behind it.*

- Switch off the pump laser. You have now aligned the beams of the pump laser and the alignment laser to the exact same beam path. This is immensely helpful as you can adjust all remaining optical elements with the alignment laser instead of the pump laser, which is both easier and safer. You can switch between the two lasers via the mirror on the magnetic base (Mirror in = Alignment, Mirror out = Pump).

7.4.3 Detector Positioning

- Put the mirror on the magnetic base back into the setup and open the alignment iris completely.
- Place the fluorescent alignment target between the alignment iris and the beam trap and adjust its height so that the beam is centered on the hole in the target. Remove the target.
- Place the screen about halfway between the alignment iris and the beam trap.
- Place the post holder with the magnetic plate and the axicon on the 21st breadboard hole from the front and the 11th from the left. The lens tube should point towards the mirror, as seen in Figure 80.
- Switch on the alignment laser. You should see parts of a circle on the screen as shown on the left side of Figure 79.
- Now adjust the height and position of the axicon until the circle on the screen shows evenly distributed intensity around the entire circle, as shown on the right side of Figure 79. Secure the position of the axicon with a CF125 clamp and a 1/4"-20 x 3/8" (M6 x 10 mm) cap screw plus washer.



Figure 79 Axicon Pattern Before (left) and After (right) Alignment

- It is important that the alignment laser hits the axicon under normal incidence. To ensure this, close the iris in front of the axicon almost completely and watch the reflection of the axicon on the back side of the iris as shown in Figure 80. Use the adjusters of the axicon holder to center the reflection on the iris. This may change the pattern on the screen. Iteratively, adjust the position, angle, and height of the axicon until you achieve **both** a centered reflection on the iris **and** a homogeneous circular pattern on the screen.

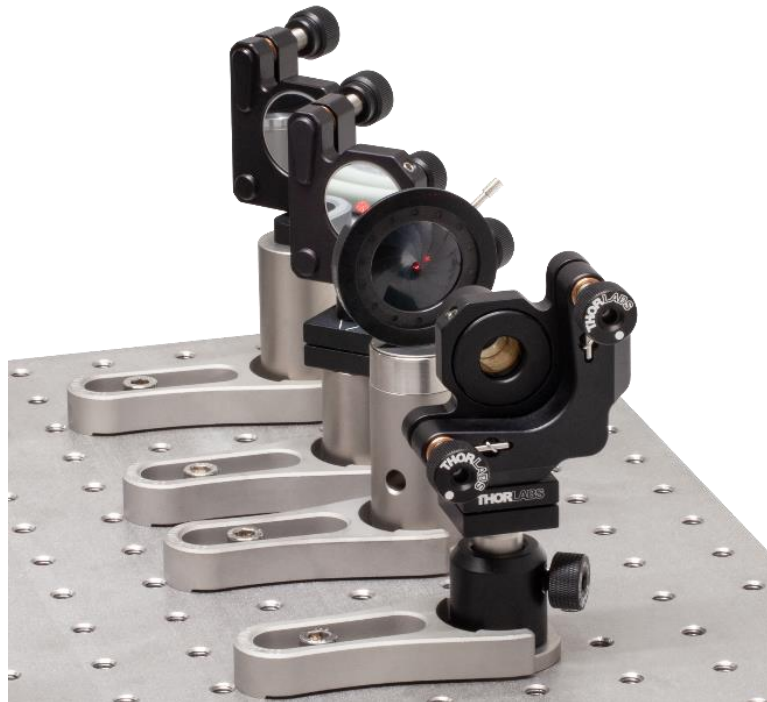


Figure 80 Axicon Reflection on the Back Side of the Iris (Should Pass Back Through Iris After Alignment)

- The axicon is designed to generate a cone of light with a half opening angle of 3° when illuminated with the wavelength of the alignment laser (635 nm). This opening angle is the same as the angle expected for the photon pairs generated by the BBO crystal. Thus, the alignment laser cone can be used to correctly position the detectors.
- Connect the lens tube with the economy beamsplitter to the detector that is labeled with “T.” Open the alignment iris completely and position the detector close to the right edge of the breadboard (about 5 cm closer to the axicon than the beam trap), so that the left part of the ring generated by the axicon hits the detector. Rotate the detector so that it points towards the axicon.
- Place the fluorescent alignment target about 10 cm in front of the detector so that the left part of the light ring passes through the hole in the target. Now adjust the height, position, and angle of the detector in such a way, that **both of the following conditions are met**:

- The reflection from the beamsplitter passes back through the hole of the target.
- The light passing the hole of the target is centered on the detector chip, as seen in Figure 81.



Figure 81 **Laser Spot Centered on Detector Chip**

Figure 82 shows the back side of the target before alignment. The curved line is part of the axicon cone (transmitted through the target), and the red spot to the right is the reflection from the beamsplitter. There may be a diffusive red spot which is the reflection from the detector chip and can be ignored.

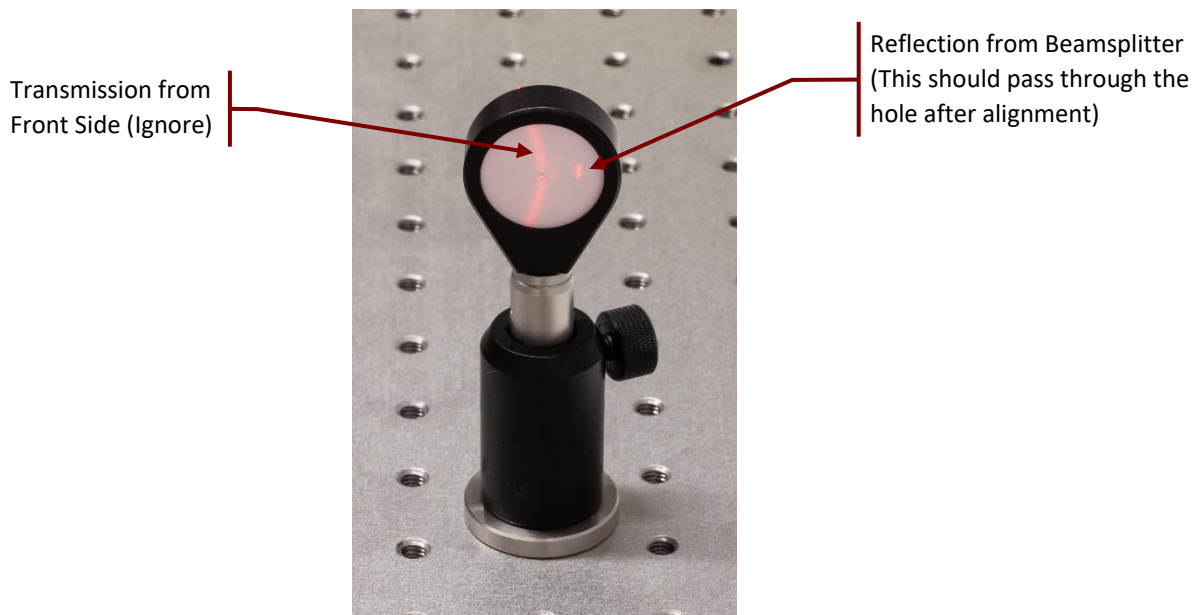


Figure 82 **Back Side of the Alignment Tool Prior To Detector Alignment**

- Secure the position of the detector with a CF125 clamp and a 1/4"-20 x 3/8" (M6 x 10 mm) cap screw plus washer. Then remove the lens tube with the beamsplitter from the detector.
- Repeat the same procedure with the detector labeled "A" for the right part of the light cone. After completion, the setup should look like Figure 83.

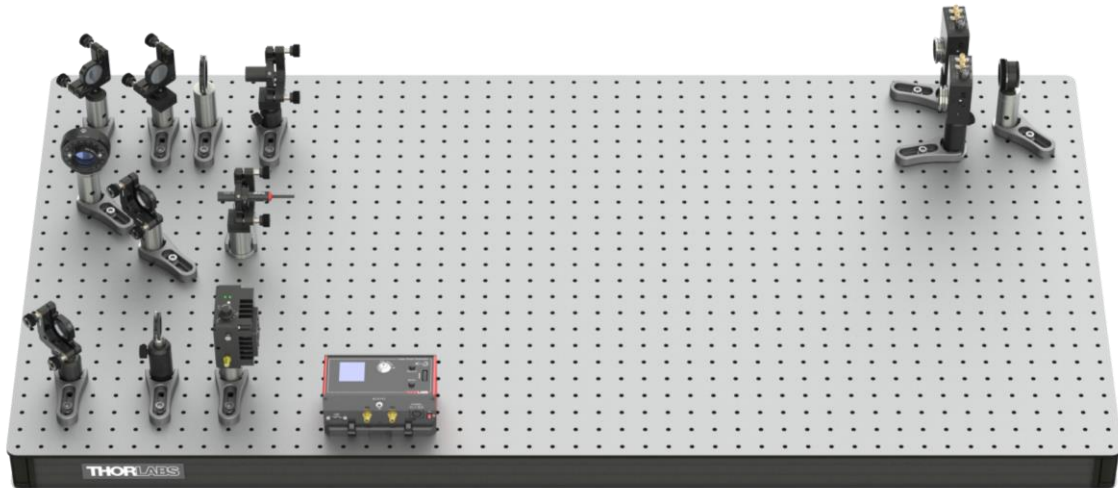


Figure 83 Setup after Detector Placement

- Take one of the prepared detector optics and loosen the locking screw of the DTSM1 dovetail adapter almost completely. Slide it over the dovetail adapter on the front of the detector labeled “T” (closer to the far breadboard edge). Rotate the optics until one of the adjusters is pointing straight upwards and the other one is pointing away from you. Then tighten the locking screw of the DTSM1 coupler to securely connect the optics to the detector⁶³.
- Repeat this step for the second detector. This time, the two differential screws should point straight up and towards you, respectively.
- The two detectors are now aligned to the expected path of the photon pairs generated by the BBO crystal, as simulated by the axicon and the alignment laser. A view from the front should look like Figure 84, with the outermost parts of the light ring passing through the iris openings of the detectors.



Figure 84 Detectors T (left) and A (right) after Alignment

7.4.4 Detector Fine Adjustment

- Replace the axicon with the colored glass filter.

⁶³ You can adjust the position of the locking screw to point upwards by repositioning the SM1NT1 locking ring.

- Close the alignment iris and adjust the adjusters of the filter holder until the reflection from the filter passes back through the iris. Then open the iris completely. Switch off the alignment laser and remove the magnetically mounted mirror from the setup.
- Position the Time Tagger on the front right corner of the breadboard (see Figure 85) and fix its position with one or two CL2 clamps. For each clamp use a 1/4"-20 x 2" (M6 x 50 mm) cap screw and a 1/4"-20 x 2.5" (M6 x 65 mm) cap screw plus washer.



Figure 85 Time Tagger Position

- Connect both detectors to the power grid via the included power supplies. You can use CS1 cable strips and 1/4"-20 x 1/4" (M6 x 6 mm) cap screws plus washers for better cable management. Use CA2924 cables to connect the outer SMA port of both detectors to the input channels 1 and 2 of the Time Tagger, respectively (labeled T and A, respectively). The detector and channel labeling should match.
- Connect the KLD101 driver and Time Tagger to your PC via the included USB cables. Start the EDU-QOP1 Software. Switch on both detectors and wait for the Signal LEDs to turn green. **Open the iris apertures of both detector optics completely.** They remain that way for all following adjustment steps.
- You might see very high count rates of both detectors in the software because of the ambient light. It may also be that you see no count rates at all because the Time Tagger is saturated.
- Darken the room as much as possible (switch off all lights, block any windows if existing, turn other light sources, such as computer screens, away from the setup). The count rates should now be significantly below 50 kHz⁶⁴. If they are higher, the room needs to be darkened further⁶⁵.
- Set the laser current in the software or at the KLD101 controller to about **5 mA below the lasing threshold** (the threshold can be determined from the spec sheet of the laser diode; see Figure 86) and switch on the pump laser. **Remember to always wear laser safety glasses when working with the pump laser!**
- The laser hits the colored glass filter in the same spot it will later hit the BBO crystal. The filter emits fluorescent light in all directions, part of which will be captured by the detectors. Thus, the detector optic can be fine-tuned to point exactly towards the future source of the photon pairs.
- Rotate the zoom housing of the T-detector to about the middle of its range (just test how far it can be turned in both directions and then try to turn it half of that from one endpoint). Now turn one of adjusters of the CXY1A mount in both directions until you observe a significant increase in the count rate of detector T (Trigger) in the software. If you see such a signal increase, then maximize the signal. If you do not see a signal increase, return the screw to the center position (align the marks on the front side of the CXY1A mount) and try the other differential screw⁶⁶.

⁶⁴ The count rates of the two detectors may be different, e.g., because some stray light source, such as a computer screen, illuminates one more than the other. This is not a problem if both count rates are below the 50 kHz threshold.

⁶⁵ If further darkening is not possible, take note of the tips at the end of Section 13.2 for dealing with large background signals.

⁶⁶ Sometimes, it seems like the count rate keeps increasing in one turning direction of the screw until the end of travel is reached, because more stray light is reaching the detector from that direction. This is not the goal of the adjustment process. You can check this by turning the laser off. If the signal does not

- Once you have found the maximum in one axis, optimize further with the other differential screw.
- Once you have maximized the count rate via the differential screws, carefully turn the zoom housing again to further increase the count rate. Afterwards, you may be able to increase the count rate further via slight changes of the differential screws. Iteratively turn the zoom housing and the screws until you have reached a stable maximum count rate. This should be at least 300 kHz (alignment iris and detector apertures completely open).
- Repeat the prior two steps for the A-detector, this time maximizing the count rate for detector A in the software. You should reach a similar count rate as the one you have for detector T⁶⁷.

7.4.5 Crystal Angle Adjustment

- Switch off the pump laser and replace the colored glass filter with the BBO crystal. Place the magnetically mounted mirror in the setup and switch on the alignment laser.
- Close the alignment iris and adjust the kinematic screws of the crystal holder until the reflection from the crystal passes back through the iris. Open the alignment iris completely, switch off the alignment laser and remove the magnetically mounted mirror.
- Set the laser current to a value that corresponds to about 13 mW output power. The current-power (LIV) curve is given on the spec sheet that comes with your laser diode, as seen in the blue curve in Figure 86 (The figure is an example, check your individual spec sheet!). Switch on the pump laser. You may already see an increase in the count rates from the detectors. Go to the Configuration tab and set the Coincidence Window to 20 ns (this helps with the alignment, as delay offsets between the detectors are not yet calibrated).

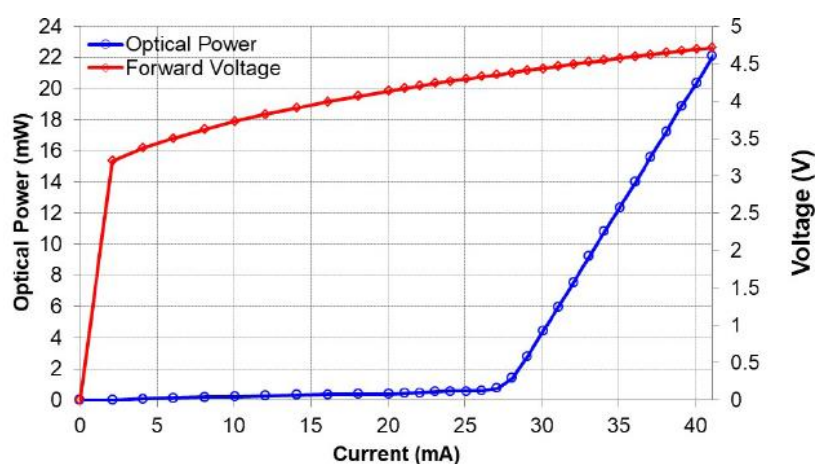


Figure 86 Current-Power Dependence (Blue Curve, Circles) in the Laser Diode Spec Sheet. In this example, the lasing threshold is at about 28 mA; 13 mW of optical output power is reached with a current of 35.5 mA.

- Go back to the Alignment tab and turn the **lower** kinematic screw of the crystal mount carefully in both directions. This changes the opening angle of the generated photon pairs and in turn the count rates of the detectors. Maximize the count rates of both detectors. As the detectors are placed symmetrically to the center axis, there should be a screw position that maximizes both the count rates of detectors T and A. You should observe count rates over 100 kHz for both detectors. At the same time, you should also observe an increase in the coincidence count rate of detectors T&A in the lower graph.

decrease significantly then you have optimized only for stray light. In this case, turn the screw back to the center position and try to find the actual signal (resulting in a much stronger and steeper count rate increase) via adjusting the other screw or the zoom housing.

⁶⁷ Slightly different count rates are not problematic, one detector might be slightly more efficient than the other (differences can be as high as 20%) or capture more stray light, resulting in an offset. Larger differences (like a factor of 2) point to one detector alignment being not fully optimized.

- If the count rates show maxima at significantly different screw positions (and no significant increase of the coincidence count rates is observed), the detectors are not symmetrically placed, and you need to remove both detectors and repeat the positioning process.
- After maximizing the count rates of the individual detectors, switch to the Delay Adjust tab of the software and set the Coincidence Window back to 5 ns. Use the standard settings of the software and start a measurement.
- The finished measurement should look like Figure 87. There should be a sharp peak with a FWHM of about 5 ns. Drag the cursor (blue vertical line) to find the delay value at the peak maximum (4.5 ns in Figure 87).
- Enter this value (4.5 ns in the example case of Figure 87) into the **Delay A to T** field.

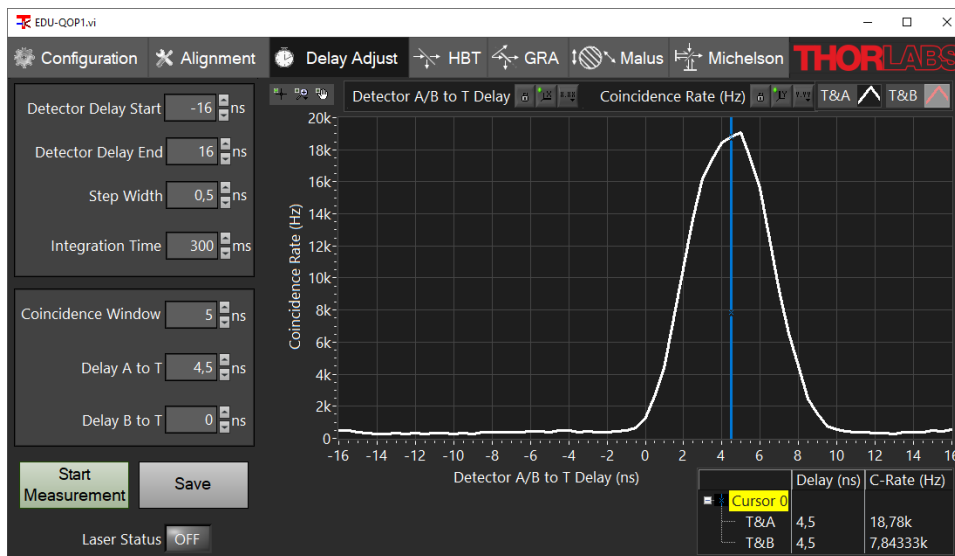


Figure 87 Example Delay Measurement

- Go back to the Alignment Tab. You should see the same count rates as before. The coincidence count rate should be above 10 kHz.
- Carefully rotate the WPH10ME-405 half-wave plate (between the first two mirrors in the pump beam) and watch the coincidence count rate. Optimize the wave plate angle for maximum count rate (this aligns the polarization of the pump beam with the crystal orientation for optimal phase matching, see Section 3.9 for details).
- Slowly close the alignment iris in front of the BBO crystal and watch the count rates as well as the coincidence count rate. At first, only the single detector count rates will decrease while the coincidence count rate remains stable. Stop closing the iris once the coincidence rate starts to drop as well. You have now found the optimal opening diameter of the alignment iris which should be somewhere between 1 mm and 3 mm. This ensures that as much stray light as possible is blocked without affecting the photon pairs. Keep the alignment iris at this diameter for all future experiments.
- Select the **$g^2(0)$** radio button on the left side of the software. The lower graph now displays the $g^{(2)}(0)$ values that are calculated live from the single detector and coincidence count rates. You should observe values significantly larger than 30.
- You have now set up and adjusted a photon pair source. This light source is the basis of all experiments in this kit.

7.5 Setting Up the Grangier-Roger-Aspect Experiment

With a working photon pair source, you can now build the setup for the Grangier-Roger-Aspect experiment as explained in Section 3.5.3. Figure 88 shows an overview of the setup with the rectangle marking the newly placed

components. The following subsections give detailed instructions for the placement and adjustment of those components.

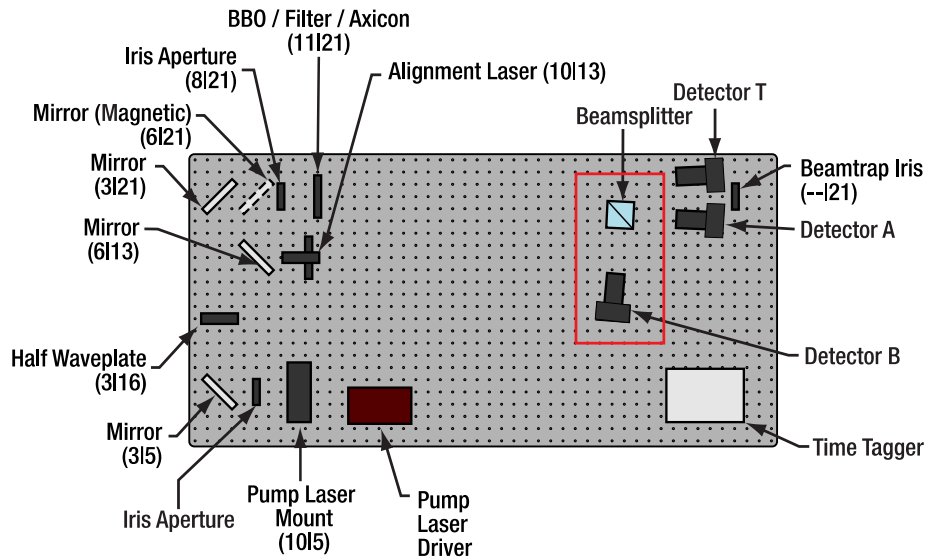


Figure 88 Setup for the GRA Experiment. Added Components are Marked with a Rectangle. The numbers in parentheses are breadboard hole numbers (from left / from bottom). Components are not to scale and exact positions may deviate slightly from those given in text.

7.5.1 Beamsplitter Positioning

- Switch off the pump laser.
- Replace the crystal with the axicon and return the magnetically mounted mirror to the setup. Switch on the alignment laser.
- Place the alignment target in the rightmost part of the light cone (viewed from the direction of the axicon).
- Place the beamsplitter with the attached iris aperture about 10 breadboard holes to the left of the detectors (iris facing the alignment target). The light passing through the target should be centered on the iris of the beamsplitter.

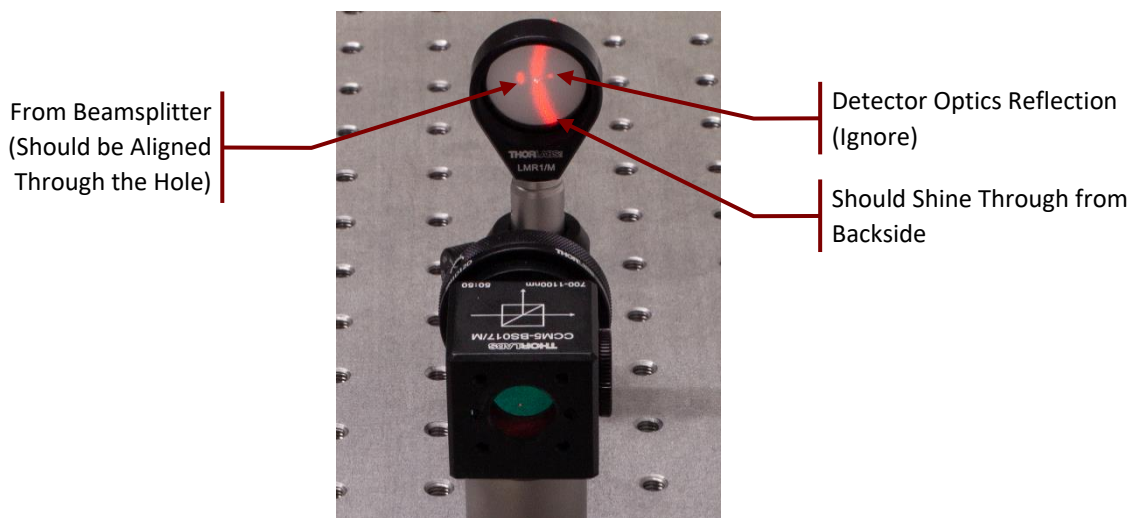


Figure 89 Beamsplitter Positioning and Orientation (Before Alignment)

- Watch the back side of the target and carefully rotate the beamsplitter until the reflection from the beamsplitter passes back through the hole in the target.

- Check that the laser is still aligned to the center of the beamsplitter iris, then secure the position of the beamsplitter with a CF125 clamp and a 1/4"-20 x 3/8" (M6 x 10 mm) cap screw plus washer.

7.5.2 Third Detector Positioning

- Take the remaining detector (labeled "B") and screw the lens tube with the economy beamsplitter on its front.
- Place the alignment target in the beam path of the light that is reflected by the beamsplitter (close to the beamsplitter) so that the light passes through the hole of the target.
- Position the detector at least 10 cm away from the target. Adjust height, position, and rotation of the detector in such a way that:
 - The light passing through the hole in the target is centered on the detector chip.
 - The reflection from the beamsplitter in front of the detector is passing back through the hole in the target.

Then secure the detector position with a CF125 clamp and a 1/4"-20 x 3/8" (M6 x 10 mm) cap screw plus washer. Remove the lens tube with the beamsplitter from the detector.

- Take the remaining detector optic and loosen the locking screw of the DTSM1 dovetail adapter almost completely. Slide it over the dovetail adapter on the front of the detector. Rotate the optics until one of the adjusters is pointing straight upwards. Then tighten the locking screw of the DTSM1 coupler to securely connect the optics to the detector. At this point, the setup should look like Figure 90.

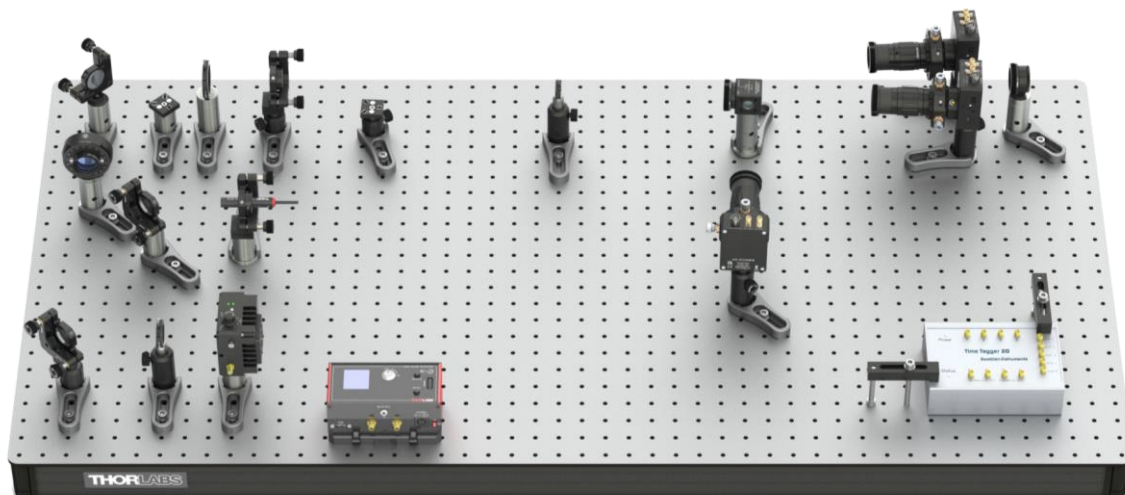


Figure 90 Setup After Placement of Third Detector

7.5.3 Third Detector Fine Adjustment

- Connect the detector to the power grid via the included power supply and connect the outer SMA port to Channel 3 of the Time Tagger (labeled "B") via a CA2924 cable. Optionally, use CS1 cable strips and 1/4"-20 x 1/4" (M6 x 6 mm) cap screws plus washers for cable management. Switch on the detector.
- Switch off the alignment laser, remove the target and the magnetically mounted mirror from the setup, and replace the axicon with the colored glass filter.
- Set the current of the pump laser to about 5 mA below the lasing threshold (check the spec sheet of your laser diode) and switch on the pump laser. **Always wear laser safety glasses when working with the pump laser!** Darken the room to similar conditions as before.
- Rotate the zoom housing of the detector to about the middle of its range (just test how far it can be turned in both directions and then try to turn it half of that from one endpoint). Now turn one of the differential

screws of the CXY1A mount in both directions until you observe a significant increase in the count rate of detector B in the software. If you see such a signal increase, then maximize the signal. If you do not see a signal increase, return the screw to the center position (align the marks on the front side of the CXY1A mount) and try the other differential screw.

- Once you found the maximum in one axis, optimize further with the other differential screw.
- Once you have maximized the count rate via the differential screws, carefully turn the zoom housing again to further increase the count rate. Afterwards, you may be able to increase the count rate further via slight changes of the differential screws. Iteratively turn the zoom housing and the screws until you have reached a stable maximum count rate. This should be at least 150 kHz.
- Switch off the pump laser and replace the colored glass filter with the BBO crystal.
- Set the laser current to the value that corresponds to about 13 mW (check the spec sheet of your laser diode). Set the coincidence window to 20 ns in the Configuration tab. Go back to the Alignment tab, then switch on the pump laser. You should see a sharp increase in the count rate of detector B in the software. The count rate should be similar to that of detector A and about half of that of detector T. The coincidence count rate between detectors T&B in the lower graph should also increase significantly.
- Slightly rotate the lower kinematic screw of the crystal holder back and forth to make sure that the maximum count rate of detector B is at a similar screw position compared to the other two detectors. If the screw positions of the maxima are significantly different (and no coincidences are observed), repeat the positioning of the third detector.
- Switch to the Delay Adjust tab of the software and set the coincidence window back to 5 ns. Use the standard settings of the software and start a measurement. In addition to the peak for detector A, you should now see an additional peak for detector B which has a similar height but may be shifted on the delay axis. Record the delay value for the center of the peak for detector B and write this value into the **Delay B to T** field. You should now see a similar coincidence count rate for T&A and T&B in the Alignment Tab.

7.5.4 Test Measurement

- Select the GRA tab of the software, choose a measurement time (20 s is recommended) and start the measurement. This will display the count rates, the absolute counts, and the calculated $g^{(2)}(0)$ values. The first value is the quality of the pair photon source as measured before and the second value is the Grangier-Roger-Aspect experiment. This value should be below 0.1 (everything below 1 is proof of a non-classical light source), as explained in detail in Section 3.5.3.
- The GRA experiment can be extended to measure Malus' Law by simply putting the polarizer component (1" diameter) between the beamsplitter and detector B, as shown in Figure 91. See Sections 3.7 and 9.6 for a detailed explanation of the Malus' Law experiment.

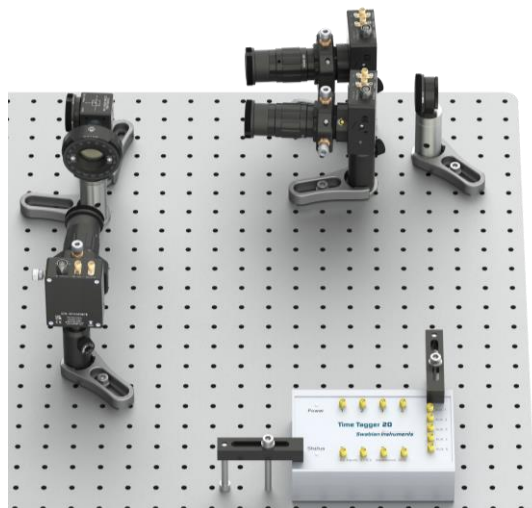


Figure 91 Setup for Malus' Law Experiment

7.6 Setting Up the Michelson Interferometer

In this Section, a Michelson interferometer for single photons (see Section 3.6) is constructed. In Figure 92, an overview over the setup is given, with the red rectangles marking the newly added or moved components.

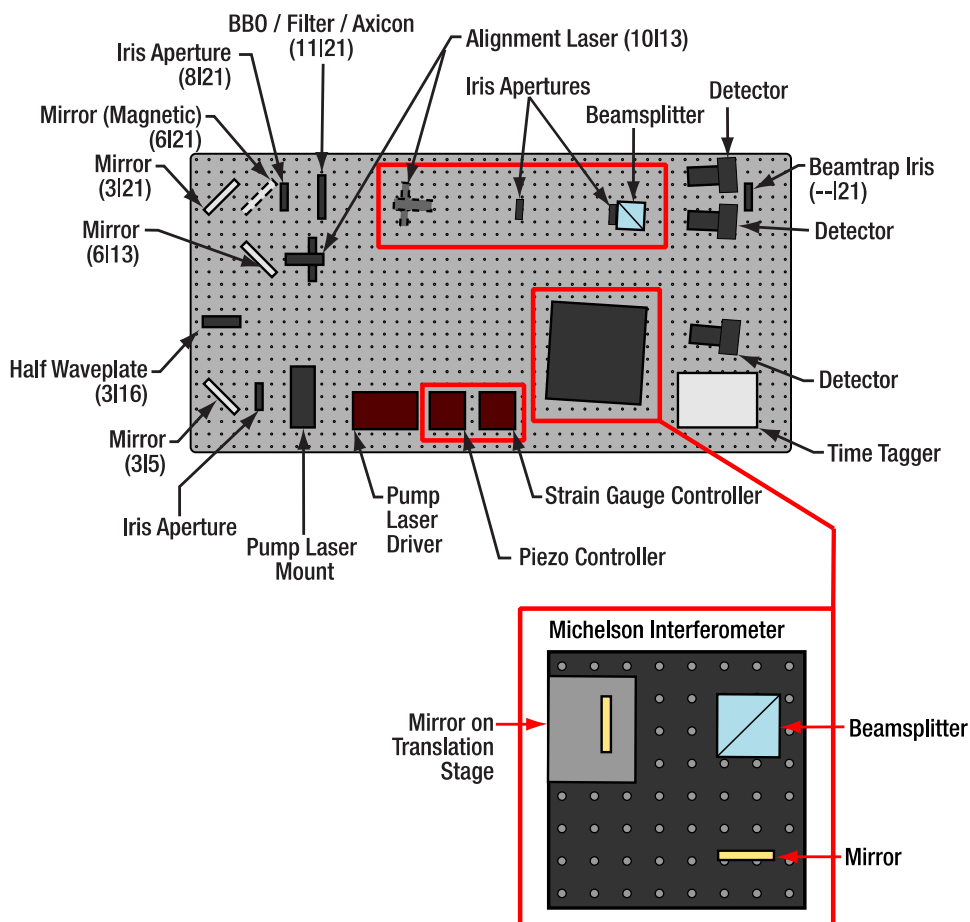


Figure 92 Overview over the Michelson Interferometer Setup. Newly added or moved parts are marked with red rectangles. The numbers in parentheses are breadboard hole numbers (from left / from bottom). Components are not to scale and exact positions may deviate slightly from those given in text.

7.6.1 Additional Alignment Path

Before setting up the interferometer, it is helpful to set up a second alignment path for the alignment laser, following the way the photons take from the crystal to the beamsplitter. Do this as follows:

- Switch off the pump laser, place the mirror on the magnetic mount in the beam path, and replace the BBO crystal with the axicon.
- Switch on the alignment laser. Place the alignment target behind the axicon in the rightmost part of the light cone.
- Place the $\varnothing 8.0$ mm iris component 30 cm behind the axicon so that it does not block the pump beam path and adjust its height and position until the light that passes the target is centered on the iris. Secure the iris position with a CF125 clamp via a 1/4"-20 x 3/8" (M6 x 10 mm) cap screw plus washer. Remove the alignment target.



Figure 93 Additional Alignment Path

- Switch off the alignment laser and transfer it to the magnetic plate in the PH1E (PH30E/M) post holder.
- Place the alignment laser between the axicon and the $\varnothing 8.0$ mm iris, as seen in Figure 93.
- Switch on the alignment laser and adjust its position until it is centered on both iris apertures. Do the following:
 - Open the $\varnothing 8.0$ mm iris completely and roughly aim the alignment laser on the beamsplitter iris by positioning the component and changing the post height. Do not use the adjusters of the laser holder in this step.
 - Close the $\varnothing 8.0$ mm iris and aim the laser on the face of the iris. Adjust the height of the iris to match the beam height.
 - Once the beam is centered on the $\varnothing 8.0$ mm axis, watch the beamsplitter iris. If the spot is to the left (right) of its center, move the whole alignment laser assembly a bit to the left (right) and rotate it until it is again centered on the iris. You may use the adjusters of the laser for fine alignment.
 - Repeat the last step iteratively until the beam is centered on both iris apertures. Figure 94 shows a completed alignment.
- Secure the position of the alignment laser with a CF125 clamp via a 1/4"-20 x 3/8" (M6 x 10 mm) cap screw plus washer. Open both iris apertures completely.

You have now completed the second alignment path. As you might have changed the laser position in its mount during the process, it is necessary to readjust the alignment of the original alignment path. Do this as follows:

- Switch off the alignment laser and move it to its original position.
- Remove the axicon and switch on the alignment laser.
- Repeat the beamwalk procedure explained in Section 7.4.2 (use only the adjusters of the mirrors, not of the alignment laser!)

You have now realigned everything. Move the alignment laser back to its position in the second alignment path and continue.



Figure 94 Additional Alignment Path After Completed Alignment (Beam Centered on Both Apertures)

7.6.2 Interferometer Adjustment

In the following steps we are going to set up the Michelson interferometer breadboard. Figure 95 shows how the board will look like after setting up the interferometer completely.

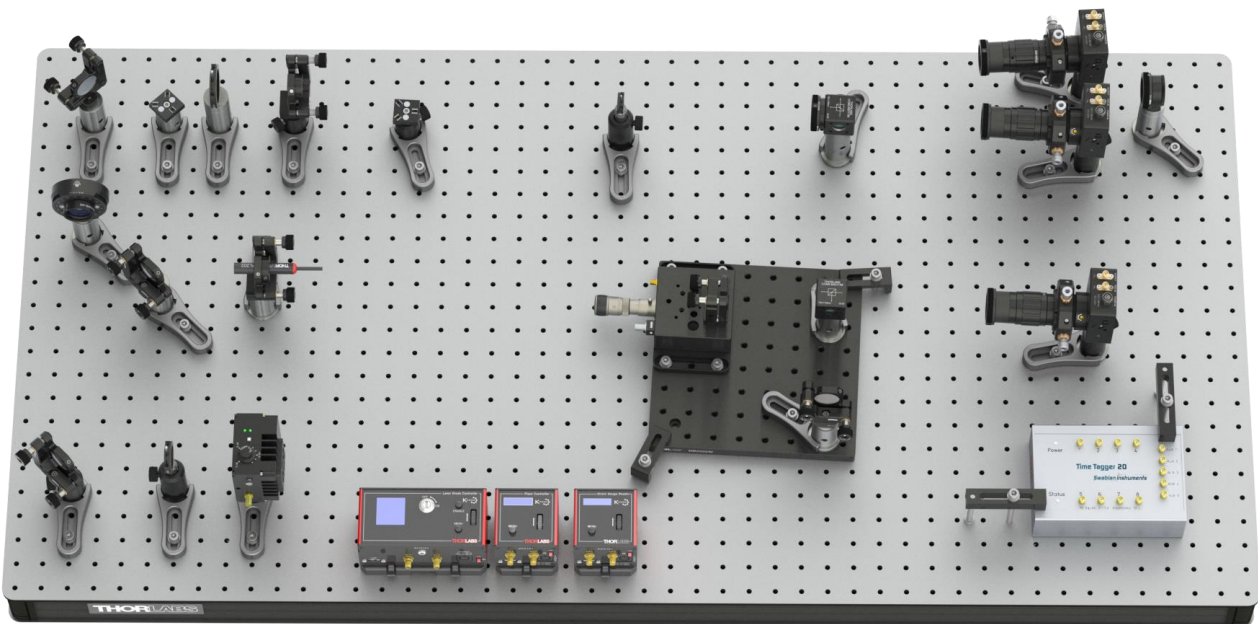


Figure 95 Setup with Fully Aligned Michelson Interferometer

- Place the alignment target in between the beamsplitter and detector B. Remove detector B from the breadboard and remove the optics from the detector (by loosening the locking screw on the dovetail coupler).
- Place the small breadboard on the free space to the right of the KLD101 laser driver.
- Place the stage with the gold mirror in the far-left corner of the small breadboard, so that the long edge of the stage and the edge of the small breadboard overlap, as seen in Figure 95. Secure its position with two 1/4"-20 x 3/8" (M6 x 10 mm) cap screws plus washers.

- Rotate the board such that the mirror on the stage faces the target. Switch on the alignment laser and adjust the board position such that the beam hits the center of the mirror, **and** the reflection passes back through the hole in the alignment target. Secure the breadboard position with two CL5A clamps, 1/4"-20 x 1" (M6 x 25 mm) cap screws, and washers. Adjust the height of the reflection with the upper adjuster of the mirror mount.
- Position the remaining beamsplitter component on the small breadboard about 10 cm in front of the mirror. For the correct orientation, see Figure 96.
- Position and rotate the beamsplitter component until the alignment laser hits it in the center **and** its back-reflection (as well as the reflection of the mirror behind) pass back through the hole in the alignment target⁶⁸. Secure the beamsplitter position with a CF028 clamp via a 1/4"-20 x 3/8" (M6 x 10 mm) cap screw plus washer.

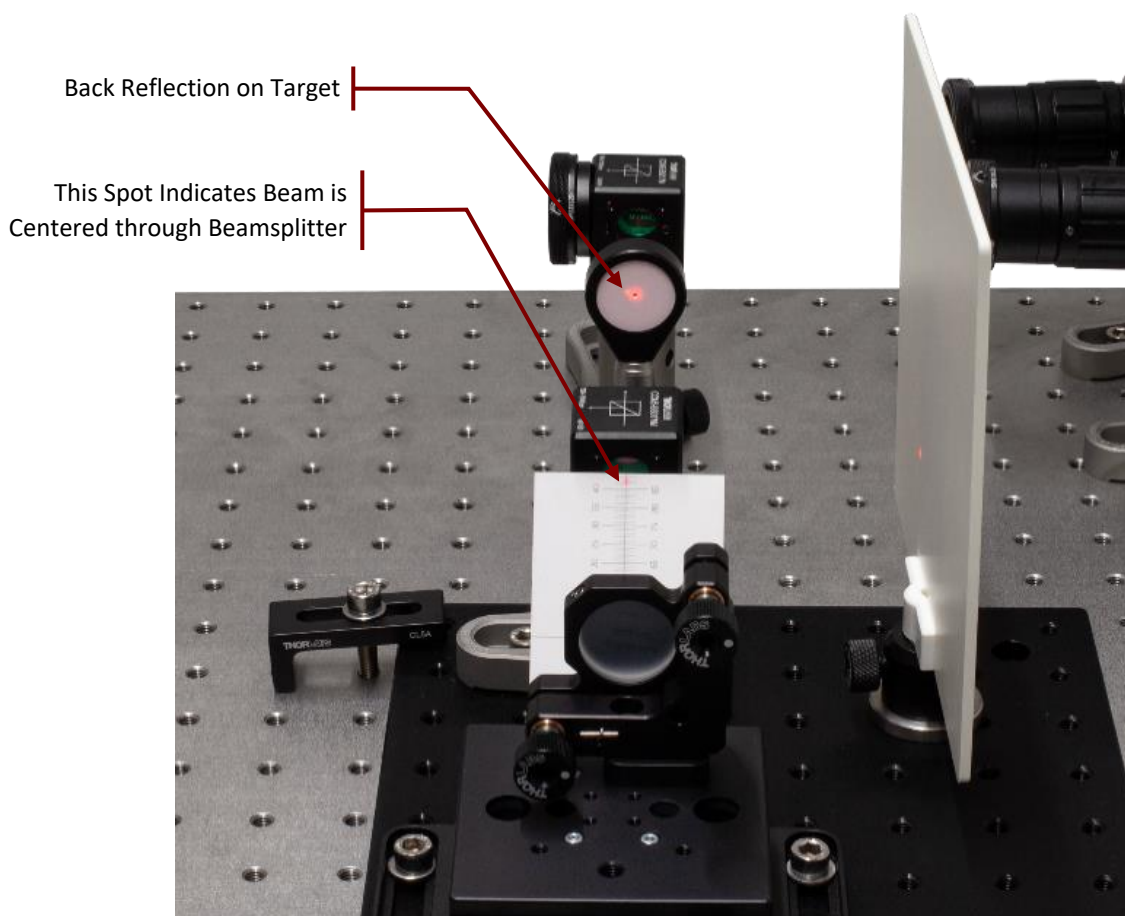


Figure 96 Alignment of the Second Beamsplitter

- Remove the clamps holding the small breadboard, then rotate it back into its original position (stage at the left edge). The distance between both beamsplitters should be about 15 - 20 cm. Align the board such that the laser hits the center of the beamsplitter **and** the reflection of the beamsplitter passes the hole in the alignment target. Then clamp the breadboard again in its final position.
- Now place the screen to block the mirror on the stage and position the gold mirror on the post in the path of the alignment laser that is transmitted by the beamsplitter. The distance between this mirror and the beamsplitter should be the same as between the mirror on the stage and the beamsplitter.

⁶⁸ Sometimes, the beamsplitter reflects the light slightly up- or downwards, so that the reflected spot cannot pass through the hole of the target. In these cases, it is sufficient to rotate the board until the reflection is right above or below the target hole. It may be helpful to cover the mirror to reduce the number of reflections on the target.

- Rotate and move the mirror until the alignment laser is centered on the mirror **and** you see its reflection on the back side of the alignment target. Then secure the mirror position with a CF125 clamp via a 1/4"-20 x 3/8" (M6 x 10 mm) cap screw plus washer, as seen in Figure 97.

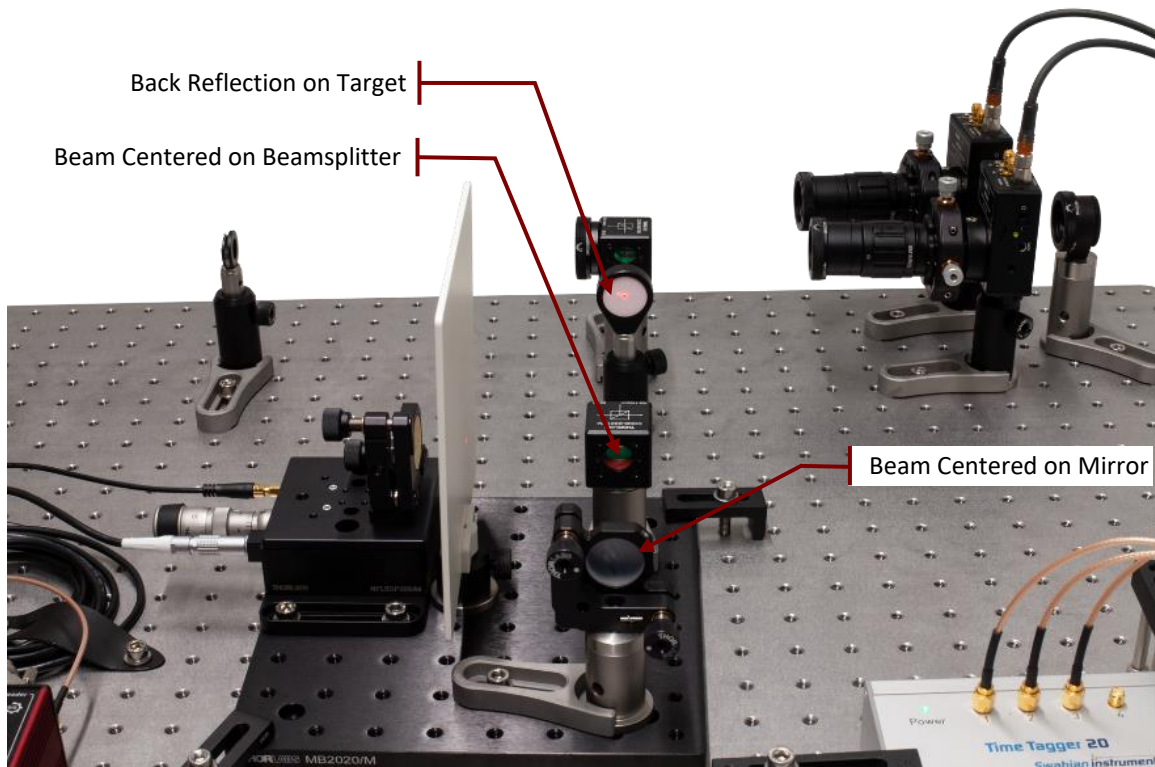


Figure 97 **Alignment of the Second Interferometer Mirror**

- Use the adjusters of the mirror mount to make the reflection pass back through the hole of the alignment target.
- Place the screen in the output arm of the interferometer (towards the right edge of the breadboard, as shown in Figure 98). You will see at least three red spots, as shown on the left side of Figure 99. If your alignment in the previous steps was very accurate, these spots already overlap. Two spots are the light coming back from the two mirrors in the interferometer (see Figure 98 b and c), the third spot (that is less intense) is a result of internal reflection in the beamsplitter (see Figure 98 a). Although this is an artifact of the beamsplitter coating not being at the same wavelength of the alignment laser, it helps with alignment. Please note that this artifact will not be present for the single photons later, as their wavelength matches the anti-reflection coating of the beamsplitter.

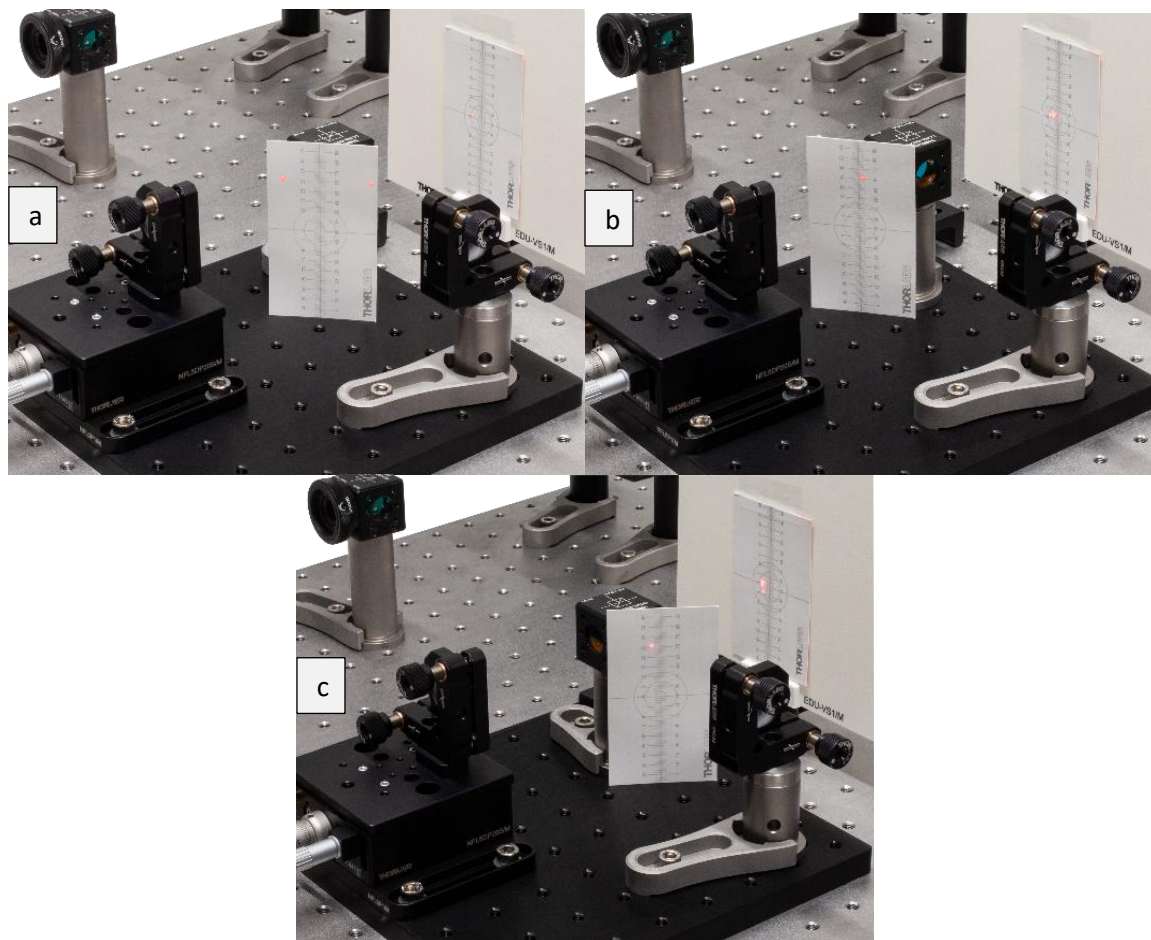


Figure 98 Alignment of Interferometer Arms

- Adjust the kinematic screws of one of the mirrors in the interferometer. You will see one of the bright spots moving. Adjust the mirror until the moving spot overlaps with the internal reflection spot. Then repeat this for the other interferometer mirror until you see only one bright spot on the screen, as shown on the right side of Figure 99. There may be less bright spots on the screen. Those are the result of multiple reflections and can be ignored.

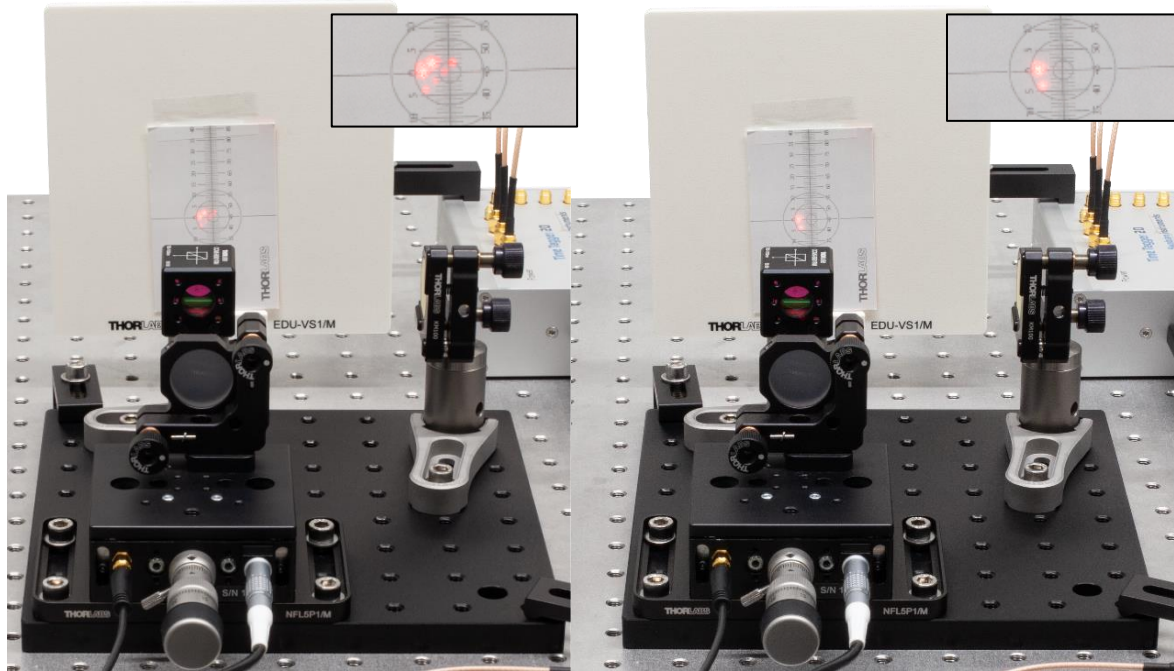


Figure 99 Spots on the Screen Before (Left) and After (Right) Adjustment of the Interferometer Mirrors

- Place the $\varnothing 1$ " lens assembly between the alignment laser and the interferometer as seen in Figure 100. Adjust the lens height and position so that the alignment laser is centered on the lens. If you block both arms of the detector, you will see a pattern from the internal reflections of the beamsplitter, which may be ignored.

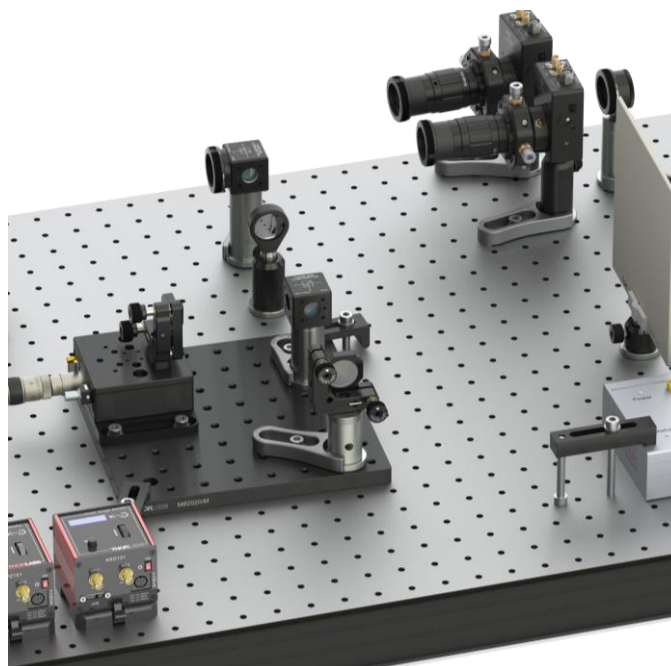


Figure 100 Position of the Lens in Front of Michelson Interferometer

- Unblock both interferometer arms. At this point you may already see an interference pattern on the screen. If that is not the case, carefully turn the kinematic screws of the mirror not on the stage back and forth until an interference pattern appears. At first, this pattern will consist of stripes, as shown on the right image in Figure 101. Use the mirror adjusters to center the pattern. If the stripes are getting broader you are turning into the right direction. If the stripes are more horizontal, use the upper adjuster, if they are more vertical, use the lower adjuster.

- You will probably see multiple interference rings (similar to the left side of Figure 101). This means that there is a significant difference between the arm lengths of the interferometer. Loosen the CF125 clamp of the mirror not on the stage and move the mirror slightly further away from the beamsplitter, then secure the clamp again. As long as there are **more than ten rings within the beam on the screen you are multiple millimeters** away from the target position.
- Adjust the kinematic screws until the interference pattern reappears, then check if the central maximum is larger or smaller than before. If it is larger, you moved the mirror in the right direction. Repeat the process until the central maximum is so large that you only see one or two interference rings on the screen (as shown on the center image of Figure 101). If the central maximum became smaller after moving the mirror, then move the mirror in the opposite direction.

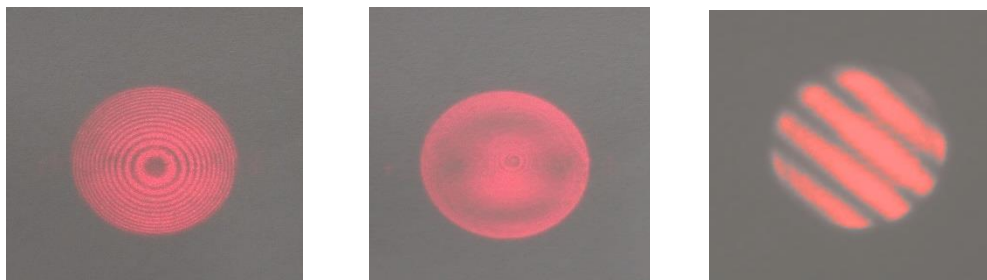


Figure 101 *Centered Interference Pattern for Large (Left) and Small (Center) Path Length Differences of the Interferometer Arms and Non-Centered Pattern (Right)*

- Once you have found a mirror position that results in only one or two interference rings, move the coarse adjuster of the differential screw of the stage (see Figure 103) slowly in one direction and check whether the central maximum of the interference pattern becomes bigger or smaller. You may have to slightly adjust the kinematic screws of one mirror from time to time to move the central maximum back into view. The goal is to find a position of the stage at which the whole spot is either completely dark or uniformly red. This corresponds to a nearly equal distance between the two mirrors to the beamsplitter.
- Once you found this position, remove the lens, and switch off the alignment laser. Place the LED in front of the beamsplitter as seen in Figure 102. Connect the LED to the power grid via the DS5 power supply.

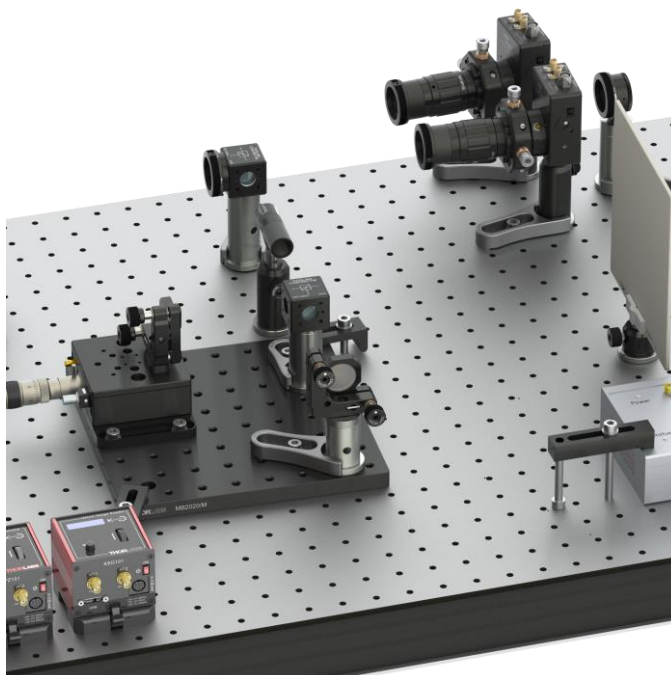


Figure 102 *Position of the LED in front of Michelson interferometer*

- Probably, you will not yet see an interference pattern on the screen. Move the fine adjuster of the differential screw of the stage (see Figure 103) very slowly (about 2 small scale markers per second) in one direction, until an interference pattern appears⁶⁹. If you reach the end of the travel range without seeing a pattern, turn the screw the other way until you see the pattern⁷⁰.

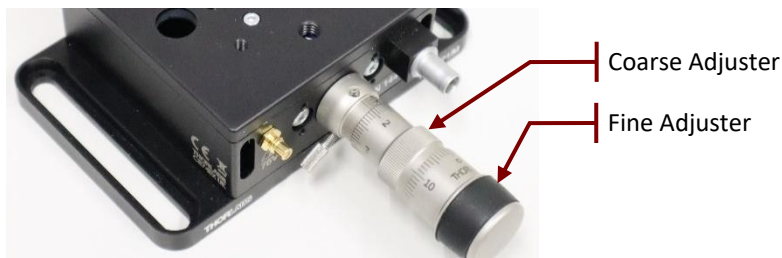


Figure 103 Coarse and Fine Adjuster of the NFL5DP20S(/M) Stage

- If you see no pattern over the entire range of the stage, you need to switch back to the alignment laser and lens and change the mirror position until you see an interference pattern with an even larger central maximum/minimum.
- Once you have found the interference with the LED, you have successfully adjusted the Michelson interferometer. Remove the LED. Check whether the beam of the alignment laser is still centered on both the $\varnothing 8.0$ mm iris aperture and the aperture on the beamsplitter, then switch it off and open both apertures completely.

The above procedure requires experience or time to find the interference pattern on the screen. As an alternative, one may continue to place the detector as described in Section 7.6.3, place and connect the KPZ101 controller and KSG101 gauge reader as described in Section 7.6.6, and visualize the count rate on detector B in the Michelson Interferometer tab of the software. The small portion of photons from the LED which pass the bandpass filter of the detector have a longer coherence length than the full LED spectrum, which makes it easier to find the correct stage position. Close the iris of the B detector completely (to avoid detector saturation) and start a measurement and let the stage run for about 2 μm . You might already see an oscillating signal with a period of 0.4 μm . If not, carefully turn the coarse adjuster screw (in steps of 5 small scale markers) in one direction until you see the count rate oscillating. Use the adjusters to maximize the amplitude of the oscillation, as shown in Figure 104.

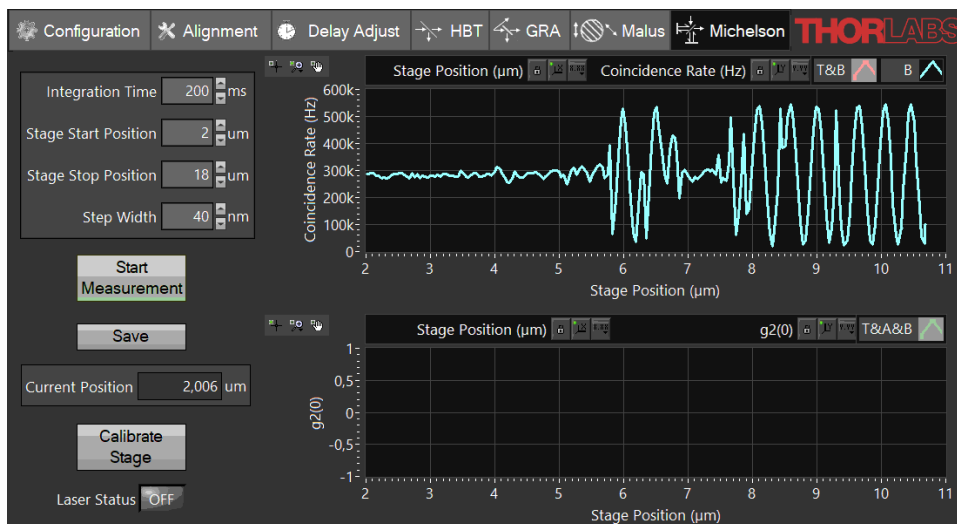


Figure 104 Adjusting the Stage Position Using the Software

⁶⁹ The LED provides less intensity than the laser and might be difficult to see on the screen in a bright room. In this case, darken the room until the LED spot is clearly visible on the screen.

⁷⁰ Due to the shorter coherence length of the LED in comparison to the alignment laser, you will only see an interference pattern when the arm length difference is nearly zero. Thus, the pattern will always consist of wide stripes, or a single maximum as shown in the center image of Figure 101.

7.6.3 Detector Positioning

- Remove the LED and switch on the alignment laser. Remove the screen. Use the screen to block the arm of the Michelson Interferometer that leads to the mirror not on the stage, as seen in Figure 105.
- Place the alignment target in the interferometer output right next to the interferometer board so that the alignment laser passes through the hole in the target.
- Take the third detector and screw the lens tube with the economy beamsplitter on its front.
- Position the detector at least 15 cm away from the target, as seen in Figure 105.

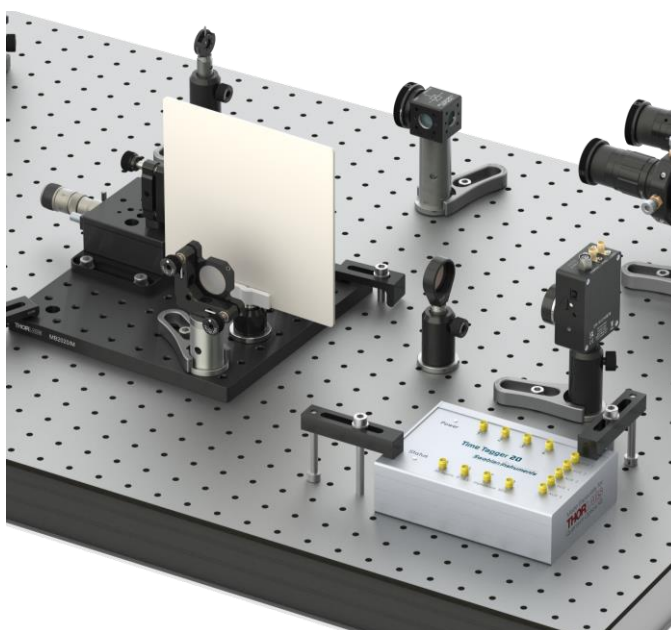


Figure 105 Setup for Positioning the Detector in the Output of the Michelson Interferometer

- Adjust height, position, and rotation of the detector in such a way⁷¹ that:
 - The light passing through the hole in the target is centered on the detector chip.
 - The reflection from the beamsplitter in front of the detector is passing back through the hole in the target.

Then secure the detector position with a CF125 clamp and a 1/4"-20 x 3/8" (M6 x 10 mm) cap screw plus washer. Remove the lens tube with the beamsplitter from the detector.

- Take the remaining detector optic and loosen the locking screw of the DTSM1 coupler almost completely. Slide it over the dovetail adapter on the front of the detector. Rotate the optics until one of the adjusters is pointing straight upwards. Then tighten the locking screw of the DTSM1 coupler to securely connect the optics to the detector.

7.6.4 Detector Fine Adjustment

- Switch off the alignment laser and transfer it to its original position in the setup, remove the target from the interferometer output, and replace the axicon with the colored glass filter.
- Set the current of the pump laser to about 5 mA **below the lasing threshold** (check the spec sheet of your laser diode) and switch on the pump laser. **Always wear laser safety glasses when working with the pump laser!** Darken the room to similar conditions as before.

⁷¹ The alignment laser has only an eighth of its original intensity at this point due to passing a beamsplitter three times. Thus, it can be difficult to see in a bright room. Darken the room until the alignment laser spot becomes clearly visible on the target and detector.

- Find the maximum count rate for detector B just like you did before by turning the two kinematic screws of the CXY1A mount and the zoom housing. To avoid inconvenient scaling of the graphs, temporarily deactivate the curves of detectors T and A (right click on the legend and deactivate the **Plot Visible** option).
- Switch off the pump laser and replace the colored glass filter with the BBO crystal.
- Set the laser current to a value corresponding to about 13 mW output power (check the spec sheet of your laser diode) and switch on the pump laser. You should see a sharp increase in the count rate of detector B in the software. The count rate will be less than detector A. The coincidences T&B should also increase but will be lower (by a factor in the range of 5 to 10) than the T&A coincidence count rate.
- Slightly rotate the lower kinematic screw of the crystal holder back and forth to make sure that the maximum count rate of detector B is at a similar screw position compared to the other two detectors. If the screw positions of the maxima are significantly different, repeat the positioning of the third detector.
- Switch to the Delay Adjust tab of the software and start a measurement with standard settings. Record the delay value for the center of the peak for detector B and write this value into the **Delay B to T** field. This value might differ from the value measured earlier because the light travels a longer distance before reaching the detector, which takes about 1 ns of additional time.

7.6.5 Single Photon Interference Adjustment

- Remove the screen from the Michelson interferometer. Turn the fine adjuster of the differential screw of the translation stage (see Figure 103) very carefully. You should see a fluctuation of the coincidence signal between detectors T&B in the software, due to the interference. Temporarily removing the T&A curve from the lower graph (right click on the legend and deactivate the **Plot Visible** option) can help with scaling.
- In case you do not see that fluctuation:
 - Switch off the pump laser. Transfer the alignment laser to the magnetic plate behind the crystal. Place the screen in front of the detector.
 - Switch on the alignment laser and check if the light from the two interferometer arms hits the screen at the same position. If not, use the Michelson mirror that is not on the stage (**do not use the one on the stage!**)⁷² to overlap the two spots.
 - Place the lens between alignment laser and interferometer. You should see an interference pattern on the screen. Use the Michelson mirror that is not on the stage (**do not use the one on the stage!**) to move the central maximum of the pattern to the center.
 - Switch off the alignment laser and move it to its original place in the setup. Remove the lens and place the LED in front of the interferometer. After switching on the LED, you should see an interference pattern on the screen. If not, turn the fine adjuster of the translation stage (see Figure 103) carefully in both directions until the pattern appears.
 - The pattern should still consist of a centered minimum or maximum. If not, then use the mirror that is not on the stage (**do not use the mirror on the stage!**) to move the central maximum to the center of the pattern.
 - Remove the LED and the screen.
 - Switch on the pump laser and repeat the above test for the fluctuation of the coincidences, which you should now see.

⁷² The position of the light leaving the interferometer on the detector was adjusted with the mirror on the stage. Therefore, this mirror should not be moved afterwards, and every fine alignment should be done with the other mirror.

7.6.6 Michelson Interferometer Test Measurement

- Remove the bottom plates from the KPZ101 controller and KSG101 strain gauge reader and fix them to the breadboard to the right next to the KLD101 controller with two 1/4"-20 x 3/8" (M6 x 10 mm) cap screws and washers each.
- Connect the controllers to their bottom plates and connect them to the power grid via the second TPS002 power supply. Connect both controllers to your PC via the USB cables included in the controller packaging.
- Connect the HV-Output port of the KPZ101 controller to the input port of the NFL5DP20S(/M) stage via the SMC-SMC cable included in the stage packaging.
- Connect the Strain Gauge I/P port of the KSG101 gauge reader with the Strain Gauge port of the NFL5DP20S(/M) stage via the TypeD-to-LEMO cable included with the stage.
- Connect the Monitor Output of the KSG101 gauge reader to the EXT IN input of the KPZ101 controller via the CA2912 cable. It is recommended you use CS1 cable strips and 1/4"-20 x 1/4" (M6 x 6 mm) cap screws plus washers for better cable management (as seen in Figure 106). Switch on the controllers. Figure 95 shows a photo of the complete Michelson Interferometer setup.



Figure 106 Cable Management for Single Photon Michelson Interferometer Setup

- Open the Michelson-Tab in the software and click the Calibrate Stage button. Wait for the calibration to finish.
- Start a measurement with the parameters that are pre-set. You should see a typical Michelson interference curve as shown in Figure 107. The maxima should be evenly spaced.

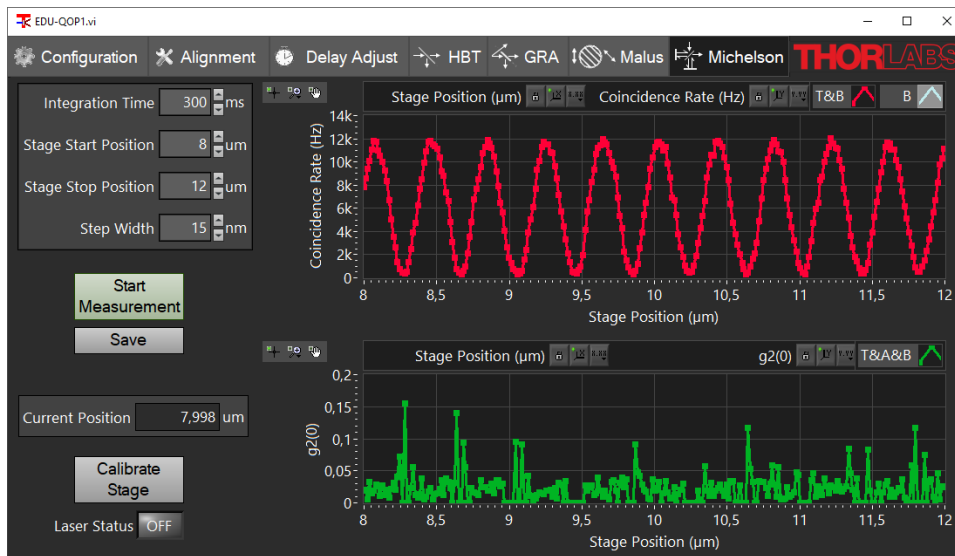


Figure 107 Typical Result of Michelson Test Measurement

- If you see the interference, then your Michelson Interferometer is aligned. For more details on the Michelson experiment, see Sections 3.6 and 9.7.

7.7 Setting Up the Quantum Eraser

As a first step, the two $\emptyset 1/2''$ polarizers need to be calibrated as follows:

- Place the $\emptyset 1''$ polarizer in front of the T-detector.
- Watch the count rate of the T-detector in the alignment tab of the software (deactivate the other two graphs).
- Check whether the count rate is higher for the 0° or 90° setting of the polarizer.
 - If the count rate is higher for the 90° setting, your polarizer axis is parallel to the table plane at the 0° setting, which is the desired case.
 - If the count rate is higher for the 0° setting, then your polarizer axis is perpendicular to the table plane at 0° . In this case, set the polarizer to 90° , lock it, and re-align the scale to show 0° to reach the desired case.
- Set the $\emptyset 1''$ polarizer to 90° and place one of the $\emptyset 1/2''$ polarizers behind the $\emptyset 1''$ polarizer (You must place the $\emptyset 1/2''$ polarizer on the PS3 spacer to make the beam heights match).
- Rotate the $\emptyset 1/2''$ polarizer until the count rate of detector T is minimized. Then tighten the locking screw. It is now perpendicular to the $\emptyset 1''$ polarizer. Set the scale of the $\emptyset 1/2''$ polarizer to 90° (loosen two screws on the front face, set scale, and retighten screws). You have now ensured that this polarizer is calibrated exactly the same as the first one.
- Replace the $\emptyset 1/2''$ polarizer with the other one and repeat the procedure.
- Remove the polarizers from the breadboard.

Now the polarizers are calibrated and can be inserted into the interferometer as follows:

- Switch off the pump laser and transfer the alignment laser to the magnetic plate behind the crystal.
- Place the alignment target between the two beamsplitters (closer to the first one) so that the alignment laser passes through the hole in the target. Set the WPH10ME-808 half-wave plate to 22.5° and place it between the two beamsplitters (as close as possible to the first beamsplitter), so that the scale of the rotation mount faces the interferometer. Make sure that the alignment laser is centered on the wave

plate and block the beam both behind the wave plate and in front of detector A either with cards (as shown in Figure 108) or with the screen.

- Rotate the wave plate component until the reflection from it passes back through the hole in the target, as seen in Figure 108. Secure the wave plate position with a CF125 clamp via a 1/4"-20 x 3/8" (M6 x 10 mm) cap screw plus washer.

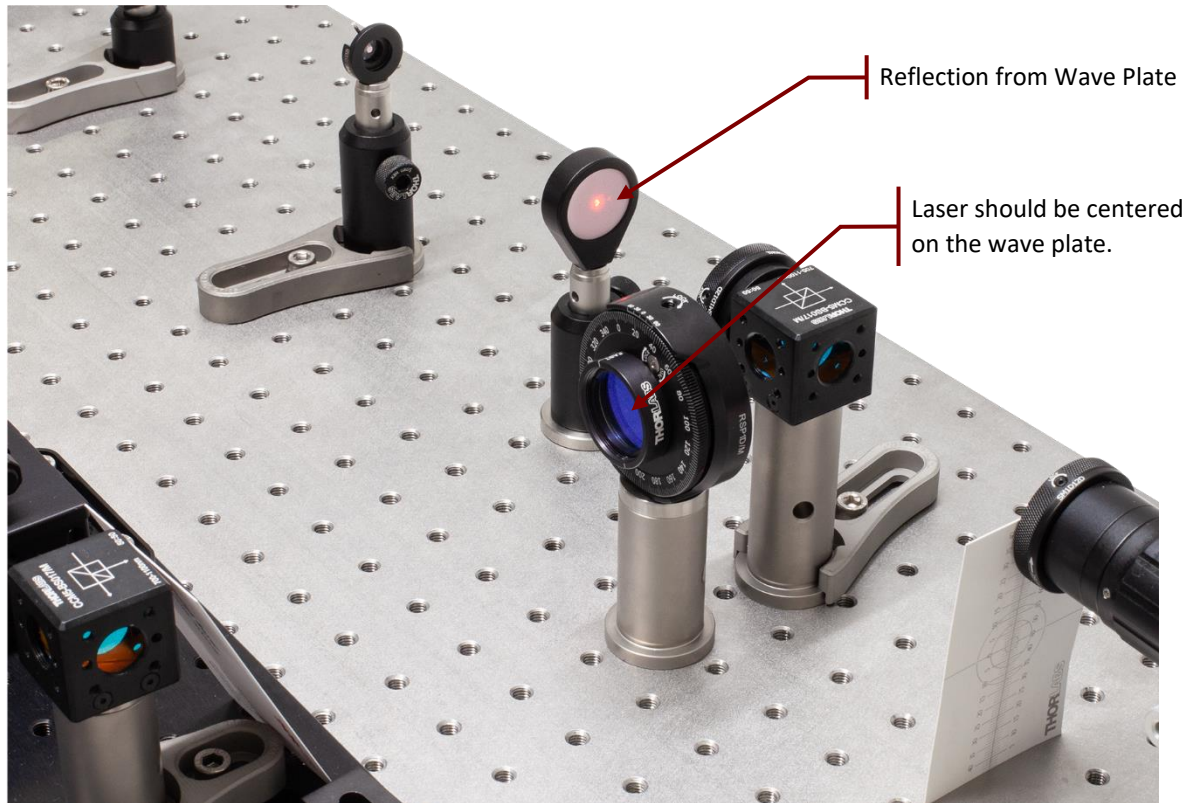


Figure 108 **Positioning of Half-Wave Plate**

- Place the alignment target in front of the interferometer beamsplitter so that the alignment laser passes through the hole in the target.
- Place one of the polarizers with 1/2" diameter in the arm of the interferometer that leads to the mirror on the stage. Make sure the alignment laser is centered on the polarizer. Block the interferometer output with the screen, block the other arm of the interferometer with a card, and rotate the polarizer component until the reflection from the polarizer passes back through the alignment target, as shown in Figure 109. Secure the polarizer position with a CF125 clamp via a 1/4"-20 x 3/8" (M6 x 10 mm) cap screw plus washer, then set it to 0°.

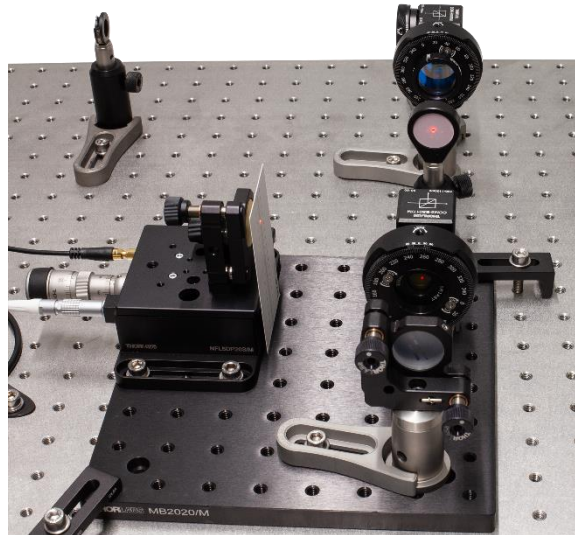


Figure 109 *Positioning of Polarizer in Interferometer*

- Repeat the above step for the second polarizer in the other arm of the interferometer (use a short clamp instead of a CF125 clamp). Set this polarizer to 0° as well. Remove the target from the breadboard, switch off the alignment laser, and transfer the laser to its original position in the setup.
- Place the LED between the two beamsplitters pointing towards the Michelson Interferometer. Place the screen in front of Detector B.
- Switch on the LED. You should see an interference pattern. If not, carefully turn the fine adjuster of the Michelson stage (see Figure 103) until you see a pattern with good contrast.
- Most likely, the pattern will consist of stripes. Use the kinematic screws of the Michelson mirror not on the stage (**do not use the one on the stage!**) to find the central maximum.
- Remove the screen and the LED from the setup. Figure 110 shows the Michelson interferometer prepared for the Quantum Eraser measurements.

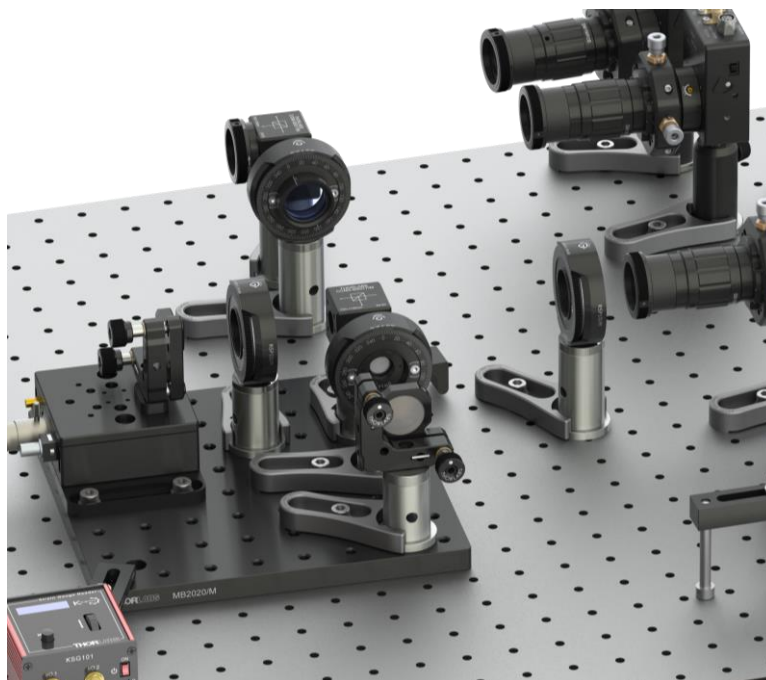


Figure 110 *Michelson Interferometer Prepared for Quantum Eraser Measurement*

- Perform the same test measurement as described in the last step of Section 7.6.6. If you see the interference minima and maxima, you have adjusted the Quantum Eraser. For more details on this experiment, see Sections 3.8 and 9.8.

Chapter 8 Learning Goals and Misconceptions

Since quantum optics is both an exciting and challenging topic, the following table summarizes the experiments and the learning goals.

Exercise	Experiment	Learning Goal	Possible Misconception
1	Attenuated Laser (Section 9.1)	Attenuated laser light is not a single photon source.	People tend to have the misconception that laser light is just a barrage of photons, visualized as little dots. In that image, attenuation leads to a reduction of photons, eventually just leaving “individually flying dots.” This image disregards the fact that photon arrival at a detector follows an underlying statistic. The attenuation of the laser light does <u>not</u> change the underlying statistic from a coherent to a non-classical source.
2	Pair Source (Section 9.2)	The BBO crystal generates photon pairs. Due to their simultaneous arrival at two detectors, the coincidence counts well exceed the expected value for an arbitrary/thermal light source.	
3	HBT in One Arm of the Pair Source (Section 9.3)	When only one arm of the pair source is considered, the light still shows classical characteristics.	The misconception here is that, once the pairs are generated, we have “two single photon sources,” namely each in one arm. This is not true. When only one arm is considered, the statistics of the light is still classical.
4	HBT with Pair Source / GRA Experiment (Section 9.4)	When both photons of the pair are considered, the light in one arm shows non-classical properties. This constitutes a photon pair source, also called a heralded single photon source (see Section 3.5.4).	
5	Fluorescent Filter (Section 9.5)	A measurement of light coming from a fluorescent filter similar to exercise 4 (i.e., with three detectors) does not yield a non-classical light source.	This exercise demonstrates to students that it is really the pair source property of the light coming from the BBO that induces the non-classical nature (and not the three-detector arrangement). If a classical light source is measured in the three-detector arrangement, the properties are still classical.
6	Malus’ Law (Section 9.6)	Behavior of single photons at a polarizer	In classical wave theory, light that is incident on a polarizer can be split into parts that are parallel and perpendicular to the polarizer’s orientation. One is absorbed, the other transmitted.

			<p>But how does this work for single photons since they cannot be split into two parts?</p> <p>In quantum optics, the photon's polarization state is expressed by a superposition of basis states. The proportionate transmission of a classical wave is replaced by the <u>probability</u> of transmitting through the polarizer. If the photon is transmitted, it retains its energy and has the polarization set by the polarizer. Otherwise, it is absorbed.</p>
7	Single Photon Michelson Interferometer (Section 9.7)	Even single photons exhibit interference.	<p>Here, the misperception of a photon as a little flying dot is revealed: similar to a double slit, a dot-like photon would only pass through either arm of the interferometer. Thus, it would not have information about the second arm and not show interference. However, an interference behavior is observable even with a heralded single photon source. The average amount of photons in the setup is about 0.02 (even less in the Michelson interferometer part), so two photons interfering with each other can be ruled out.</p>
8	Quantum Eraser (Section 9.8)	Orthogonal polarizers in two interferometer arms yield a path information, thus losing interference. A suitable polarizer after the interferometer can erase that path information, thus recovering the interference.	<p>Suppose the eraser is not yet in the system. The misconception is that the photon would have to decide on one of the paths. This misconception is debunked by the fact that the polarizer after the interferometer can retrieve the interference.</p> <p>Fundamentally, the photon is a superposition of states and only once it is measured, an individual state is assumed. If the measurement is not designed in this regard, the photon does not have to "decide" for a path in the interferometer.</p>

Chapter 9 Experiments

In this chapter, experiments that can be performed with the kit are described in detail. The learning goals of the experiments and common misconceptions that may be worth addressing in a lab course are summarized in Chapter 8.

If switching back and forth between experiments is intended, the Michelson board can be marked with additional clamps and moved in and out of the setup. For detailed instructions, see Section 12.11.

9.1 HBT-Experiment with Attenuated Laser

Goal: Test whether an attenuated laser is a suitable single photon source.

Setup: The alignment laser is attenuated by an ND filter and then hits a beamsplitter. The detectors A and B are placed in the output ports of the beamsplitter. For the adjustment of the setup, see Section 7.3.

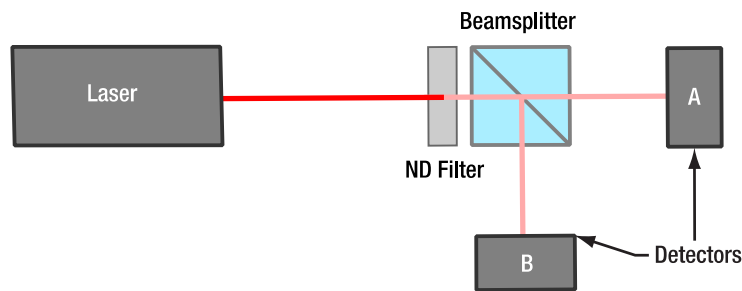


Figure 111 Schematic Setup for the Attenuated Laser HBT Experiment

Measurement: Darken the room, open the HBT-Tab in the software, switch on the alignment laser, and start a measurement with a measurement time of 20 s. Save the result.

Result Analysis: The correlation $g_{HBT}^{(2)}(0)$ is calculated automatically via the following equation (for the derivation, see Section 3.5.2):

$$g_{HBT}^{(2)}(0) = \frac{R_{AB}}{R_A \cdot R_B \cdot Dt}$$

The measured $g_{HBT}^{(2)}(0)$ will be close to 1. Less laser intensity would only increase the error bar (or increase the measurement time required to reach the same error bar), it does not change the result⁷³. Table 1 shows the results of an example measurement.

Spec	Measured Value
R_A	391118.45 Hz
R_B	315945.65 Hz
R_{AB}	619.1 Hz
$g_{HBT}^{(2)}(0)$	1.00201

Table 1 Results of Example Measurement (HBT with Attenuated Laser)

Interpretation: Let us start with an assumption that is very compelling, **but totally wrong**: The laser emits a stream of photons with a constant time interval between them. The photon energy per time fits the laser power and when attenuating this laser by a factor x , every x th photon passes the attenuator. In this case, we could calculate the number of photons n that are in the setup at average from the length of the setup l , the speed of light c and the frequency f of photons per second as follows:

⁷³ If you want to show this experimentally, it is possible to use a second ND filter with higher optical density. Be aware that the measurement time to reach a meaningful statistic will be tens of minutes in this case.

$$n = \frac{l}{c} \cdot f$$

In our case, we measure about 300 kHz of count rate at both detectors, so the overall frequency f would be 600 kHz. The setup is about 1 m long. We get as a result:

$$n = \frac{l}{c} \cdot f = \frac{1 \text{ m}}{3 \cdot 10^8 \frac{\text{m}}{\text{s}}} \cdot 6 \cdot 10^6 \text{ Hz} = 0.02$$

We have only 0.02 photons in the setup on average! All photons that we measure should be single photons! Those cannot be split at the beamsplitter, so we expect no double coincidences and $g_{HBT}^{(2)}(0) \ll 1$.

However, this is not what we measure: We get $g_{HBT}^{(2)}(0) = 1$, irrespective of the attenuation. This is because the initial assumption of the “evenly spaced photons” **was totally wrong**.

In reality, laser light is quantum mechanically represented by a coherent state, as seen in Section 3.3.2. For this state, the photon statistic is a Poisson distribution (see Figure 6). Irrespective of the attenuation, the laser always emits multiple photons often enough to make $g_{HBT}^{(2)}(0) = 1$ the expected result. Simply attenuating the laser does not change the underlying statistics of the light.

This means that **it is not possible to perform single photon experiments with an attenuated laser**, even a strongly attenuated one!

9.2 Photon Pair Source

Goal: Test, whether the source is indeed emitting photon pairs.

Setup: The pump laser is generating photon pairs in the BBO crystal. One single photon detector is placed in each path, as seen in Figure 112. For the adjustment of the setup, see Section 7.3.

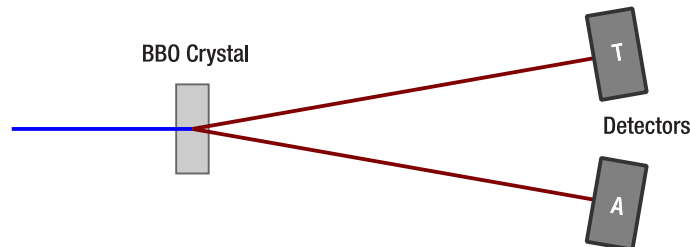


Figure 112 Schematic Setup for the Photon Pair Source

Measurement: Darken the room, open the Adjustment Tab in the software and start the laser. Record the count rates for detectors T and A in the upper graph and the coincidence count rate T&A in the lower graph.

Result Analysis: Calculate the correlation $g_{PS}^{(2)}(0)$ between the two detectors via the following formula (for the derivation, see Section 3.5.2):

$$g_{PS}^{(2)}(0) = \frac{R_{TA}}{R_T \cdot R_A \cdot \Delta t}$$

Here, R_T and R_A are the single count rates of detectors T and A, respectively, R_{TA} is the coincidence count rate of the two detectors, and Δt is the coincidence window of the experiment.

Interpretation: For completely uncorrelated light, one would expect the coincidences to be completely random, resulting in a $g_{PS}^{(2)}(0)$ value of 1. However, due to the photon pairs generated by the BBO crystal, there are many more coincidences than what would be expected in the random case. The value of $g_{PS}^{(2)}(0)$ is the factor between the measured and expected coincidences and should be at least 50 in the measurement you have taken. Such a large $g_{PS}^{(2)}(0)$ proves the generation of photon pairs. For a more detailed explanation, see Section 3.5.2.

9.3 HBT Experiment with one Arm of the Pair Source

Goal: Test if one arm of the photon pair source is a single photon source.

Setup: Take the setup from Section 9.2, place a beamsplitter in one of the detection arms and place single photon detectors at both outputs of the beamsplitter, see Figure 113. For the adjustment of the setup, see Section 7.5. Then block the arm leading to detector T with the screen.

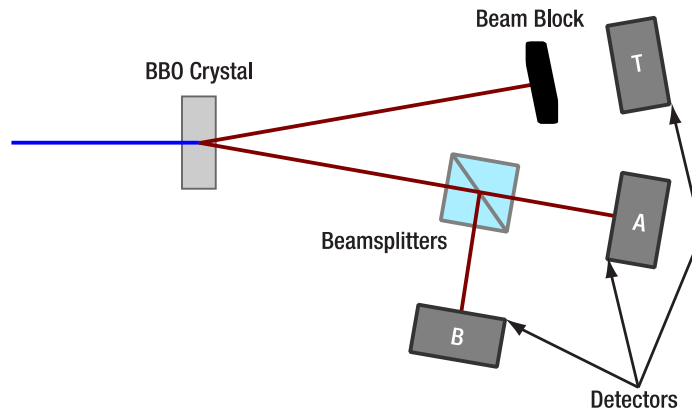


Figure 113 Schematic Setup for the HBT Experiment with one Arm of the Pair Source

Measurement: Darken the room and open the HBT tab in the software. Set the measurement time to 10 s, perform 10 measurements, and record the results of each measurement.

Result Analysis: The correlation $g_{HBT}^{(2)}(0)$ is calculated automatically via the following equation (for the derivation, see Section 3.5.2):

$$g_{HBT}^{(2)}(0) = \frac{R_{AB}}{R_A \cdot R_B \cdot Dt}$$

The result will be $g_{HBT}^{(2)}(0) = 1$ within the error of the measurement for every one of the 10 measurements.

Interpretation: A single arm of the photon pair source is not a single photon source. The photons are actually in a thermal state, so one would expect $g_{HBT}^{(2)}(0) = 2$ with ideal detectors. However, as explained in Section 3.5.2, the time resolution of the detectors used here is far too low and integration leads to the result $g_{HBT}^{(2)}(0) = 1$. To perform single photon experiments with a pair source, one must use the information of the second photon of a pair to create a single photon state, which is shown in the next experiment.

9.4 Grangier-Roger-Aspect Experiment

Goal: Test whether the pair source is a single photon source when counts are measured only in coincidence with the trigger detector.

Setup: Take the setup from Section 9.3 and remove the screen. This setup reproduces the experiment by Grangier, Roger, and Aspect (GRA) that is explained in Section 3.5.3.

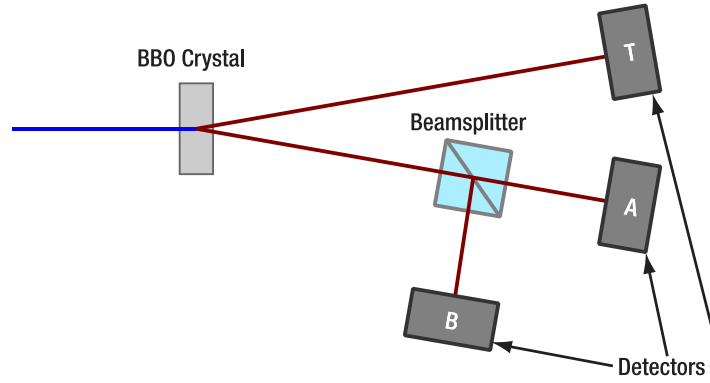


Figure 114 Schematic Setup for the Grangier-Roger-Aspect Experiment

Measurement: Darken the room and open the GRA tab in the software. Set the measurement time to 1 s, perform 10 measurements, and record the results of each measurement. Then set the measurement time to 10 s and again record ten measurements.

Result Analysis: The correlation $g_{GRA}^{(2)}(0)$ is calculated automatically via the following equation (for the derivation, see Section 3.5.4):

$$g_{GRA}^{(2)}(0) = g_{GRA}^{(2)}(0) = \frac{R_{TAB} \cdot R_T}{R_{TA} \cdot R_{TB}}$$

Here, R_T is the single count rate of detector T, R_{TA} and R_{TB} are the twofold coincidence count rates of detector T with detectors A and B, respectively, and R_{TAB} is the triple coincidence count rate.

Compare the measurement series with 1 s and 10 s measurement time, respectively. Calculate the expectation value as well as the standard deviation of $g^{(2)}(0)$ for both cases.

Interpretation: For classical light, one would expect a certain number of triple coincidences depending on the number of trigger events, resulting in a $g^{(2)}(0)$ value between 1 and 2. However, the experiment results in $g^{(2)}(0)$ values much lower than 1, proving that we are dealing with a non-classical light source. For a more detailed explanation, see Section 3.5.4.

The expectation value of $g^{(2)}(0)$ does not depend on the measurement time. The standard deviation on the other hand can be reduced by longer measurements. Table 2 shows an example measurement.

Spec	Measured Value
Total Measurement Time	20.000 s
Counts (Detector T)	4.638 M
Counts (Detector A)	2.905 M
Counts (Detector B)	2.925 M
Coincidence Counts (T&A)	385,865
Coincidence Counts (T&B)	324,688
Coincidence Counts (T&A&B)	513
$g^{(2)}(0)$ - Correlation T&A	114.547
$g^{(2)}(0)$ - Correlation A&B Triggered by T (GRA Setup)	0.0190

Table 2 Example Measurement of the Grangier-Roger-Aspect Experiment

9.5 GRA Experiment with Classical Light

Goal: Perform the GRA experiment with a non-pair source.

Setup: Use the setup of Section 9.4 and replace the BBO crystal with the fluorescent filter. The filter will emit fluorescent light in all directions, so that you can perform the GRA experiment with it. A schematic of the setup is shown in Figure 115.

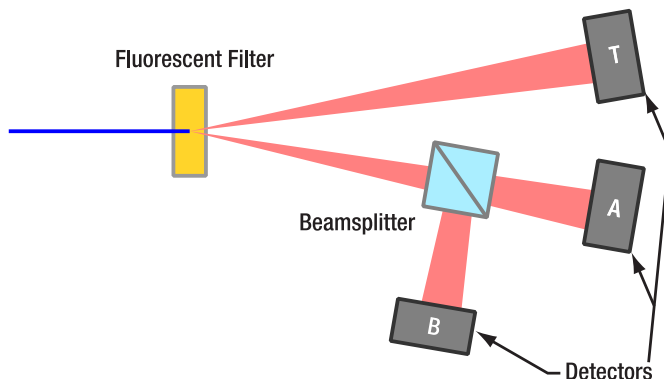


Figure 115 Schematic Setup of GRA Experiment with Fluorescent Filter (Only Relevant Parts of the Fluorescent Light Cone are Shown)

Measurement: Darken the room, set the laser current to about 5 mA below the lasing threshold (check the spec sheet of your laser diode), open the GRA tab of the software and perform 10 measurements with 10 s measurement time each.

Result Analysis: The results are generated with the same formula as in Section 9.4.

$$g_{GRA}^{(2)}(0) = g_{GRA}^{(2)}(0) = \frac{R_{TAB} \cdot R_T}{R_{TA} \cdot R_{TB}}$$

However, this time, the result will always be close to 1.

Interpretation: The light from the filter is in a thermal state. The fluorescent photons are not generated as pairs but randomly. Thus, there is no correlation between events on detector T and detectors A and B. In this case the triple coincidence detection scheme produces the same result as the simpler HBT experiment: $g^{(2)}(0) = 1$. This proves that the result measured in Section 9.4 was not generated only by the change of the detection scheme, but that a pair photon source is required to be able to generate single photon states this way.

9.6 Malus’ Law for Single Photons

Goal: Test the polarization properties of single photons.

Setup: Take the setup from Section 9.4 and place a rotatable linear polarizer between the beamsplitter and detector, as seen in Figure 116. For the adjustment of the setup, see Section 7.5.4.

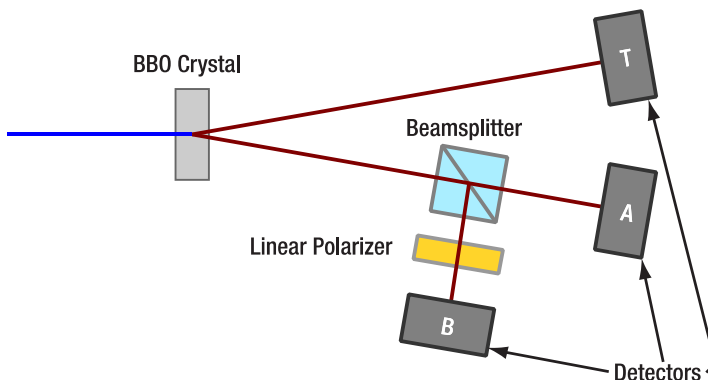


Figure 116 Schematic Setup for the Single Photon Malus’ Law Experiment

Measurement: Set the polarizer to 0° . Darken the room and open the GRA Tab in the software. Set the measurement time to 10 s and record a measurement (the important data points are $g_{GRA}^{(2)}(0)$ and $R_{T\&B}$). Then rotate the polarizer by 10° and repeat the measurement. Record measurements in 10° steps between 0° and 180° (or 360° for a larger dataset).

Result Analysis: Plot the coincidence count rate $R_{T\&B}$ and the correlation $g_{GRA}^{(2)}(0)$ over the polarizer angle.

Interpretation: The coincidence count rate shows a \cos^2 -dependence on the polarizer angle. This is known as Malus' law (for more details, see Section 3.7). However, the simultaneously measured correlation values $g_{GRA}^{(2)}(0)$ are always well below 1, showing that the experiments were always in the single photon regime. The higher values for $g_{GRA}^{(2)}(0)$ at 0° , 180° , and 360° are a result of the extremely low count rates at those angles, significantly increasing the noise and the contribution of uncorrelated stray light to the signal. In summary, the experiment shows that single photons can possess a linear polarization (see Section 3.7) and that their probability to pass through a linear polarizer shows the same behavior as the intensity of a classical electromagnetic wave. An example measurement is shown in Figure 117.

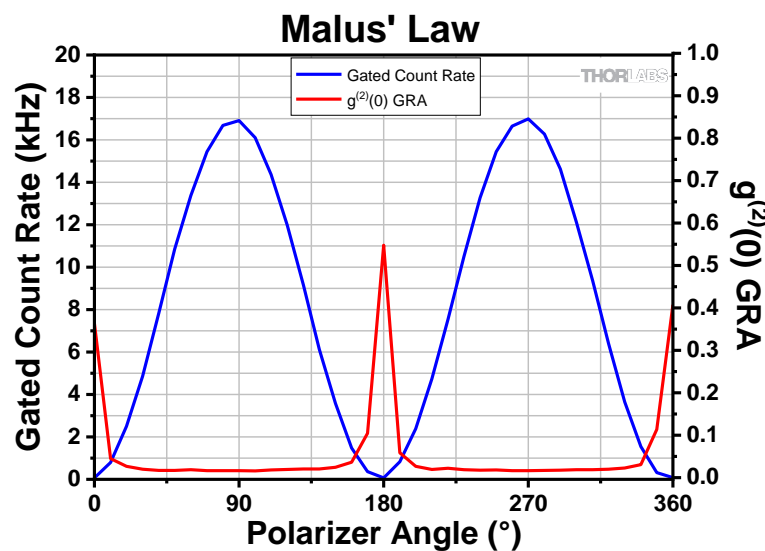


Figure 117 Example Measurement for Malus' Law for Single Photons

9.7 Single Photon Michelson Interferometer

Goal: Test the interference properties of single photons and determine their wavelength.

Setup: Take the setup from Section 9.4 and place a Michelson interferometer in one of the beamsplitter outputs. Place detector B in the output of the interferometer, as seen in Figure 118. For the adjustment of the setup, see Section 7.6.

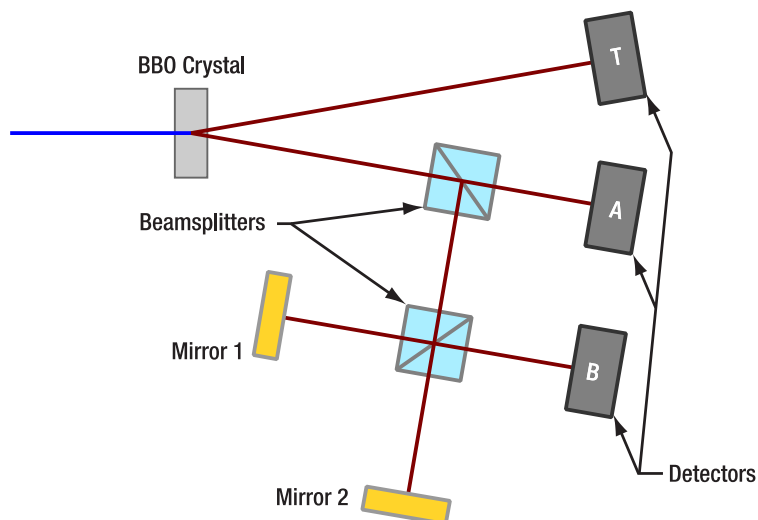


Figure 118 Schematic Setup for the Single Photon Michelson Interferometer

Measurement: Darken the room and open the Michelson Tab in the software. Start a measurement with a long range of stage positions (for example $2\ \mu\text{m}$ - $18\ \mu\text{m}$), a short integration time (such as 400 ms) and a medium step width (such as 25 nm). After the measurement is completed, save the data (see Section 11.3).

Record a second measurement, this time with a reduced measurement range (for example $9\ \mu\text{m}$ Start Position and $11\ \mu\text{m}$ End Position), a longer integration time (such as 1200 ms)⁷⁴, and a smaller step width (such as 10 nm). Again, save the results after completion of the measurement.

Result Analysis: Open the .csv file of the first measurement with a spreadsheet software and plot the data for the coincidence count rate and the $g_{GRA}^{(2)}(0)$ in one graph (use two different y-axes). Determine the average spacing of the maxima and calculate the wavelength of the single photons (see Section 3.6).

Open the spreadsheet of the second measurement and plot it in the same way. Compare the $g_{GRA}^{(2)}(0)$ curves of both measurements.

Interpretation:

The first measurement shows the interferogram over nearly the entire range of the interferometer. An example measurement is shown in Figure 119. The interferogram resembles a sine curve. The maxima are evenly spaced, and the wavelength calculation should result in a value close to 810 nm (twice the pump laser wavelength; see Section 3.9), with an error of up to 3% due to the accuracy of the stage position control⁷⁵. The amplitude of the interference is not changing significantly over the whole measurement range, pointing to a coherence length of the photons larger than $20\ \mu\text{m}$. Quantitatively determining the coherence length requires additional measurements (see Section 10.1).

⁷⁴ You could also reduce the step width below 15 nm to improve spatial resolution. However, there are small oscillations in the interferometer signal due to air currents that become more apparent at smaller step widths, negating most of the resolution gain. If you want to reduce these oscillations, we recommend placing a closed box over the interferometer (with openings for entry and exit of the beam; see Section 12.3).

⁷⁵ If higher precision is required, you can use the PL202 laser to do an interferometric calibration measurement of the stage. Compare the measured wavelength to the actual wavelength of the PL202 (given in the datasheet included with the laser) to determine a correction factor. Apply this factor to all future measurements to obtain more precise wavelength results.

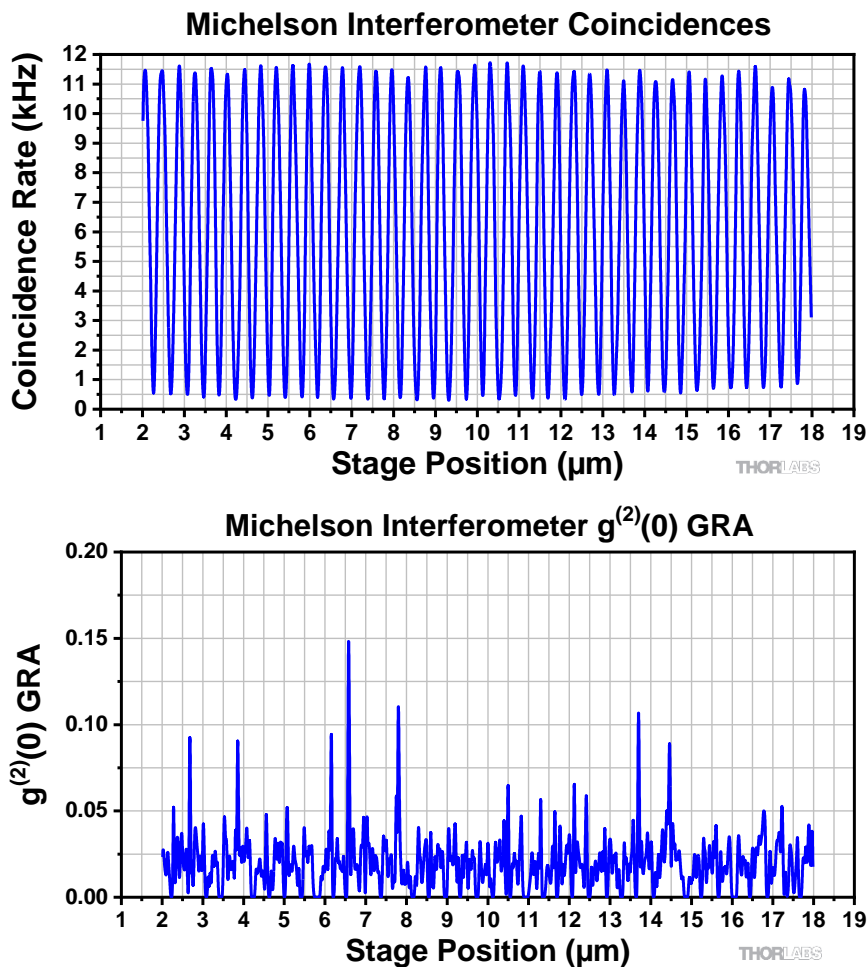


Figure 119 Michelson Interferometer Measurement (Range: 2 μm - 18 μm ; Step Size: 20 nm; Time per Data Point: 300 ms)

The $g_{GRA}^{(2)}(0)$ graph of the first measurement shows significant noise, as seen in Figure 119. For some data points $g^{(2)}(0)$ is measured as 0, but can reach up to 0.15 at some points. The reason for this behavior is the short measurement time per data point. As the calculation of $g_{GRA}^{(2)}(0)$ is highly sensitive to the number of triple coincidences (see Section 3.5.4), and those occur at a much lower rate than two-detector coincidences, more time is required to get meaningful values. However, the average $g_{GRA}^{(2)}(0)$ is still well below 1, pointing to the single-photon regime.

For the second measurement, a larger time per data point and a smaller measurement range were used. An example measurement is shown in Figure 120. As a result of the increased time per data point, the noise of the $g_{GRA}^{(2)}(0)$ curve is significantly lower than for the first measurement. The value of the function is always below 0.1, clearly proving that the whole measurement was performed with non-classical light. Around the minima of the interferogram, all coincidence count rates are much lower. This results in higher noise and a higher relative contribution of uncorrelated stray light to the signal for the $g_{GRA}^{(2)}(0)$ values of these data points.

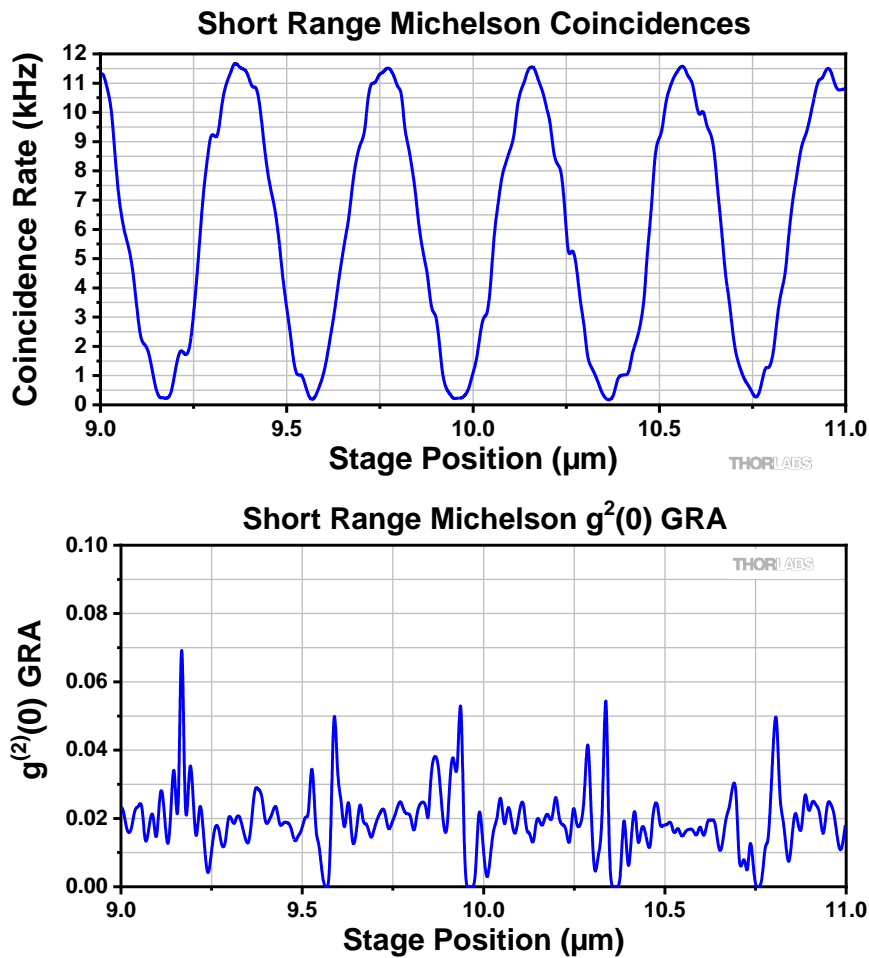


Figure 120 Michelson Measurement (Range: 9 μm - 11 μm, Step Size: 10 nm, Time per Data Point: 1200 ms)

9.8 Quantum Eraser

Goal: Show the quantum eraser effect for single photons.

Setup: Take the setup from Section 9.7 and place one 1/2" diameter polarizer in each arm of the Michelson Interferometer, as seen in Figure 121. For the adjustment of the setup, see Section 7.7.

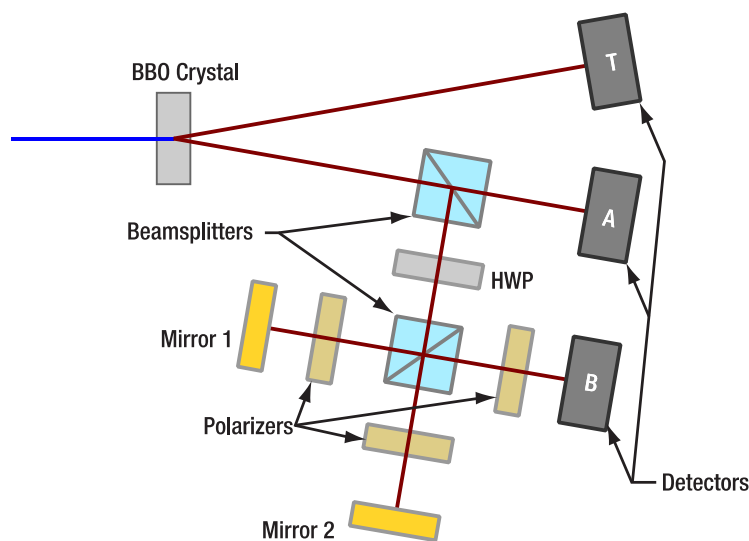


Figure 121 Schematic Setup for the Quantum Eraser Experiment

Measurement: Set both polarizers to 0° , darken the room, and open the Michelson Tab in the software. Set the start and end positions of the stage at about $1\ \mu\text{m}$ apart. Record a measurement. Rotate one of the polarizers to 90° and record a measurement with the same parameters as before. Now place a linear polarizer set to 45° directly in front of detector B and repeat the measurement a third time.

Result Analysis: Plot the R_{TB} coincidence count rate with respect to the stage position for all three measurements in one plot.

Interpretation: An example measurement is shown in Figure 122. The first measurement (both polarizers at 0°) shows a typical interferogram (blue curve) as the polarizations in both arms are parallel.

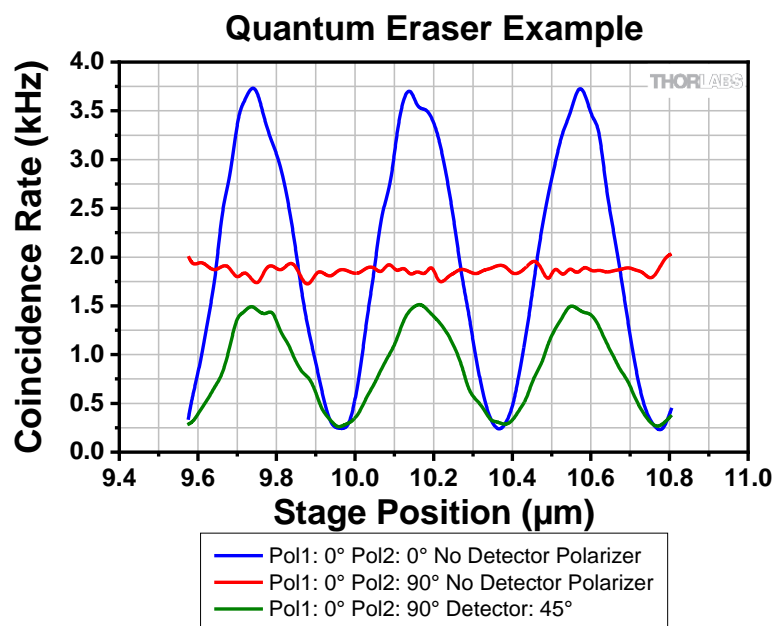


Figure 122 **Quantum Eraser Example Measurement**

In the second measurement (the red curve in Figure 122), the polarization in the arms is set to be perpendicular to each other. Because it would now be possible to determine which arm the photon took at the position of detector B (via a simple polarization measurement), no interference is observed anymore. The constant coincidence count rate is about half of the maximum rate of the first measurement.

The information about the path can be “erased” by the 45° polarizer in the third measurement (the green curve in Figure 122). The probability of a photon reaching the detector is now again the same for both arms, hence an interference curve is observed in the third measurement. The third polarizer is absorbing half of the remaining photons, so the amplitude of the curve in the third measurement is much lower than the first measurement. For more details, see Section 3.8.

Chapter 10 Additional Experiments

10.1 Coherence Length

The coherence length l_c of a light source can be determined by evaluating the envelope of the interferogram taken with the source, as seen in Figure 123.

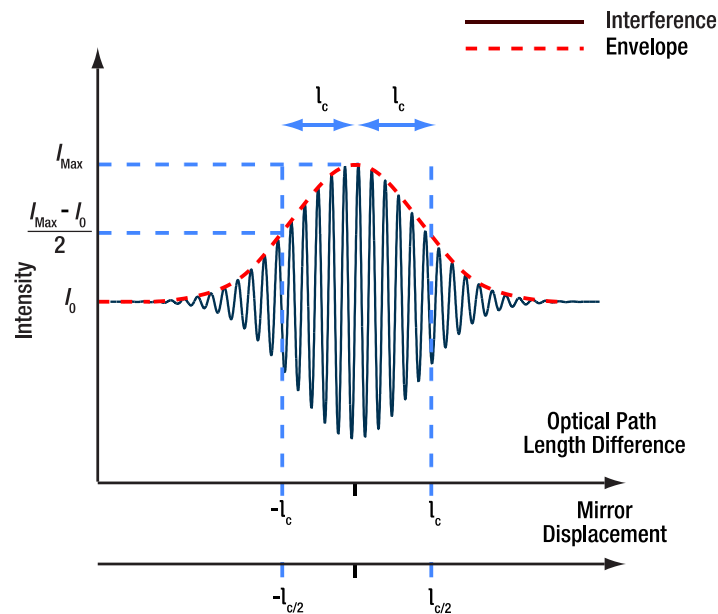


Figure 123 How to Determine the Coherence Length l_c from an Interferogram

It can also be approximated by:

$$l_c = \frac{\lambda^2}{\Delta\lambda}$$

With λ being the center wavelength of the spectrum of the source and $\Delta\lambda$ being the FWHM of the spectral distribution. The photons generated by the SPDC process in the BBO crystal have $\lambda = 810 \text{ nm}$. The spectral width of the photon wavelength distribution is larger than the window of the bandpass filters in front of the detectors. Hence, $\Delta\lambda = 10 \text{ nm}$ is given by the filter window size. This yields:

$$l_c = \frac{\lambda^2}{\Delta\lambda} = \frac{810^2}{10} \text{ nm} = 65.6 \text{ } \mu\text{m}$$

As the piezo moving the stage in the Michelson interferometer of the kit has a maximum range of $20 \text{ } \mu\text{m}$, a single interferogram does not include the whole envelope. Therefore, the following method must be applied to measure the coherence length.

1. Make sure that the fine adjuster is close to the center of its travel range (6 full turns or $300 \text{ } \mu\text{m}$) for the maximum contrast with the red LED. If needed, use the coarse adjuster to ensure the fine adjuster has the full travel range.
2. Then use the fine adjuster to move the stage about two revolutions ($50 \text{ } \mu\text{m}$ per revolution) away from the point of maximum contrast with the red LED.
3. Set the piezo travel range such that about 2 periods of the interferogram are covered. The exact position is not important, but it must be kept the same for all following measurements.
4. Take an interferogram measurement with the above settings and read out the amplitude. Note the value together with the current fine adjuster position.
5. Use the fine adjuster screw to move the stage by $5 \text{ } \mu\text{m}$ in the opposite direction compared to step 2.

- Repeat steps 4 and 5 until enough points have been taken for a good visualization or fit of the envelope (about 40 points).

The coherence length is equal to the full width half maximum (FWHM) of the envelope when the stage position is plotted on the x-axis (see Figure 123). An example measurement is shown in Figure 124. The FWHM of the example measurement is about 55 μm , which is in good agreement with the approximation made above. The small side maxima are caused by the spectral function not being a Gaussian but closer to a rectangle (due to the bandpass filters). For a rectangular spectrum, the envelope is expected to resemble the shape of a $\text{sinc}^2(x) = \left(\frac{\sin(x)}{x}\right)^2$ function.

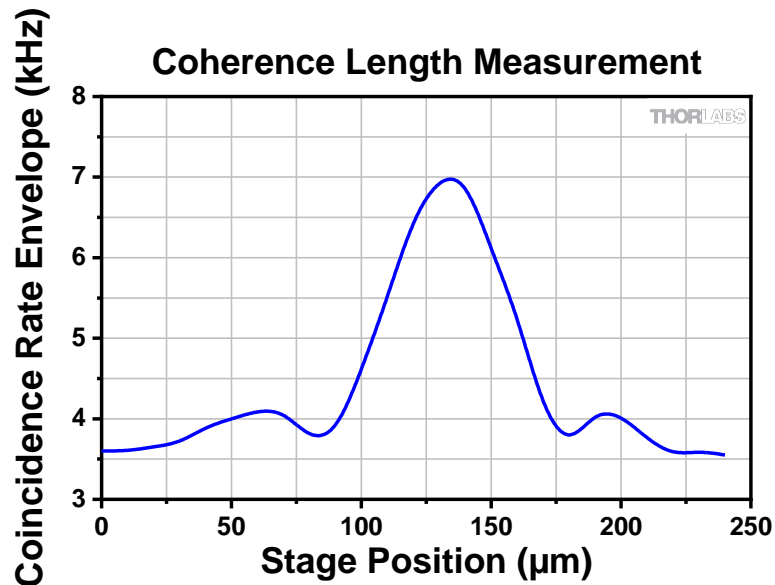


Figure 124 Example Measurement for the Coherence Length of the SPDC Source with Bandpass Filters

An additional experiment could be to exchange the bandpass filters in front of all three detectors with filters with a broader window, such as Thorlabs’ FBH800-40 filter. This way, the coherence lengths would decrease, so that the “true” spectrum of the SPDC source could be measured even with a single interferogram over the whole piezo range. Additionally, the side maxima should disappear due to the spectrum being closer to a Gaussian than to a rectangle. Figure 125 and Figure 126 show two measurements with the FBH800-40 filters, with different positions of the envelope maximum.

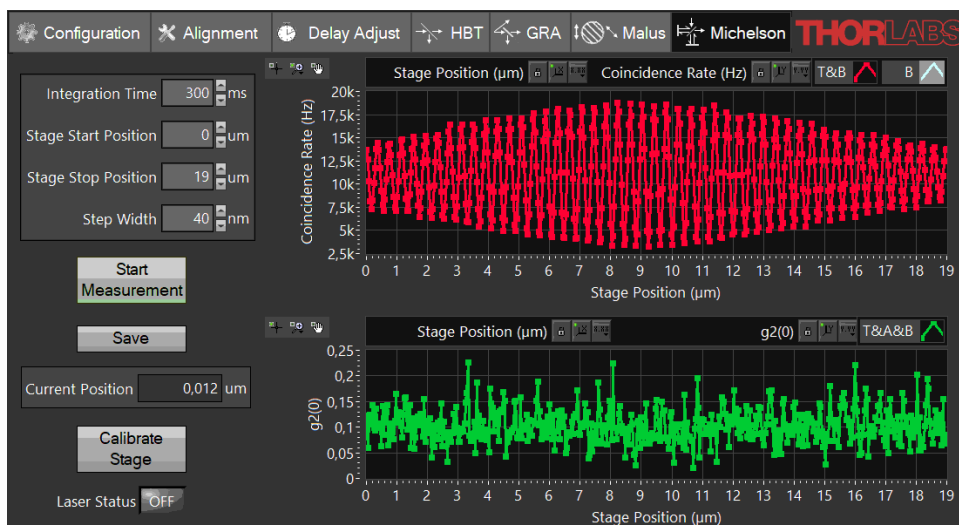


Figure 125 Michelson Measurement with FBH800-40 Filters, Envelope Maximum Centered

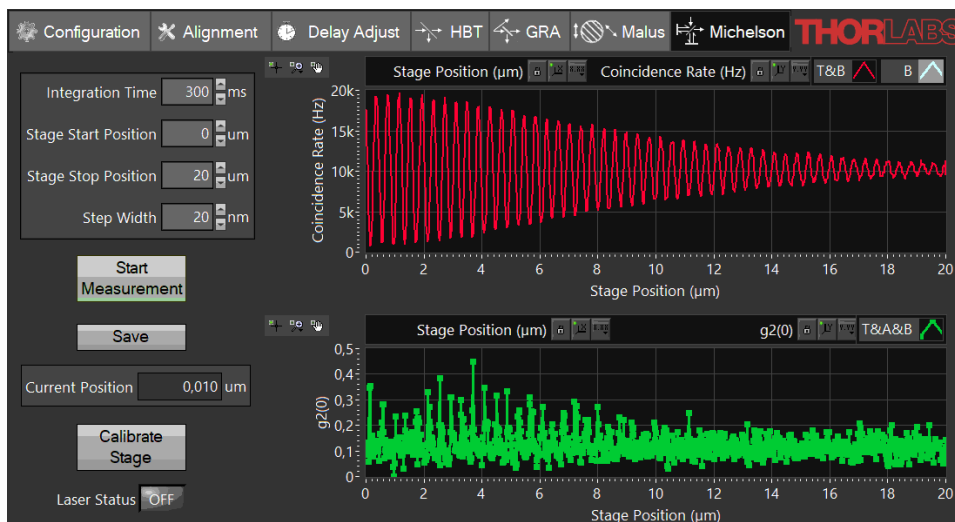


Figure 126 Michelson Measurement with FBH800-40 Filters, Envelope Maximum at 1 μm

10.2 The Three-Polarizer-Paradox

The three-polarizer-paradox describes a situation where the transmission through two crossed polarizers is zero. Upon adding a third polarizer at 45° rotation (with respect to the polarization axis of the other two polarizers) in between, the intensity increases again. This may be counterintuitive when thinking about single photons. From a quantum mechanics perspective, there is a chance that a photon gets either absorbed or transmitted at each polarizer (according to Malus' law, see Section 3.7).

If there were nothing more to it, the increase of the transmitted signal could not be explained, as adding a third polarizer should only decrease the chance of transmission through all polarizers.

But in terms of quantum mechanics, each polarizer must be viewed as a measurement device. As such, the measurement does not just give a reading of the probability to end up in this polarization state, but also projects the incoming state onto the state of the measurement result (see Section 3.2.9).

Therefore, in the case of two crossed polarizers, the first polarizer projects the state onto its own axis and the second polarizer has zero probability for photons to transmit in this state. But once the third polarizer is introduced in between, the state projected by the first polarizer is measured and projected by the intermediate polarizer again. According to Malus' law, the probability to measure a transmitted photon after the 45° rotated polarizer is $\frac{1}{2}$. The last polarizer again measures the probability for the photons projected to the 45° rotated polarization to pass the 90° oriented polarizer, which also is $\frac{1}{2}$. Multiplying the probabilities at each polarizer yields $\frac{1}{4}$ for the transmission through both polarizers after the first one.

This experiment can be set up with the components in this kit. All three polarizers can be placed in front of detector B (setup similar to Section 9.6) and the alignment laser can be used to properly line up the components. To achieve the same height for all three polarizers, you may use the Michelson interferometer breadboard or one PS3 spacer for each $\frac{1}{2}$ " polarizer (one is included in the kit).

A more detailed analysis of this topic and its implications for teaching can be found in the literature⁷⁶, including the optical analogue of the Stern-Gerlach experiment.

10.3 Quantum Computing

Since the experiments in this kit already show that we are dealing with (heralded) single photons, we can use these photons to demonstrate photonic quantum computing (QC). A detailed introduction to quantum computing would be out of scope of this kit. Please refer to cited literature within this section for more context.

⁷⁶ J. M. Brom and F. Rioux, *The Chemical Educator*, **7**, 200 (2002).

In the following, we give a short description of basic quantum computing algorithms with a strong focus on the general concept and the concrete technical implementation based on this kit. It is important to note that these algorithms can only deliver answers to highly specialized problems and are by no means suitable for general purpose calculations we are used to from modern PCs.

The goal is not to provide a complete understanding of QC algorithms in general. The teaching value of this experimental realization lies in an actual implementation of a qubit system and to demonstrate the actions of QC operations in an environment that can also be understood from a purely optical perspective. It further serves to demonstrate challenges, like phase-noise, in real-world implementations and how this influences the outcome of quantum computations.

This section is structured in the following way: We start by briefly introducing the concept of qubits and gate operations. Then, we present the algorithm that can be implemented based on this educational kit, the Deutsch-Jozsa algorithm (DJA). Next, we explain how the DJA is implemented in a purely optical fashion, followed by the actual experimental realization and sample measurements.

10.3.1 Qubits and Gates

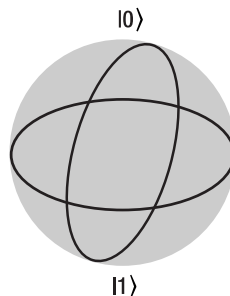
Generally, the power of QC stems from superpositions of states: While a classical bit can only be in one state (off/on; 0/1), in QC a so-called qubit can be in any superposition of both states.

$$(a|0\rangle + b|1\rangle) \quad a, b \in \mathbb{C}$$

Since in quantum mechanics, the total amplitude must fulfill a norm condition and the global phase does not influence a measurement outcome, the two complex coefficients can be reduced to two real valued angles and any superposition state can be written as:

$$\left(\cos\frac{\theta}{2}|0\rangle + e^{i\varphi}\sin\frac{\theta}{2}|1\rangle\right)$$

Using this representation, any single qubit superposition state can be graphically represented on the surface of the so-called Bloch sphere.



In the following we will not only discuss a single qubit state, but also the combination of two qubits, labeled x and y . To make it clearer which state belongs to which qubit, we use $|x\rangle$ and $|y\rangle$ to label the state of each qubit and x, y indices to indicate which qubit the basis state belongs to. For example, the combined state $|x\rangle|y\rangle = \frac{1}{\sqrt{2}}(|0\rangle + |1\rangle)_x \cdot |1\rangle_y$ means that qubit x is in an equal superposition state of 0 and 1, while the other qubit y is only in the 1 basis state.

Operations that change the state of one or more qubits are called gates in resemblance of the classical bit counterparts.

One example would be the Hadamard gate, which transforms the single qubit input states:

$$|0\rangle \leftrightarrow \frac{1}{\sqrt{2}}(|0\rangle + |1\rangle) \quad \text{and} \quad |1\rangle \leftrightarrow \frac{1}{\sqrt{2}}(|0\rangle - |1\rangle)$$

and thus, can be used to transform back and forth between a qubit basis state and a superposition state.

Another often used quantum gate involving two qubits is the controlled-not (CNOT) gate. It inverts the state of one qubit y based on the state of the other (control) qubit x :

$$|0\rangle_x: |y\rangle \text{ is left unchanged}$$

$$|1\rangle_x: |0\rangle_y \leftrightarrow |1\rangle_y$$

Such multi-qubit operations can create system states that cannot be written as simple products of the single qubit states (separable states). Such states can be mixed or entangled qubit states.

In photonic QC, various properties of a single photon⁷⁷ can be used to represent orthogonal bases for qubits.

For example, one qubit basis could be defined by the orthogonal polarization basis $|V\rangle$ & $|H\rangle$, i.e., the vertical and horizontal linear polarizations, that span the space of all polarization states. Here, the Bloch sphere is in a one-to-one correspondence to the Poincaré sphere. A halfwave plate (HWP) can be used to define a range of different gates, for example:

- If the HWP is oriented with an optic axis at 45° to the vertical axis, it flips a photon with vertical polarization to horizontal polarization upon transmission, $|V\rangle \leftrightarrow |H\rangle$. This is a NOT gate, also known as an X-gate.
- If the HWP is oriented with an optic axis at 22.5° to the vertical axis, the photon is projected onto the polarization states $|V\rangle \rightarrow \frac{1}{\sqrt{2}}(|V\rangle + |H\rangle)$ and $|H\rangle \rightarrow \frac{1}{\sqrt{2}}(|V\rangle - |H\rangle)$ which corresponds to the definition of the Hadamard gate above.
- If the HWP is oriented with its slow axis vertical, it introduces a 180° phase shift to the $|V\rangle$ basis. This is a phase gate (P-gate).

Another representation of a qubit makes use of the path state of a single photon in an interferometer. Here we label the two arms of the interferometer with states $|A\rangle$ & $|B\rangle$. As the experiments in this kit show, the photon will be in a superposition state of both arms. The coefficients for both states are described by the relative probability amplitudes (in the examples of this kit both arms always have the same amplitude) and the phase difference. In this representation of a qubit, beamsplitters serve as a close analog to a Hadamard gate⁷⁸.

Combining the polarization state with the path state of a single photon yields a two-qubit system. Both qubit states can be manipulated independently by either changing the polarization (e.g. rotation) or the path state (e.g. a phase shift in one arm). Also, a two-qubit operation like the CNOT gate would for example flip the polarization state between horizontal and vertical polarization depending only on one arm of the interferometer.

In principle, further qubit states can be added to a single photon state, e.g., by creating more path states when nesting interferometers within each other⁷⁹, or making use of the photons' orbital angular momentum⁸⁰. Both notably increase the complexity of the optical setup, so we do not recommend this for introductory student setups.

10.3.2 Deutsch-Jozsa Algorithm

The Deutsch-Jozsa algorithm⁸¹ (DJA) is one of the first proof-of-principle algorithms to run on any quantum computation platform. In the Qiskit textbook⁸², DJA is the first quantum algorithm presented to new learners.

Given an n -bit binary function $f: \{0,1\}^n \mapsto \{0,1\}$, the DJA is designed to determine whether the function is constant (same output for any input) or balanced (half of the inputs are mapped to 0 and the other half to 1). In the following we only consider the case for $n = 1$ (also known as the Deutsch algorithm), which can be solved by a two-qubit quantum computer in one run, while a classical computer would need to evaluate both $f(0)$ and $f(1)$ using two function calls.

⁷⁷ While it is possible to use additional photons to increase the number of qubits, it is not easy to let the states of these photons interact in a controlled way.

⁷⁸ Strictly speaking, beamsplitters introduce different phase shifts than Hadamard gates, but this can be compensated by other optical elements or adjusting the interferometer path lengths accordingly.

⁷⁹ P. G. Kwiat et al., *Journal of Modern Optics*, **47**(2-3), (2000).

⁸⁰ J. Leach et al., *Optics Express*, **17**(10), 8287 (2009).

⁸¹ D. Deutsch and R. Jozsa, *Proceedings of the Royal Society of London. Series A: Mathematical and Physical Sciences*, **439**(1907), 553 (1992).

⁸² <https://learn.qiskit.org/course/ch-algorithms/quantum-circuits>

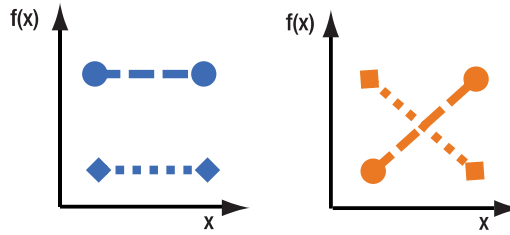


Figure 127 The four possible functions for the Deutsch algorithm: constant (left) or balanced (right) output.

One possible two-qubit quantum circuit which solves the Deutsch problem is shown in Figure 128. The two rows show the operations done on each qubit from left to right.

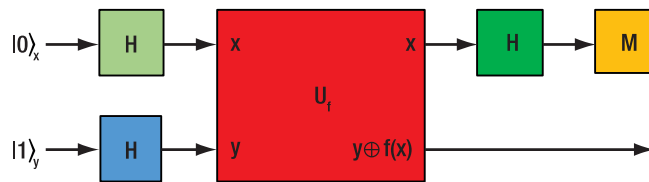


Figure 128 Quantum circuit to solve the Deutsch problem, based on two qubits labeled x and y . It uses three Hadamard gates (H) and a two-qubit gate (U_f) described in the text. The result is obtained from measuring the state of qubit x (M).

The Hadamard gates are used to prepare a separable superposition input state for both qubits (x and y), i.e.

$$|x\rangle |y\rangle = \frac{1}{\sqrt{2}}(|0\rangle + |1\rangle)_x \cdot \frac{1}{\sqrt{2}}(|0\rangle - |1\rangle)_y$$

The two-qubit gate $U_f: |x\rangle |y\rangle \rightarrow |x\rangle |y \oplus f(x)\rangle$ essentially flips the state of the second qubit based on the defined function value for the first qubit’s states and can be simply realized by (controlled) NOT gates. After this operation the qubit state is

$$|x\rangle |y\rangle = \frac{1}{2} \left((-1)^{f(0)} |0\rangle + (-1)^{f(1)} |1\rangle \right)_x \cdot (|0\rangle - |1\rangle)_y$$

Note that due to the properties of the chosen input superposition state, the resulting y -qubit state remains identical to the input, while the information about the solution is imprinted onto the x -qubit via a process called phase-kickback⁸³.

Thus, depending on whether the function is constant or balanced, the x -qubit will be in one of two superposition states $|x\rangle \propto (|0\rangle \pm |1\rangle)$. After the last Hadamard gate the x -qubit ends up in a clean $|0\rangle$ or $|1\rangle$ basis state which, theoretically, can be measured without uncertainty. If the measurement returns the $|0\rangle$ state, the function is constant. If the $|1\rangle$ state is measured, the function is balanced.

10.3.3 Optical Implementation

The above quantum circuitry can be mapped onto an optical interferometry setup⁸⁴ with a 1:1 correspondence between quantum gates and optical elements, as can be seen in Figure 129.

⁸³ <https://learn.qiskit.org/course/ch-gates/phase-kickback>

⁸⁴ M. Scholz et al., *Physical Review Letters*, **96**(18), 180501 (2006).

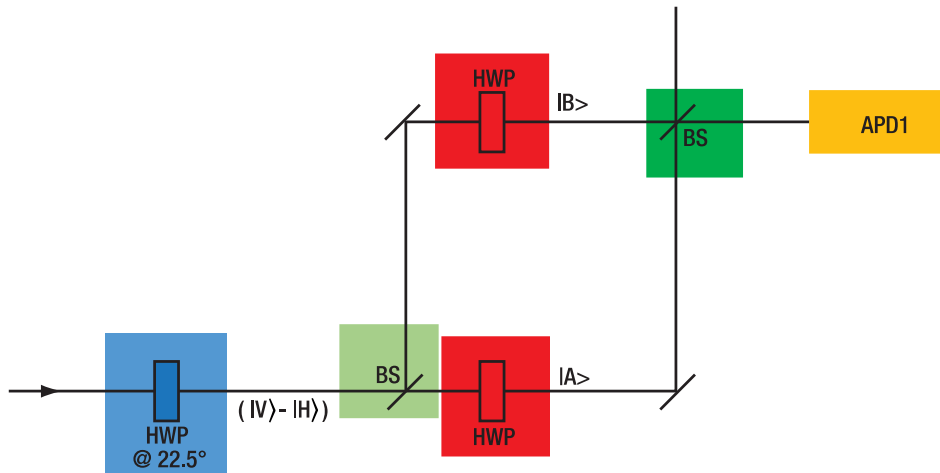


Figure 129 Scheme for the optical implementation of the Deutsch algorithm in a Mach-Zehnder interferometer configuration. The color-highlighted elements correspond to elements of the quantum circuit in Figure 128.

Here, the first qubit state $|x\rangle$ is represented by the two path states of the single photon in an interferometer and the qubit $|y\rangle$ is given by its polarization state.

State initialization is performed by setting the polarization to $|y\rangle \propto |V\rangle - |H\rangle$, i.e., linear polarization is rotated by 45° against the vertical axis. This can be done using a polarizer or a half-wave plate. The $|x\rangle \propto |A\rangle + |B\rangle$ state is generated by a 50:50 beamsplitter and the relative phase is adjusted via the path lengths of the interferometer.

Depending on which kind of function is used to demonstrate the Deutsch algorithm (constant or balanced function), the polarization states $|V\rangle \leftrightarrow |H\rangle$ must be flipped if $f(x) = 1$. This is done by introducing HWP(s) set to 45° with respect to the vertical into one of the interferometer arms for a balanced function or to none or both arms for a constant function.

The last Hadamard gate is again represented by combining both arms at a beamsplitter, where due to interference between states $|A\rangle$ & $|B\rangle$ photons exit through only one of the outputs, depending on the type of the function.

A second way to interpret what is happening in the interferometer does not require any knowledge of quantum mechanics and just considers the effects of the optical elements onto the photons:

An interferometer is set up in a way, that all photons are linearly polarized and exit through one output of the recombining beamsplitter (constructive interference). Now if a HWP is introduced to one of the arms, such that the slow axis is aligned with the polarization axis, the relative phase difference between the arms is shifted by π , which makes all photons exit at the other output port of the beamsplitter. Introducing HWPs in both arms keeps the phase difference and output port unchanged compared to the initial situation. When the photon's polarization is aligned with the slow axis of the HWP, its polarization state also remains unchanged, fully in line with the conclusions that can be drawn from the quantum circuitry analysis.

In the kit we use an interferometer in Michelson configuration instead of the above discussed Mach-Zehnder configuration. The latter one is beneficial for theoretical discussion, as each gate operation corresponds to a single optical element. The Michelson interferometer is more practical for experimental realizations, as it is easier to align and control the phase difference between both arms. The analogy with the quantum circuitry is left unchanged, but we require only one beamsplitter element for both Hadamard operations on the path qubit. In the Michelson configuration, the elements in the interferometer arms are passed in both directions; therefore, the phase shifts are doubled. To achieve the same phase shifts as in the Mach-Zehnder configuration, we use quarter-wave plates (QWP) instead of HWPs.

10.3.4 Experimental Realization

For experimental realization, the following extra components which are not included in this kit are required:

- 2 x LCC1111-B
- 2 x KLC101
- 1 x TPS002
- 2 x Mounting kit, each:
 - RS1.5P8E (RS1.5P4M)
 - RS4M
 - 8-32 (M4) setscrew, 3/4" (20 mm) long⁸⁵
 - RSP1D(/M)



We recommend using a 20 x 20 cm stainless steel board instead of the MB8 (MB2020/M) aluminum breadboard as the basis for the Michelson interferometer to reduce thermal drift effects. This can be ordered from Thorlabs as a special, comparable to the MB6S (MB15S/M) breadboard.

The phase difference between the arms of the interferometer plays a crucial role for the quantum computation. Since manual alignment attempts, such as moving a wave plate, strongly disturb this phase relation, we use a pair of liquid crystal cells (LCC) to control the phases in both arms and switch the effective presence of a wave plate in each arm without moving mechanical parts. This way, the setup needs to be aligned only once, analog to the quantum eraser experiment (Section 7.7), to correct for beam deviations introduced by the cells. As the glass walls of the cells add a considerable amount of dispersion, a cell must be used in each arm or a suitable compensation plate must be placed in the arm without a liquid crystal cell.

The KLC101 controllers are used to apply the correct alternating voltage signals for long life-time operation of the LCCs. The controllers can be operated manually using their front panel controls or with the Kinesis software (recommended)⁸⁶. Their operation is not integrated in the software for this kit. Please refer to the KLC101 controller manual for operation details.

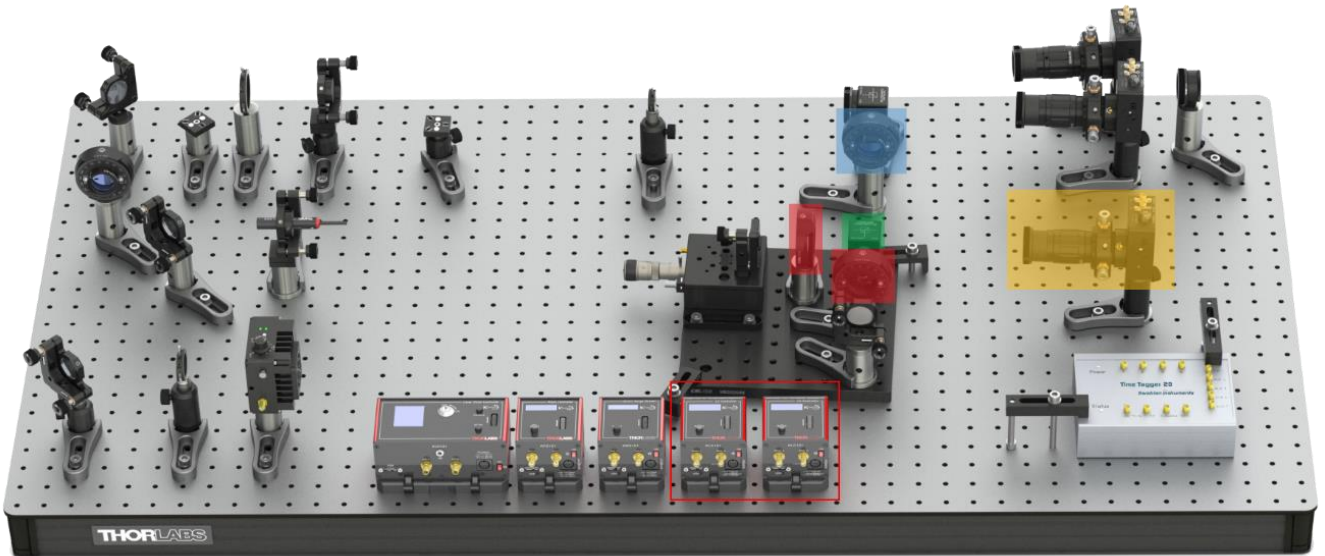


Figure 130 Fully set up Deutsch algorithm. The color-highlighted elements correspond to elements of the quantum circuit in Figure 128 and Figure 129. Details are given in the text. Additional KLC101 controllers are placed in the red rectangle.

⁸⁵ These screws can be ordered as packs of 50 under the part number SS8S075 (SS4MS20).

⁸⁶ When using the Kinesis software, do not connect to the KLD101, KSG101, and KPZ101 controllers, otherwise the EDU-QOP1 software cannot connect to them. We recommend starting the EDU-QOP1 software first; then only the KLC101 controllers will be listed in Kinesis.

Figure 130 shows the implementation of the DJA based on this kit, using two LCC1111-B liquid crystal retarders and KLC101 liquid crystal controllers. The HWP between the two beamsplitters and the rest of the setup stay in the same orientation in the quantum eraser experiment. When viewed from the Michelson board towards the first beamsplitter, the fast axis of the HWP should be oriented at 22.5° counterclockwise.

1. Assemble the LCC components in their mounts as shown in the explosion rendering and insert them into the Michelson interferometer in the same way as the polarizers in the Quantum Eraser experiment (see Section 7.7). The orientations of the slow axis of the LCCs can be seen in Figure 131.
 - a. When looking from the **fixed mirror** towards the beamsplitter, the slow axis of the wave plate in this arm should be oriented at **45° counterclockwise** from the 12 o'clock (vertical) position.
 - b. When looking from the **stage mirror** towards the beamsplitter, the slow axis of the wave plate in this arm should be oriented at **45° clockwise** from the 12 o'clock (vertical) position.



Figure 131 Orientation of the LCCs in the Michelson interferometer

2. Set both KLC101 controllers to $V_{\text{HIGH}} = 20 \text{ V}$, where the LCC acts like there is no wave plate in the system. This voltage can be saved as “Preset 1” in the KLC101 controller. On the front panel of the KLC101 controller, use the menu button and scroll wheel to navigate to “LC config” → “Set Preset 1” → “Set Volt 1: 20V” and confirm to save the preset. To actually select a preset navigate to “LC output” → “Preset1 V1 enabled” → “Preset V1 20V”. In the Kinesis software you only need to click on the Preset indicators to select them (will light up green) and set the voltage of the preset with the blue “set” arrow.
3. Align the interferometer, analog to the description for the Quantum Eraser (see Section 7.7), such that you see an interference pattern from the LED.
4. Use the Michelson tab in the software to record a single photon interference pattern. Look for a stage position with a minimum in the interference signal (see Figure 132). Enter this value as the start position in the Michelson tab. The stage will be kept at this position as long as no scan is started.

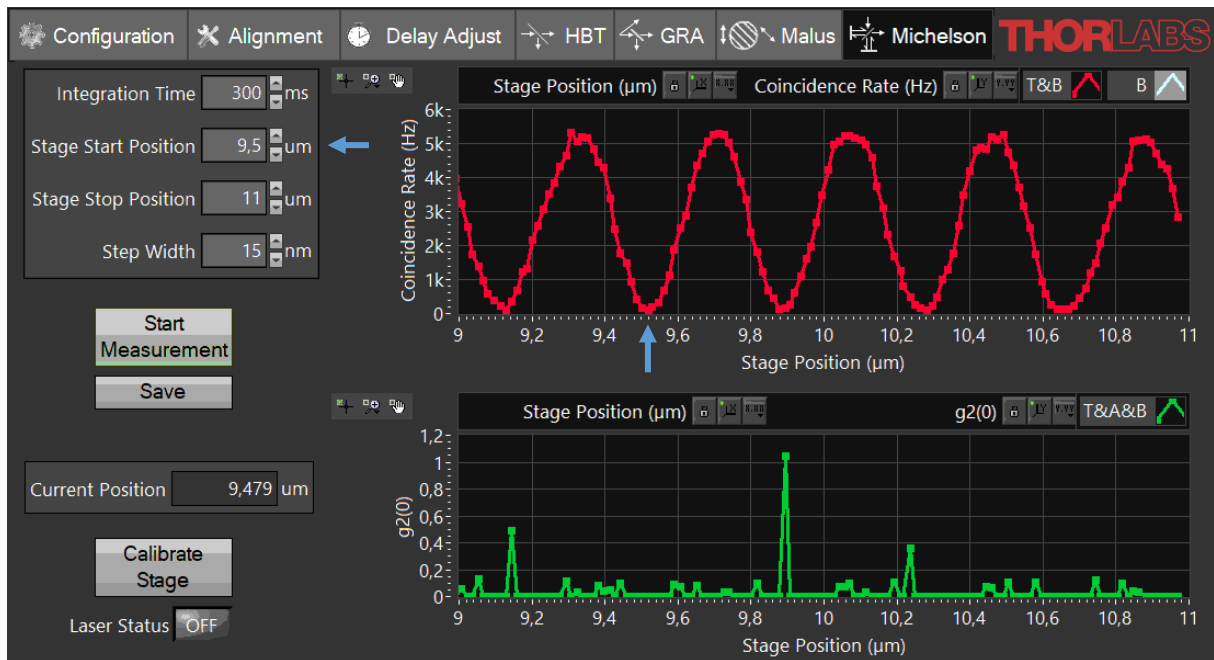


Figure 132 Choosing a Working Point in the Interference Signal. Here 9.5 μm is selected.

- This will be the working point for calibration of the LCCs and later measurements. If the Michelson breadboard changes temperature and expands or contracts, this affects the phase of the interferogram at the working position. During calibration of the LCCs the phase must be stable. Should you observe notable phase drift during calibration, you need to start again with a new working point.
- Move to the Alignment tab of the software and monitor the T&B coincidence count rate while adjusting the voltage V_{LOW} ("Preset 2") of one of the KLC101 controllers between 1.5 and 2.5 V⁸⁷. Once a maximum in the rate is reached, you have calibrated the correct voltage setting for the desired (relative) quarter-wave retardance. The interference patterns in the Michelson tab should exhibit a half-wave phase shift, when changing between the two defined high and low voltage settings at the controller, as shown in Figure 133.
- Reset both KLC101 controllers to $V_{\text{HIGH}} = 20 \text{ V}$ and repeat the process to calibrate the second liquid crystal cell as well.
- Changing environmental conditions, such as temperature and humidity, shift the phase of the interference pattern over time. In order to get correct results from the Deutsch algorithm, you have to readjust the stage position as explained in the fourth step to update the working point from time to time. See also Section 10.3.6.

⁸⁷ From the factory test sheet of the liquid crystal cell, it is possible to calculate a narrower voltage range where quarter-wave retardance can be found.

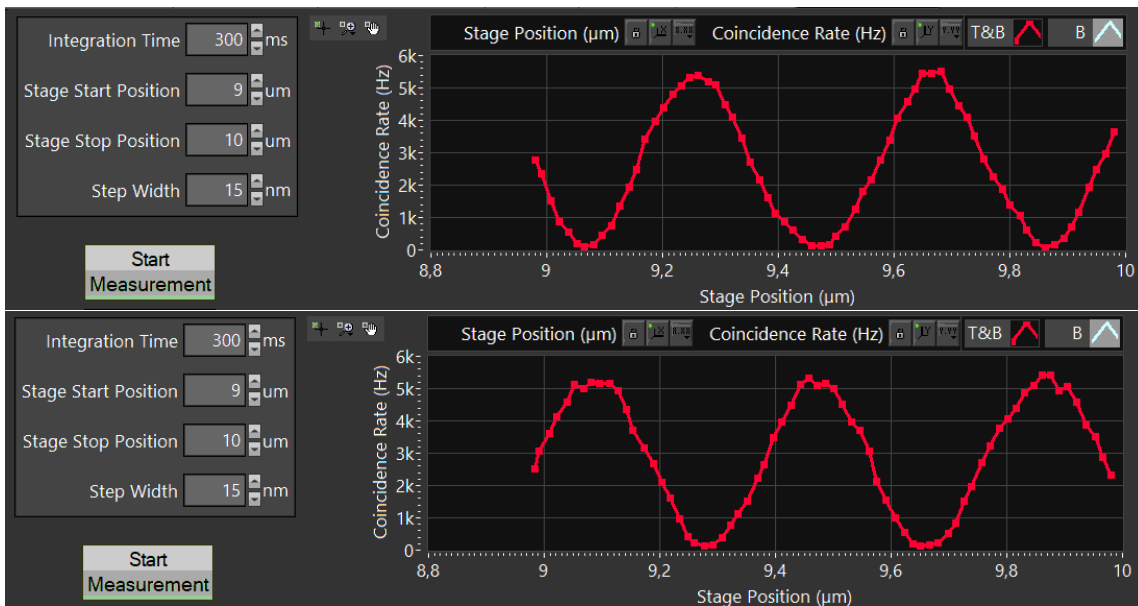


Figure 133 Michelson signal with both LCC voltages at 20 V (top) and one LCC voltage at calibrated low voltage (bottom).

10.3.5 Sample Measurements

The Deutsch algorithm can now be tested for any of the four possible function inputs:

- Two constant functions – Minimum T&B coincidence count rate:
 - Both LCC voltages are set to V_{HIGH} . Effectively, no arm contains a wave plate.
 - Both LCC voltage are set to V_{LOW} . Effectively, both arms contain a wave plate.
- Two balanced functions – Maximum T&B coincidence count rate:
 - Only one LCC voltage is set to V_{HIGH} , the other is at V_{LOW} . Only the arm set at V_{LOW} voltage effectively contains a wave plate.

Figure 134 shows the output state of the Deutsch algorithm for all four possible functions. All single photons exit the Michelson interferometer either at the output with the detector in case of balanced functions (maximum count rate) or leave through the input in case of constant functions (minimum count rate). This way, we may differentiate both types of functions from our detector signal.

While the results can be fully interpreted by the quantum-mechanical formalism introduced above, there is another explanation which requires no quantum mechanics at all:

- The linear input polarization of our single photons is aligned exactly with the slow axes of the LCCs. Therefore, there is no net change of the polarization state, but only additional retardance by a quarter wavelength with each pass through the cell, if the voltage is set at V_{LOW} .
- With both LCCs at minimum retardance (set at V_{HIGH}), the working point for the interferometer has been chosen such, that destructive interference is obtained at the detector output and all photons leave through the input.
- Switching one of the LCCs to low voltage (V_{LOW}) introduces a half-wavelength phase shift in the respective interferometer arm. This inverts the interference conditions for the output ports and all photons now leave at the detector port.
- Switching both LCCs to low voltage (V_{LOW}) introduces the same phase shift in both arms and the interference conditions are analog to the first condition.

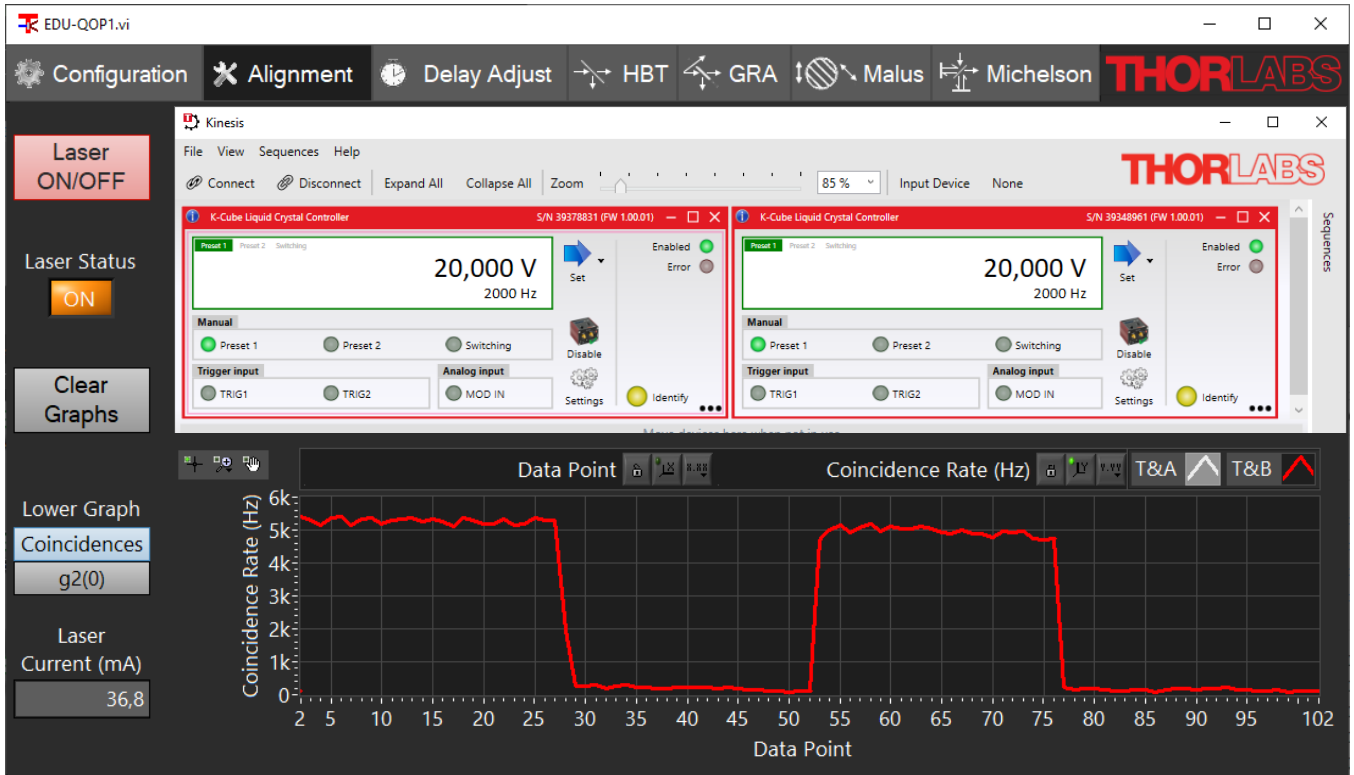


Figure 134 T&B Coincidence Signal for All Four Functions of the Deutsch Algorithm with Voltage Combinations $V_{HIGH}V_{LOW} \rightarrow V_{LOW}V_{LOW} \rightarrow V_{LOW}V_{HIGH} \rightarrow V_{HIGH}V_{HIGH}$. The inset shows the Kinesis settings for the last combination.

10.3.6 Discussion of Error Sources

Unless the setup is perfectly in thermal equilibrium with its environment, the Michelson breadboard’s temperature changes over time and contracts or expands. This may lead to a drift of the relative phase between both interferometer arms, which decreases the count rate contrast between both output states and eventually may even invert the meaning of minimum and maximum rate states. This visualizes the immense importance that phase stability and phase noise play in quantum circuitry and is a good opportunity to discuss this challenge in modern research. In this example, the noise affects the phase difference between $|A\rangle&|B\rangle$ of the $|x\rangle$ qubit state.

- Replacing the aluminum breadboard with a stainless-steel counterpart reduces thermal drift effects.
- Air currents also introduce phase noise and can be suppressed by housing the interferometer in a box (see Section 12.3).

Furthermore, we can demonstrate the importance of clean qubit state initialization: It is possible to rotate the HWP between both beamsplitters, which defines the input polarization state, i.e., the initial qubit state $|y\rangle$. This changes the results for the balanced function configuration. As soon as the HWP is rotated out of the optimal position, the coincidence count rate of the balanced functions state decreases. If we only use a single photon to detect the state, our calculation would not be reliable anymore, as there is a chance that the photon does not reach the detector but leaves at the input port of the Michelson interferometer. Finally, identical count rates are obtained for all functions if the input polarization is rotated by 90° onto $|y\rangle \propto |V\rangle + |H\rangle$. Using the quantum-mechanical formalism, one can show that the DJA does not work with this input state. From the optical perspective, it can be understood like this: The input polarization is now perpendicular to the slow axes of the LCCs. Therefore, switching the retardance of the LCC does not have any effect for the transmitted photons.

10.3.7 Further Algorithm Ideas

Other optical implementations of QC algorithms, such as Grover's⁸⁸ and Shor's^{89,90} algorithm, can be found in literature. If you have concrete implementations that could usefully extend the scope of this kit, please do not hesitate to contact us.

10.4 Direct Event Pulse Observation

For educational purposes one may want to view the TTL pulses generated by the three detectors directly. Observing the incoming pulses can be helpful to establishing an understanding of the different temporal distribution for the pair source compared to a classical light source. Based on these observations the statistical quantities described in the theory section can be motivated further.

Viewing the pulses directly also helps when discussing technical aspects of the detectors, like pulse length, jitter, or afterpulsing.

To view the detector pulses, you can use any kind of oscilloscope or logic level analyzer with a timing resolution on the order of nanoseconds, i.e., a minimum bandwidth of about 1 Gigahertz. The Time Tagger included in the kit also has a logic level scope integrated as a software module, which will be described at the end of this section.

Recommended general settings for any kind of scope are:

- A displayed time window of 200 - 500 nanoseconds
- A maximum voltage level of 5 V
- A trigger level at 0.5 - 2 V
- A negative trigger delay of a few 10s of nanoseconds, to show what happens before the trigger pulse arrives
- Trigger input on pulses of detector T

You may choose to trigger on detectors A or B instead as well. However, triggering on detector T will show similar relative frequencies of coincidence events as in the experiments described above. As the detection rates on detector T are highest (while A or B have at maximum half the rate due to the beamsplitter), many trigger events will only show a trigger pulse without coincidence. Even without the beamsplitter, as stated in Section 4.1, the chances of coincidences are relatively low, as the detection efficiency of the SPDMA detectors is below 50% meaning that often only one photon of a pair will be detected.

To use the scope module of the time tagger, start the Time Tagger Lab software that comes with the installation of the drivers required for the kit. Choose the Time Tagger that is connected to detectors, as seen in Figure 135.

⁸⁸ P. G. Kwiat et al., *Journal of Modern Optics*, 47(2-3), (2000).

⁸⁹ C. Y. Lu et al., *Physical review Letters*, 99(25), 250504 (2007).

⁹⁰ B. P. Lanyon et al., *Physical Review Letters*, 99(25), 250505 (2007).

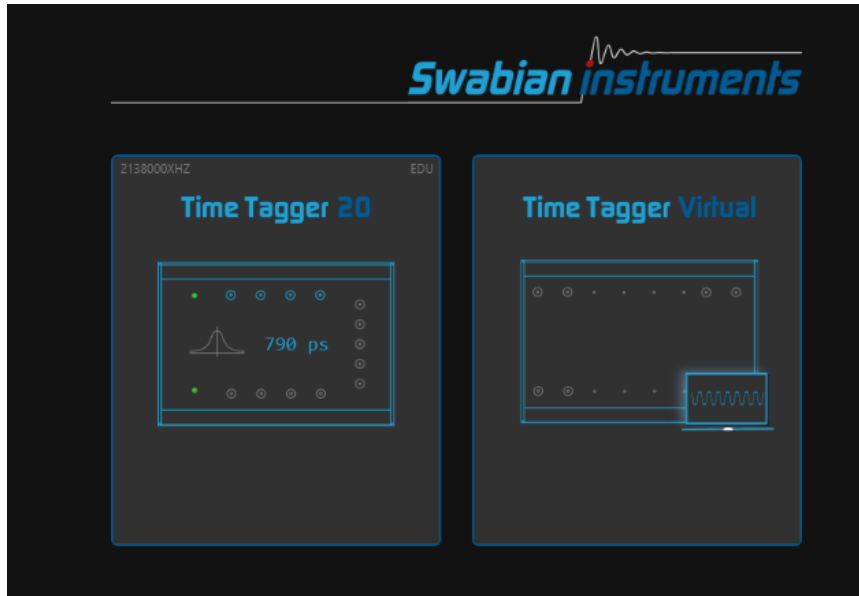


Figure 135 Startup Page of the Time Tagger Software

After connecting to your Time Tagger, you will see the “Home” tab with a visual representation of the device and a live view of incoming count rates at the three connected detector inputs. Use the switch above to change to the detailed view, where you can set the input delays (see Figure 136). Note that you must set the same delay values for rising and falling flanks for the scope module to show the true input signals. You may use zero delay for channel T (1) and the same input delay values for channels A (2) and B (3) as calibrated using the delay tab of this kit’s software. It is also possible to assign names to the channels here, which will be shown throughout the software.

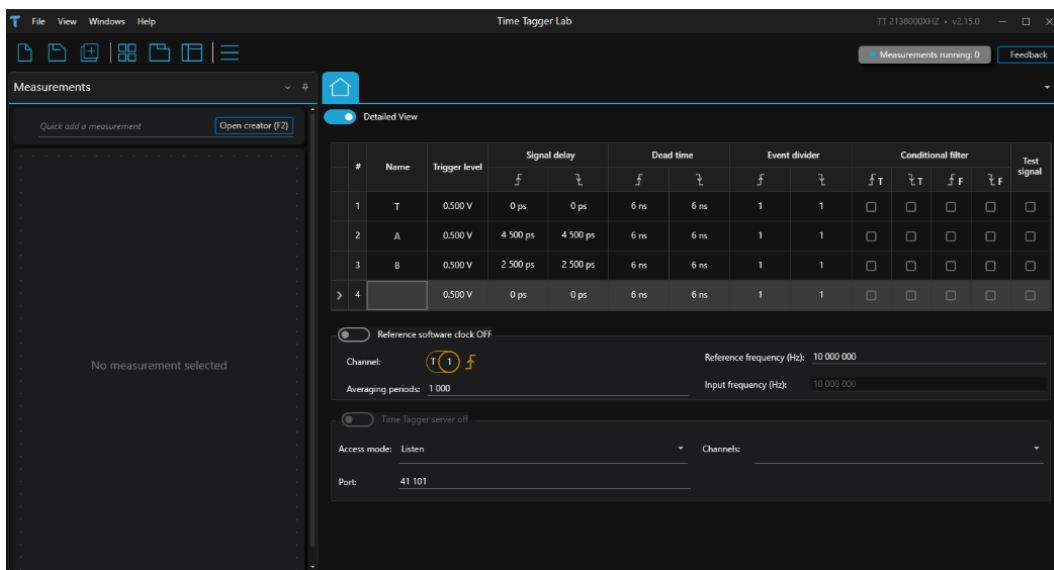


Figure 136 Detailed View of the Home Screen in the Time Tagger Software

In the left “Measurements” side panel click “Open creator” (or press the F2 key) and choose “Logic level time trace – Scope” in the new window. Here you may already adjust the scope settings as given below (see Figure 137). After clicking on the “Add measurement” button in the lower left corner, the scope tab opens.

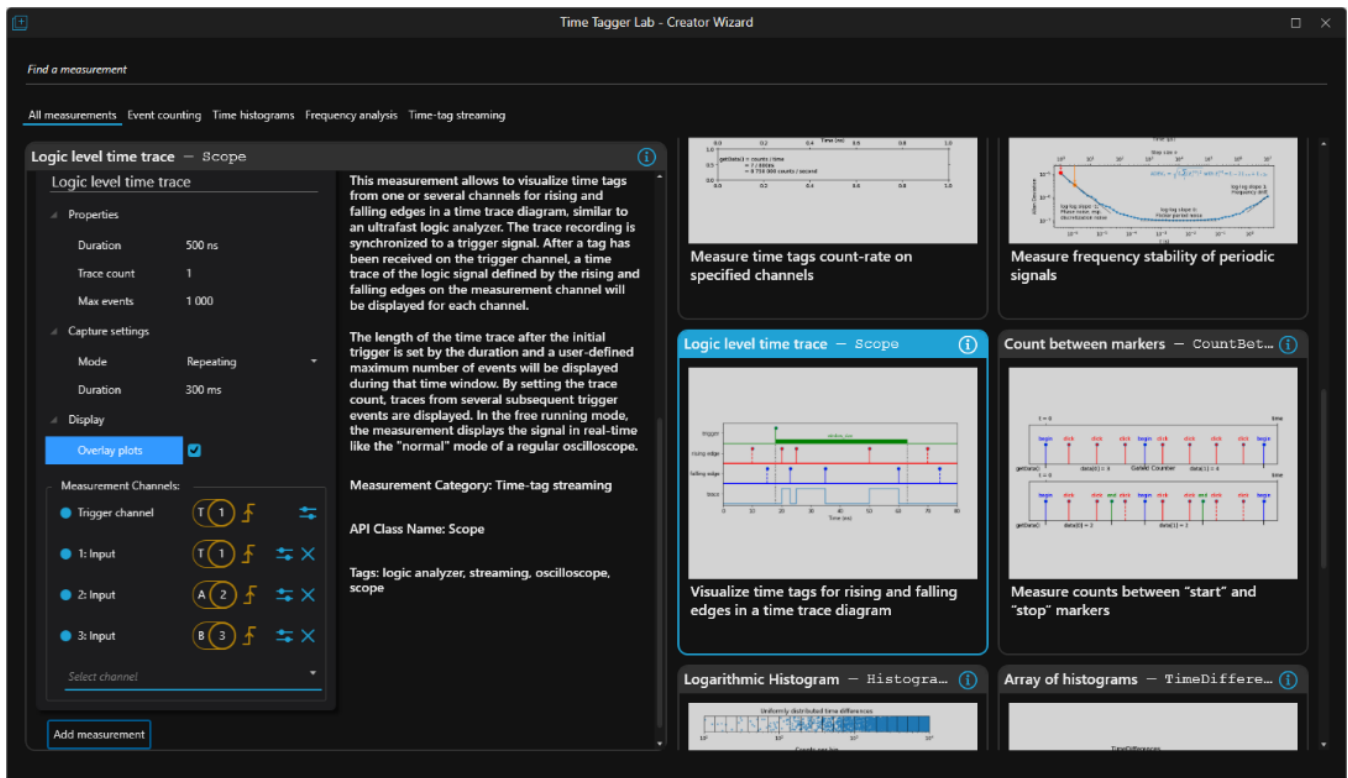


Figure 137 Setting Up the Scope in the Time Tagger Software

In the “Logic level time trace” tab (see Figure 138), the top graph displays the time trace, as set in the properties panel on the left. You may need to start the measurement using the play button to the left of the top graph. The bottom graph shows a visualization of the count rates at the input ports from the start of the measurement. The measurement of these rates is not restricted to the duration set for the time trace display.

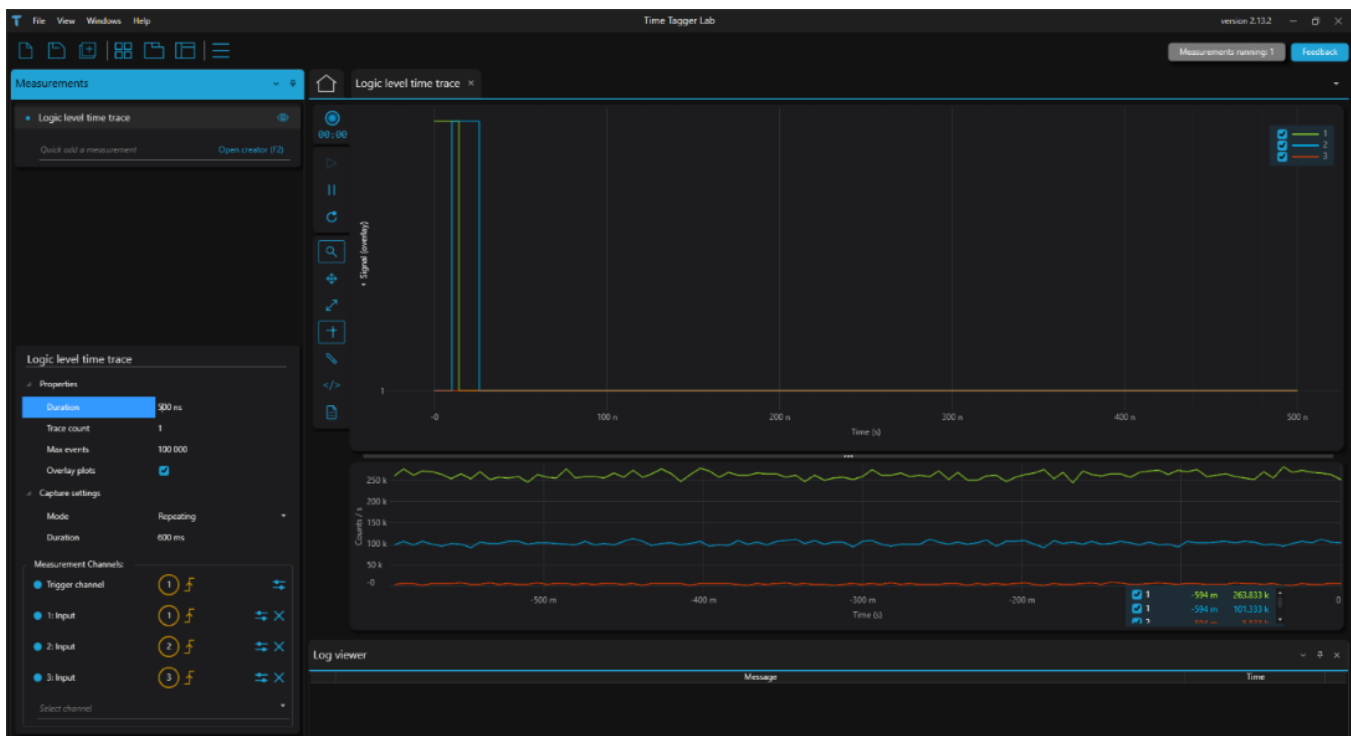


Figure 138 Logic Level Time Trace Tab in the Time Tagger Software

Note that the Time Tagger hardware can only be used by one software application at a time. To use the software for the kit, you need to close the Time Tagger Lab (and the other way round).

Chapter 11 Software

11.1 Software Installation

- Connect the USB-Stick that is included in the kit to your PC.
- The folder contains four installers (EDU-QOP1 software, Thorlabs Kinesis, Swabian Instruments Time Tagger software, and dotnet-runtime). Install all four elements (the dotnet-runtime file has to be installed before the Time Tagger software).
- Alternatively, you can visit the Thorlabs, Swabian Instruments, and Microsoft webpages⁹¹ to install the most recent version of the respective software.

11.2 General Remarks

- Upon starting the software, a connection check for the Time Tagger is performed. If the device is not connected to the PC, an error message will be displayed. The software will still start but will not have any functionality. In this case, close the software, connect the time tagger to the PC and start the software again.
- The software is optimized to run with the KLD101 laser driver included in the kit but can in principle be used with any laser. In case a different laser driver is used, functions like the on/off button or setting the laser power will not be functional in the software and must be controlled manually.
- With the standard settings, the software will not control the laser switch (except for the On/Off button in the alignment tab). It is possible to automatize the laser (see Section 11.9) so that it is switched on when a measurement starts and switched off when it ends as well as when the tab is changed, or the software is closed.
- The second order autocorrelation function $g^{(2)}(0)$ is displayed as **g2(0)** in the software UI.
- You can change the displayed curves in all graphs by right-clicking on the line symbols in the legend (top right of the graph) and checking/unchecking the “Plot Visible” option. You can also turn the automatic scaling of the axes on and off and zoom in and out with the standard LabVIEW options on top of every graph.
- The standard values for most of the control elements in the software are loaded from a config file named **Settings.xml**. This file will automatically be created upon the first start of the software and is located in your documents folder under **\Thorlabs\EDU-QOP1**. If you wish to have different standard values than the ones supplied, you can either use the respective button in the Configuration tab, see Section 11.9 or change the values in the config file directly. The first option is preferred as it ensures that only valid parameters are set. You can always revert to the original values by deleting the config file. It will then be created again upon the next software start.

11.3 Saving Results

- After clicking a **Save** button in any tab, a dialog window to select the path and filename appears. It is sufficient to just enter the name without the data type suffix as the file will automatically be saved as a .csv file. If activated (see Section 11.9), a screenshot of the current tab will also be saved in the same folder.
- If the dialog is cancelled, the measurement will not be saved. If you choose a file that already exists, you will be asked whether to overwrite or not. If you choose not to overwrite, the measurement will not be saved. If you choose to overwrite and the file is currently opened, an error message will be displayed.

⁹¹ For Kinesis, the link is: https://www.thorlabs.com/software_pages/ViewSoftwarePage.cfm?Code=Motion_Control

- Along with the measurement data, the current values of all settings will be saved to a separate .xml file. This file has the same name as the measurement file with an added “_Settings” at the end.
- If a new measurement is started before the current one is saved, the current data is lost. The same is true for exiting the software without saving first. Changing the tab, however, does not result in a data loss. It is possible to go back and save the last measurement if you do not start a new one beforehand.
- It is also possible to directly export data from any graph by right-clicking in the graph and choosing **Export** → **Copy to Clipboard**. Then it can be pasted into any spreadsheet software.

11.4 Alignment Tab

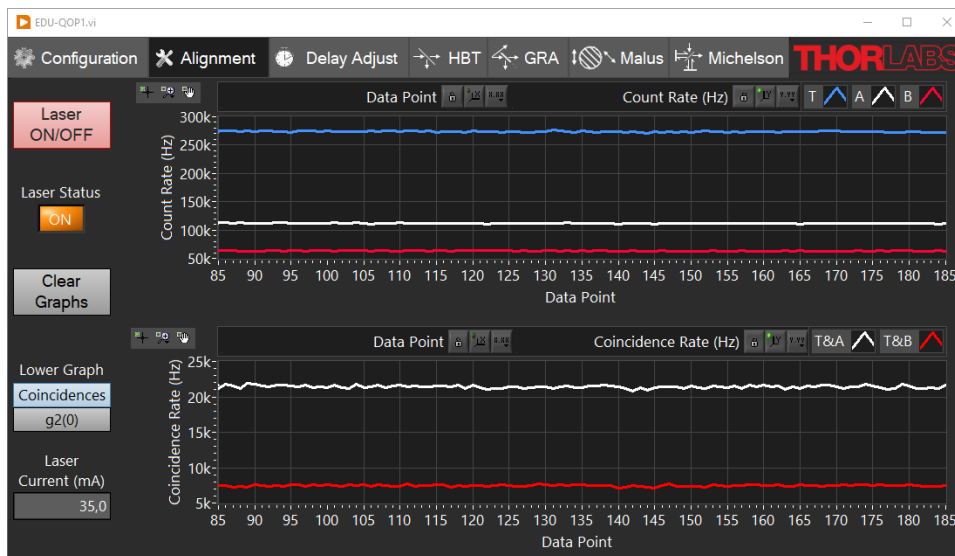


Figure 139 Alignment Tab

This tab, as shown in Figure 139, is used to align the setup before taking measurements. The count rates of the three detectors T, A, and B are shown in the upper graph, while the lower graph can be selected to either show the coincidence count rates between T&A and T&B, respectively or the second order autocorrelation $g^{(2)}(0)$ for these detector pairs (for details on the calculation of these values, see Section 3.5.2). Count rates are measured over intervals of 0.5 s and both graphs are updated at the corresponding rate (twice per second).

On the left side of the graphs are the following control elements:

- The **Laser ON/OFF** button switches the pump laser on and off (if a KLD101 laser driver is connected to the PC and switched on).
- The **Laser Status** LED displays the current laser status.
- The **Clear Graphs** button deletes all data from both graphs.
- The **Lower Graph** radio buttons switch this graph between showing the coincidence count rates or the $g^{(2)}(0)$ values calculated from the coincidences and single channel count rates (see Section 3.5.2).
- **Laser Current (mA)**: Here, you can set the laser current for the pump laser to adjust the pump power. The maximum is 100 mA, but the current will be limited by the maximum current setting of the KLD101 controller (see Section 7.2.2).

11.5 Delay Adjust Tab

In this tab, as shown in Figure 140, the delay compensation measurement is performed, as described in Sections 4.2.3, 7.4.5, and 7.5.3. The graph displays the coincidence count rates between detectors T&A and T&B, respectively, in dependence of the delay offset between the detectors.

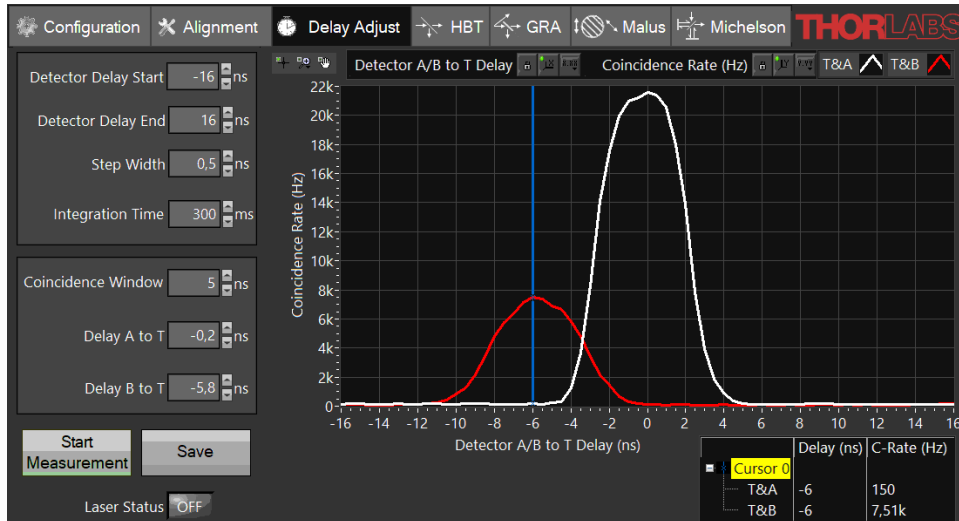


Figure 140 Delay Calibration Tab

To the left of the graph are the following control elements:

- **Detector Delay Start / Detector Delay End:** Here, the start and end points of the delay offset are set. Detectors A and B are delayed by the specified amount in relation to detector T. The minimum value is -100 ns, and the maximum value is 100 ns. The standard range from -16 ns to 16 ns should cover most experimental cases. Smaller ranges can be chosen to speed up the measurement.
- **Step Width:** Here, the step width of the measurement is set. The minimum is 0.001 ns. The standard value of 0.5 ns offers a good compromise between measurement time and precision. Larger step widths can be chosen to speed up the measurement.
- **Integration Time:** Here, the time over which counts are collected for a single data point is set. The minimum is 10 ms. Longer times lead to less noise but increase the measurement time. The standard value of 300 ms offers a good compromise.
- **Coincidence Window:** Set the time window for when two events are counted as a coincidence, as defined in Section 4.2.2.
- **Delay A/B to T:** Set the time delay compensation for each channel as read out from the measurement. These values will be used for all other measurements in the software and compensate the delay caused by electronics and optical path length differences.
- **Start Measurement:** Clicking this button will trigger a measurement. If the automatic laser control is turned off (standard setting) and the software detects that the laser is not activated, a reminder to switch on the laser will be displayed. During a running measurement, the button changes to **Stop Measurement** and can be used to end the measurement.
- **Save:** This button saves the last measurement in this tab as a delimited text file (.csv) that can easily be imported in spreadsheet programs. Additionally, the current software settings are saved to a separate .xml file at the same directory. A screenshot of the software is also saved if the respective setting is activated, see Section 11.9.

The laser status is displayed below the buttons.

Once a measurement is finished, the values of the curves can be read out by dragging the cursor (vertical blue line in the graph) left and right and monitoring the values in the cursor table (bottom right corner of the tab).

11.6 HBT and GRA Tabs

In these tabs, as shown in Figure 141 and Figure 142, the Hanbury-Brown-Twiss experiment and the Grangier-Roger-Aspect experiment, as explained in Sections 3.5.1 and 3.5.3, respectively, can be performed. Both tabs have a similar structure, only differing in the shown quantities.

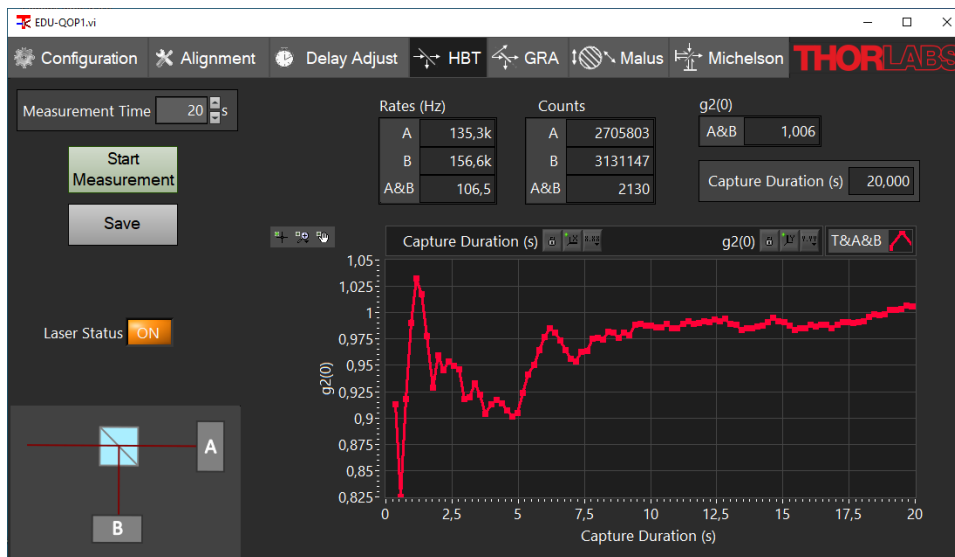


Figure 141 HBT Tab

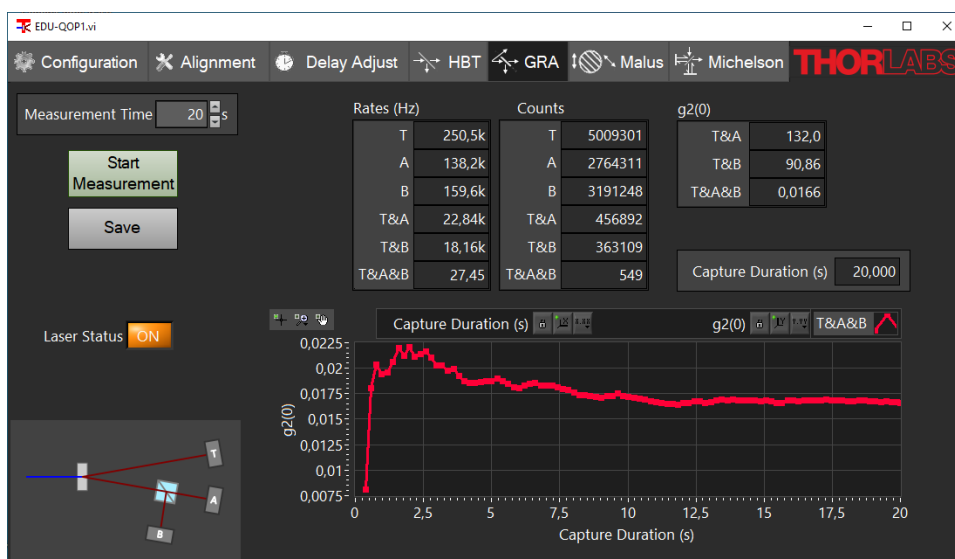


Figure 142 GRA Tab

On the left side of the tabs, the following control elements are located:

- **Measurement Time:** This value sets the overall time of the measurement. Longer times lead to higher count totals and in turn decrease the statistical uncertainty of the calculated autocorrelation functions.
- **Start Measurement:** Clicking this button will trigger a measurement. If the automatic laser control is turned off (standard setting) and the software detects that the laser is not activated, a reminder to switch on the laser will be displayed. During a running measurement, the button changes to **Stop Measurement** and can be used to end the measurement.
- **Save:** This button saves the last measurement in this tab as a delimited text file (.csv) that can easily be imported in spreadsheet programs. Additionally, the current software settings are saved to a separate .xml file at the same directory. A screenshot of the software is also saved if the respective setting is activated, see Section 11.9 for details.

The laser status is displayed below the buttons.

The boxes in the right part of the tab contain the measurement results:

- The count rates
- The absolute count numbers
- The $g^{(2)}(0)$ value calculated by the software. In the GRA tab, three different $g^{(2)}(0)$ functions for different detector correlations are acquired. For details on those values and their calculation, see Section 3.5.4.
- Below the result boxes, the $g^{(2)}(0)$ values are plotted over time, making it possible to see how the correlation function stabilizes with increasing measurement duration.

11.7 Malus' Law Tab

This tab, as shown in Figure 143, is used for the measurement of Malus' law for single photons, as described in Sections 3.7 and 9.6.

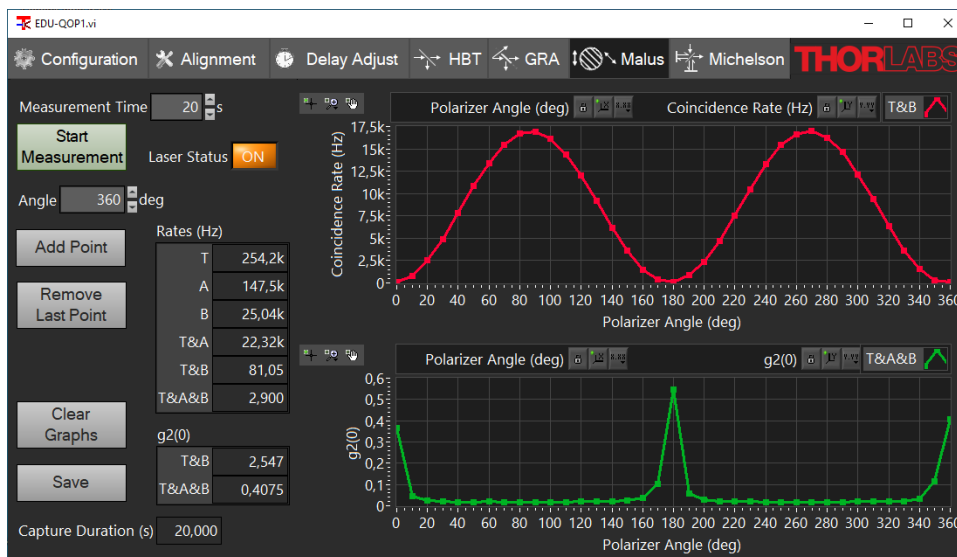


Figure 143 Malus' Law Tab

In this tab, you can perform several Grangier-Roger-Aspect-like measurements for different polarizer angles and add those data points to two plots. The collected results can then be saved in a single file.

On the left side of the tab are the following elements from top to bottom:

- **Measurement Time:** This value sets the overall time of the measurement. Longer times lead to higher count totals and in turn decrease the statistical uncertainty of the calculated autocorrelation functions.
- **Start Measurement:** Clicking this button will trigger a measurement for a single data point (polarizer angle). If the automatic laser control is turned off (standard setting) and the software detects that the laser is not activated, a reminder to switch on the laser will be displayed. During a running measurement, the button changes to **Stop Measurement** and can be used to end the measurement.
- **Results Box:** Here, the results of the current measurement are displayed, similar to the result of the GRA tab, as seen in Section 11.6.
- **Angle:** Here, you can set the angle of your polarizer for the current measurement. This value will be taken as the x-coordinate of the data point in the plot, when using the **Add Point** button.
- **Add Point:** This button adds the last completed measurement to the plots. The x-coordinate is read from the **Angle** field.

- **Remove Last Point:** This button removes the last data point from the plots (e.g., if you accidentally used the wrong angle value). It can be used multiple times to remove more than one point. Please note that removed data points are lost and cannot be restored.
- **Save:** This button saves the current plots as a delimited text file (.csv) that can easily be imported in spreadsheet programs. Additionally, the current software settings are saved to a separate .xml file at the same directory. A screenshot of the software is also saved if the respective setting is activated, see Section 11.9 for details.
- **Clear Graphs:** This button clears all data points from both graphs. Please note that the data is lost if not saved prior to clearing.

On the right side of the tab are the data plots:

- The upper plot shows the T&B coincidence count rates as a function of the polarizer angles.
- The lower plot shows the $g^{(2)}(0)$ values calculated from the count rates as a function of the polarizer angle.

The laser status is displayed to the right of the Start Measurement button.

11.8 Michelson Interferometer Tab

In this tab, as shown in Figure 144, the single photon interference experiments (see Sections 3.6 and 9.7) as well as the quantum eraser experiment (see Sections 3.8 and 9.8) can be performed.

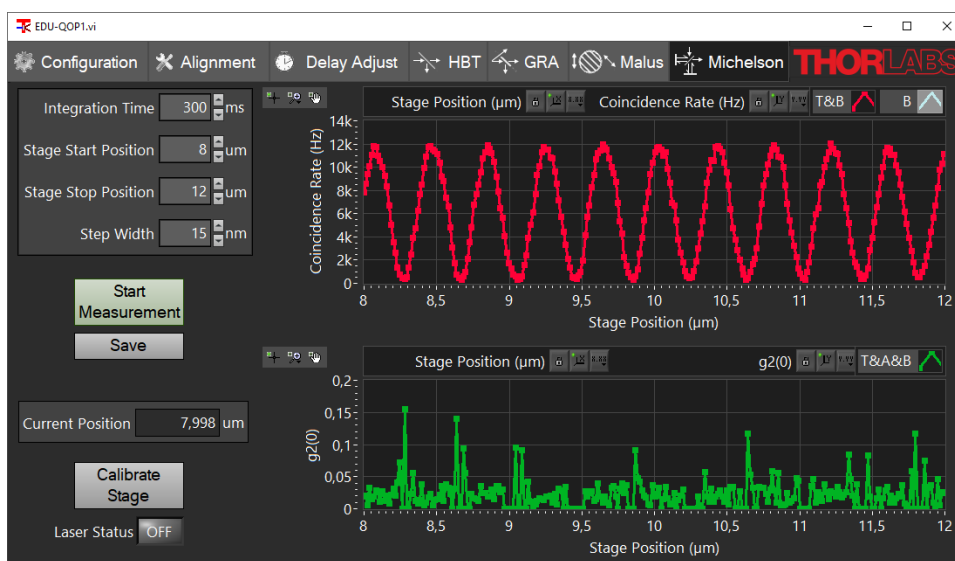


Figure 144 Michelson Interferometer Tab

This software tab utilizes the KPZ101 and KSG101 K-cube piezo stage controllers. The connection for each controller is checked automatically when the software is started. If one or both are disconnected or switched off, an error message will be displayed. You can still view the tab, but the measurement will not move the stage. The stage should be calibrated before first use, as described below.

The graphs show the coincidence count rate of detectors T&B (upper graph) and the autocorrelation $g^{(2)}(0)$ (lower graph) as a function of the stage position of the Michelson interferometer. For details on the calculation of $g^{(2)}(0)$, see Section 3.6.

On the left side of the tab are the following control elements:

- **Integration Time:** Here, the time over which counts are collected for a single data point is set. The minimum is 100 ms. Longer times lead to less noise (especially in the $g^{(2)}(0)$ calculation) but increase the measurement time. For measurements where only the upper graph is of importance and for large

measurement ranges, we recommend the minimum setting of 300 ms. For smaller ranges and if the $g^{(2)}(0)$ value is of interest, significantly longer times (e.g. 5000 ms) are advantageous.

- **Stage Start Position / Stage End Position:** Here, the start and end point of the measurement are set.
- **Step Width:** Here, the step width of the measurement is set. The minimum value is 1 nm, and the maximum is 20000 nm. Larger step widths speed up the measurement at the cost of spatial resolution. The typical period of the interferogram is about 400 nm.
- **Start Measurement:** Clicking this button will trigger a measurement. If the automatic laser control is turned off (standard setting) and the software detects that the laser is not activated, a reminder to switch on the laser will be displayed. During a running measurement, the button changes to **Stop Measurement** and can be used to end the measurement.
- **Save:** This button saves the last measurement in this tab as a delimited text file (.csv) that can easily be imported in spreadsheet programs. Additionally, the current software settings are saved to a separate .xml file at the same directory. A screenshot of the software is also saved if the respective setting is activated, see Section 11.9.
- **Calibrate Stage:** Clicking this button starts the calibration process for both the KPZ101 and the KSG101 controller. This process is required to obtain precise position readings. It is highly recommended to calibrate the stage at the first start of the software, else the software loads an emergency calibration which may lead to deviations in the position reading. If optimal accuracy is required, re-calibrating the stage at each start of the software or after alterations to the setup/environment is recommended. The calibration process takes about 30 seconds. During the process, all software controls are deactivated.

The current position is displayed above the Calibrate Stage button and the laser status is displayed below the button.

11.9 Configuration Tab

This tab (shown in Figure 145) displays all the settings made in the other tabs as well as additional global settings. Those are:

- **Laser Current (mA):** Here, you can set the laser current for the pump laser to adjust the pump power. The maximum is 100 mA, but the current will be limited by the maximum current setting of the KLD101 controller (see Section 7.2.2).
- **Lock KLD Front Panel:** If this checkbox is activated, the front panel of the KLD101 controller is locked and the laser power can only be set via the software. The standard setting is an unlocked front panel.
- **Switch Laser On/Off Automatically:** If this checkbox is activated, the software is allowed to control the laser. It will turn on the laser with the beginning of every measurement and turn it off at the end of a measurement, when a different tab is chosen, or when the software is closed. The standard setting is no automatic control.
- **Save Settings on Exit:** If this checkbox is activated (standard setting), the software will write all values displayed in the configuration tab in a config file and load them upon the next start of the software. If the setting is deactivated, the config file will not be overwritten when closing the software.
- **Save Screenshot with Data:** If this checkbox is activated (standard setting), a screenshot of the current tab will be saved every time a **Save** button is clicked in any tab.
- **Save Current Settings:** With this button, you can write the current settings in the config file to be loaded after the next software start. Make sure to deactivate the **Save Settings on Exit** checkbox in this case or the config file will be overwritten again upon closing the software.
- **Restore Default Settings:** With this button, you can restore the settings to the state that is set when opening the software for the first time (default state).

- Check for Latest Version Online:** With this button, you can check whether there is a newer version of the software available for download. If that is the case, the new version number is displayed and you may choose to open a direct download link via your browser, open the software information web page, or do nothing at all.

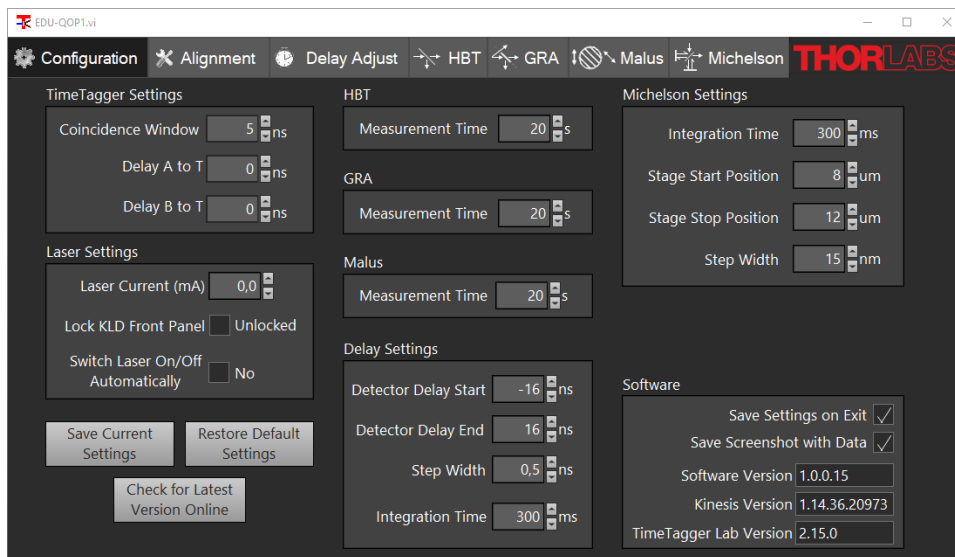


Figure 145 Configuration Tab

11.10 Hidden Settings

There are two settings that make more complex changes and are therefore not controllable via the software. Those settings can be changed directly via the config file, which is located in your documents folder under \Thorlabs\EDU-QOP1. The hidden settings are:

- Coincidence Mode:** In Section 12.1, we describe three different ways to define coincidences and their advantages and disadvantages. The software can use all three modes. The mode can be changed via the lines in the config file that are shown in Figure 146. A value of 2 (standard setting) is the Coincidence of Coincidence mode, a value of 1 is the Gated Counting mode and a value of 0 is the standard definition of triple coincidences (see Section 12.1).

```

<EW>
<Name>Coincidence mode</Name>
<Choice>Triple Coincidences</Choice>
<Choice>Gated Counting</Choice>
<Choice>Coincidences of Coincidences</Choice>
<Val>2</Val>
</EW>
    
```

Figure 146 Settings File Code for Changing the Coincidence Mode. The red circle marks the important value.

- Laser Operation Mode:** The laser can be operated in the Constant Current mode (standard setting) or in the Constant Power mode. If you want to use the latter, search for the lines displayed in Figure 147 in the config file and change the value from 0 to 1. To use the Constant Power Mode, the slope of the current-power curve needs to be set. Please refer to the KLD101 driver manual for details.

```

<EW>
<Name>Laser Operation mode</Name>
<Choice>Constant Current (mA)</Choice>
<Choice>Constant Power (mW)</Choice>
<Val>0</Val>
</EW>
    
```

Figure 147 Settings File Code for Changing the Laser Mode. The red circle marks the important value.

Chapter 12 Technical Notes

12.1 Different Detection Schemes

12.1.1 Standard Triple Coincidences

When looking at the Time Tagger in this kit and many coincidence electronics in the literature, the standard way to define triple coincidences deviates from the definition used in Section 3.5.4. (from here on called “coincidence of coincidences” (CC)).

In the standard definition, a triple coincidence works like double coincidences, i.e., a triple coincidence is counted whenever **both** other detectors fire within the tagger window after an event on any detector. This definition is stricter than the CC definition, meaning that there are count sequences that are counted as a triple coincidence in the CC definition but not in the standard definition. Such a sequence is shown in Figure 148. It is not a triple coincidence by the standard definition, as the count on detector B is not in the window after the first count of the sequence (detector A). It is a triple coincidence by the CC definition because the counts at detectors A and B are both in coincidence with the count on detector T.

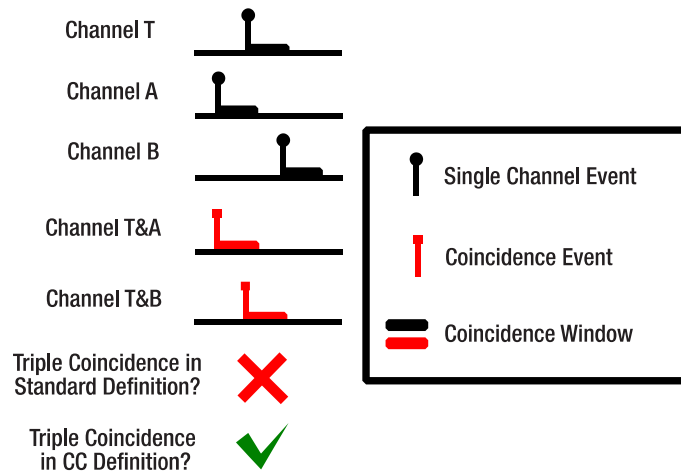


Figure 148 An event sequence that is counted as a triple coincidence in CC definition but not in the standard definition (since there is no overlap between all three windows).

When deciding which definition to use for the quantum optics experiments, the decisive factor is whether Equation (101) results in the correct values for the second order correlation function. Performing an experiment with completely uncorrelated light (such as explained in Section 9.5), one expects $g_{GRA}^{(2)}(0) = 1$.

In the uncorrelated case, all coincidences are purely accidental. The expected rate of accidental counts for double coincidences of two detectors T and A is given in the literature⁹² as:

$$R_{TA}^{(acc)} = 2 \cdot R_T \cdot R_A \cdot \Delta t$$

The rate of accidental triple coincidences between three detectors T, A, and B in the **standard definition** is:

$$R_{TAB_{st}}^{(acc)} = 3 \cdot R_T \cdot R_A \cdot R_B \cdot \Delta t^2$$

In the uncorrelated case, the rates in Equation (101) are given by the purely accidental rates which yields:

$$g_{GRA_{st}}^{(2)}(0) = \frac{R_{TAB_{st}}^{(acc)} \cdot R_T}{R_{TA}^{(acc)} \cdot R_{TB}^{(acc)}} = \frac{3 \cdot R_T^2 \cdot R_A \cdot R_B \cdot \Delta t^2}{4 \cdot R_T^2 \cdot R_A \cdot R_B \cdot \Delta t^2} = \frac{3}{4}$$

⁹² C. Eckart and F. R. Shonka, *Physical Review*, **53**(9), 752 (1938)

This deviates from the expectation $g_{GRA}^{(2)}(0) = 1$ for uncorrelated light and shows that the standard definition of triple coincidence is not perfectly suited for the GRA experiment.

A stochastic view helps to calculate $g_{GRA}^{(2)}(0)$ for the CC definition of triple coincidences. The probability for an event on detector T to be coincident both with events on detector A and B is $P(TA \cap TB)$. As we are dealing with completely uncorrelated events, TA and TB are stochastically independent and the joint probability becomes:

$$P(TA \cap TB) = P(TA) \cdot P(TB)$$

The probabilities of the double coincidences are simply:

$$P(TA) = \frac{R_{TA}^{(acc)}}{R_T} \quad \text{and} \quad P(TB) = \frac{R_{TB}^{(acc)}}{R_T}$$

Hence, the rate $R_{TAB_CC}^{(acc)}$ of trigger events that occur in coincidence with events **both** on detector A and detector B (the CC definition of triple coincidences) is:

$$R_{TAB_CC}^{(acc)} = R_T \cdot P(TA \cap TB) = R_T \cdot P(TA) \cdot P(TB) = R_T \cdot \frac{R_{TA}^{(acc)}}{R_T} \cdot \frac{R_{TB}^{(acc)}}{R_T} = \frac{R_{TA}^{(acc)} \cdot R_{TB}^{(acc)}}{R_T}$$

Substituting this in Equation (101) for the uncorrelated case yields:

$$g_{GRA_CC}^{(2)}(0) = \frac{R_{TAB_CC}^{(acc)} \cdot R_T}{R_{TA}^{(acc)} \cdot R_{TB}^{(acc)}} = \frac{R_{TA}^{(acc)} \cdot R_{TB}^{(acc)} \cdot R_T}{R_{TA}^{(acc)} \cdot R_{TB}^{(acc)} \cdot R_T} = 1$$

This result is reproduced when using the CC definition for triple coincidences. However, as fewer triple coincidences are counted with the standard definition, but the number of twofold coincidences stays the same, using the standard definition results in $g_{GRA}^{(2)}(0) < 1$ (the experiments in this kit show $g_{GRA}^{(2)}(0) = 0.75$) for uncorrelated light, which is counterintuitive. For this reason, the CC definition for triple coincidences is used in this kit.

12.1.2 Gated Detection Scheme

In this scheme (which was used in the original GRA experiment), gated counts are registered instead of coincidences. In this case one of the detectors (in our case: T) is specified as the gate detector. A count on this detector opens a gate window of length Δt_g . Counts at the other detectors are only registered when they occur during an open gate window. All other events are discarded. For example, instead of the coincidence rate R_{TA} one registers the gated count rate $R_A^{(g)}$. The main difference between the two is that in the gated case, the event at the gate detector T must come first, while the order of the events is irrelevant in the coincidence case.

In the gated scheme, gated coincidences are counted instead of triple coincidences. A gated coincidence between channels A and B occurs when both detectors A and B register an event during the **same** gate window after a count on detector T, as seen in Figure 149. The gated coincidence rate is denoted $R_{AB}^{(g)}$.

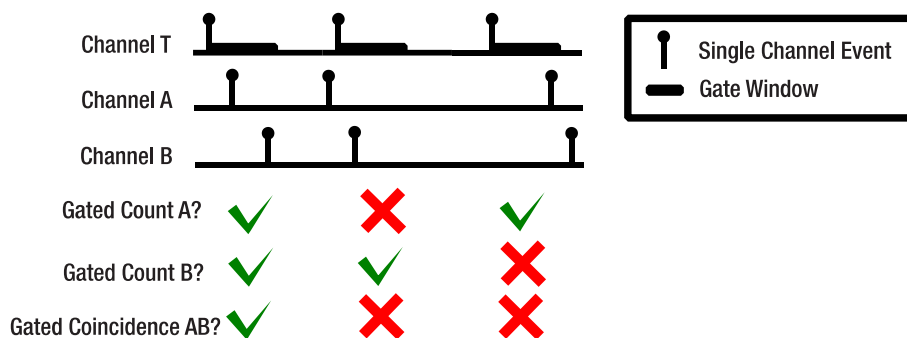


Figure 149 Gated Detection Scheme, Definition of Gated Counts and Gated Coincidences

The equations for the second order correlation function in the GRA experiment become:

$$g_{GRA}^{(2)}(0) = \frac{R_{AB}^{(g)} \cdot R_T}{R_A^{(g)} \cdot R_B^{(g)}}$$

The time window used for gating Δt_g is the same as the coincidence window Δt used in Equation (98) amongst others, i.e., $\Delta t_g = \Delta t$.

The photon pairs produced by the SPDC process induce a correlation to the events at the detector. We expect counts at detector T to occur at the same time as counts on detector A. Here, we see a disadvantage of the gated scheme. Half of those simultaneous events will not be detected as gated counts because statistically, the event on A will be registered slightly before the event on T half of the time and thus will be discarded. In the triple coincidence scheme, the order of the events is irrelevant, and all simultaneous events will be counted as twofold coincidences.

This can be avoided by introducing an artificial delay to the counts on detectors A and B. If this delay is not larger than the gate window, all events that occur simultaneously will be counted as gated counts, because the count on A (B) is ensured to be registered after the one on T. In fact, if the artificial delay is chosen to be exactly half the size of the gate window, the gated scheme becomes identical to the triple coincidence scheme (with the CC definition of triple coincidences) for all count sequences, whether correlated or uncorrelated, which is shown in Figure 150.

For any count on T (black marker) there is a gate window (black bar) and a tagger coincidence window of half the size of the gate window (red bar). In the triple coincidence scheme any count on A or B must be in a time window that is symmetric around T with a width of twice the tagger window to be counted as a coincidence. This window is the grey rectangle on the second line. In the gated scheme, counts on A or B must simply lie in the gate window to be counted as a gated count, as marked by the grey rectangle in the third line. It becomes apparent that the windows have the same size but are shifted by half the size of the gate window to each other. Hence, shifting all counts on A and B by this amount relative to T results in the same position of the counts relative to the grey rectangle as in the triple coincidence scheme, making them identical.

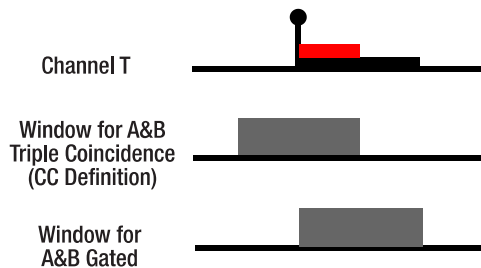


Figure 150 Comparison for Triple Coincidence and Gated Scheme. The window in which counts on A and B must lie to be counted as coincidences is marked by the grey rectangles. The black bar in the upper line marks the gate window and the red bar marks the tagger coincidence window.

It is important to stress that the gated scheme produces the same results for the second order correlation function $g_{GRA}^{(2)}(0)$ with or without the artificial delay, as the rates for gated counts and gated coincidences are both affected by the ordering issue described above. However, the overall count rates will be lower without the artificial delay, making the experiments less efficient.

To avoid the complication of setting up the artificial delay and the risk of missing all coincidence counts when setting the delay wrong, this kit uses the triple coincidence scheme (with the CC definition of triple coincidences) instead of the gated scheme.

12.1.3 Changing the Detection Scheme in the Software

While we recommend sticking with the triple coincidence scheme with the CC definition, the software is prepared to operate with the gated scheme or the standard definition of triple coincidences. To change the scheme, open

the Settings.xml file in the software folder, search for the code shown in Figure 151 and change the value in the second to last line to “0” to use the triple coincidence scheme with the standard definition or to “1” to use the gated detection scheme. The changed detection mode is loaded with the next start of the software (make sure not to overwrite your changes to the settings file automatically when closing the software). Delay times and coincidence window definition set in the Time Tagger are updated automatically to match the changed mode.

```
<EW>
  <Name>Coincidence mode</Name>
  <Choice>Triple Coincidences</Choice>
  <Choice>Gated Counting</Choice>
  <Choice>Coincidences of Coincidences</Choice>
  <Val>2</Val>
</EW>
```

Figure 151 Part of the Settings.xml File that Allows Choosing the Detection Scheme. The important value is highlighted by the circle.

12.2 Environmental Conditions

We recommend using the setup in rooms that can be completely darkened (no windows, or shutters) since the best performance is reached in darkness. Sunlight is especially problematic as its spectrum includes the transmission range of the bandpass filter in front of the detectors and thus results in large background count rates.

If you want to use the setup but do not have the possibility to block sunlight from entering the room, you can use a box with transparent wavelength-filtering walls, like the one depicted in Figure 152.



Figure 152 Setup with Wavelength Filtering Enclosure

Please contact Techsupport@thorlabs.com for a part list recommendation and a construction manual for such a box.

12.3 Avoiding Fluctuations in the Michelson Interferometer

The Michelson Interferometer is an extremely sensitive instrument. Slight changes in the parameters can have significant influence on the measured signal. For example, the miniscule changes in the refractive index of air at different temperatures can introduce visible fluctuations in the interferogram, when temperature gradients or air currents are present. An example measurement is shown in Figure 153.

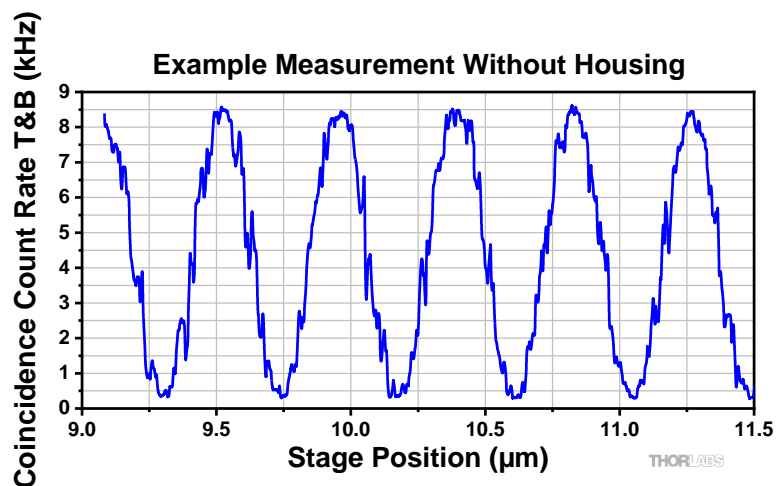


Figure 153 Example Interferogram with Air Current in the Michelson Interferometer

This problem can be alleviated by housing the interferometer in a box that prevents air currents from entering the interferometer. An example of such a housing is shown in Figure 154. This is made of acrylic glass with custom recesses for entry and exit of the light and for the clamps to fix the board. A measurement with the same parameters as Figure 153 but with the housing is displayed in Figure 155, clearly showing the noise-reducing effect of the housing.

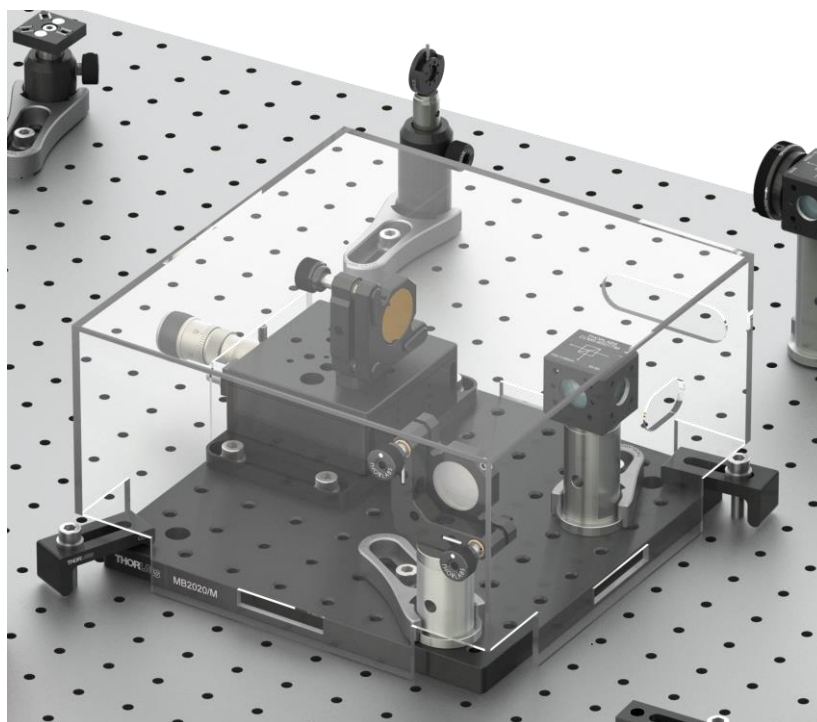


Figure 154 Acrylic Housing for Michelson Interferometer

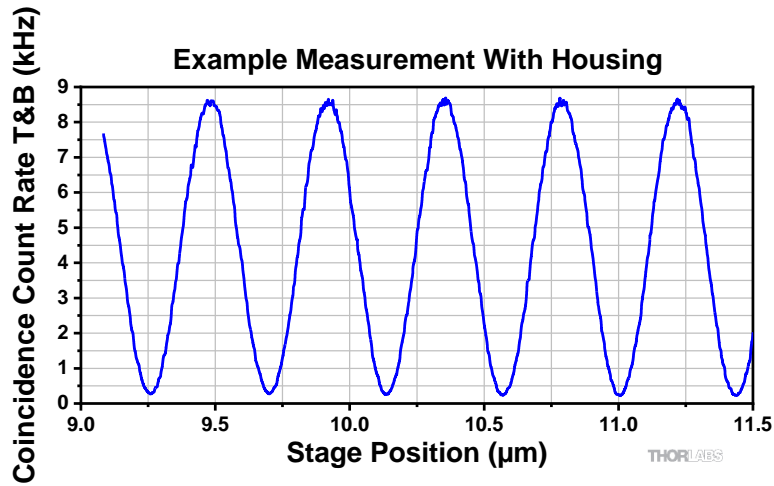


Figure 155 Example Measurement with Interferometer Housing

12.4 Accidental Coincidences

In Section 3.5.7, we discussed the influence of the count rate and the coincidence window on the rate of accidental coincidences and the measurement results of $g_{GRA}^{(2)}(0)$. In this section, we lay out a simplified example calculation to quantify and visualize the effect.

The following assumptions are made:

- The count rates caused by background (detector dark counts and stray light) are small against the signal count rates and can be ignored.
- The overall detection efficiency for photons incident on a detector is $\eta = 0.5$
- The splitting ratio of the beamsplitter is perfectly 50:50.

Under these assumptions, the trigger count rate R_T is:

$$R_T = \eta \cdot R_{pp} = \frac{R_{pp}}{2}$$

Here, R_{pp} is the rate of photon pairs emitted in the direction of the detectors. The count rates on detectors A and B are then (due to the beamsplitter ratio):

$$R_A = R_B = 0.5 \cdot \eta \cdot R_{pp} = \frac{R_{pp}}{4}$$

The rate of double coincidences R_{TA} (R_{TB}) can be determined stochastically. The coincidence is registered only if both chances come true, so:

$$R_{TA} = R_{TB} = 0.5 \cdot 0.25 \cdot R_{pp} = \frac{R_{pp}}{8}$$

The rate of accidental triple coincidences is then (see Section 3.5.7):

$$R_{acc}^{2+1} = (R_{TA} \cdot R_B + R_{TB} \cdot R_A) \cdot \Delta t = \left(\frac{R_{pp}^2}{32} + \frac{R_{pp}^2}{32} \right) \cdot \Delta t = \frac{R_{pp}^2}{16} \cdot \Delta t$$

The correlation function $g_{GRA}^{(2)}(0)$ is then:

$$g_{GRA}^{(2)}(0) = \frac{R_{acc}^{2+1} \cdot R_T}{R_{TA} \cdot R_{TB}} = \frac{R_{pp}^2 \cdot \Delta t \cdot 8 \cdot 8 \cdot R_T}{R_{pp}^2 \cdot 16} = 4 \cdot R_T \cdot \Delta t = 4 \cdot \frac{N_T}{T} \cdot \Delta t$$

with N_T being the absolute number of measured counts at the trigger detector and T being the measurement duration.

For the calculation of the $g_{GRA}^{(2)}(0)$ measurement's statistical error, we assume that the error is dominated by the event counting measurements. In turn, the errors of the coincidence window width Δt and the measurement duration T are neglected. The distribution of the measured counts is Poissonian, so for example the error $\Delta(N_T)$ is:

$$\Delta(N_T) = \sqrt{N_T}$$

As the error of the measurement duration is neglected, the relative error of a count rate is the same as that of the corresponding absolute count number (at the example of R_T):

$$\frac{\Delta(R_T)}{R_T} = \frac{\Delta(N_T)}{N_T} = \frac{1}{\sqrt{N_T}} = \frac{1}{\sqrt{R_T \cdot T}}$$

The statistical errors of different count measurements are independent. The relative error for $g_{GRA}^{(2)}(0)$ is then:

$$\begin{aligned} \frac{\Delta(g_{GRA}^{(2)}(0))}{g_{GRA}^{(2)}(0)} &= \sqrt{\left(\frac{\Delta(R_{acc}^{2+1})}{R_{acc}^{2+1}}\right)^2 + \left(\frac{\Delta(R_T)}{R_T}\right)^2 + \left(\frac{\Delta(R_{TA})}{R_{TA}}\right)^2 + \left(\frac{\Delta(R_{TB})}{R_{TB}}\right)^2} \\ &= \sqrt{\frac{1}{R_{acc}^{2+1} \cdot T} + \frac{1}{R_T \cdot T} + \frac{1}{R_{TA} \cdot T} + \frac{1}{R_{TB} \cdot T}} \approx \frac{1}{\sqrt{R_{acc}^{2+1}}} \cdot \frac{1}{\sqrt{T}} \end{aligned}$$

In the last step, we neglected all terms under the square root but the first as the accidental count rate is much smaller than all other count rates. It becomes apparent that a lower rate of accidental count rates results in an increase of the relative error of $g_{GRA}^{(2)}(0)$.

The complete calculation is visualized in Figure 156 (constant coincidence window, varying trigger count rate) and Figure 157 (vice versa).

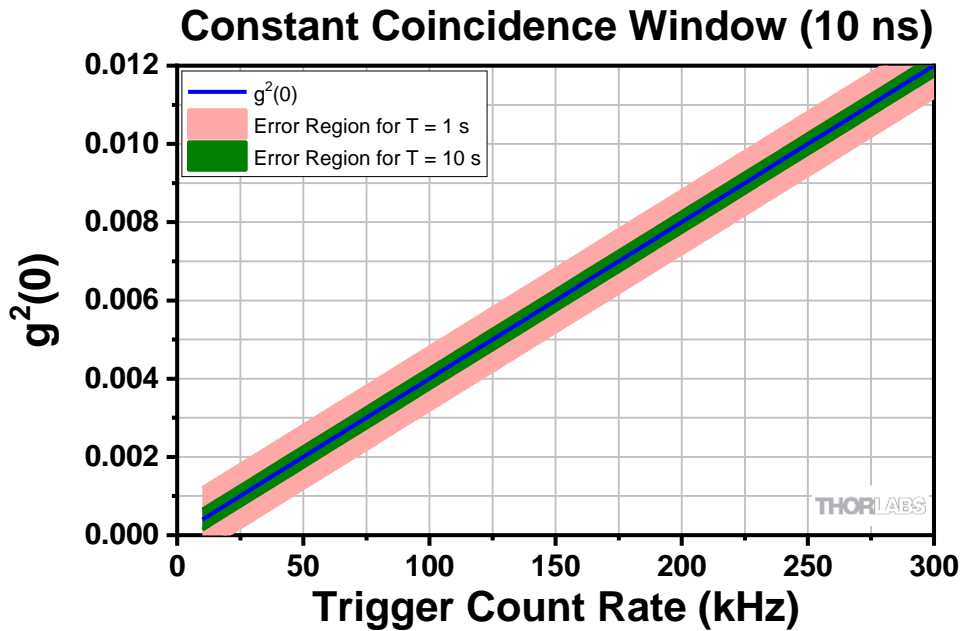


Figure 156 Expected measurement results as a function of the trigger count rate for a constant coincidence window of 10 ns.

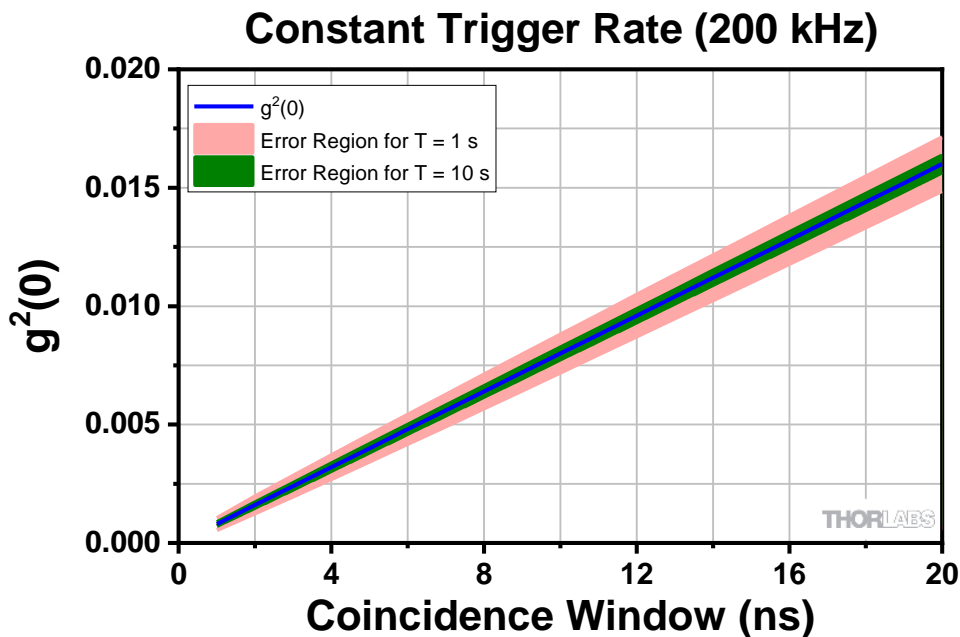


Figure 157 Expected measurement results as a function of the coincidence window width for a constant trigger count rate of 200 kHz.

The following conclusions can be drawn from the calculation results:

- When aiming to measure values of $g_{GRA}^{(2)}(0)$ as close to the ideal result of 0 as possible, it is best to first reduce the coincidence window, as this does not influence the relative error of the measurement. However, the coincidence window cannot be reduced infinitely, as the jitter of the electronics and detectors act as a lower limit.
- Reducing the trigger count rate (via lowering the pump laser power) results in a lower expectation value of $g_{GRA}^{(2)}(0)$, i.e., one closer to the ideal result but at the same time the relative uncertainty of the measurement increases.
- The increased uncertainty can of course be compensated for by increasing the measurement duration.

In the end, the user must formulate the degree of uncertainty and deviation from the ideal result they are willing to accept and choose the parameters accordingly. The standard values recommended throughout this manual provide a good balance between the competing goals.

It is important to note that the assumptions made here break down for very low trigger count rates, as background signal and dark counts cannot be neglected any more in this case. These effects will increase the measured value of $g_{GRA}^{(2)}(0)$.

12.5 Maximizing the Count Rate

If you want higher count rates, there are several ways to do that:

- Increase pump laser power. Make sure not to exceed the maximum current/power for the laser diode. You can see the characteristics of your individual laser diode in its spec sheet.
- Reduce the distance between detectors and BBO crystal (more photons of the cone pass the detector aperture).
- Rotate the BBO crystal and the polarization of the pump beam (by rotating the HWP in the pump beam path) by 90°. In our tests, this configuration increased the coincidence count rate by about 20%. However, be aware that in this configuration, the polarization of the photons in the two arms is not parallel anymore but shifted by about 6° in relation to each other.

Please be aware that higher count rates are not always beneficial. For a fixed coincidence window, higher count rates result in more accidental coincidences, thus moving the $g^{(2)}(0)$ closer towards 1, as explained in Section 12.4.

12.6 Choice of Polarizers

We use two distinct types of linear polarizers in this kit, one LPNIRE100-B polarizer and two LPNIRB050 polarizers.

The LPNIRE100-B polarizer is the more cost-efficient solution and its extinction ratio of >1000:1 is good enough for all experiments in this kit. However, its parallelism is only about 20 arcmin, which leads to a significant deviation of the beam path when rotating the polarizer. This makes the LPNIRE100-B polarizer unsuitable for usage inside the Michelson interferometer during the Quantum Eraser experiment, as even small angular deviations in the interferometer can lead to a significant loss of contrast in the measurement. Thus, we include the more expensive LPNIRB050⁹³ polarizers, which have a parallelism of <0.5 arcmin.

The LPNIRE100-B polarizer can still be used whenever the angular deviation is of no consequence, such as directly in front of the detectors in the Malus' Law experiment or as the "eraser-polarizer" in the Quantum Eraser experiment.

12.7 Polarizers vs. Quarter-Wave Plates

Changing the polarization of the photons in the interferometer arms is possible by either using polarizers as in this kit or by inserting a quarter-wave plate (QWP) in one arm of the interferometer. In the Michelson interferometer, the beam passes through the QWP twice, effectively acting as a half-wave plate (HWP), i.e., rotating the linear polarization of the incoming photon by twice the angle difference between photon polarization and fast axis orientation.

Advantage of QWP

A QWP has the advantage of being nearly absorption-free, so using one will result in reaching higher count rates in the experiment.

Disadvantage of QWP

The function of the QWP is highly wavelength-sensitive, and optimal functionality is only guaranteed at exactly the design wavelength of the QWP. As the wavelength of the photons generated by the SPDC process varies by up to several nanometers, the QWP induces ellipticity to the polarization of the photons instead of just turning the linear polarization. This in turn makes a complete suppression of the interference pattern in the quantum eraser experiment impossible. Even when the polarizations are theoretically crossed and no interference pattern should appear, there will be a residual interference pattern due to the elliptical polarization component.

Due to this reason, polarizers are used in the kit. They are achromatic and do not suffer from the same problems as the QWPs. A complete suppression of the interference can be reached, which is important for a didactic experiment. The count rates in this kit are high, so a loss of half the counts is not critical.

Important Parameters

If you want to use QWPs in your kit instead of polarizers, be aware of the following points:

- The QWP should be achromatic, i.e., offer a retardation of very close to 0.25 for a range of at least 800 - 820 nm.
- The QWP must have a low beam deviation. Deviations below 1 arcmin are recommended. Higher deviations will result in a significant loss of interference contrast when turning the QWP due to misalignment of the beam paths from the interferometer arms.

⁹³ The LPNIRB050 polarizers are based on nanoparticles. Thus, their polarization axis can change when operated outside their specified wavelength range. For example, if used with the 405 nm pump laser, the axis will be tilted by about 90°.

12.8 Axicon Design

The axicon is designed to emulate the cone of photon pairs generated in the BBO crystal. A schematic is shown in Figure 158.

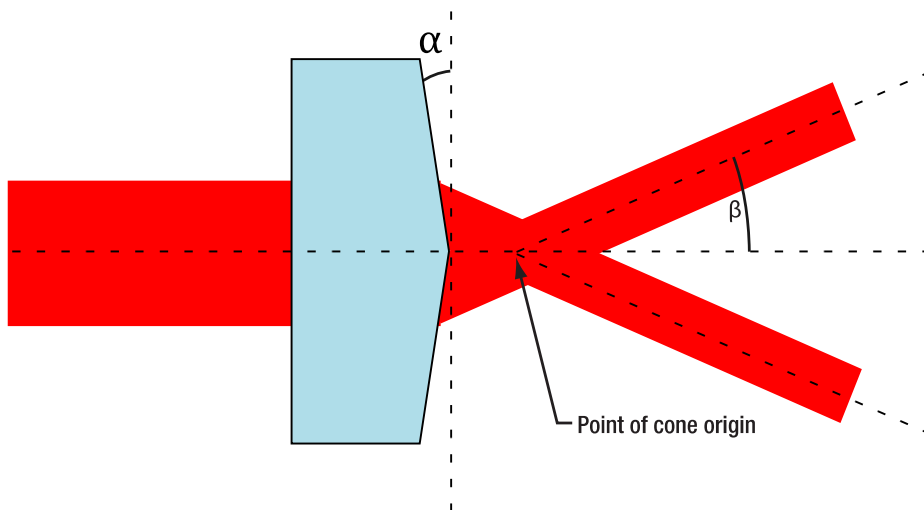


Figure 158 Schematic of the Axicon

As the BBO is designed for a half opening angle of 3°, the axicon parameters are chosen to produce a cone with an opening angle of 3° when illuminated with the alignment laser (635 nm wavelength). The following equation was used to determine the required axicon angle α :

$$\alpha = \tan^{-1} \left(\frac{\sin \beta}{n(\lambda) - \cos \beta} \right)$$

Here, β is the desired half-opening angle of the cone (3° in our case) and $n(\lambda)$ is the spectrally dependent index of refraction for the axicon material.

The glass used for our axicon has $n(635 \text{ nm}) = 1.4584$ leading to $\alpha = 6.49$.

The equation above can be used to design axicons for different alignment laser wavelengths or cone-angles.

In Figure 157, one can see that the origin of the output cone is not exactly on the axicon tip, but some distance after it. The exact distance depends on the beam diameter of the alignment laser. To ensure that the origin of the cone is the same for the axicon and the BBO crystal, we offset the axicon by 15 mm via the lens tube spacers.

12.9 Temperature Dependence of Pump Laser Wavelength

The center wavelength of the L405P20 laser diode depends on the temperature. The wavelength increases linearly with temperature and the coefficient is about $0.05 \frac{\text{nm}}{\text{K}}$. This means that the wavelength can be tuned by 0.5 nm over the full temperature range of the LDM9T/(M) diode mount. Please note that the diode temperature is influenced not only by the setpoint of the controller, but also by the laser current. A higher current increases the temperature and therefore leads to slightly longer wavelength at the same controller setpoint. Vice versa, a change in temperature can change the output power at the same current.

12.10 Adjustable Count Rate Ratio

In some of the experiments, it can be desirable to adjust the ratio of photons that go to detector A and B. This can be achieved by a combination of a half-wave plate and a polarizing beamsplitter in the arrangement displayed in Figure 159.

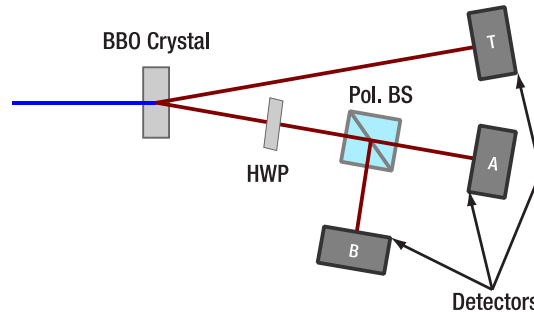


Figure 159 Using a polarizing beamsplitter to adjust the count rate ratio between detectors A and B.

By turning the HWP, the polarization of the photons incident on the polarizing beamsplitter is changed, so that different ratios of photons are transmitted/reflected. Thus, the count rate ratio can be continuously varied. Exercise caution when using this arrangement for polarization sensitive experiments. A suitable wave plate (Item # WPH10ME-808) is part of the kit and Thorlabs offers other suitable beamsplitters such as the CCM5-PBS202(/M) beamsplitter.

12.11 Movable Michelson Interferometer

Our standard setup procedure involves clamping the Michelson interferometer board to the table at its final position, such that it cannot move in any direction during operation. The fine alignment of the Michelson depends on the force and position of clamping. If you want to be able to move the interferometer in and out of the beam path, e.g. for switching between the GRA configuration and the Michelson experiment, there is another option to define a repeatable position for the Interferometer board, as shown in Figure 160. Additional clamps and screws are not included in the kit.

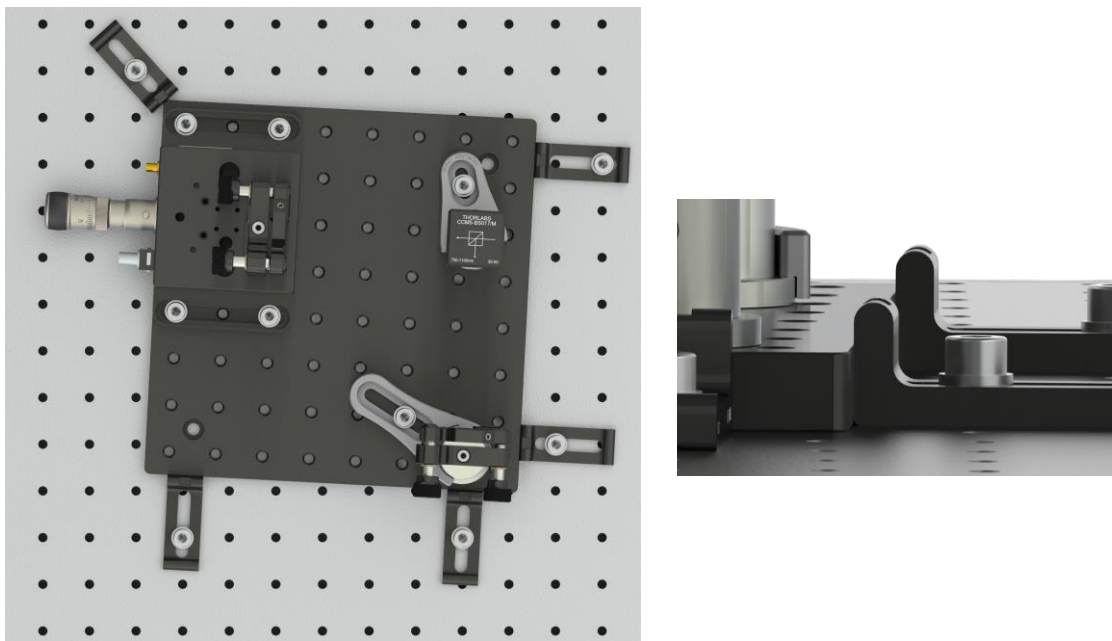


Figure 160 Repeatable positioning of the Michelson interferometer board, using 5 additional CL5A clamps (not included). The inset shows a side view.

- Set up the Interferometer in its final position (see Section 7.6) and use at least one clamp to fix the position temporarily. Fine alignment using the LED is not yet required.
- Press four CL5A clamps (or similar) flat against two neighboring sides of the breadboard and fix their position using 1/4"-20 x 1/2" (M6 x 12 mm) cap screws plus washers (not included). Larger spacing between clamps on the same side improves positioning accuracy.

- Remove the temporary clamps from the first step. Now the Michelson board can be moved in and out of the measurement position.
- In the measurement position, the board should be secured against lateral movement by a fifth clamp which is pressed against the board diagonally to the axes defined by the other clamps.
- With the board fixed in this position, you can do the fine alignment procedure of the Michelson. Moving the board carefully around the table usually does not affect the alignment of the Michelson much, such that comparable amplitudes of the interferometer signal can be achieved between multiple repositions.

12.12 Polarization In the SPDC Process

Since the light in this setup has various orientations of linear polarization, we shortly follow the light path from pump laser to detector:

- The pump laser polarization is perpendicular to the plane of the optical table.
- The first half-wave plate (at 45°) rotates the pump beam polarization parallel to the table plane.
- The BBO crystal is oriented such that its optical axis lies parallel to the table plane. The marking on the housing shows the axis of rotation which is used to tune the phase matching and should be perpendicular to the table, as well as the polarizations of the pump, signal, and idler photons, see Figure 161. The text on the crystal mount also denoted the wavelength range of the anti-reflection coating (400 nm - 500 nm) and the thickness of the crystal (3 mm).
- The photon pair polarization is perpendicular to the table plane and remains unaffected by the beamsplitter in the arm of detector A.
- The HWP (at 22.5°) rotates the single photon polarization by 45° counterclockwise, when viewed against the beam direction from the HWP towards the first beamsplitter.
- This way, the polarization axis is aligned exactly with the slow axis of the liquid crystal cell in the interferometer arm with the fixed mirror, in case of the additional experiments for Quantum Computing (see Section 10.3 for details).
- In the interferometer arm with the moving mirror, the polarization axis is rotated 45° clockwise, when viewed from the moving mirror towards the interferometer beamsplitter. This is due to the reflection in the beamsplitter.

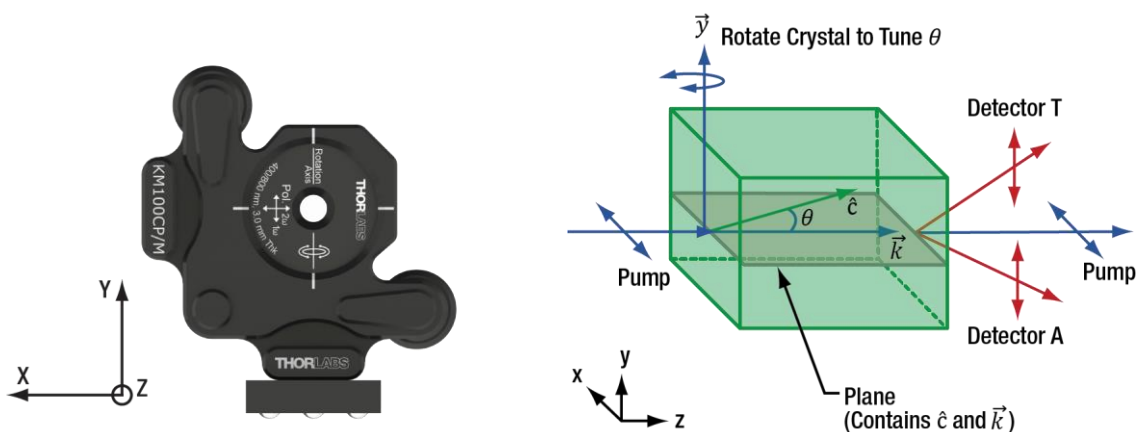


Figure 161 Polarization Vectors and Crystal Axes of the Setup (\hat{c} is the optic axis of the crystal and \vec{k} is the propagation vector of the light). The red arrows for detectors T and A are in the same plane as \hat{c} and \vec{k} .

Chapter 13 Troubleshooting

13.1 Pump Laser not Working

Problem: The pump laser is not lasing.

Solution:

- Make sure that the KLD101 driver and LDM9T(/M) mount are securely connected via the CAB400 cable.
- Make sure that the LDM9T(/M) mount is connected to the power grid and switched on.
- Make sure that the KLD101 driver is set to “Cathode Grounded” and that you have set a laser current between 25 and 40 mA (compare to the spec sheet of the laser diode).
- Make sure that the internal switches and jumpers of the LDM9T(/M) mount are set exactly as described in Section 7.1.
- Make sure that the connection of the laser diode to the LDM9T(/M) mount is exactly as described in Section 7.1.

In rare cases, the laser diode might have burned out. If you have checked all the above points and the pump laser is not working, please contact Techsupport@thorlabs.com.

13.2 Low Count Rates with Filter

Problem: In Section 7.4.4, the count rates are much smaller than 300 kHz.

- If the count rates are 0, the detectors might still be switched off or the detectors are connected to the wrong channel of the Time Tagger.
- Make sure that the pump laser is switched on and that the laser current is about 5 mA below the lasing threshold of your diode (check the spec sheet).
- Make sure that all iris apertures in front of the detectors are opened as far as possible.
- Check all other iris apertures in the setup. None of them should be completely closed.
- Make sure that the gain of the detectors is set to maximum (rotate gain screw clockwise until you reach hard stop).

If the above points do not solve the problem, recenter the CXY1A mount (turn adjusters until markings on the front align) and repeat the detector positioning process, as explained in Section 7.4.3. An experimental environment with significant stray light leads to large background signals. This complicates the adjustment process, but satisfactory results can still be reached by applying the following methods:

- When adjusting the detector optics to maximize for count rate (either with the alignment laser in Section 7.3 or with the colored glass filter), switch the laser off and on again. If the count rate in the alignment tab changes, you are optimizing on actual signal, keep going. If it does not change, you are seeing only signal from stray light and are far away from the target adjustment.
- Use higher pump laser power to more clearly separate actual signal from stray light. When adjusting the third detector, you might need to temporarily close the iris apertures in front of the other detectors to avoid saturation of the Time Tagger. Lower the pump laser power once you are sure that you are optimizing on actual signal rather than stray light (see prior point).

13.3 Low Count Rates with BBO crystal

Problem: In Section 7.4.4, the count rates are correct, but after inserting the BBO crystal in Section 7.4.5., the count rates are too low.

- Make sure that the laser current is set to a value that corresponds to about 13 mW of output power (compare the spec sheet of your individual laser diode).
- Make sure that the crystal is oriented correctly (see Figure 37)
- Make sure that the 405 nm half-wave plate is positioned between the two mirrors of the pump beam path and is set to 45°. Turn the HWP to see if there is a significant increase in the count rates.
- Check, whether the pump laser is still centered on both the alignment iris and the beam trap iris. If that is not the case, use the two mirrors in the pump beam to re-center the pump laser on both iris apertures (see Section 7.4.2).
- Make sure that the BBO crystal is perpendicular to the pump beam (back reflection with target and alignment laser) before trying to tilt it to maximize the count rate.

If the above points do not solve the problem, repeat the detector positioning process, as described in Section 7.4.3.

13.4 Low Coincidence Count Rates

Problem: In Section 7.4.5, you see high single detector count rates (>100 kHz), but low coincidence count rates (<1 kHz).

- Make sure you have calibrated the detector delay offset as described in Section 7.4.5
- Check that the maximum single detector count rates are at the same crystal tilt angle. If the maxima are at significantly different angles, you must repeat the positioning process (Sections 7.4.3 and 7.4.4)

13.5 Malus' Law Measurement is Asymmetric

Problem: The measurements for Malus' law (Section 9.6) show an asymmetric signal rate. An example is shown in Figure 162.

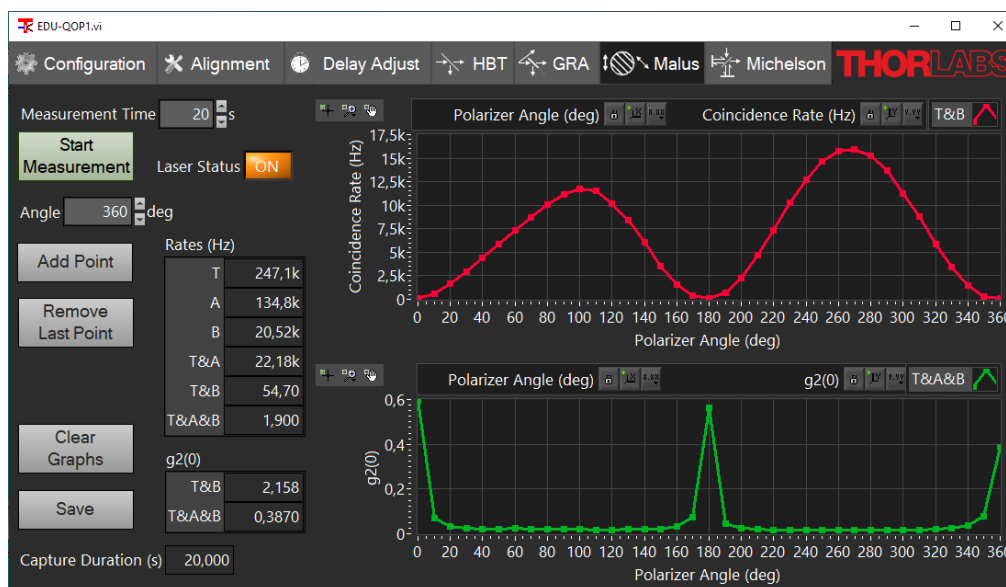


Figure 162 Example measurement with asymmetric signal for Malus' experiment.

- Make sure the polarizer is centered with respect to the alignment laser and that its reflection goes back through the alignment target (similar to the alignment of the half-wave plate in Section 7.7)
- The $\varnothing 1''$ economy polarizer can give rise to a beam deviation, which walks the spot out of the active detector area if it is close to the edge. In the Alignment tab, optimize the T&B coincidence signal for the smaller maximum (in the above example with the polarizer at 90-100°) by turning the two kinematic screws of the CXY1A mount and the zoom housing.

13.6 Michelson Interferometer Problems

If in Section 7.6.6, you see a very low count rate on detector B and/or a very low coincidence count rate T&B:

- Move the alignment laser to the magnetic post behind the crystal and use it to check whether all iris apertures and optical elements are correctly positioned (the beam should pass through the center). If an iris is not hit correctly, repeat the beamwalk as described in Section 7.6.1. If an element is not positioned correctly, move the element (or the whole Michelson board until the positioning is correct; check back reflections with the target to ensure normal incidence).

In Section 7.6.6, you see coincidence count rates, but no interference pattern when moving the stage.

Softly press against the holder of the Michelson mirror that is not on the stage. If you do not see any variation of the coincidence count rate:

- Test your interferometer adjustment: Put the LED in front of the interferometer and check whether you see an interference pattern at the output.
- Make sure that the interference pattern is centered on detector B.

If you see a variation with the above test, but not when moving it via the software:

- Make sure that the stage is connected to both the KPZ101 and KSG101 controllers.
- Make sure that the KPZ101 and KSG101 controllers are connected to power and switched on. Sometimes the power supply cable is not fully connected to the controllers. This will result in their display to work, but not any other functionality.
- Make sure that the K-Cube controllers are connected to each other via an SMA-to-SMA cable (from KSG-Monitor to KPZ-EXT IN)
- Perform the zeroing procedure in the software.

If you see an interference pattern in the software, but the contrast is low:

- Slightly move the differential screw of the stage and check whether the contrast improves.
- Very carefully turn the kinematic screws of the interferometer mirror not on the stage. Use a hex key to be able to turn as slow as possible. Check whether this improves the contrast.
- Alternatively, use the LED for the alignment process, as described in Section 7.6.2.

13.7 Quantum Eraser Problems

In Section 7.7, if you see the interference pattern with both polarizers at 0° , but you also still see a pattern with crossed polarizers, this is a sign for a non-optimal calibration of the polarizers or polarization changes induced by a slight inclination of the beamsplitter. In this case, try the following:

- Put the $\emptyset 1''$ polarizer in front of detector B and set it to 0°
- Block one arm of the interferometer, turn the $\emptyset 1/2''$ polarizer in the other arm until the coincidence count rate T&B is minimized.
- Block the other arm of the interferometer, turn the $\emptyset 1''$ polarizer to 90° , and then turn the $\emptyset 1/2''$ polarizer in the open arm until the coincidence count rate T&B is minimized.
- Now, you have ensured that the light coming from the arms of the interferometer is perpendicularly polarized. Remove the $\emptyset 1''$ polarizer, unblock both arms, and test whether the interference pattern is indeed fully suppressed (and whether it can be recovered when inserting the $\emptyset 1''$ polarizer set to 45°)

Chapter 14 Laser Safety Calculation

14.1 Laser System

In this EDU-Kit we are using the **L405P20** laser diode. Each institution that uses this educational kit should have a laser safety officer to determine the safety requirements. However, here we give one approach to calculate the risk assessment based on the laser used in this kit.

This laser has a maximum output power of 20 mW and emits in the wavelength range of 405 nm \pm 5 nm. There is a lens on the laser, which provides a collimated beam. The beam divergence is not known but will be in the range of a few mrad. The laser beam is not circular, it has an elliptical shape with widths of 3 mm x 1 mm.

During normal operation, the laser beam is guided by optics and directed to a working area. As the laser beam is not shielded, there is direct access to this laser radiation. As a result, a reflection (single fault case) of the complete laser radiation could leave the working area.

14.2 Laser Class Calculation

For the classification of laser devices, the accessible emission limits (AEL) must be considered. The AEL for the respective protection classes are defined according to the possible hazards that can be caused by the light radiation for the human body and especially for the human eye.

The limit values depend on several factors defined in the EN60825-1 standard to cover different parameters influencing the hazard.

To determine the laser class of the system, the maximum emitted laser power in the case of a fault must be considered. According to the measuring conditions described in the DIN EN60825-1 Norm, the measurement is performed according to condition 3 at a distance of 100 mm from the source with a measuring aperture diameter of 7 mm. Only the laser radiation detected with this measuring aperture is relevant for the evaluation.

The laser radiation has a maximum output power of $P=20$ mW, a wavelength range of 405 nm \pm 5 nm, and is not pulsed. Due to the beam widths of 3 mm x 1 mm, the complete power of the laser radiation is relevant for the classification. The following table shows the laser classes and their power limits for operating the laser in CW mode.

Laser class	Accessible Emission Limits for CW Mode	
1	AEL_{LC1}	0.39 mW
2	AEL_{LC2}	1 mW
3R	AEL_{LC3R}	5 mW
3B	AEL_{LC3B}	500 mW

Table 3 Accessible Emission Limits for CW Mode

The table shows that the L40P20 laser exceeds the limits of laser classes 1, 2 and 3R and is thus classified in **class 3B**.

For class 3B laser systems, looking into the direct beam is normally dangerous, including short-time accidental irradiation.

14.3 Laser Safety Glasses Calculation

Using personal safety equipment (such as laser safety glasses), ensures that the user will not encounter emission that exceeds laser class 1. The standard DIN EN 207:2017 provides a guideline for the selection and application of laser safety eyewear. The following calculations are based on the specification of this standard.

With a laser power of 20 mW and a limit value of 0.39 mW, a maximum transmittance of 10^{-2} is relevant for laser safety eyewear.

In addition to the transmittance, the resistance of the safety goggles to the laser radiation is also relevant. For this purpose, the maximum irradiance of the laser beam must be determined. The beam as a 3 mm x 1 mm beam

profile, but as a worst case, it was assumed that the beam is circular with a diameter of 1 mm. With the laser power of 20 mW, the irradiance is:

$$E = \frac{P}{A} = \frac{P}{\pi \cdot r_{beam}^2} = \frac{20mW}{\pi * (0.5 \cdot 10^{-3}m)^2} \cdot 2 = 50.93 \cdot 10^3 \frac{W}{m^2}$$

The additional factor 2 in the formula describes the maximum irradiance in the center of the Gaussian beam. This irradiance must be used for the selection of the laser safety eyewear.

Both the transmittance and the maximum irradiance must be complied with by the used safety eyewear. For an Irradiance $<100.000 \frac{W}{m^2}$, safety goggles with scale number of D LB4 are required according to the EN207:2017 norm (see green field in Figure 163).

From the Thorlabs portfolio, the **LG3** glasses are therefore a viable choice, as it has a protection level of **D LB4** in the relevant wavelength range.

		Max. Power Density (E, W/m ²) & Energy Density (H, J/m ²) in Specified Wavelength Range								
Wave-length Range		180 - 315 nm			>315 - 1400 nm			>1400 nm - 1000 μm		
		For Pulse Duration (seconds)								
Scale Number	T	D > 3·10 ⁻⁴	I, R 10 ⁻⁹ to 3·10 ⁻⁴	M <10 ⁻⁹	D >5·10 ⁻⁴	I, R 10 ⁻⁹ to 5·10 ⁻⁴	M <10 ⁻⁹	D >0.1	I, R 10 ⁻⁹ to 0.1	M <10 ⁻⁹
LB1	10 ⁻¹	0.01	3 · 10 ²	3 · 10 ¹¹	10 ²	0.05	1.5 · 10 ⁻³	10 ⁴	10 ³	10 ¹²
LB2	10 ⁻²	0.1	3 · 10 ³	3 · 10 ¹²	10 ³	0.5	1.5 · 10 ⁻²	10 ⁵	10 ⁴	10 ¹³
LB3	10 ⁻³	1	3 · 10 ⁴	3 · 10 ¹³	10 ⁴	5	0.15	10 ⁶	10 ⁵	10 ¹⁴
LB4	10 ⁻⁴	10	3 · 10 ⁵	3 · 10 ¹⁴	10 ⁵	50	1.5	10 ⁷	10 ⁶	10 ¹⁵
LB5	10 ⁻⁵	10 ²	3 · 10 ⁶	3 · 10 ¹⁵	10 ⁶	5 · 10 ²	15	10 ⁸	10 ⁷	10 ¹⁶
LB6	10 ⁻⁶	10 ³	3 · 10 ⁷	3 · 10 ¹⁶	10 ⁷	5 · 10 ³	1.5 · 10 ²	10 ⁹	10 ⁸	10 ¹⁷
LB7	10 ⁻⁷	10 ⁴	3 · 10 ⁸	3 · 10 ¹⁷	10 ⁸	5 · 10 ⁴	1.5 · 10 ³	10 ¹⁰	10 ⁹	10 ¹⁸
LB8	10 ⁻⁸	10 ⁵	3 · 10 ⁹	3 · 10 ¹⁸	10 ⁹	5 · 10 ⁵	1.5 · 10 ⁴	10 ¹¹	10 ¹⁰	10 ¹⁹
LB9	10 ⁻⁹	10 ⁶	3 · 10 ¹⁰	3 · 10 ¹⁹	10 ¹⁰	5 · 10 ⁶	1.5 · 10 ⁵	10 ¹²	10 ¹¹	10 ²⁰
LB10	10 ⁻¹⁰	10 ⁷	3 · 10 ¹¹	3 · 10 ²⁰	10 ¹¹	5 · 10 ⁷	1.5 · 10 ⁶	10 ¹³	10 ¹²	10 ²¹

Figure 163 Table 1 of the EN207:2017 Norm. The important value for this kit is marked in green.

Chapter 15 Acknowledgements

We are grateful for the various insights we have collected over the years from numerous committed educators who have taken on the challenge of experimentally teaching quantum optics to students.

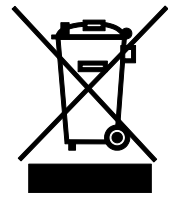
The experimental realization in this kit was heavily influenced by our collaborators from the Leibniz University Hannover. We cordially thank Dr. Kim-Alessandro Weber and Dr. Rüdiger Scholz for their outstanding contributions to this kit. Between them, they have more than 40 years of experience in designing quantum optics and photon statistics experiments. This kit's design borrows many ideas from the experiments they set up to teach both college students as well as teachers and students from high schools. We are grateful for their enthusiasm to share this experience with the rest of the teaching community by means of this kit. Moreover, they have been invaluable partners to discuss matters of quantum optics in general and didactics in particular. Finally, we thank them for testing and providing extensive feedback on the SPDMA single-photon detector incorporated into this kit during its development.

We cordially thank Paul Schlummer, Adrian Abazi, Carsten Schuck, and Wolfram Pernice from the University of Münster for supporting the development of this educational quantum optics setup. We acknowledge countless fruitful discussions, both on the physical as well as the teaching aspects of quantum systems. In particular, we are grateful for the thorough comparison to a type-II BBO system and their detailed feedback on our SPDMA single photon detector.

We also gratefully acknowledge the contributions of Prof. Dr. Jan-Peter Meyn who was one of the early adopters of real quantum optics experiments in the German teaching community (e.g., P. Bronner *et al* 2009 *Eur. J. Phys.* **30** 1189). His expertise and the optical design of his setups helped spread knowledge among educators and was also an inspiration to certain design elements in the setups from Dr. Kim-Alessandro Weber and Dr. Rüdiger Scholz.

Chapter 16 Warranty and RMA Information

Thorlabs verifies our compliance with the WEEE (Waste Electrical and Electronic Equipment) directive of the European Community and the corresponding national laws. Accordingly, all end users in the EC may return “end of life” Annex I category electrical and electronic equipment sold after August 13, 2005 to Thorlabs, without incurring disposal charges. Eligible units are marked with the crossed out “wheelie bin” logo (see right), were sold to and are currently owned by a company or institute within the EC and are not disassembled or contaminated. Contact Thorlabs for more information. Waste treatment is your own responsibility. “End of life” units must be returned to Thorlabs or handed to a company specializing in waste recovery. Do not dispose of the unit in a litter bin or at a public waste disposal site. It is the user’s responsibility to delete all private data stored on the device prior to disposal.



Annex I

16.1 Return of Devices

This precision device is only serviceable if returned and properly packed into the complete original packaging including the complete shipment plus the cardboard insert that holds the enclosed devices. If necessary, ask for replacement packaging. Refer servicing to qualified personnel.

Chapter 17 Thorlabs Worldwide Contacts

For technical support or sales inquiries, please visit us at www.thorlabs.com/contact for our most up-to-date contact information.



USA, Canada, and South America

Thorlabs, Inc.
sales@thorlabs.com
techsupport@thorlabs.com

Europe

Thorlabs GmbH
europe@thorlabs.com

France

Thorlabs SAS
sales.fr@thorlabs.com

Japan

Thorlabs Japan, Inc.
sales@thorlabs.jp

UK and Ireland

Thorlabs Ltd.
sales.uk@thorlabs.com
techsupport.uk@thorlabs.com

Scandinavia

Thorlabs Sweden AB
scandinavia@thorlabs.com

Brazil

Thorlabs Vendas de Fotônicos Ltda.
brasil@thorlabs.com

China

Thorlabs China
chinasales@thorlabs.com



THORLABS
www.thorlabs.com
